NASA CR-132717

CARBON MONOXIDE POLLUTION EXPERIMENT
FINAL REPORT

BY M. H. BORTNER
R. DICK*
H. W. GOLDSTEIN
R. N. GRENDA

January 1975

Prepared under Contract No. NAS1-10139 by
GENERAL ELECTRIC COMPANY
SPACE PRODUCTS DIVISION
SPACE SCIENCES LABORATORY
P.O. Box 8555
Philadelphia, Pa. 19101

for

NATIONAL AERONAUTICS AND SPACE ADMINISTRATION

*Barringer Research Limited

NASA CR-132717

CARBON MONOXIDE POLLUTION EXPERIMENT
FINAL REPORT

BY M. H. BORTNER
R. DICK*
H. W. GOLDSTEIN
R. N. GRENDA

January 1975

Prepared under Contract No. NAS1-10139 by
GENERAL ELECTRIC COMPANY
SPACE PRODUCTS DIVISION
SPACE SCIENCES LABORATORY
P.O. Box 8555
Philadelphia, Pa. 19101

for

NATIONAL AERONAUTICS AND SPACE ADMINISTRATION

*Barringer Research Limited

INDEX

FIGURES

LIST OF TABLES

FORWORD

This report was prepared for NASA as part of contract NAS1-10139 with Langley Research Center under the Advanced Applications Flight Experiments (AAFE) Program. The objective of this contract is the development of the Carbon Monoxide Pollution Experiment (COPE). This experiment is designed primarily to obtain data for the investigation of mechanisms by which CO is removed from the earth's atmosphere. The approach uses an orbiting platform to remotely map global CO concentrations and determine vertical CO profiles using a correlation interferometer measurement technique developed by Barringer Research Ltd. The instrument is to be capable of measuring CO over the range of expected atmospheric burdens and of measuring other trace atmospheric constituents.

Since various parts of the program have been reported in detail in other reports they are only briefly described to herein. These parts include the CO problem (ref. 1), the Breadboard (ref. 2), and the Engineering Model (ref. 3). The major topic covered in this report is that of flight measurements of carbon monoxide and methane.

ACKNOWLEDGEMENTS

The authors would like to express their appreciation to several co-workers who have contributed significantly to this work - specifically to Dr. F. N. Alyea who organized the analytical work on the CO feasibility studies; Dr. G. R. Liebling who did much of the programming for the analysis; Dr. S. L. Neste who assisted in performing calculations; G. M. Levy whose thorough understanding contributed much of the information and answered questions related to the meteorological aspects of the program; Dr. S. H. Chandra who investigated the effects of possible scintillations on the measurement; Dr. J. C. Burns who made numerous helpful suggestions and reviewed the analytical work; A. E. Kreft who assisted with GE laboratory tests; D. W. Grantham who designed the interface equipment and assisted in the installation of equipment in the jet and helicopter aircraft; A. M. Karger who performed much of the laboratory work done in conjunction with the applicability of the technique to other gases, G. A. Griffith who handled the computing for both the feasibility studies for other gases and the treatment of the flight data; Miss L. Beaudette who handled many of the calculations done at Barringer Research; J. H. Davies who served as program manager of the Barringer Research portion of the work; Dr. A. R. Barringer whose stimulating ideas and discussion were vital to the development of the technique and the practical solutions of problems of its application; Dr. L. Steg who contributed the needed backing of General Electric Company management; W. Rohrbach and L. Mayo of NASA LaRC who assisted in the tunnel tests of the breadboard instrument; M. Jarret of NASA LaRC who assisted with the computer treatment of the tunnel data; E. Hooper of NASA LaRC whose assistance during the work at that location was invaluable; and Dr. R. H. Kummler, now of Wayne State University, who contributed many valuable suggestions in the formulation of the program and in his consultation throughout the work.

The authors were extremely interested in and appreciative of the study of the use of the correlation interferometer for the measurement of carbon monoxide from an orbiting platform carried out by a group at the Department of Aerospace Engineering at the University of Michigan under Prof. Wilbur C. Nelson.

The authors appreciate the cooperation of Dr. Peter Wilkness of the Naval Research Laboratory in making available data before publication.

The authors would also like to express their great appreciation to E. McLaren, Maj. E. Gardiner, and the many other members of the Canada Centre for Remote Sensing for their cooperation and interest in planning and carrying out the flights on the Falcon.

The support and cooperation of R. N. Parker, NASA LaRC AAFE program manager, and P. J. LeBel, NASA LaRC Technical Project Manager on the COPE program, have been much appreciated throughout the program.

1. EXPERIMENT DEFINITION

1.1 CO in the Atmosphere

Carbon monoxide (CO) is a toxic pollutant which is continually introduced into the Earth's atmosphere in significant quantities. It is the most widely distributed and most commonly occurring air pollutant. Although in recent years the effort to measure CO in the atmosphere has increased significantly, there is still a need for a much expanded program of CO measurements both in urban and rural areas and on a more global scale. Such data are needed because of the need to have sufficient data to evaluate pollution hazards as such, to quantitatively evaluate sources of CO, to determine transport effects and to investigate sink mechanisms. That is, data are needed both for the investigation of localized short-term problems and for large-scale long-term effects.

One of the latter questions is that of the CO "sink". There are apparently some mechanisms operating which destroy most of the CO in the atmosphere, i.e., a CO "sink". These mechanisms have not as yet been established in a quantitative sense. If there were no mechanism of destruction, then the CO concentrations would be expected to double in two or three years. This apparently is not occurring at present, but it is impossible to extrapolate CO concentrations without a knowledge of the sink mechanism. Thus, the potential of CO as an ecological problem in the future can not be determined. There is, therefore, substantial interest in ascertaining the global balance of CO. Such a consideration involves a knowledge of the sources, the present global concentrations and the sinks of CO. The CO balance in the atmosphere has been discussed in detail elsewhere (ref. 1).

The problem of carbon monoxide in the atmosphere is still replete with unsettled questions. Although over the past several years significant new information has been obtained relating to sinks, to sources, and to concentrations, none of these questions have been definitely and quantitatively answered. The present status of information concerning the sink question indicates that the most likely sinks are interaction with soil bacteria, reaction with OH near the ground, and transport to and reaction with OH in the stratosphere. With these singly, or in combination, lifetimes of a few tenths of a year could be accounted for although for the definite establishment of a sink mechanism both better data on various parameters involved and better CO concentration data are needed.

Sinks are most likely rather extensive covering significant global areas Since they are extensive and could occur anywhere on the globe, a satellite-based remote measurement technique is ideally suited for the measurement. Of course, if the sink covers the entire globe, the measurement of concentrations will not show the sink region. If it is localized to some extent to regions which are rather extensive, as would be effected by most sink mechanisms, the measurement of CO densities with spatial resolution of the order of 25 to 50 miles should provide the information needed to locate the sink.

The carbon monoxide produced by the various sources has time to circulate around the globe and at least mix in each hemisphere, although perhaps not

enough time for appreciable inter-hemispheric transfer. There may or may not be enough time for transfer of significant amounts to the stratosphere. Just how much mixing is possible depends on the sink and the resultant lifetime which is probably somewhere between 0.1 and 1 year, most likely around 0.4 year.

There are logical indications that there may be some unidentified significant natural source of CO. If this is the case, it suggests that the sink strength is much larger than previously supposed. Data are needed to determine this.

All parts of the CO question require further investigation. Data are needed on both localized and global CO measurements, at ground level, in the troposphere and in the stratosphere. Data best found by remote and in some cases by remote global measurements are needed on other sources of CO, on both urban and rural variations, on hemispheric differences, and on CO transport. Data are needed related to certain sink processes. Also important are various laboratory data such as those required for the analysis of atmospheric chemistry and for those required to quantify biological CO removal processes. The sink mechanism problem can be solved only by obtaining sufficient atmospheric CO measurement data, supporting atmospheric measurements of related species, supporting laboratory data, and ground measurements of the characteristics of any sink region found, thus permitting the quantitative determination of the sink strength and allowing extrapolation to determine the trend of world-wide CO concentration in the future.

1.2 Measurements Needed

In order to obtain sufficient data to understand and eventually be able to solve both short-term and long-term CO problems, measurements of CO are needed on a global scale. That is, measurements are needed on a scale which permits areas of about the size of cities and of the size of significantly large, rather uniform areas which may in some way affect the CO balance to be isolated. These measurements must also cover the entire globe so as not to overlook the possibility of any major sources or sinks. Thus an ideal platform is a spacecraft with an orbit such that essentially all the globe can be covered with a spatial resolution of the order of 25 miles and with a reasonable frequency. It is also advisable to be able to investigate certain areas, especially those areas found from spacecraft-based measurements to be interesting, by more frequent measurements with higher spatial resolution, such as those which could be obtained from an aircraft.

The study described herein is on an instrument which seems most ideally suited for such measurements - both spacecraft-based and aircraft-based.

2. FEASIBILITY OF THE MEASUREMENT

2.1 The Feasibility Problem

An important question in the application of the correlation interferometric technique to the measurement of atmospheric burdens of CO concerns the effect of variations in atmospheric conditions and profiles. Specifically, variations in atmospheric temperature and its profile including inversion layers, atmospheric pressure, surface temperature, surface emissivity, surface reflectivity, the atmospheric profile of the gas to be measured, the atmospheric profile of gases which interfere with the measurement, cloud cover, the velocity of the platform, atmospheric scintillations, and certain other properties were studied to determine their effect on the radiation incident on an instrument on a spacecraft. This was done by a simulation which consisted of defining a representative model atmosphere and subsequently solving the radiative transfer equation to obtain the spectrum falling on the instrument. Effects such as reflected sunlight, earthshine, atmospheric absorption and atmospheric emission were considered in order to yield physically meaningful solutions to the equation. For carbon monoxide transmission was computed for the spectral regions of the fundamental and first overtone bands, i.e., the 4.6 and 2.3 μm regions. The calculations to that point were applicable to any instrument. The action of the instrument on the incident radiation was then calculated to determine the signal produced. For the case in which the instrument is an interferometer, the Fourier transform of the spectrum is then calculated to produce an interferogram. Treatment of the interferogram produces the measurement of the pollutant.

The model has been used to investigate the feasibility of the use of the correlation interferometer to measure CO, to consider the usefulness of the measurement in looking for a CO sink (ref. 4), and to define the exact spectral band which should be used for most reliable and useful results. The following section summarizes the work done on the feasibility study. It is covered in detail elsewhere (ref. 5).

2.2 Atmospheric Models

2.2.1 Composition Models.- The analytical work performed employed several variations of the carbon monoxide, water, and temperature profiles and one carbon dioxide and one methane profile.

Specifically, ten CO profiles were used. These are shown graphically in Figure 2.1. Profile 1 is that for a constant mixing ratio of 0.1 ppm; profile 2 is that for 10 ppm up to 2 km and 0.1 ppm above that; profile 3 is that for a constant mixing ratio of 0.01 ppm; profile 4 is that representing a sink in the 20-45 km range with the mixing ratio dropping from 0.1 to 0.01 over this altitude range; profile 5 is that representing a low altitude sink with an effect up to 9 km, having a mixing ratio of 0.01 ppm at 0 km and 0.1 ppm at 9 km; profile 6 represents a low altitude sink with an effect up to 1 km, having a mixing ratio of 0.01 ppm at 0 km increasing to 0.1 ppm at 1 km; profile 7 also represents a low altitude sink with an effect up to 3 km, having a mixing ratio of 0.005 ppm at 0 km and 0.1 ppm at 3 km; profile 8 represents a low altitude

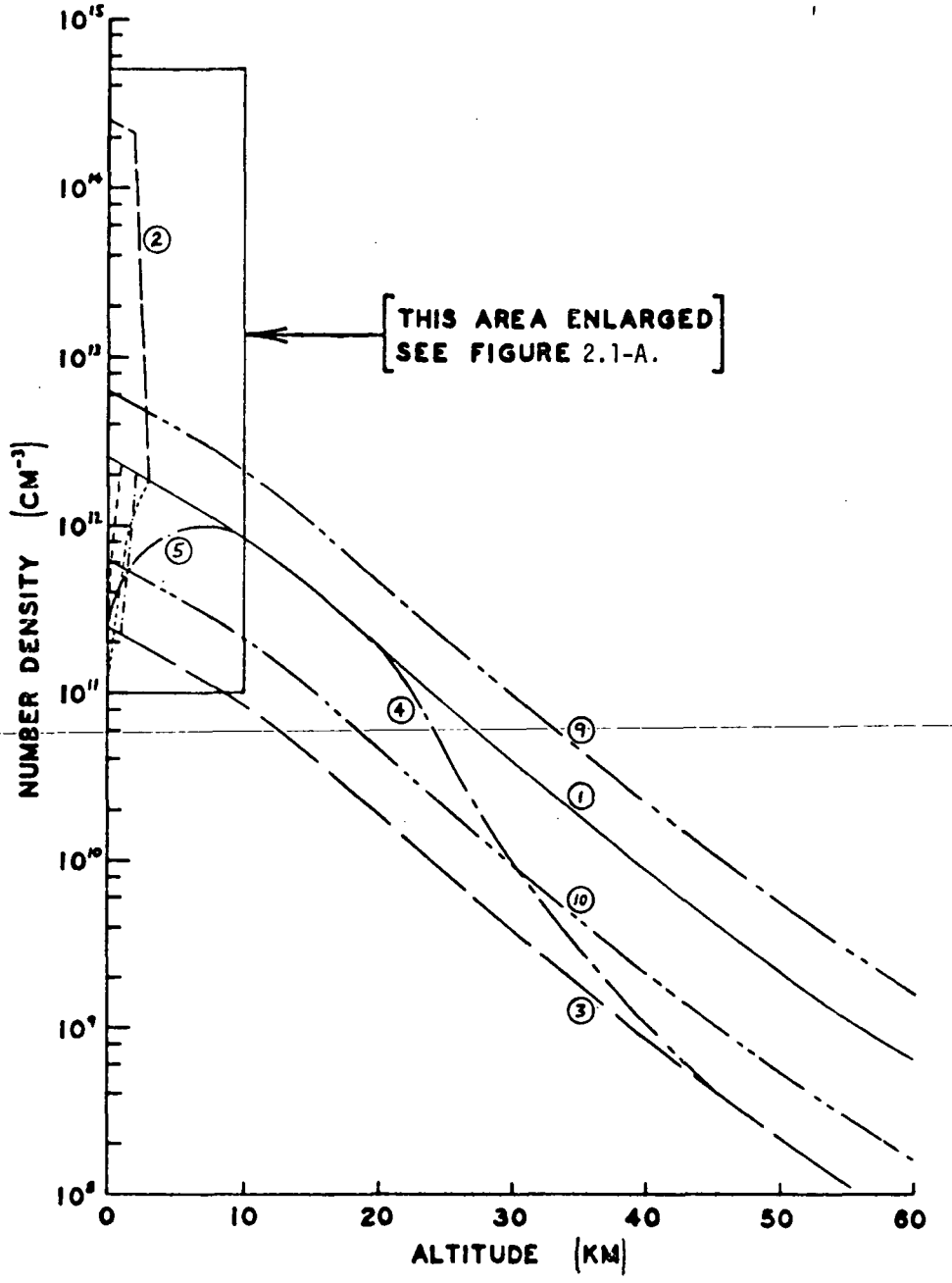

Figure 2.1 CO Profiles

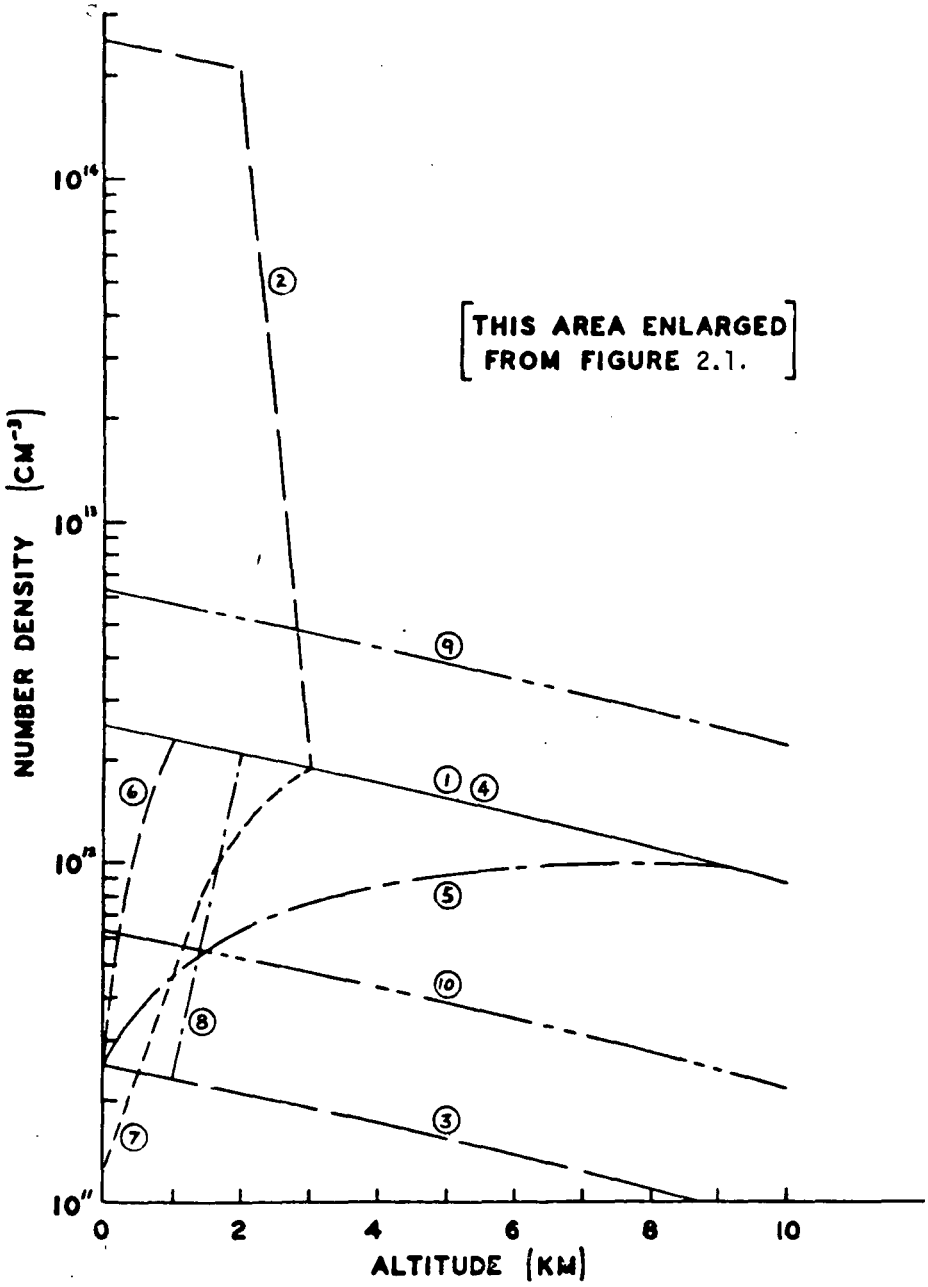

Figure 2.1-A CO Profiles

sink with an effect up to 1 km as in profile 6, but having a mixing ratio of 0.01 ppm up to 1 km and 0.1 ppm above. Models 9 and 10 representing 0.025 and 0.25 ppm CO were used for other purposes discussed later. It is important for the mapping measurements to show the effects of these differences except for profile 4, the effect of which should be shown in the limb experiment. The total number densities from which the CO number densities were obtained with the above mixing ratios were taken from Bortner and Kummler (ref. 6) in which they were derived mainly from CIRA (ref. 7) representing mean conditions throughout the year for latitude near 30°. The CO optical thickness (total number of CO molecules per cm^2 column of sight) is given for the mapping experiment in Figure 2.2 and for the limb experiment in Figure 2.3.

The CO_2 profile used was based on a constant mixing ratio of 320 ppm. The CH_4 profile used was based on a constant mixing ratio of 2 ppm (ref. 8). The three water profiles, corresponding to a dry model (1), normal (2), and a wet (3) atmosphere, were taken from Gutnick (ref. 9), Oppel (ref. 10), and Linquist (ref. 11), respectively, as summarized by Anding (ref. 12). These are given in Figure 2.4. These are equivalent to approximately 0.2, 1.5, and 3 percipitable cm H_2O.

2.2.2 Temperature and Pressure Models.- Four specific temperature profiles were used. These are shown in Figure 2.5. Profile 1 corresponds to a cold atmosphere (ref. 13); profile 2 corresponds to an average atmosphere (ref. 13); profile 3 corresponds to a hot atmosphere (ref. 13); profile 4 involves a low altitude inversion layer (up to 2 km), based on average values for Vandenberg AFB, June 1970. It is important that these variations should have no large effect on the CO measurements. Any such effects require detailed accurate supplemental measurements and make the interpretation of the data much more complex and, for practical purposes, means that many fewer data can be interpreted. Analysis of such effects is covered in subsequent sections of this report.

2.3 Vehicle Effects

The planned satellite experiment may be best carried out in an approximately polar orbit. Without noting reasons, advantages, and disadvantages, this is excellent for the mapping experiment, but restricts the limb measurements to the polar regions. This is not a problem, however, since above the tropopause, it is to be expected that there is no appreciable latitude effect on the concentrations. Keneshea (ref. 14) has calculated the OH concentration at different latitudes and found little variation. Since the chief CO removal mechanism at these altitudes is, in all probability, CO + OH reaction, the rate of CO removal should be about constant with latitude. The small temperature effect on the rate constant should not cause significant variation of CO with latitude.

One effect which must be considered in remote sensing from a fast moving vehicle is the possibility of a Doppler shift. If there is a large velocity component in the direction of the observed radiation, there is a Doppler shift which is determined by $\Delta\nu = \nu\frac{v_s}{c}$ where v_s is the velocity component in the line-

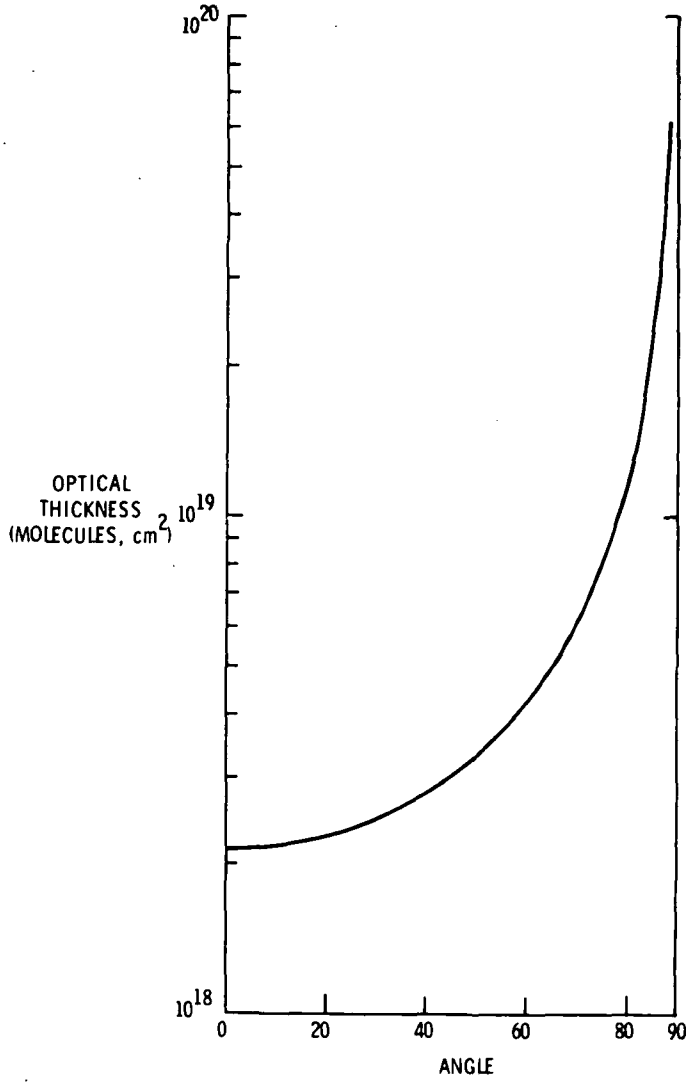

Figure 2.2 Optical Thickness as a Function of Angle from Vertical

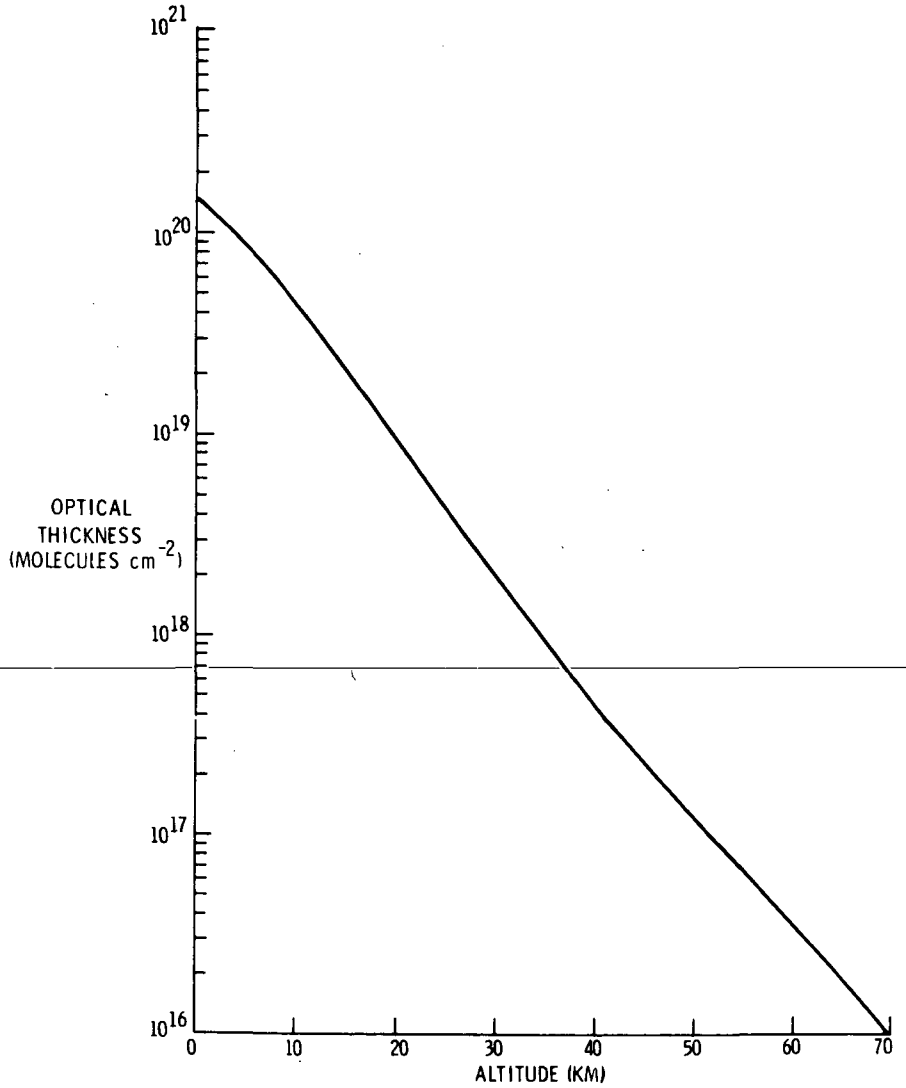

Figure 2.3 Optical Thickness for Limb Transmission Experiment as a Function of Grazing Altitude

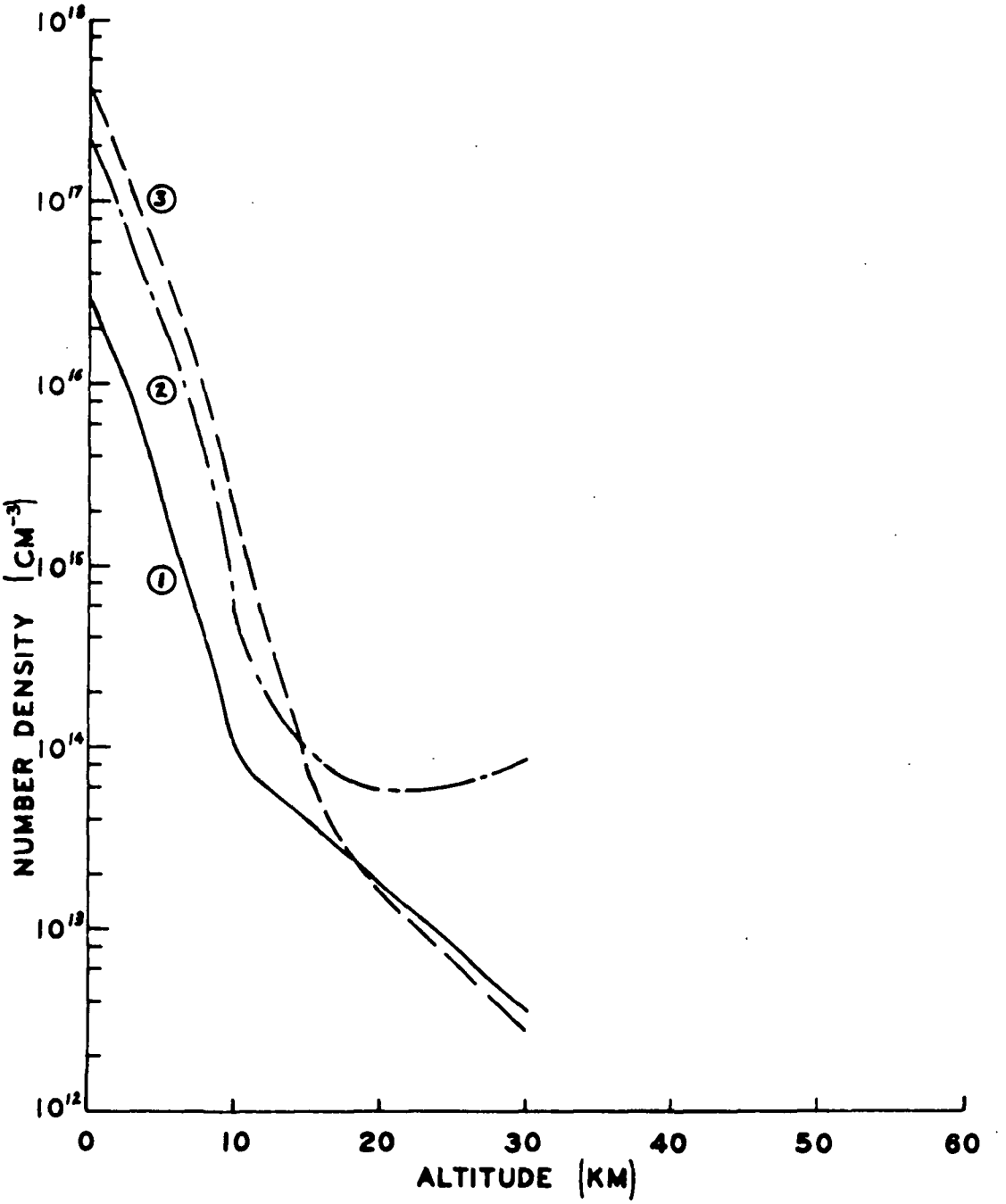

Figure 2.4 H_2O Concentrations

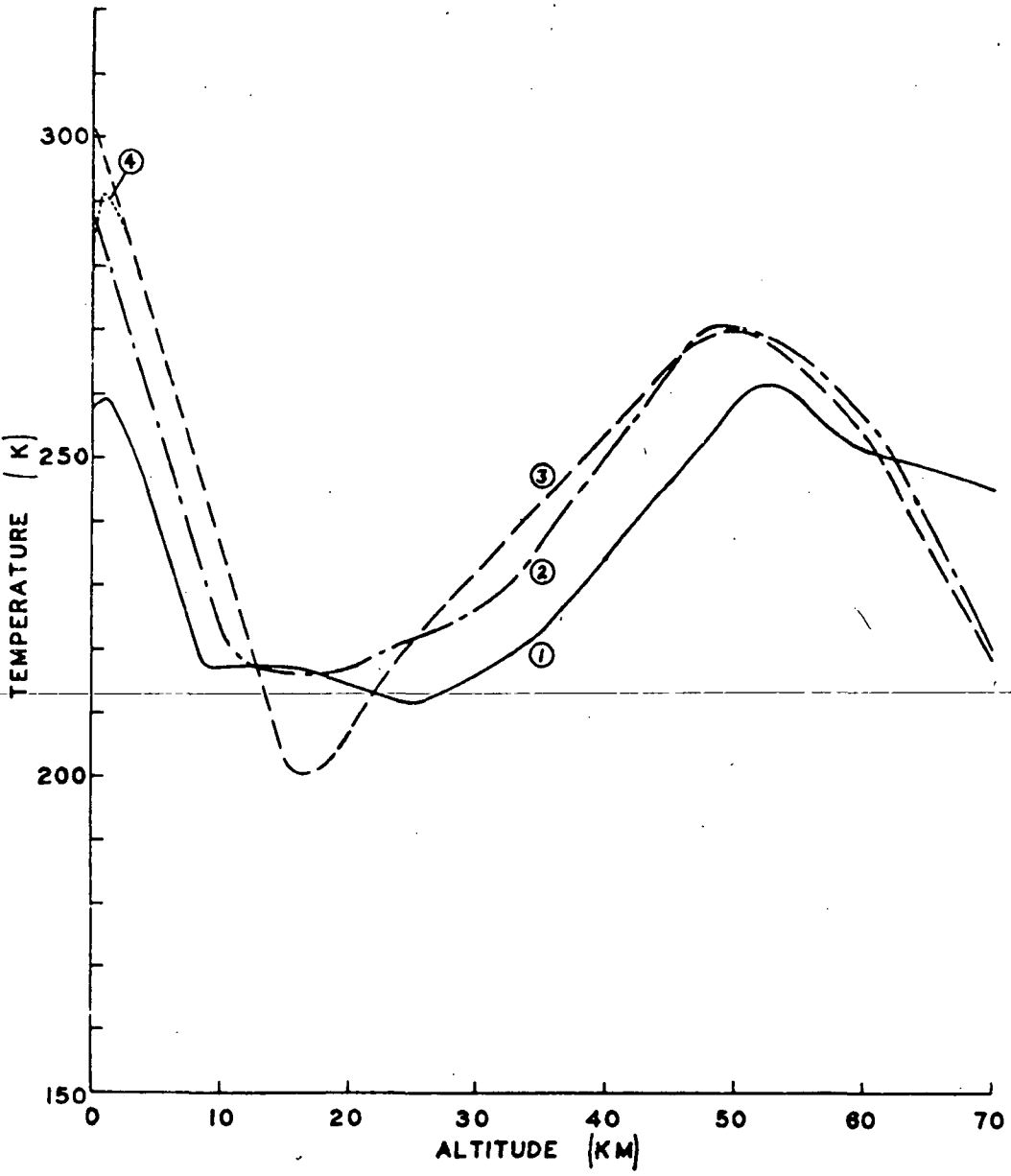

Figure 2.5 Temperature Profiles

of-sight, or $\Delta\nu = \nu\frac{v}{c} \cos\Theta$ where Θ is the angle between the line-of-sight and the vehicle movement. In the limb experiment, the satellite may be traveling very nearly direct toward or away from the sun so that $\cos\Theta \approx 1$, and v_s is of the order of 7×10^5 cm sec^{-1}. Thus $\frac{v_s}{c} = \frac{\Delta\nu}{\nu}$ is of the order of 2.3×10^5. Thus at 2.3 μm, $\Delta\nu = 0.1$ cm^{-1}; and at 4.6 μm, $\Delta\nu = 0.05$ cm^{-1}. These shifts are of the order of a Doppler line-width, which is the width of the line at the upper altitudes, i.e., those of interest in the limb experiment. If the technique is spectral and employs a reference cell of any sort on board this is extremely important and probably means that the technique is not suitable for the limb measurement. For the correlation interferometric technique a Doppler shift essentially appears as a phase shift which can be readily taken into account.

As mentioned above, a desirable spatial resolution is of the order of 25 to 50 miles. From spacecraft altitudes, such as those of the Nimbus vehicle, a 2° field-of-view gives approximately a 25 mile spatial resolution, a distance which is traversed in about four seconds of satellite flight. For the instrument described herein, a 2° telescope was therefore used in some measurements to narrow the normal field-of-view of the instrument from 7°.

2.4 Spectral Consideration

2.4.1 CO Spectra.- The problem of measuring a variety of CO burdens or of locating and explaining a CO sink depends on having a reliable technique applicable to remote sensing. Early in this work, correlation interferometry was compared with various other remote techniques considering specificity to CO, sensitivity, signal/noise, dynamic range, observation time, spatial resolution, stability and data interpretation. Correlation interferometry was found to be the most suitable. Such techniques are mainly spectral and involve the measurement of the amount of absorption or of emission of spectral radiation. Consideration of the energy levels of CO and their populations shows that the potentially useable spectral features lie in the ultraviolet, infrared, and microwave regions. However, in the region of the ultraviolet at which there is significant CO absorption or emission, the atmosphere does not transmit appreciably due to the presence of various dissociation and ionization continua. Microwave techniques are also not practical for this measurement. The infrared has no such continua but has many lines and bands. There are thus a number of windows in the infrared, particularly in high resolution spectra of which the most notable are the 10-12, 8-9.5, 3.5-4, 2-2.5 and 4.5-5 μm windows (ref. 15). CO bands include the following:

V_{upper}	V_{lower}	Band
1	0	
1	1	
1	0	Fundamental
2	1	
2	0	1st Overtone
3	0	2nd Overtone

The pure rotational lines ($V_u = V_l$) of CO occur in the microwave region. The other bands ($V_u > V_l$) are in the infrared (between about 1 and 5 microns).

The fundamental and the first overtone are the bands of most interest here. The energies and wavelengths for the lines of these systems are given in Tables 2.1 and 2.2, respectively. The fundamental band is the strongest. The first overtone is about two orders of magnitude weaker and the second overtone is approximately that much weaker than the first overtone. The transitions involving only excited vibrational states (e.g., 2-1, 3-2, 3-1) are weak because of the low populations of the lower state, that of the first excited state being some four orders of magnitude lower than the ground vibrational state and the second excited state being another four or more orders of magnitude lower.

The R branch consists of transitions in which the rotational state of the upper vibrational level is one greater than that of the lower vibrational level. Similarly, the P branch consists of those transitions in which the rotational state of the upper vibrational level is one less than that of the lower vibrational level. That is for $v' > v''$, the R branch has $J' = J'' + 1$, the P branch has $J' = J'' - 1$. The lines, R or P, are given a subscript denoting the rotational level of the lower vibrational state. Thus the R_0 line of the fundamental is between the $v = 1$, $J = 1$ and $v = 0$, $J = 0$ states. Thus the lines in the R branch have a higher energy (lower wavelength) than those in the P branch of the same band.

The strengths of the individual lines in both the fundamental and first overtone bands are given in Table 2.3. The integrated band intensities are:

Fundamental (ref. 16):	260 cm^{-2} atm^{-1}
Overtone (refs. 17,18):	1.64 cm^{-2} atm^{-1}

The advantages and disadvantages of the two bands are discussed later.

It should be mentioned that the energies and wavelengths given are for the normal, most prevalent, isotope of CO, i.e., $C^{12}O^{16}$. Other isotopes have similar levels and lines with the lines shifted slightly but significantly. For example, the center of the fundamental and first overtone bands of several isotopes of CO are given in Table 2.4, together with the relative abundances (ref. 19). They play essentially no role in this work.

2.4.2 Intensity of Reflected Solar Radiation and Earthshine.-

2.4.2.1 Solar reflection: The solar radiation reaching the earth and being reflected can be calculated for any wavelength as follows. From blackbody radiation tables (ref. 20) the radiant intensity, J, for a 5900 K blackbody is calculated to be 9.3×10^1 watt cm^{-2} sr^{-1} μm^{-1} at 2.3 μm and 8.0×10^0 at 4.6 μm. The average irradiance, H, incident on the earth's atmosphere (and incident on the earth's surface in the absence of any atmospheric attenuation) is 6.8×10^{-3} watts cm^{-2} μm^{-1} at 2.3 μm and 5.5×10^{-4} watts cm^{-2} μm^{-1} at 4.6 μm (ref. 21).

The reflected solar radiation, N, from the earth's surface is

TABLE 2.1 ENERGY AND WAVELENGTH OF VIBRATION-ROTATION LINES OF CO (1-0)

R BRANCH 1 - 0			P BRANCH 1 - 0		
J' - J''	CM^{-1}	λ(μm)	J' - J''	CM^{-1}	λ(μm)
1- 0	2147.083	4.65748	0- 1	2139.428	4.67415
2- 1	2150.858	4.64931	1- 2	2135.548	4.68264
3- 2	2154.598	4.64124	2- 3	2131.634	4.69124
4- 3	2158.301	4.63327	3- 4	2127.684	4.69994
5- 4	2161.970	4.62541	4- 5	2123.701	4.70876
6- 5	2165.602	4.61765	5- 6	2119.683	4.71769
7- 6	2169.198	4.61000	6- 7	2115.631	4.72672
8- 7	2172.759	4.60244	7- 8	2111.545	4.73587
9- 8	2176.282	4.59499	8- 9	2107.426	4.74513
10- 9	2179.770	4.58764	9-10	2103.273	4.75449
11-10	2183.220	4.58039	10-11	2099.086	4.76398
12-11	2186.634	4.57324	11-12	2094.867	4.77357
13-12	2190.011	4.56619	12-13	2090.614	4.78328
14-13	2193.351	4.55923	13-14	2086.328	4.79311
15-14	2196.653	4.55238	14-15	2082.010	4.80305
16-15	2199.918	4.54562	15-16	2077.659	4.81311
17-16	2203.145	4.53897	16-17	2073.275	4.82329
18-17	2206.334	4.53240	17-18	2068.860	4.83358
19-18	2209.486	4.52594	18-19	2064.412	4.84399
20-19	2212.599	4.51957	19-20	2059.932	4.85453
21-20	2215.674	4.51330	20-21	2055.421	4.86518
22-21	2218.713	4.50712	21-22	2050.878	4.87596
23-22	2221.708	4.50104	22-23	2046.303	4.88686
24-23	2224.667	4.49505	23-24	2041.697	4.89789
25-24	2227.587	4.48916	24-25	2037.060	4.90903
26-25	2230.469	4.48336	25-26	2032.393	4.92031
27-26	2233.310	4.47766	26-27	2027.694	4.93171
28-27	2236.113	4.47205	27-28	2022.965	4.94324
29-28	2238.875	4.46653	28-29	2018.205	4.95490
30-29	2241.598	4.46110	29-30	2013.415	4.96669
31-30	2244.281	4.45577	30-31	2008.595	4.97860
32-31	2246.924	4.45053	31-32	2003.745	4.99065
33-32	2249.527	4.44538	32-33	1998.865	5.00284
34-33	2252.089	4.44032	33-34	1993.956	5.01516
35-34	2254.611	4.43536	34-35	1989.017	5.02761
36-35	2257.092	4.43048	35-36	1984.049	5.04020
37-36	2259.532	4.42573	36-37	1979.051	5.05293
38-37	2261.931	4.42108	37-38	1974.025	5.06579
39-38	2264.289	4.41643	38-39	1968.970	5.07880
40-39	2266.605	4.41188	39-40	1963.886	5.09194

TABLE 2.2 ENERGY AND WAVELENGTH OF VIBRATION-ROTATION LINES OF CO (2-0)

R BRANCH 2 - 0			P BRANCH 2 - 0		
J' - J''	CM^{-1}	λ(μm)	J' - J''	CM^{-1}	λ(μm)
1- 0	4263.831	2.34531	0- 1	4256.211	2.34951
2- 1	4267.536	2.34327	1- 2	4252.296	2.35167
3- 2	4271.170	2.34128	2- 3	4248.311	2.35388
4- 3	4274.734	2.33933	3- 4	4244.257	2.35612
5- 4	4278.227	2.33742	4- 5	4240.133	2.35842
6- 5	4281.649	2.33555	5- 6	4235.940	2.36075
7- 6	4285.000	2.33372	6- 7	4231.678	2.36313
8- 7	4288.280	2.33194	7- 8	4227.347	2.36555
9- 8	4291.488	2.33019	8- 9	4222.947	2.36801
10- 9	4294.625	2.32849	9-10	4218.479	2.37052
11-10	4297.690	2.32683	10-11	4213.942	2.37307
12-11	4300.684	2.32521	11-12	4209.337	2.37567
13-12	4303.605	2.32363	12-13	4204.664	2.37831
14-13	4306.454	2.32210	13-14	4199.923	2.38100
15-14	4309.231	2.32060	14-15	4195.114	2.38373
16-15	4311.935	2.31914	15-16	4190.237	2.38650
17-16	4314.567	2.31773	16-17	4185.293	2.38932
18-17	4317.125	2.31636	17-18	4180.282	2.39218
19-18	4319.611	2.31502	18-19	4175.203	2.39509
20-19	4322.024	2.31373	19-20	4170.058	2.39805
21-20	4324.363	2.31248	20-21	4164.845	2.40105
22-21	4326.628	2.31127	21-22	4159.567	2.40410
23-22	4328.821	2.31010	22-23	4154.221	2.40719
24-23	4330.939	2.30897	23-24	4148.810	2.41033
25-24	4332.983	2.30788	24-25	4143.332	2.41352
26-25	4334.953	2.30683	25-26	4137.788	2.41675
27-26	4336.849	2.30582	26-27	4132.179	2.42003
28-27	4338.670	2.30485	27-28	4126.504	2.42336
29-28	4340.417	2.30393	28-29	4120.763	2.42674
30-29	4342.089	2.30304	29-30	4114.957	2.43016
31-30	4343.686	2.30219	30-31	4109.086	2.43363
32-31	4345.208	2.30139	31-32	4103.150	2.43715
33-32	4346.654	2.30062	32-33	4097.149	2.44072
34-33	4348.026	2.29989	33-34	4091.083	2.44434
35-34	4349.321	2.29921	34-35	4084.953	2.44801
36-35	4350.541	2.29856	35-36	4078.759	2.45173
37-36	4351.685	2.29796	36-37	4072.501	2.45549
38-37	4352.753	2.29740	37-38	4066.178	2.45931
39-38	4353.745	2.29687	38-39	4059.792	2.46318
40-39	4354.660	2.29639	39-40	4053.342	2.46710

TABLE 2.3 CO LINE STRENGTHS (cm^{-2} atm^{-1})

	FUNDAMENTAL (ref. 19)		OVERTONE (ref. 22)	
	R	P	R	P
0	1.970		.0163	
1	3.878	1.927	.0321	.0158
2	5.643	3.707	.0467	.0303
3	7.100	5.251	.0592	.0428
4	8.261	6.491	.0691	.0527
5	9.059	7.386	.0760	.0598
6	9.482	7.920	.0797	.0638
7	9.544	8.105	.0805	.0651
8	9.286	7.980	.0785	.0638
9	8.760	7.591	.0742	.0604
10	8.032	7.002	.0682	.0555
11	7.170	6.278	.0610	.0495
12	6.240	5.480	.0532	.0430
13	5.301	4.665	.0453	.0365
14	4.400	3.876	.0376	.0301
15	3.568	3.145	.0306	.0243
16	2.830	2.494	.0243	.0192
17	2.196	1.934	.0189	.0148
18	1.668	1.486	.0144	.0112
19	1.241	1.091	.0107	.00828
20	0.904	0.793	.00779	.00597
21	0.645	0.566	.00557	.00423
22	0.451	0.395	.00390	.00294
23	0.309	0.290	.00268	.00200
24	0.208	0.181	.00180	.00133
25	0.137	0.119	.00119	.000872
26	0.0884	0.0766	.000765	.000556
27	0.0589	0.0483	.000486	.000350
28	0.0349	0.0300	.000302	.000215
29	0.0212	0.0182	.000184	.000130
30	0.0127	0.0108	.000110	.0000770
31	0.00743	0.00634	.0000642	.0000446
32	0.00427	0.00364	.0000371	.0000254
33	0.00241	0.00205	.0000209	.0000142
34	0.00134	0.00113	.0000116	.0000078

TABLE 2.4 CO BAND CENTERS FOR ISOTOPES

Isotope	V_o (Fundamental)	V_o (1st Overtone)	Abundance
$C^{12}O^{16}$	2143.273	4260.056	.98654
$C^{12}O^{17}$	2116.111	4206.675	.00037
$C^{12}O^{18}$	2092.124	4161.021	.00202
$C^{13}O^{16}$	2116.075	4206.825	.01106
$C^{13}O^{17}$	2068.460	4112.264	.0000041
$C^{13}O^{18}$	2043.701	4062.639	.0000226

$$N(\text{watts cm}^{-1}\ \text{sr}^{-1}\ \mu\text{m}^{-1}) = \frac{\rho H}{\pi}$$

The values of N are thus 2.16×10^{-3} ρ watt cm^{-2} sr^{-1} μm^{-1} at 2.3 μm and 1.68×10^{-4} ρ watt cm^{-2} sr^{-1} μm^{-1} at 4.6 μm. The intensities (in watt cm^{-1} sr^{-1} μm^{-1}) are shown in Figure 2.6 for various reflectivities.

2.4.2.2 Earthshine: From blackbody radiation tables (ref. 20) the radiant intensity is given for a 300 K blackbody by the ratio

$$\frac{R_T}{R_{300}} = \frac{e^{1.439 \times 10^4\ \lambda \times 300}-1}{e^{1.439 \times 10^4\ \lambda\ T}-1}$$

the intensities (watts cm^{-2} sr^{-1} μm^{-1}) for 273.2 and 288 K blackbodies were calculated giving the following, as shown in Figure 2.6

T_g	2.3 μm	4.6 μm
273.2	2.0×10^{-8}	6.15×10^{-5}
288	7.54×10^{-8}	1.11×10^{-4}
300	1.60×10^{-7}	1.71×10^{-4}

2.4.2.3 Ratio of reflected solar radiation and earthshine intensities: As seen in Figure 2.6 the radiation seen in this experiment in the overtone band region would consist almost exclusively of reflected sunlight while that radiation for the fundamental band region would be mainly earthshine with some effect of reflected sunlight and serious atmospheric emission effects. These factors will be discussed later.

From the above numbers the ratios of reflected sunlight to earthshine at 2.3 μm are found to be

ρ	T_g: 273.2 K	288 K	300K
0.02	2×10^3	5.4×10^2	2.5×10^2
0.1	1×10^4	2.7×10^3	1.2×10^3
1.0	1×10^5	2.7×10^4	1.2×10^4

and the ratios of earthshine to reflected sunlight at 46 μm are:

ρ	T_g: 272.2K	288 K	300 K
0.02	1.78×10^1	3.20×10^1	4.95×10^1
0.1	3.56×10^0	6.40×10^0	9.90×10^0
1.0	3.56×10^{-1}	6.40×10^{-1}	9.90×10^{-1}

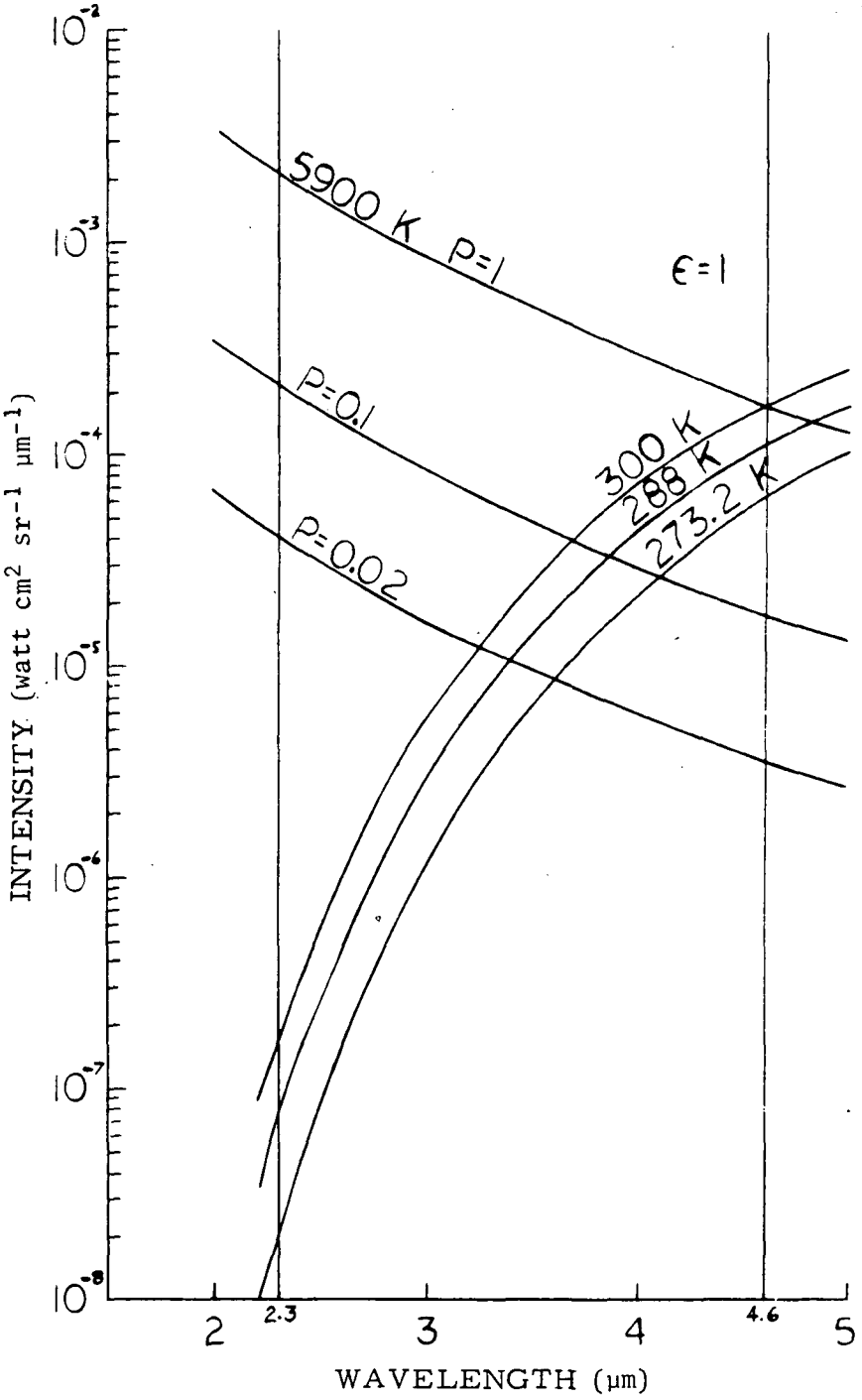

Figure 2.6 Reflected Solar Radiation and Earthshine

2.5 Radiative Theory

To study the feasibility of the CO density measurements and the effect of various atmospheric parameters on such measurements, calculations have been made using the radiative transfer theory described in this section. The model used includes absorption and emission of photons along a ray from the source to the detector. The two geometries considered are direct solar observation - limb experiment, and absorption of the earth's albedo - mapping experiment. Provisions are made for adding earthshine to reflection of sunlight from the earth's surface. However, phenomena such as scattering resonance fluorescence and radiation trapping have been neglected. Boltzmann populations, as described by the local atmospheric temperature, have been assumed for the upper and lower states of all transitions and the line profiles are given by the Voigt function at all altitudes. Doppler shifts as caused by atmospheric winds and by relative motion between the atmosphere and the satellite have been neglected.

The monochromatic radiative transfer equation (ref. 23) is given by:

$$\frac{dI_\nu}{dS} = \varepsilon_\nu - I_\nu \alpha_\nu \tag{2.1}$$

Where:

I_ν = spectral intensity (watts/cm^2-sr-cm^{-1})

S = distance along ray (cm)

ε_ν = spectral emission coefficient (watts/cm^3-sr-cm^{-1}), as a function of S

α_ν = spectral absorption coefficient (cm^{-1}), as a function of S

Formally,

$$I_\nu = C \exp(-\int \alpha_\nu dS') + \exp(-\int \alpha_\nu dS') \int \varepsilon_\nu \exp(\int \alpha_\nu dS'') \, dS' \tag{2.2}$$

For the limb boundary condition:

$$I_\nu(z) = I_{o,\nu} \exp(-\int_o^z \alpha_\nu dS'') + \exp(-\int_o^z \alpha_\nu dS'') \int_o^z \varepsilon_\nu \exp(\int_o^{S'} \alpha_\nu dS'') \, dS' \tag{2.3}$$

or

$$I_\nu(z) = I_{o,\nu} \exp(-\int_o^z \alpha_\nu dS'') + \int_o^z \varepsilon_\nu \exp(-\int_{S'}^z \alpha_\nu dS'') \, dS' \tag{2.4}$$

The geometry for this situation is shown in Figure 2.7.

For the mapping experiment, two conditions are required. The solar energy is attenuated as it penetrates to the earth's surface. At this point, it is reflected and the total intensity increased by earthshine. The resulting flux

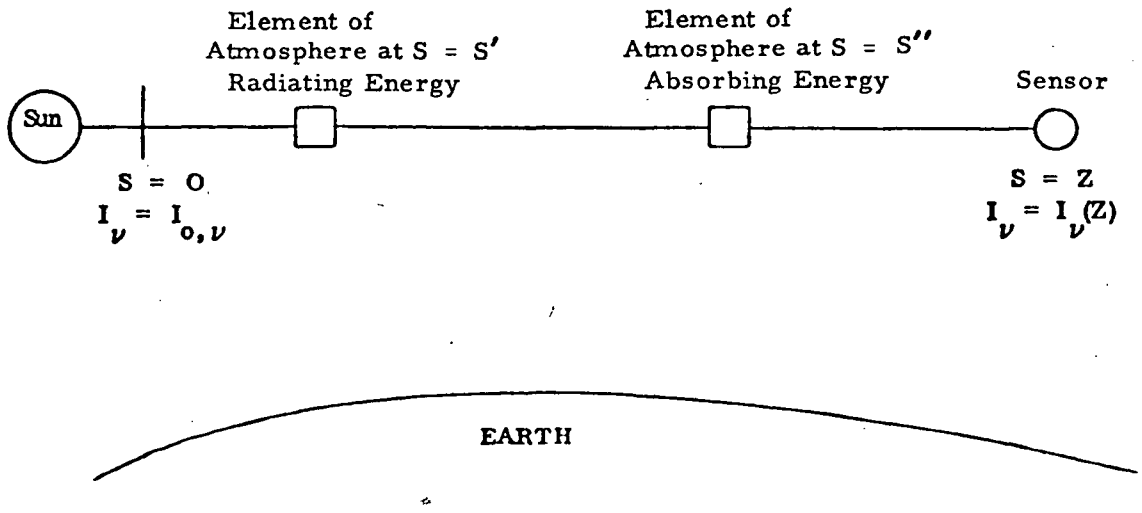

Figure 2.7 Geometry for Limb Conditions

is then further attenuated by the atmosphere until the satellite is reached. It is pointed out that atmospheric emission which is reflected by the earth into the field-of-view of the detector is negligible and therefore not included in the model. The geometry of the mapping experiment is given in Figure 2.8 and is described mathematically by Equation 2.5.

$$I_x = \rho_\nu \left[I_{o,\nu} \exp\left(-\int_o^{z_1} \alpha ds''\right) + \int^{z_1} \varepsilon_\nu \exp\left(\int_s^{z_1} \alpha_\nu ds''\right) ds' \right] \qquad (2.5)$$

$$+ I_e \exp\left(-\int_o^{z} \alpha_\nu dx''\right) + \int_o^{z} \varepsilon_\nu \exp\left(-\int_x^{z} \alpha_\nu dx''\right) dx'$$

Where

I_e = earthshine (watts/cm^2-sr-cm^{-1})

ρ_ν = earth reflection coefficient

Equations 2.4 and 2.5 have been numerically integrated along the rays indicated in Figures 2.7 and 2.8 using Simpson's rule. The properties ε_ν and α_ν are functions of altitude which must be evaluated prior to integration. This is considered below.

On a microscopic basis, for a single rotational line (ref. 24),

$$\varepsilon_\nu = \varepsilon\phi_\nu = \frac{n_u h c\nu}{4\pi} A_{u\ell} \phi_\nu \qquad (2.6)$$

$$\alpha_\nu = (\alpha_A - \alpha_S)\ \phi_\nu = (n_\ell\ B_{\ell u} - n_u\ B_{u\ell}) \frac{hc\nu}{4\pi}\ \phi_\nu \qquad (2.7)$$

Where

ϕ_ν = Voigt profile (1/cm^{-1})

n_u, n_ℓ = upper and lower state number densities (particles/cm^3)

$hc\nu$ = energy per transition (watt sec/transtion)

α_A = absorption coefficient (cm^{-1}/cm)

α_S = stimulation emission coefficient (cm^{-1}/cm)

$A_{u\ell}$ = Einstein coefficient for spontaneous emission

$$\left(\frac{\text{Transitions}}{\text{Sec. Particle}} \right)$$

$B_{\ell u}$ = Einstein coefficient for absorption

$$\left(\frac{\text{Transitions}}{\text{Particle}} \cdot \frac{\text{Cm-Ster}}{\text{Watt Sec.}} \right)$$

$B_{u\ell}$ = Einstein coefficient for stimulated emission

$$\left(\frac{\text{Transitions}}{\text{Particle}} \cdot \frac{\text{Cm-Ster}}{\text{Watt Sec.}} \right)$$

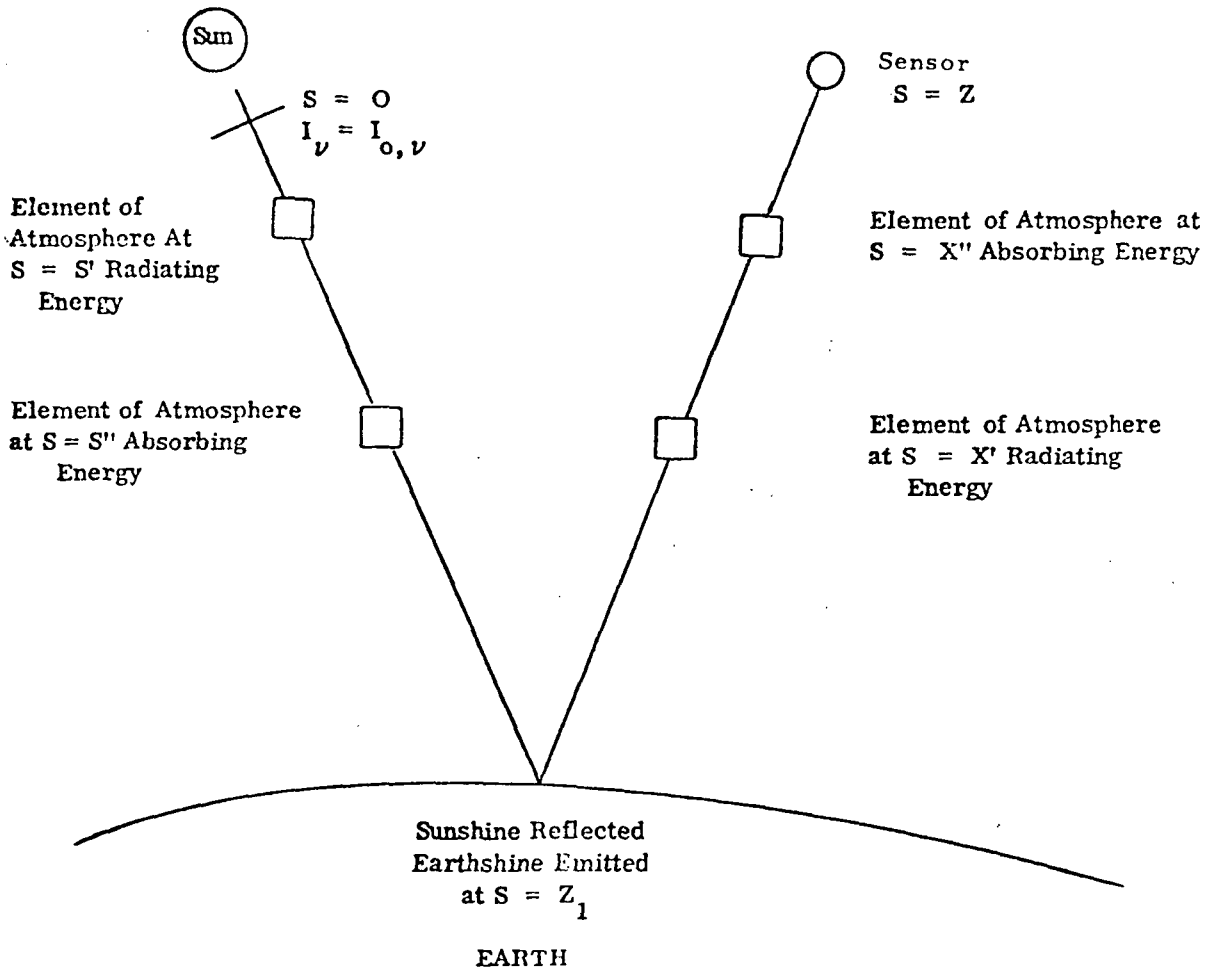

Figure 2.8 Geometry for Mapping Conditions

It is noted that the definition of the Einstein coefficients is arbitrary but that they are related by Kirchoff's Law for equilibrium at temperature, T.

$$\varepsilon_\nu = B_\nu(T)\ \alpha_\nu \tag{2.8}$$

$$B_\nu(T) = \frac{2\ hc^2\ \nu^3}{e^{hc\nu/kT}-1}\ (\text{watts/cm}^2\text{-sr-cm}^{-1})$$

Thus,

$$n_u\ A_{u\ell} = (n_\ell\ B_{\ell u} - n_u\ B_{u\ell})\ B_\nu(T) \tag{2.9}$$

or

$$\frac{A_{u\ell}/B_{u\ell}}{(n_\ell\ B_{\ell u}/n_u\ B_{u\ell})} = \frac{2\ hc^2\ \nu^3}{\exp(hc\nu/kT)-1} \tag{2.10}$$

But, at equilibrium the Boltzmann distribution is:

$$\frac{n_\ell}{n_u} = \frac{g_\ell}{g_u}\exp(hc\nu/kT) \tag{2.11}$$

and by comparison

$$g_\ell\ B_{\ell u} = g_u\ B_{u\ell} \tag{2.12}$$

$$A_{u\ell} = B_{u\ell} \cdot 2hc^2\ \nu^3 \tag{2.13}$$

The Voigt profile, ϕ_ν, is defined in terms of the Doppler and Lorentz half widths, i.e., half the line width at half the peak intensity (ref. 25).

$$\phi_\nu = \frac{1}{\alpha_D}\left(\frac{\ln 2}{\pi}\right)^{1/2} K(x,y) \tag{2.14}$$

$$K(x,y) = \frac{y}{\pi}\int_{-\infty}^{\infty}\frac{\exp(-t^2)}{y^2 + (x - t)^2} \tag{2.15}$$

$$y = \frac{\alpha_L}{\alpha_D}(\ln 2)^{1/2} \tag{2.16}$$

$$x = \frac{(\nu - \nu_o)}{\alpha_D}(\ln 2)^{1/2} \tag{2.17}$$

$$\alpha_D = \text{Doppler half width } (cm^{-1}) \tag{2.18}$$

$$= \frac{\nu_o}{c}\left(\frac{2R(\ln 2)\ T}{M}\right)^{1/2} = 3.58 \times 10^{-7}\ \nu_o \left(\frac{T}{M}\right)$$

$$\alpha_L = \text{Lorentz half width } (cm^{-1}) \tag{2.19}$$

$$= \Gamma/2\pi c$$

$$= \frac{1.4\ p\ \sigma_{12}^2\ N_O \left(\frac{8\pi}{\bar{M}\ R\ T}\right)^{1/2}}{2\pi^2\ c}$$

Where

Γ = gas collision frequency (sec^{-1})

p = pressure ($dynes/cm^2$)

σ_{12}^2 = optical collision cross-section (cm^2)

$\bar{M}$ = reduced mass of the colliding species (gm/gm mol)

R = gas constant (erg/gm mol K)

T = temperature (K)

N_O = Avagadro's number (particles/gm mol)

c = velocity of light (cm/sec)

The Doppler and Lorentz widths are functions of temperature and pressure and thus are easily obtained at any point along the ray from the atmospheric properties. The integral, K(x,y), is then calculated using a subroutine developed by Armstrong (ref. 25). It should be noted that

$$\int_{-\infty}^{\infty} K(x,y)\ dx \cong \pi^{1/2}$$

The emission coefficient number density product necessary for Equations 2.6 and 2.7 is most easily obtained by scaling experimentally derived line strengths which are defined as (ref. 26).

$$S_{\ell u} = \frac{1}{8\pi c\nu^2}\frac{\bar{N}_\ell}{\bar{P}} A_{u\ell}\frac{g_u}{g_\ell}\left[1 - \exp\ -\left(\frac{hc\nu}{k\bar{T}}\right)\right] \tag{2.20}$$

Where

$S_{\ell u}$ = line strength (cm^{-2}-atm^{-1})

ν = wavenumber (cm^{-1})

$\bar{P}$ = pressure (atm)

$\bar{N}_\ell$ = lower state population for conditions where $S_{\ell u}$ is measured (particles/cm^3)

g_u, g_ℓ = statistical weights (2J + 1)

$A_{u\ell}$ = Einstein coefficient $\left(\frac{\text{Transitions}}{\text{Sec. Particle}}\right)$

Using equation 2.11 and rearranging

$$n_u A_{u\ell} = \frac{8\pi c\nu^2 \bar{P}}{[\exp(hc\nu/k\bar{T}) - 1]} S_{\ell u} \tag{2.21}$$

Where

n_u = upper state population for conditions where $S_{\ell u}$ is measured (particle/cm^3).

But

$$\frac{n_u}{\bar{n}_u} = \frac{n_t}{\bar{n}_t} \cdot \frac{Q}{\bar{Q}} \cdot \frac{\exp(-hc\nu/kT)}{\exp(-hc\nu/k\bar{T})} \tag{2.22}$$

Where

n_t = total number density

Q = partition function

E = upper state energy

Thus, combining Equations 2.19 and 2.20

$$n_u A_{u\ell} = 8\pi c\nu^2 \bar{P} S_{\ell u} \frac{\exp\left(-\frac{hc\nu}{k}\left[\frac{1}{T} - \frac{1}{\bar{T}}\right]\right)}{\exp\left[-\left(\frac{hc\nu}{k\bar{T}}\right) - 1\right]} \frac{\bar{Q}}{Q} \frac{n_t}{\bar{n}_t} \tag{2.23}$$

If several lines contribute to the absorption at a specific wavenumber the total absorption coefficient is obtained by summation. The computational algorithm then uses $S_{\ell u}$ as a basis. $n_u A_{u\ell}$ from Equation 2.21 gives $(n_\ell B_{\ell u} - n_u B_{u\ell})$ from Equation 2.9. This, in conjunction with ϕ_ν, leads to α_ν via Equation 2.7. Equation 2.5 can then be integrated over altitude.

2.6 Feasibility Analysis

2.6.1 Programs.- Calculations have been made with several programs. Initial calculations were made with a single-line model. For each of several lines of the overtone and fundamental bands, calculations were made of absorption across the line, the line shape as a function of altitude, net absorption as a function of altitude for various CO density profiles (including sinks and various temperature and emissivity, and of other factors which influence the net intensity). With a second program, calculations were made, for the limb mode, of the effect of instrument error on the inversion of measured total CO densities in the path to obtain a CO profile. With a multi-line program which computes the spectrum incident on the instrument, generates the corresponding interferogram, and, with another program, inverts this to CO densities in the path, calculations were made to determine the sensitivity of the technique and the effects of various atmospheric parameters.

Parameters which can be varied by means of input data include temperature and species concentration profiles of the atmosphere, ground temperature and emissivity, reflectivity, viewing angles, incident radiation angle, and grazing height.

The net change in intensity for the R7 line of the fundamental is given in Figure 2.9. This shows by the solid curve the results obtained by the single-line model and by the x's the results obtained by the multi-line model. These agree within 1% and it can be concluded that the comparison of the fundamental and overtone bands can be carried out using the single-line model.

For all calculations discussed in the following pages, the following conditions were used, as standard and variations made therefrom:

CO Profile 1
Temperature Model 2
Ground Temperature = 0 km Atmospheric Temperature
Emissivity = 1.0
Reflectivity = 0.1
Bandpass = 20 cm^{-1}
Lorentz Half-Width (R7) = 0.06 cm^{-1}

Calculations have been made for the CO profile models 1 through 6 described in Section 2.2.1 (Figure 2.1). These models were used to evaluate the emission and absorption coefficients and compute the CO absorption spectrum which would be observed at an altitude of 80 km.

2.6.2 Single-Line Model.-

2.6.2.1 Line shapes: The absorption and emission coefficients are functions of pressure, temperature, and CO number density. This is illustrated by Figure 2.10 which shows the spectral absorption coefficient of the 4.6 μm P8 line as a function of altitude for the standard temperature and CO models. At low altitudes the lines are Lorentz broadened and then as altitude increases, Doppler broadening dominates. The variation in the magnitude of the absorption coefficient with altitude is controlled by the variation of the CO number den-

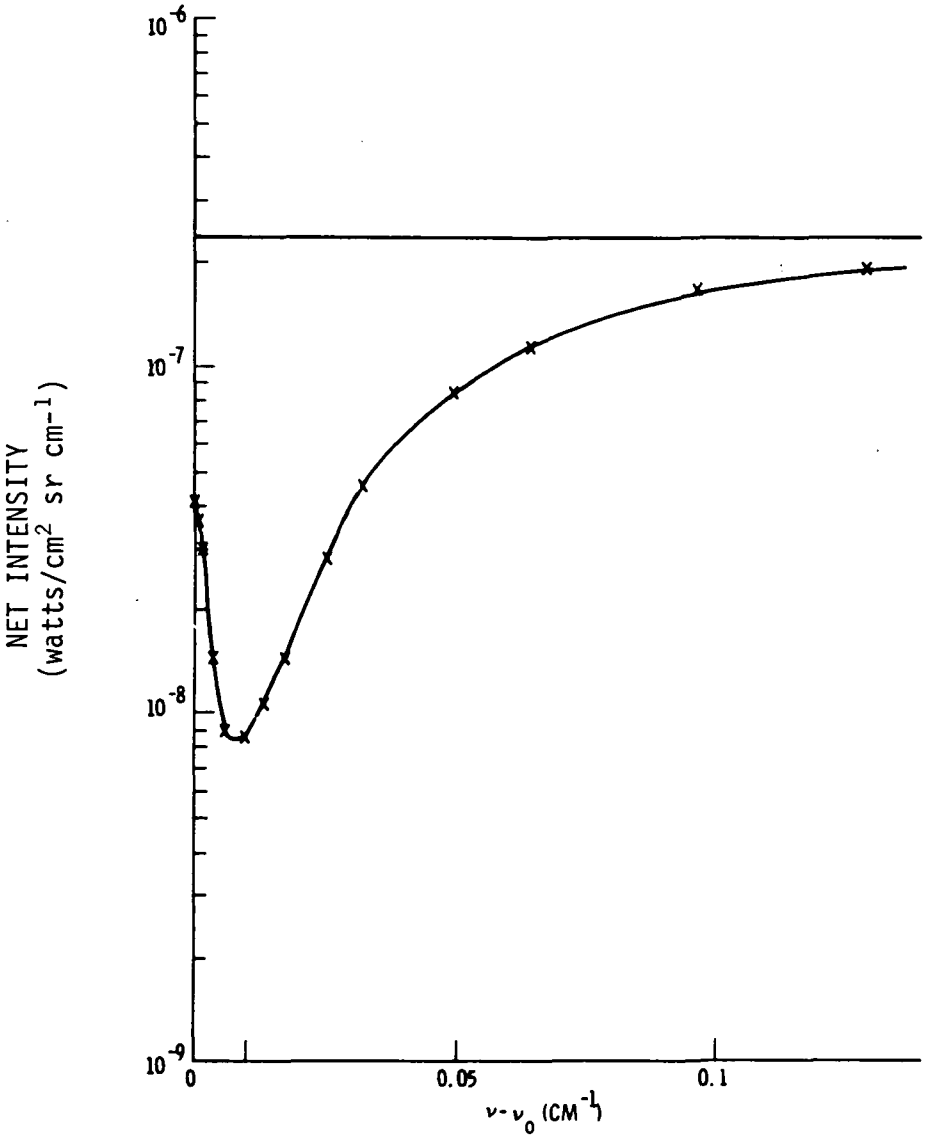

Figure 2.9 Comparison of Single and Overlapping Line Absorption Spectra Through Standard Atmosphere

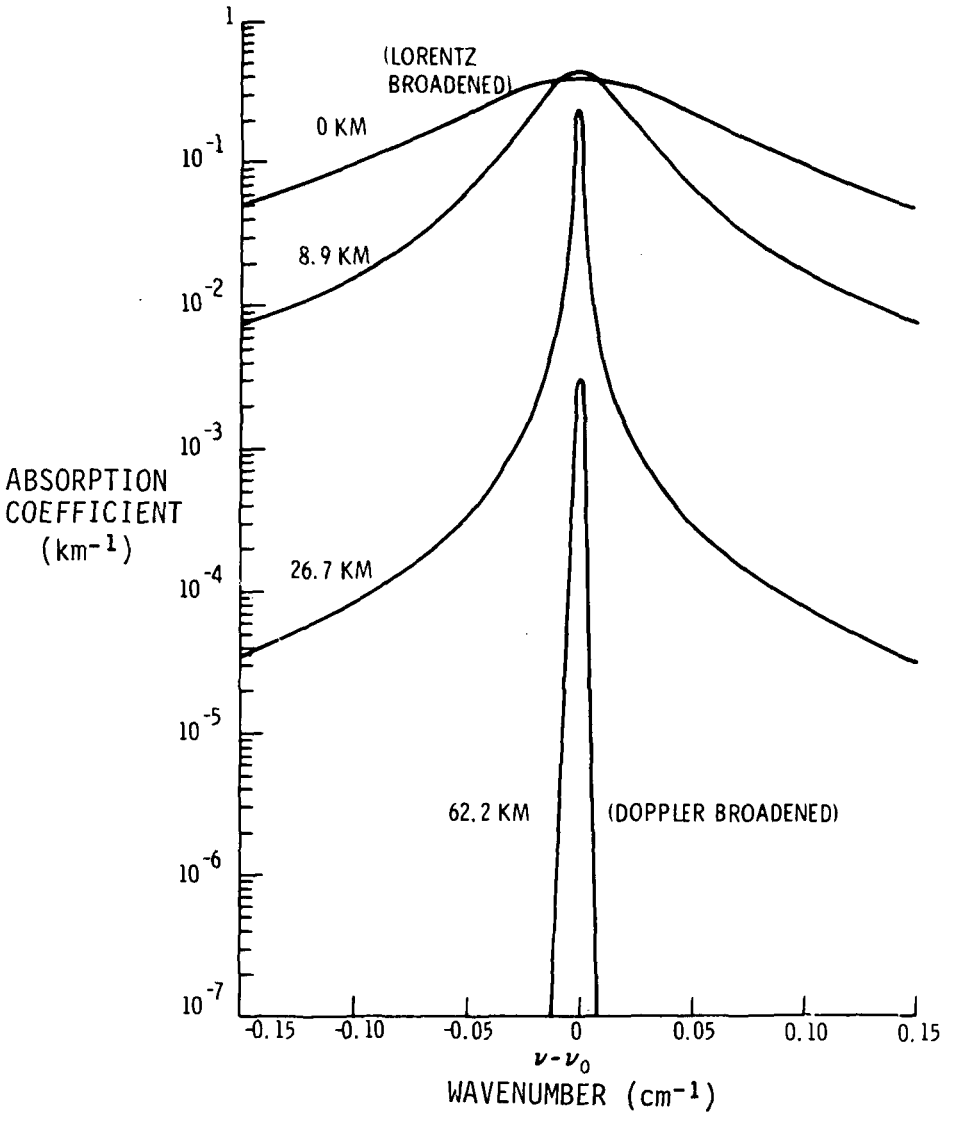

Figure 2.10 Absorption Line Profile (P8)

sity. When these absorption coefficients are integrated over the atmosphere, the line profile variation with altitude is manifested by an emission peak at the center of the absorption line. This behavior is illustrated in Figure 2.11. Physically, earthshine is absorbed up to an altitude of about 30 km. At this point, the atmospheric temperature rises and the light flux is increased by emission. However, because the line profiles are very sharp at this altitude, the emission is observed only near the line center.

A second example of the importance of atmospheric emission is illustrated in Figure 2.12. Here the net change in absorbed intensity with altitude as integrated over the P8 line of the fundamental is shown as a function of altitude for the four temperature models and the standard CO model. Two temperature profiles have inversion layers which cause a net increase in the light flux (negative absorption). When the temperature drops there is less photon emission and the net absorption increases. For the case of the P8 line of the overtone this behavior is not observed, as shown in Figure 2.13. The reason for this is source temperature. In the case of the overtone, reflected sunshine dominates the intensity at the earth's surface, whereas at 4.6 μm earthshine is the dominant contributor to the ground intensity. The atmospheric temperature can be higher than the ground temperature and hence atmospheric emission becomes important.

2.6.2.2 CO profile effects: The effect of CO number density profile on the intensity has been examined using the standard temperature profile and the six CO models. The results for the change of intensity with altitude for the P8 line of the fundamental are shown as a function of altitude in Figure 2.14. In all cases, except the urban atmosphere, the change in intensity peaks between 6 to 10 km whereas it should peak at ground level except for the low-altitude sink models. This peak is caused by a balance between the changing CO concentration and the emission. In the case of the urban atmosphere, the CO concentration profile dominates. This balance should be emphasized in that the change in absorption at 4.6 μm is not directly proportional to the CO concentration. On the other hand, similar calculations for the P8 line at 2.3 μm are a direct measure of the CO number density. This is shown in Figure 2.15. The difference between the two wavelengths is again caused by the effective source temperature.

The data shows that absorption spectra as observed from 80 km depend on the atmospheric profiles of the absorbing species and on temperature. The temperature dependence on the spectra is controlled by the temperature of the absorbed source. For the case where earthshine is important the absorption profiles are strongly effected by the atmospheric temperature profile. Also in this case, the change in absorption with altitude is not a direct measure of the absorbing species. On the other hand, when the absorbed source is the sun, the absorbed signal is almost independent of the temperature profile and the change in absorption with respect to altitude is directly proportional to the concentration of the absorbing species.

The results are shown in Table 2.5 for the six models and in Table 2.6 for models in which concentrations of the CO were multiples (.1, .2, .4, .8, 1., 1.6, 3.2, and 6.4) of the standard atmosphere at all altitudes.

The effect of low altitude sinks on measured CO densities is seen in Tables 2.7 and 2.8 using temperature models 2 and 4, respectively. The numbers pre-

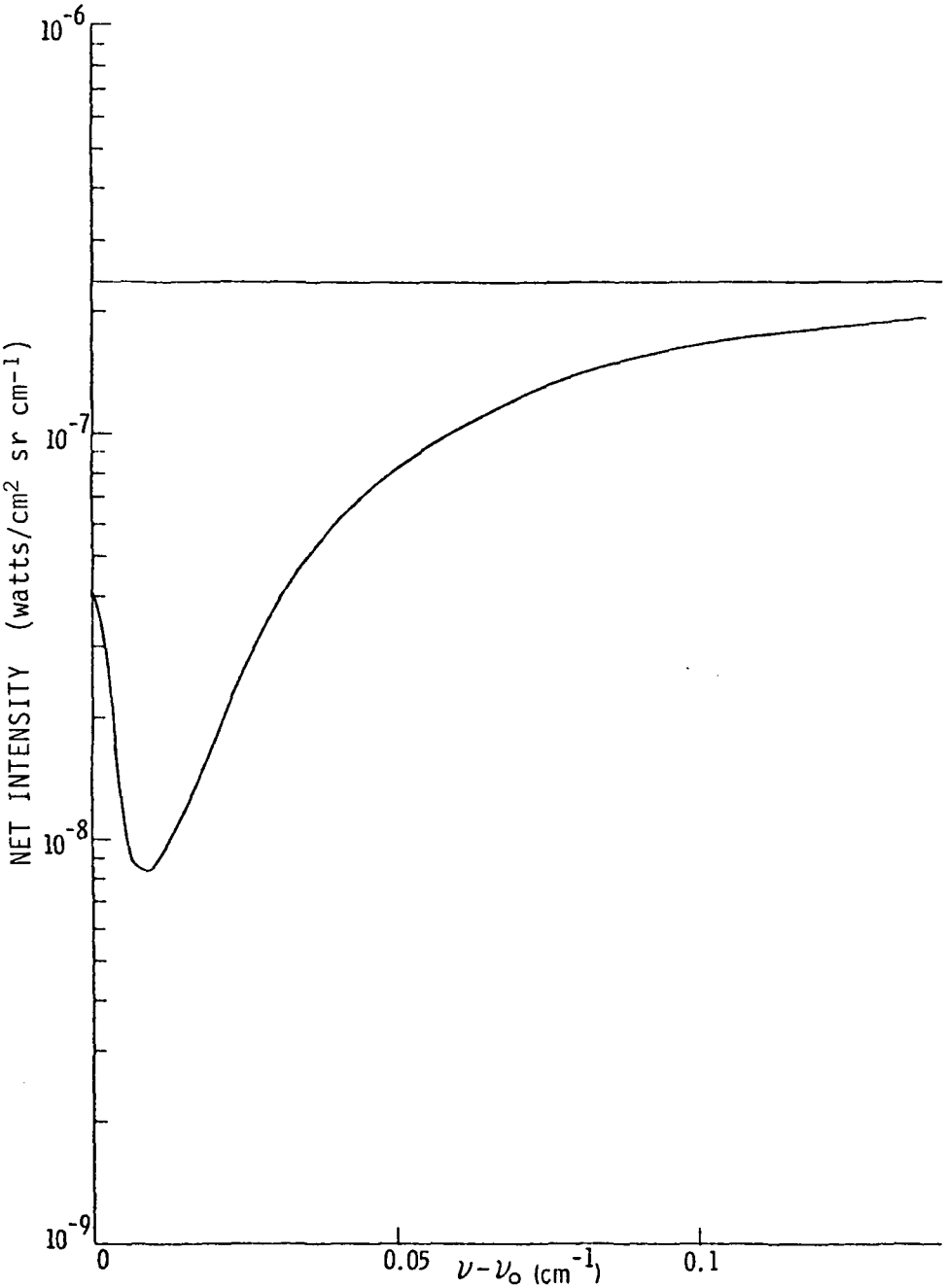

Figure 2.11 Line Profile Showing Emission Peak at Center

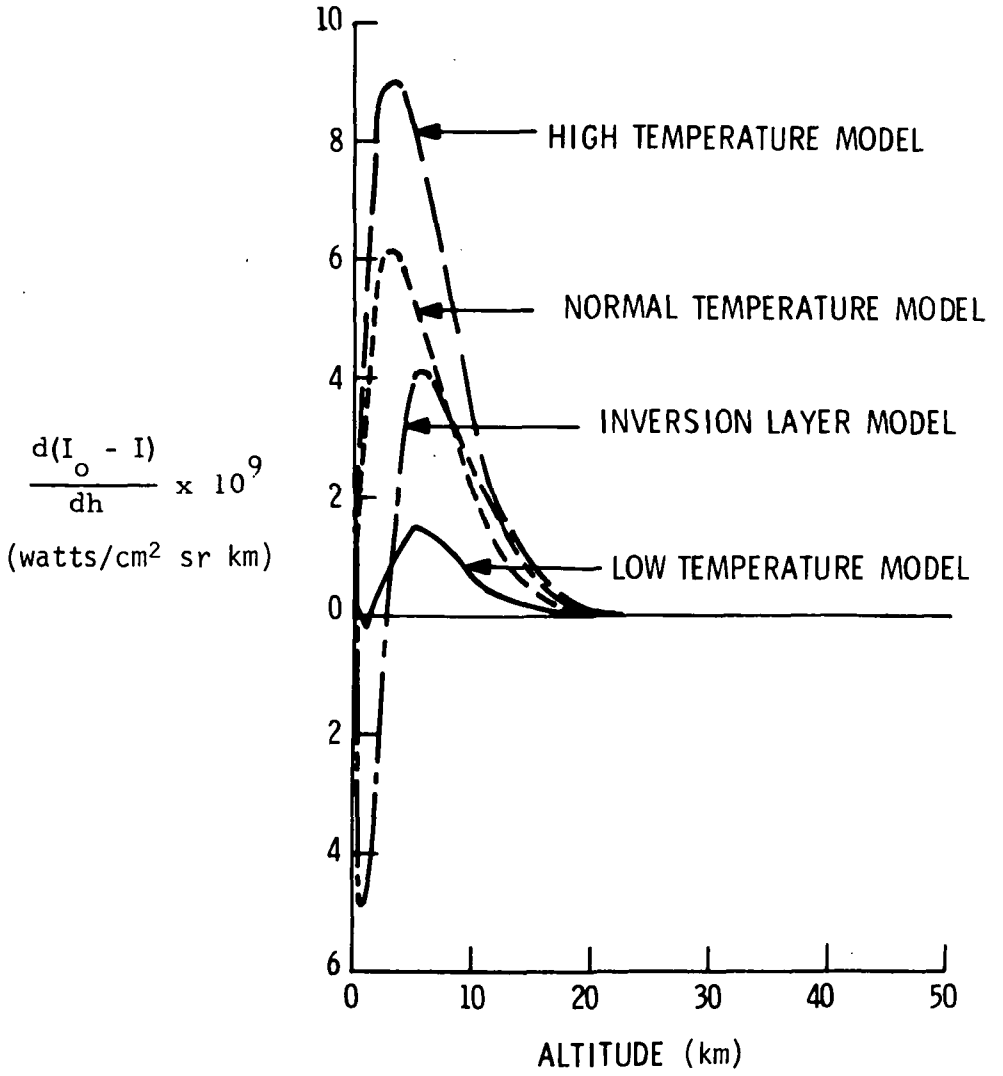

Figure 2.12 Variation of Rate Change in Absorbed Intensity Fundamental (4.6 μm) (R7 Line)

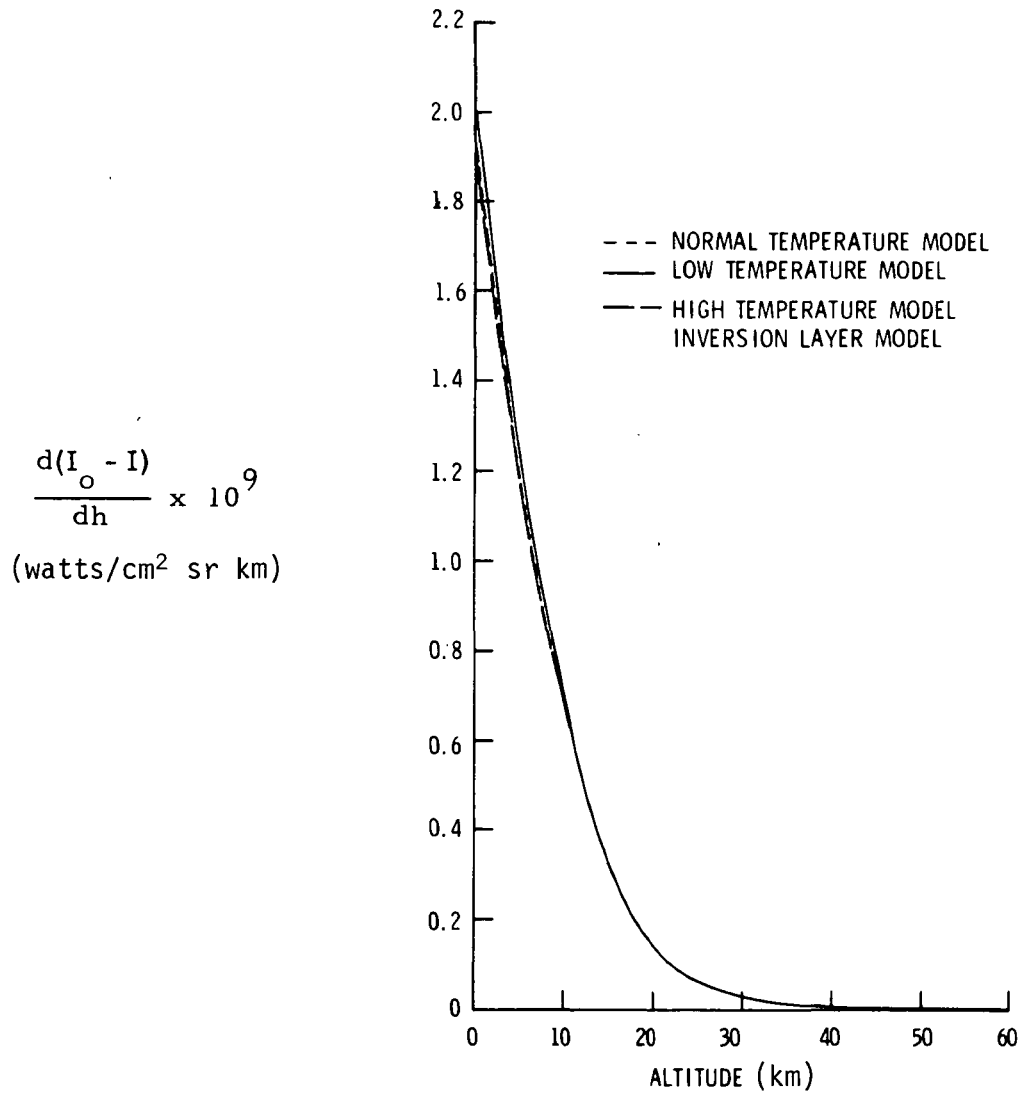

Figure 2.13 Variation of Rate of Change in Absorbed Intensity Overtone (2.3 μm)(R7 Line)

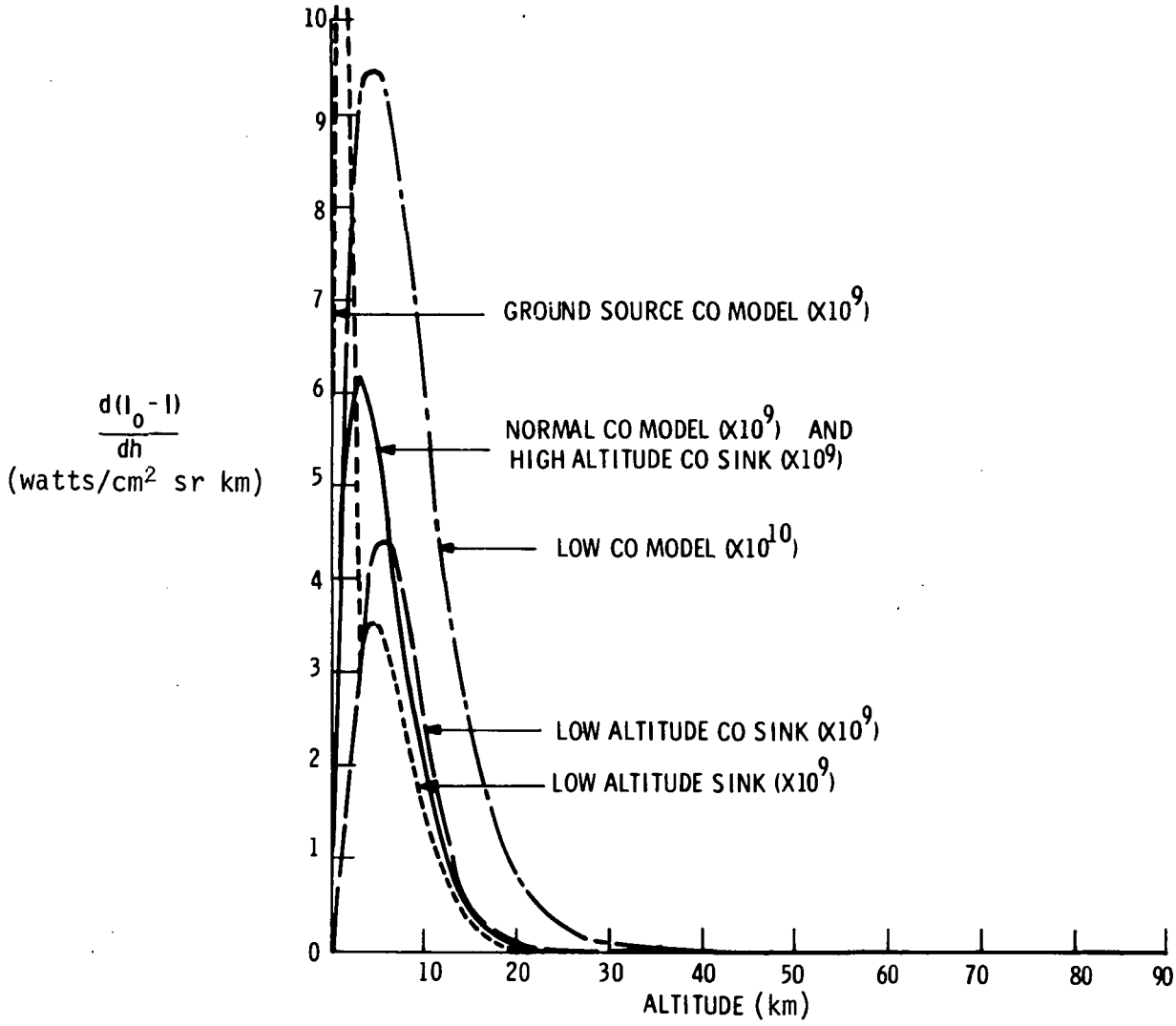

Figure 2.14 Variation of Rate Change in Absorbed Intensity Fundamental (4.6 μm)

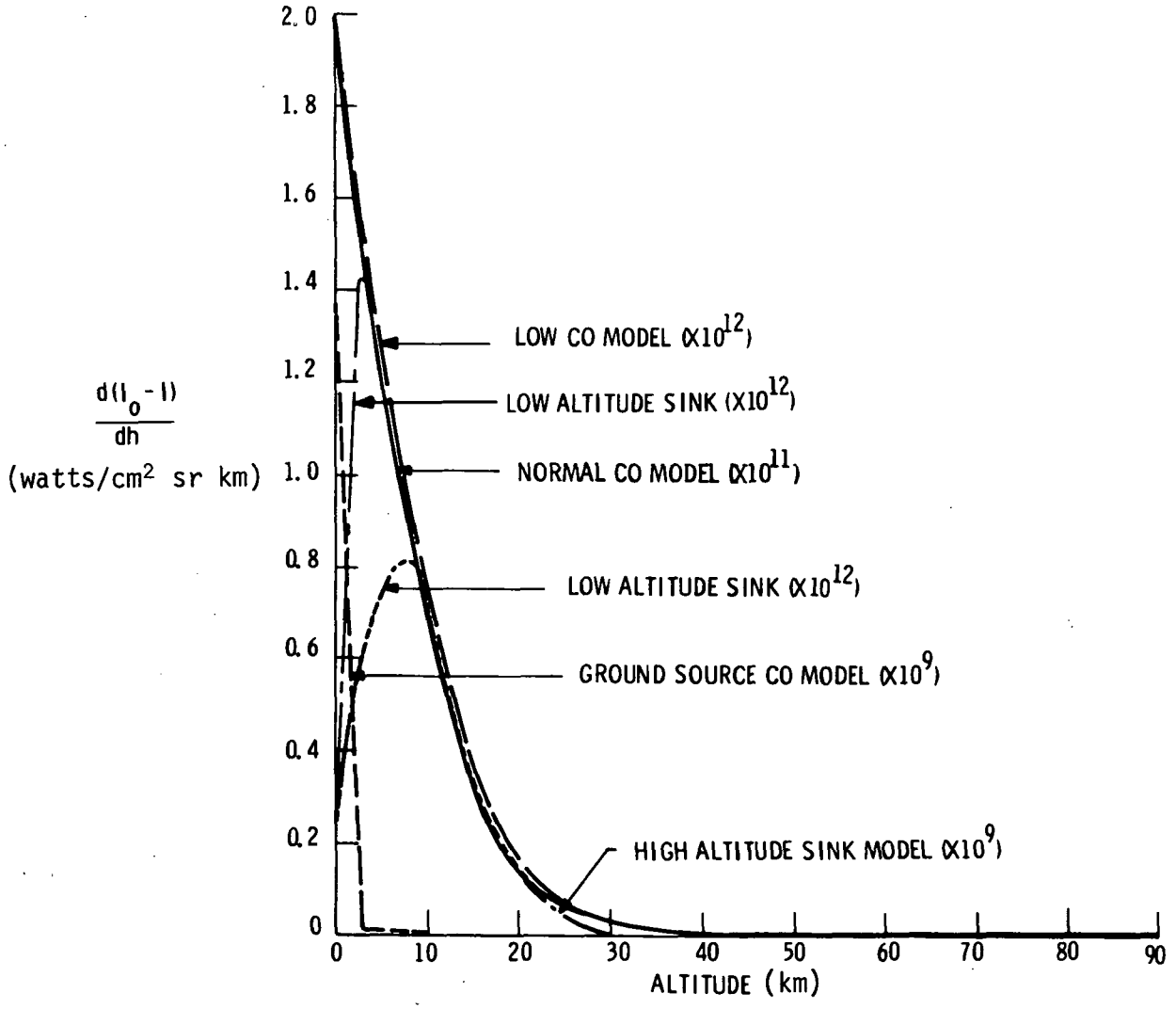

Figure 2.15 Variation of Rate of Change in Absorbed Intensity Overtone (2.3 μm)

TABLE 2.5 EFFECT OF CO PROFILES ON ABSORPTION

FUNDAMENTAL (4.6 μm)

CO MODEL	$n_{CO}(cm^{-2})$	R7	P1	P8	P26
STANDARD	2.15 (18)	.2002	.0810	.1700	.00104
LOW ALTITUDE SOURCE	5.21 (19)	.6620	.2974	.5695	.0167
LOW CO	2.15 (17)	.0439	.0119	.0350	.000107
HIGH ALTITUDE SINK	2.09 (18)	.2006	.0807	.1703	.00102
LOW ALTITUDE SINK (9 km)	1.37 (18)	.1580	.0642	.1335	.000614
LOW ALTITUDE SINK (3 km)	1.93 (18)	.1963	.0795	.1666	.000965

OVERTONE (2.3 μm)

CO MODEL	$n_{CO}(cm^{-2})$	R7	P1	P8	P26
STANDARD	2.15 (18)	.00647	.00144	.00462	.0000098
LOW ALTITUDE SOURCE	5.21 (19)	.1226	.0299	.0953	.000431
LOW CO	2.15 (17)	.000662	.000146	.000471	.0000011
HIGH ALTITUDE SINK	2.09 (18)	.00631	.00140	.00451	.0000097
LOW ALTITUDE SINK (9 km)	1.37 (18)	.00418	.00095	.00292	.0000037
LOW ALTITUDE SINK (3 km)	1.93 (18)	.00582	.00130	.00413	.0000068

TABLE 2.6 EFFECT OF CO COLUMN DENSITY ON FRACTIONAL NET ABSORPTION

FUNDAMENTAL (4.6 μm)

$n_{CO}(cm^{-2})$	R7	P1	P8	P26
2.15 (17)	.0439	.0119	.0350	.000107
4.3 (17)	.0741	.0223	.0604	.00020
8.6 (17)	.1174	.0405	.0978	.000410
1.72 (18)	.1769	.0692	.1496	.000820
2.15 (18)	.2002	.0810	.1710	.00104
3.44 (18)	.2585	.1108	.2205	.00163
6.88 (18)	.3714	.1683	.3183	.00322
1.37 (19)	.5292	.2470	.4545	.00629

OVERTONE (2.3 μm)

$n_{CO}(cm^{-2})$	R7	P1	P8	P26
2.15 (17)	.000662	.000146	.000471	.0000011
4.3 (17)	.00131	.000286	.000926	.0000015
8.6 (17)	.00260	.000569	.00185	.0000032
1.72 (18)	.00518	.00115	.00369	.0000071
2.15 (18)	.00647	.00144	.00462	.0000099
3.44 (18)	.0102	.00228	.00729	.000014
6.88 (18)	.0197	.00455	.0142	.000030
1.37 (19)	.0370	.00895	.0272	.000059

TABLE 2.7 EFFECT OF CO PROFILES ON DERIVED CO CONCENTRATIONS (% DEVIATION)

FUNDAMENTAL (4.6 μm)

CO MODEL	$n_{CO}(cm^{-2})$	R7	P1	P8	P26
HIGH ALTITUDE SINK	2.09 (18)	0.2	0.0	8.3	2.5
LOW ALTITUDE SINK (9 km)	1.37 (18)	14.6	10.5	18.0	4.9
LOW ALTITUDE SINK (3 km)	1.93 (18)	8.1	2.7	12.7	1.0

OVERTONE (2.3 μm)

CO MODEL	$n_{CO}(cm^{-2})$	R7	P1	P8
HIGH ALTITUDE SINK	2.09 (18)	3.5	4.5	3.5
LOW ALTITUDE SINK (9 km)	1.37 (18)	6.1	6.1	6.1
LOW ALTITUDE SINK (3 km)	1.93 (18)	2.7	2.7	2.7

TABLE 2.8 EFFECT OF PROFILES ON DERIVED CO CONCENTRATIONS - TEMPERATURE INVERSION (% DEVIATION)

FUNDAMENTAL (4.6 μm)

CO MODEL	$n_{CO}(cm^{-2})$	R7	P1	P8	P26
LOW ALTITUDE SINK (9 km)	1.37 (18)	13.3	10.4	17.0	0.04
LOW ALTITUDE SINK (3 km)	1.93 (18)	0.9	29.5	32.6	35.2

OVERTONE (2.3 μm)

CO MODEL	$n_{CO}(cm^{-2})$	R7	P1	P8
LOW ALTITUDE SINK (9 km)	1.37 (18)	7.4	7.4	7.4
LOW ALTITUDE SINK (3 km)	1.93 (18)	3.6	4.7	2.6

sented are those of the precent difference of the actual CO density in the model and that calculated using the computed net absorption for that model and converting that by means of the data of Table 2.6. It can be seen that at 4.6 μm the errors are larger than the differences in the amounts of CO in the standard and the sink models. To improve these results, an atmospheric CO profile would have to be known for measured CO densities; this cannot be assumed to be obtainable. The errors for the temperature model 2 are less drastic than those of model 4 which has an inversion layer. The latter errors are extremely large for the 4.6 μm band.

2.6.2.3 Temperature profile effects: Calculations have been made for temperature models 1, 2, 3, and 4 (Table 2.9, Figure 2.12) using the 0.1 ppm CO model. The calculations shown in Figures 2.12 and 2.13 were made for the R7, P1, P8, and P26 lines of the fundamental band and the R7, P1, P8 and P26 lines of the overtone band, using CO model 1. The results for this are shown in Table 2.9. The tabulated results show a great dependence on the atmospheric temperature model for the 4.6 μm band and little dependency on the 2.3 μm band. The graphical data of Figures 2.12 and 2.13 show the contribution of various altitudes to the net absorption. The 2.3 μm band shows absorption as a function of altitude to be as would be expected whereas the 4.6 μm band shows much less absorption below about 5 km (and, in fact, a significant net emission in some regions) which is an important region for CO sink studies.

2.6.2.4 Ground temperature effects: The calculations described above include a ground temperature of each model at 0 km. Calculations have also been made for a different ground temperature. The following cases were carried out.

T_{Ground}	Atmospheric Temperature Model	$T_{Model\ Atm.\ at\ 0\ km}$
288.2	2	288.2
288.2	1	257.3
288.2	3	302.6
288.2	4	283.2
273.2	2	288.2
284.2	2	288.2
287.2	2	288.2
289.2	2	288.2
291.2	2	288.2
308.2	2	288.2

The results of these calculations are shown in Table 2.10. Drastic effects are seen for the fundamental band (4.6 μm) and negligible effects are seen for 2.3 μm.

2.6.2.5 Emissivity effects: In calculations described above, an emissivity of 1 was used. Since certain ground areas have appreciably different emissivities, calculations have been made using emissivity values of 0.95, 0.9, 0.8, and 0.7 for the 4.6 μm band and a value of 0.7 for the 2.3 μm band, with each of the four temperature models. Drastic effects in the fractional net apparent absorption are seen by the data in Table 2.11 at 4.6 μm while those at 2.3 μm are negligible.

TABLE 2.9 EFFECT OF TEMPERATURE PROFILE ON ABSORPTION

4.6 μm	R7	P1	P8	P26
LOW TEMPERATURE	.1613	.0677	.1328	.000489
NORMAL TEMPERATURE	.2002	.0810	.1700	.00104
HIGH TEMPERATURE	.1942	.0772	.1662	.00134
INVERSION LAYER	.1270	.0521	.1063	.000433
2.3 μm				
LOW TEMPERATURE	.00660	.00152	.00462	.0000062
NORMAL TEMPERATURE	.00647	.00144	.00462	.0000098
HIGH TEMPERATURE	.00637	.00140	.00461	.000014
INVERSION LAYER	.00639	.00140	.00461	.000013

TABLE 2.10 EFFECT OF GROUND TEMPERATURE ON ABSORPTION

FUNDAMENTAL (4.6 μm)

		R7	P1	P8	P26
LOW TEMPERATURE	257.3	.1613	.0677	.1328	.000489
	288.2	.2500	.1030	.2117	.00104
HIGH TEMPERATURE	302.6	.1942	.0772	.1662	.00134
	288.2	.1342	.0550	.1128	.00415
INVERSION LAYER	283.2	.1270	.0521	.1063	.000433
	288.2	.1540	.0622	.1302	.000793

OVERTONE (2.3 μm)

		R7	P1	P8	P26
LOW TEMPERATURE	257.3	.00660	.00152	.00462	.0000061
	288.2	.00657	.00150	.00459	.0000053
HIGH TEMPERATURE	302.6	.00637	.00140	.00461	.0000137
	288.2	.00634	.00138	.00457	.0000122
INVERSION LAYER	283.2	.00639	.00140	.00461	.0000128
	288.2	.00635	.00139	.00458	.0000144

TABLE 2.11 EFFECTS OF EMISSIVITY ON FRACTIONAL NET ABSORPTION FOR R7 LINES

TEMPERATURE MODEL	ϵ	4.6 μm	2.3 μm
LOW TEMPERATURE	1	.161	.00660
	0.95	.155	
	0.9	.149	
	0.8	.133	
	0.7	.113	.00657
NORMAL TEMPERATURE	1	.200	.00647
	0.95	.196	
	0.9	.191	
	0.8	.180	
	0.7	.165	.00644
NORMAL TEMPERATURE T_g = 288.2	1	.200	
	0.9	.191	
	0.7	.165	
HIGH TEMPERATURE	1	.194	.00637
	0.95	.190	
	0.9	.184	
	0.8	.172	
	0.7	.156	.00634
INVERSION LAYER	1	.127	.00639
	0.95	.119	
	0.9	.110	
	0.8	.0886	
	0.7	.0710	.00635

It can be seen that atmosphere and ground temperatures and ground emissivities would have to be very accurately measured to be able to interpret any CO data obtained by remote measurements at 4.6 μm. It appears that the best expected temperature data will have an accuracy of ± 2 K (refs. 27, 28, 29). These data would not be expected to be this accurate if an inversion layer exists. Even ± 2 K would present substantial effects at 4.6 μm, since the emissivity may vary with wavelength.

2.6.2.6 Effects of other parameters: Calculations made to test the effect of reflectivity show this effect to be small for the 4.6 μm band and negligible for the 2.3 μ band. The effect is due to a change in source intensity with no accompanying change in atmospheric emission.

Calculations were made to show the effect of Lorentz half-width on absorption. Significant effects were found for some conditions for the 4.6 μm band while the effects on the 2.3 μm band were small. Results are shown in Tables 2.12 and 2.13. This shows that the value of σ_{12}^2 in Equation 2.21 must be known to accuracies of the order of 10% for the fundamental, while for the overtone an accuracy of 50% is sufficient.

Calculations to test the effect of bandpass (the distance from the center of the line over which the absorption is integrated) were made. As expected this has an appreciable effect if too small a bandpass is taken. Data for four lines of the 4.6 and 2.3 μm bands are given in Tables 2.14 and 2.15 for bandpasses ($\nu = \nu_o$) of 20, 2, and 0.1 cm^{-1}.

2.6.2.7 Comparison of overtone and fundamental bands: Using the data given in the preceding tables, a summary may be made of the two general wavelength regions, the 2.3 μm band of the first overtone of CO and the 4.6 μm band of the fundamental of CO.

The absorption of the 2.3 μm radiation has been found to be sufficient to produce the required sensitivities and ranges using the correlation interferometer technique for optical thicknesses appropriate to both the mapping and the limb experiments, considering nominal ambient atmospheric concentrations and reasonable fractions thereof.

The absorption of the 4.6 μm radiation is, of course, sufficient for the experiments. One difficulty arises at the higher optical thicknesses appropriate to the lower altitude limb measurements. Under such conditions the absorption is so strong that it is well off the linear portion of the curve-of-growth with ambient atmospheric CO concentrations resulting in a loss of sensitivity in the CO measurements.

The data show that there is considerably more error in measurement at 4.6 μm of the CO column density in the important case of a low altitude sink than for the same measurement at 2.3 μm. Since a major objective of the experiment is to search for a potential low altitude sink, this indicates a definite advantage for 2.3 μm. In the case of a temperature inversion drastic errors are found in the case of a low altitude sink. Since temperature inversions are common the 2.3 μm has another distinct advantage. In general it can be said that

TABLE 2.12 EFFECT OF LORENTZ HALF-WIDTH ON APPARENT ABSORPTION OF FUNDAMENTAL (4.6 μm)

		R7	P1	P8	P26
STANDARD CO	.06	.2002	.0810	.1700	.0010
	.09	.2387	.0905	.2012	.0010
LOW ALTITUDE SOURCE	.06	.6620	.2974	.5695	.0167
	.09	.8052	.3555	.6921	.0178
LOW CO	.06	.0439	.0119	.0350	.0001
	.09	.0470	.0121	.0370	.0001
HIGH ALTITUDE SINK	.06	.2006	.0807	.1703	.0010
	.09	.2390	.0898	.2014	.0010

TABLE 2.13 EFFECT OF LORENTZ HALF-WIDTH ON ABSORPTION OVERTONE (2.3 μm)

		R7	P1	P8	P26
STANDARD CO	.06	.00647	.00144	.00462	.0000098
	.09	.00647	.00142	.00461	.0000085
LOW ALTITUDE SOURCE	.06	.1226	.0299	.0953	.000431
	.09	.1312	.0303	.1005	.000420
LOW CO	.06	.000662	.000146	.000471	.0000011
	.09	.000649	.000140	.000457	.0000006
HIGH ALTITUDE SINK	.06	.00631	.00140	.00451	.0000097
	.09	.00631	.00139	.00450	.0000083

TABLE 2.14 EFFECT OF BANDPASS ON FRACTIONAL NET APPARENT ABSORPTION - FUNDAMENTAL (4.6 μm)

FUNDAMENTAL (4.6 μm)

		R7	P1	P8	P26
LOW TEMPERATURE	20	.1613	.0677	.1328	.00049
	2	.1593	.0670	.1314	.00047
	0.1	.1086	.0142	.0951	.00042
NORMAL TEMPERATURE	20	.2002	.0810	.1700	.00104
	2	.1979	.0804	.1682	.00102
	0.1	.1286	.0635	.1155	.00093
HIGH TEMPERATURE	20	.1942	.0772	.1662	.00134
	2	.1921	.0766	.1646	.00133
	0.1	.1264	.0610	.1138	.00120
INVERSION LAYER	20	.1270	.0521	.1063	.00043
	2	.1260	.0518	.1056	.00041
	0.1	.0977	.0450	.0852	.00040

TABLE 2.15 EFFECT OF BANDPASS ON FRACTIONAL NET APPARENT ABSORPTION - OVERTONE (2.3 μm)

OVERTONE (2.3 μm)

		R7	P1	P8	P26
LOW TEMPERATURE	20	.00660	.00152	.00462	.0000062
	2	.00656	.00150	.00459	.0000053
	0.1	.00544	.00125	.00383	.0000053
NORMAL TEMPERATURE	20	.00647	.00144	.00462	.0000098
	2	.00643	.00143	.00459	.0000089
	0.1	.00531	.00118	.00381	.0000087
HIGH TEMPERATURE	20	.00637	.00140	.00461	.000014
	2	.00633	.00138	.00457	.000012
	0.1	.00521	.00114	.00378	.000012
INVERSION LAYER	20	.00639	.00140	.00461	.000013
	2	.00635	.00139	.00458	.000012
	0.1	.00523	.00115	.00378	.000011

the 4.6 μm is greatly affected by the temperature profile. This is as expected due to contribution of atmospheric emission. The 2.3 μm radiation is essentially unaffected., as is desired. Similarly the ground temperature and the ground emissivity, have larger effects (not desired) on the CO absorption signal at 4.6 μm but not at 2.3 μm.

The calculations show that, assuming measurement of CO absorption can be made on the 2.3 μm band, that band is much to be preferred over the 4.6 μm band for data interpretation. The advantages are:

1. Measurements of temperature of the atmosphere, ground temperature, and emissivity are not needed for 2.3 μm but accurate values are required for 4.6 μm.

2. The signal at 2.3 μm is affected significantly, as desired by the CO concentration in the lowest few kilometers in the atmosphere, but not significantly at 4.6 μm and in a manner very difficult to interpret.

3. The measurements at 2.3 μm are readily interpreted directly in terms of CO densities whereas those at 4.6 μm must be interpreted by use of an atmospheric model calculation at each point, assuming the required atmospheric data are available for the latter.

Calculations using CO models 9 and 10 (Figure 2.1) were made of upwelling radiation in the 4.6 μm CO band for conditions as nearly as possible duplicating those used elsewhere (ref. 30). Results of these calculations (ref. 5) show very good agreement. It can be concluded that the calculations reported here and in more detail (ref. 5) can be used for application to any instrument employing radiation in these bands.

2.6.3 Limb Inversion Analysis.- The limb experiment has been analyzed for the effects of instrumental error on the inversion of the instrument values of total CO in the path to yield CO concentration vs altitude. The calculations have been performed for the three CO sink models to which the limb experiment is relevant. These are the constant mixing ratio model with 0.1 ppm at ground level, the upper atmosphere sink, and the low level sink with maximum concentration at 9 km. The error sources, which have been introduced, include a random error with standard deviation of 2%, 5%, or 10% and systematic errors of ± 2%, ± 5%, or ± 10%.

For these calculations the atmosphere below an altitude, h_1, was divided into n speherical shells (j = 1, 2, ---n), a distance, Δh, apart (Figure 2.16). The atmospheric properties within a shell are assumed to be constant. The altitude of the first shell is given by

$$h_1 = n\Delta h,$$

and the altitude of the jth shell is

$$h_j = h_1 - (j-1)\ \Delta h$$

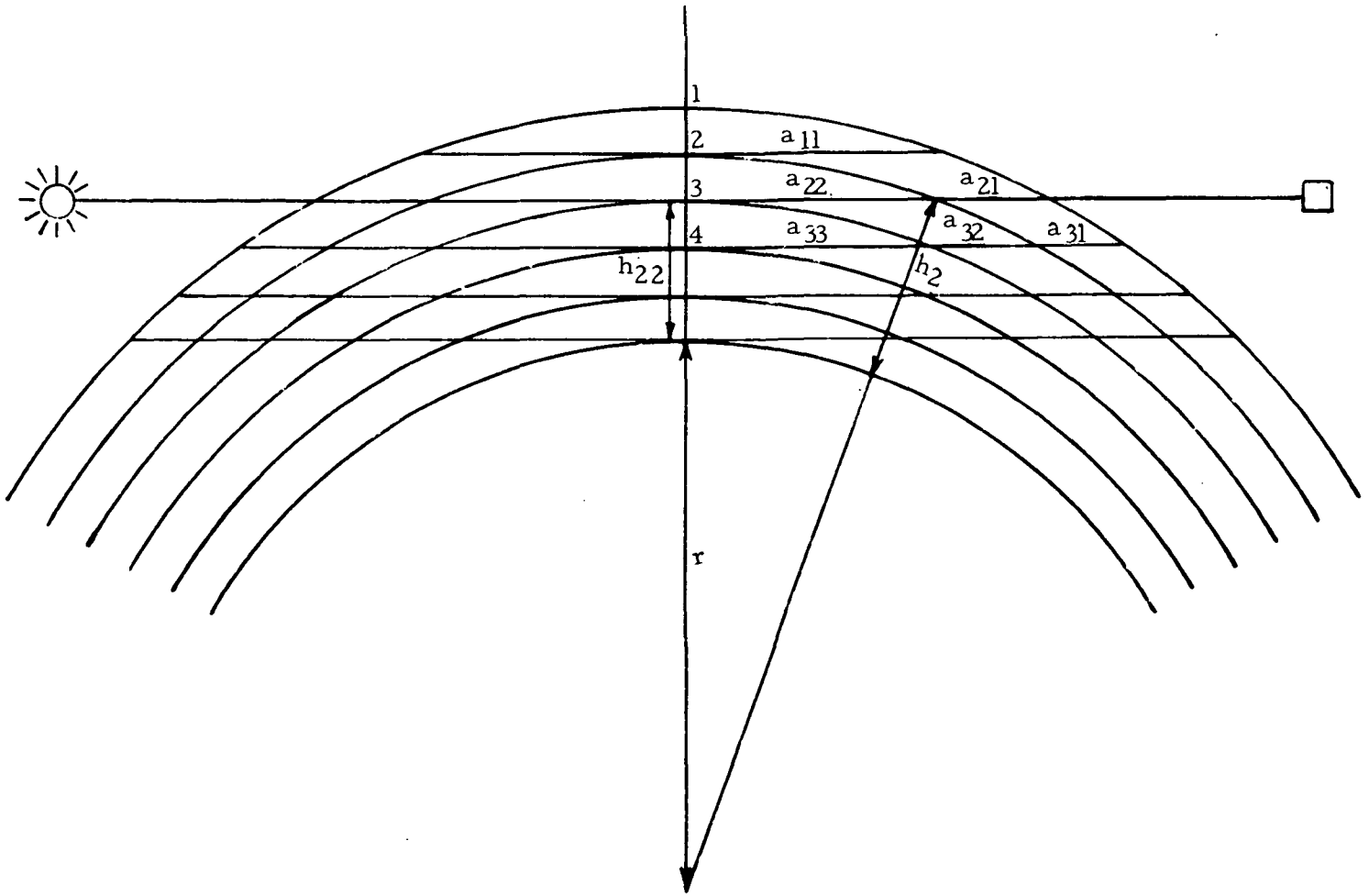

Figure 2.16 Shell Model for Limb Inversion Analysis

The ith ray from the sun to the instrument passes horizontally through the lower edge of the ith shell (j = i). The height of this ray is

$$h_{ii} = h_i - \Delta h$$

The rays passing through the shells can be divided into lengths, a_{ij}, over which the atmospheric properties are assumed to be constant. The lengths a_{ij} are given by:

$$a_{ij} = \left\{ (r + h_j)^2 - (r + h_{ii})^2 \right\}^{1/2} \qquad \text{if } i = j$$

$$a_{ij} = \left\{ (r + h_j)^2 - (r + h_{ii})^2 \right\}^{1\ 2} - \sum_{k = j + 1}^{k = i} a_{ik} \qquad \text{if } i \pm j$$

A square matrix (n x n) of the elements a_{ij} can be formed.

In a shell j, the average concentration of CO is given by:

$$c_j = c(h_j - 1/2\ \Delta h)$$

The integrated amount of gas in a horizontal path is given by:

$$\{u_i\} = 2\{c_j\}[a_{ij}]$$

where

$\{u_i\}$ ≡ column matrix of integrated amount of CO

$\{c_i\}$ = column matrix of the average concentration of CO

$[a_{ij}]$ = square matrix of path length elements within the shells.

The calculations were carried out with a 40 shell atmospheric model with a 2 km distance between shells. The matrix elements u_i were calculated for the three CO models (1, 4, and 5) in Figure 2.1. The correlation interferometer gives an instrument output which is proportional to the total CO in the path, or u_i. In this case the known parameters will be u as a function of altitude, and the a_{ij} elements will be known. A set of equations can then be set up to solve for the concentrations c_i.

$$\{c_i\} = 1/2\{u_j\}[a_{ij}]^{-1}$$

where $[a_{ij}]^{-1}$ is the inverted matrix $[a_{ij}]$.

To test for the effects of random or systematic instrument errors, the values of u were computed for each of the three concentration models from the relation $\{u_i\} = 2\{c_j\}[a_{ij}]$. The computed values were then changed by fixed amounts

a) random error with 2%, 5%, or 10% standard deviation

b) systematic error of ±2%, ±5%, or ±10%.

For each of these types of errors, the concentration profile was calculated and compared with the exact profile used as the original input. Some results of the calculation are shown in Figure 2.17.

With measurement errors of the order of 5 and 10%, the computations show that it is possible to distinguish the carbon monoxide constant mixing ratio concentration profile from the concentration profile which assumes a high altitude sink. The computations with a 2% random error show the same result with a much smaller error.

The computations indicate that instrumental errors of the order of 10% in the measurement of the total CO in the horizontal sight path through the atmosphere do not result in significantly larger errors in the computed CO concentration profile at high altitudes. While the measurement errors are more significant in the case where an inversion in the CO concentration profile occurs (i.e., the low-level sink), they do not invalidate the limb transmission experiment at the higher altitudes. The limb experiment was primarily intended for searching for an upper atmosphere sink, and in this case the effects of reasonable measurement errors are not of sufficient magnitude to permit the upper atmosphere sink profile to be mistaken for the standard constant mixing ratio CO profile.

2.6.4 Multi-Line Model Calculations.-

2.6.4.1 The program: The first step in the theoretical determination of the feasibility of using the correlation interferometric technique for the measurement of CO levels in the atmosphere is the computation of theoretical transmission spectra of the atmosphere in the wavelength regions of interest. Theoretical spectra were calculated by a fairly elaborate computer program, developed by GE. This program has been described in greater detail elsewhere (ref. 5).

Additional subroutines, patterned after Cooley (ref. 31) and Gentleman (ref. 32) then compute the Fourier transforms of the resultant spectra. These Fourier transforms which are closely related to interferograms form the data base for the theoretical feasibility study.

The computer program was used to generate a large number of theoretical spectra and transforms of CO in the presence of H_2O. Spectra were generated in the 2.3 μm spectral region (using geometry case 2) and in the 4.6 μm region

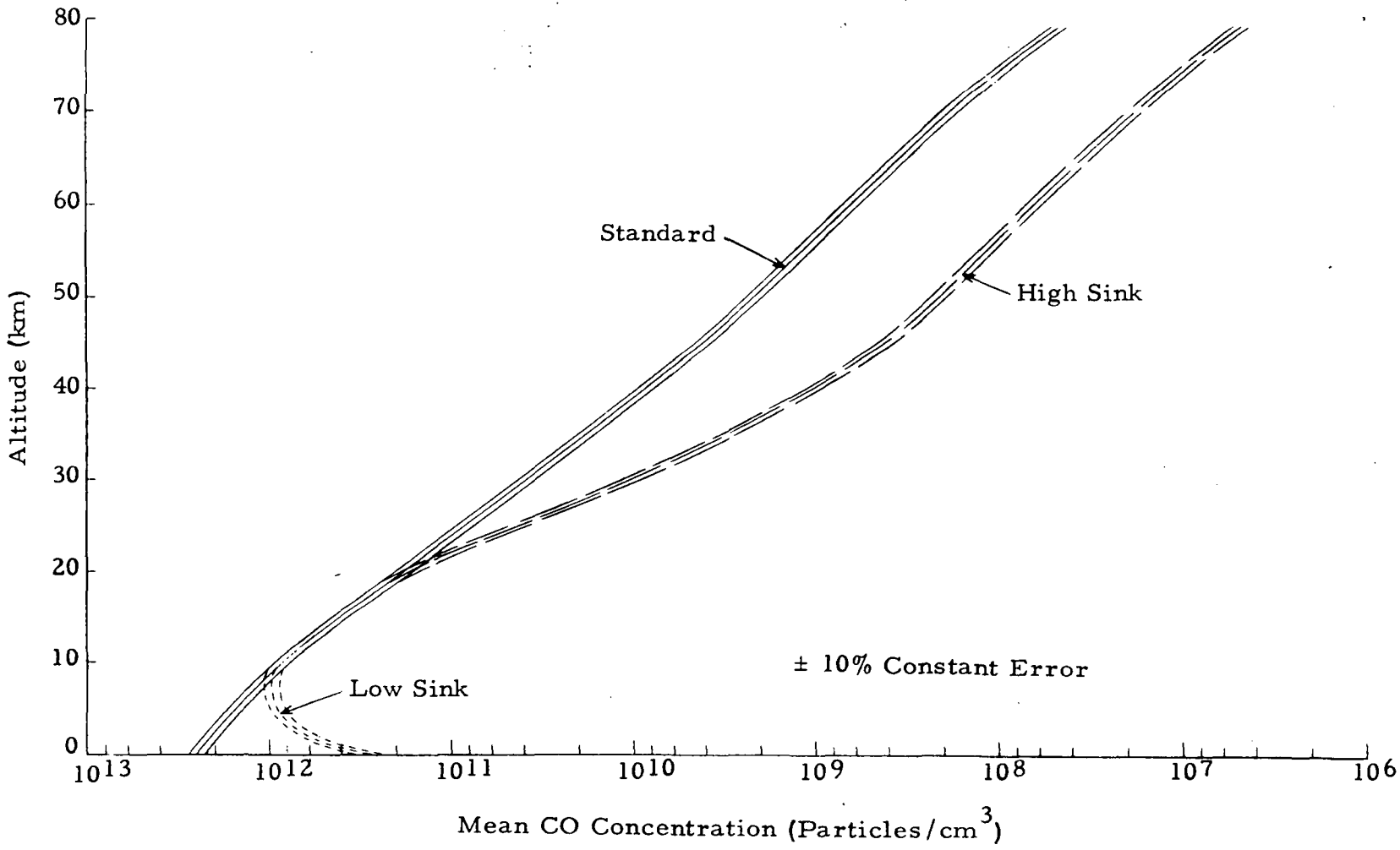

Figure 2.17 Computed Atmospheric CO Concentrations with Simulated Instrument Error

(using geometry case 1). The regions covered were 4230 - 4330 cm^{-1} and 2100 - 2200 cm^{-1}, respectively. Spectra included combinations of CO models 1, 2, 3, and 4, as described in Section 2. Ground emissivity was varied in the 4.6 μm spectra, and albedo was varied in the 2.3 μm spectra. In all, 53 theoretical spectra and transforms were computed at 2.3 μm and 19 at 4.6 μm. Although there are many additional combinations which would have been desirable, extremely long running time of the program (about 10 - 15 minutes on a GE 635 or IBM 360) makes a full gamut of combinations prohibitively costly.

Following generation of these theoretical Fourier transforms, analyses were performed by use of a weighting function computer program. This program, (ref. 5) patterned after a program furnished by Barringer Research, is an implementation of the weighting function concept described in detail in Section 6.

The weighting function can be considered a correlation function which, when multiplied by the Fourier transform of a spectrum gives a measurement of the CO level. Inputs to the weighting function program consist of a basic set of several Fourier transforms of spectra generated from a constant amount of CO and various combinations of other variables, e.g., temperature profile, H_2O level, etc. One of these transforms is designated as the nominal case. One additional transform is input, designated as the target case, which is identical to the nominal case with the exception of a variation in the CO level. The weighting function generated from these cases is then applied to other transforms which were not included in the basic set. It is this operation of generating weighting functions from one set of data and applying them to another set which determines the feasibility of the correlation operation.

The theoretical spectra Fourier transforms described above were used in various combinations as basic sets for the weighting function program. Two groups of studies were made, at 2.3 μm and 4.6 μm. The results of these studies are described below.

Calculations were made using the principles outlined in Sections 5 and 6. The intent of these calculations is to determine the sensitivity of the method in the determination of CO densities, the accuracy to be expected in the measurements, the effects of various atmospheric parameters, the optimum wavelength region to be used, and in general, to establish the feasibility of the technique in obtaining the data needed to determine the CO sink.

While the theoretical feasibility studies will be necessary, the establishment of the feasibility will only be accomplished after the instrument is shown to be capable of measuring CO in the atmosphere.

2.6.4.2 Calculations: It must be remembered in examining the results that in the measurement of CO burdens as such or for their measurement to find the CO sink, it is important to be able to see an effect produced by a rather small variation from normal CO column density, since, although at ground level the concentration may drop off by a large factor, the total column density may only have small drops, as little as about 10%. Further non-sink areas should not appear as sinks and the accuracy for very low CO column density may be poor, as long as it is good enough to show it to be less than the normal atmospheric amount. It must be emphasized that the most accurate measurements are needed at densities near those of a normal CO profile.

Further, the results should not be affected significantly by variations in atmospheric or ground properties, e.g., atmospheric temperature profile, temperature inversion layer, ground temperature, ground emissivity, reflectivity, and the shape of the CO profile.

The results which are presented in the following table are given as an example of the results of the many similar calculations made. This table (2.14) gives the results for all interferograms, using a specified set of interferograms to determine the weighting functions and then using these weighting functions to determine the CO density in all the interferograms. The table gives the percentage difference of the calculated value from the actual amount of CO in the model. The four left-hand columns give data on this model, the first column giving the actual amount of CO and the second column giving the CO profile shape, the CO model numbers being those of Figure 2.1. The third column gives the total water burden and the fourth column gives the water profile shape. Water models correspond to water models 1, 2, and 3 of Figure 2.4, multiplied at all altitudes by a constant factor. The middle four columns are for the 2.3 μm (overtone) band and the right four columns are for the 4.6 μm (fundamental) band. These last eight column headings note the four corresponding temperature models of Figure 2.5.

The table presents the results using a specific set of runs to obtain the weighting functions and gives the accuracy of the calculated CO for each interferogram of either the 2.3 or 4.6 μm band as noted. The sets used in obtaining the weighting functions are indicated by the x's.

Some of the results presented in Table 2.16 show accuracy which will fit the accuracy requirements detailed above while some show inaccuracies which are too large to be acceptable. This is as expected. The calculated accuracy of the calculations are dependent on the conditions which were used for determining the weighting functions. It is evident that, for the overtone band, the results are quite acceptable. The data of this table are typical of the many calculations carried out on this band. The calculated errors near the standard profile, that is for burdens near that of the normal clean atmosphere, are less than 5% for all temperature models. Although the errors are greater for the very small and very large CO burdens they are certainly not so great that their size is not readily distinguishable from that of the standard. This is not the case for the fundamental band. Here small and large burdens give excessive errors which make them, in many cases, indistinguishable from the standard. And for the case of a temperature inversion the errors are extremely large. This example for the fundamental band shows smaller errors than most other calculations made on that band. Such calculations were so unfavorable that many fewer calculations were made for this band than for the overtone band.

Many more conditions were calculated and are reported in detail elsewhere (ref. 5). All show similar results - quite useable for 2.3 μm and very poor for 4.6 μm.

Some general conclusions can be drawn from the results for the 2.3 μm band. If the conditions used in obtaining weighting functions for CO are within the range of CO where absorption is about linear, that is within the range from very low CO densities to slightly above our standard model, the results will be good

TABLE 2.16 CALCULATED ERRORS IN CO MEASUREMENT

ACTUAL CO (atm-cm)	CO MODEL SHAPE	WATER (atm-cm)	WATER MODEL SHAPE	% Error (2.3 μm meas.) T MODEL 1	T MODEL 2	T MODEL 3	T MODEL 4	% Error (4.6 μm meas.) T MODEL 1	T MODEL 2	T MODEL 3	T MODEL 4
.0162	3	3	3	X		X					
.0162	3	2.25	2			-22.5					
.0162	3	1.5	2	X		X			X		470.0
.0162	3	0.8	1	-22.5	31.1	34.1					
.0162	3	0.2	1	X		X					
.0324	3	3	3			2.1					
.0324	3	1.5	2	3.8		1.0					
.0324	3	0.2	1	1.9		- 0.6					
.0486	3	3	3	5.6							
.0486	3	0.8	1	- 4.0	11.1	11.5					
.0486	3	0.3	1			- 5.5					
.1488	6	3	3			1.8			3.7		
.1488	6	1.5	2	4.3		0.2		- 2.8	3.8	7.7	26.4
.1488	6	0.2	1	1.1		- 3.0					
.1618	1	3	3	4.8		0.6			X		
.1618	1	2.25	2			- 2.4					
.1618	1	1.5	2	3.4	4.7	- 1.0	1.3	X	X	X	22.3
.1618	1	0.8	1	- 0.1	2.7	1.1					
.1618	1	0.2	1	X		- 4.2					
.2426	1	3	3			- 1.4					
.2426	1	1.5	2	1.5		3.0			-14.1		
.2426	1	0.2	1	- 1.7		- 6.3					
4.3376	2	3	3			-40.7					
4.3376	2	1.5	2	-37.5		-41.6			-102.4		-110.7
4.3376	2	0.2	1	-39.4		-43.5					
4.7696	2	3	3			-42.5					
4.7696	2	1.5	2	-39.4		-43.4					
4.7696	2	0.2	1	-41.3		-45.2					

within the range of water density and temperature covered in the weighting function runs and probably not good outside such range. That is, if water density models 1 and 3 are used, those for in-between water densities have the desirable accuracy, but if models 2 and 3 are used, the results for water model 1 are inaccurate. That is, interpolation gives reasonable results but extrapolation does not.

In these models the total water content was varied by a factor of fifteen. Such a variation in total column density is probably as much as the variation over the year for any one region. Seasonal variations for a region range up to a factor of four (ref. 33) while shorter term variations may be somewhat larger. Hence, in treating the data for any one area, weighting functions based on the range of conditions for that area can be used rather than those which bracket the range of conditions for all areas.

Conslusions about sinks and sources can also be made. These results show that sinks (even those at low altitude having only a 9% lower CO optical thickness than the standard model) are detected readily and regions of high CO concentration are also readily seen. It is also to be noted that the presence of a temperature inversion layer does not interfere with the results for this (2.3 μm) band. The effects of surface reflectivity, temperature, and emissivity and of atmospheric temperature are negligible.

In all 4.6 μm cases, the source runs show up with large negative errors. In almost all urban model runs, negative CO densities are calculated. These are meaningless and undoubtedly smaller sources would show up as sinks. This is an intolerable situation.

Certain other tests were made to help show the effects of atmospheric and earth-surface parameter variations. Results show that surface temperature and emissivity and atmospheric pressure all appreciably affect the results and would have to be included in the interpretation of any measurements with the 4.6 μm band.

2.6.5 Conclusions.- The accurate measurement of atmospheric trace species by the correlation interferometric technique has been shown by analysis to be feasible. Specifically, it has been shown to measure atmospheric amounts of carbon monoxide with an accuracy of about 10%. Thus the technique should be capable of picking out CO sinks which are only about 10% lower in CO column density using measurements which are made by determining the absorption in a part of the first overtone band of CO in the 2.3 μm region of the spectrum. It has been determined that the use of this band is preferable to the use of the fundamental band in the 4.6 μm region. The latter is unsuitable because of the effect of atmospheric parameters including the atmospheric temperature profile (and the associated atmospheric emission), the ground temperature, the ground emissivity at wavelengths being used, atmospheric pressure and atmospheric path length. For that band, atmospheric emission causes an enhancement of the radiation which is a function of temperature and must be taken into account. If at some altitude the atmospheric temperature is greater than the ground temperature the effect of absorption below is minimized. Effectively, the instrument cannot see well below an atmospheric temperature peak. Then the absorption does not follow the CO profile at low altitude but rather there is less net absorption

per CO molecule near the ground even for CO profiles when there is more CO in that region (see Figures 2.14 and 2.15). These difficulties arise for any species with all spectral techniques which are primarily involved with radiation of wavelengths greater than about 3.5 μm. This is because of the predominance of earthshine over reflected solar radiation at these wavelengths (see Figure 2.6). The overtone band is not affected significantly by variations in the parameters noted above and absorption in this band follows closely the atmospheric CO profile for any reasonable atmospheric model. Atmospheric scintillations have little effect at either wavelength region.

The conclusions for the two wavelengths studied may be summarized on the basis of the following considerations.

Optical Thickness:

4.6: For much of the range, the absorption curve is not linear. The higher optical thicknesses may be so high that there is little sensitivity in that range.

2.3: The optical thickness is suitable for the range of concentrations of interest. The only limit is the upper limit of the limb experiment but it will be suitable for a sink at any reasonable expected altitude.

Interpretation:

4.6: Very difficult because of the need for accurate atmospheric temperature data as a function of altitude, ground temperature, and ground emissivity at 4.6 μm.

2.3: Data directly presented in terms of CO density.

Sensitivity to Low Altitude Sink:

4.6: Sensitivity to low altitude CO is very low and errors introduced are likely to be larger than the CO decrease effect being sought.

2.3: Sensitivity at low altitude same as the similar effect at high altitude. Sinks of less than 10% CO density decrease appear to be detectable.

Temperature Inversion Layer:

4.6: Drastic effects on calculated CO densities prohibit detection of significant sinks.

2.3: No appreciable effect.

Line Strengths:

4.6: *Strong.*

2.3: About 1% of 4.6 lines. This is strong enough.

Atmospheric Emission:

4.6: Considerable emission in this band causes much variation from straight absorption model and leads to difficulty in interpretation as mentioned.

2.3: Emission negligible.

Night Use:

4.6: Possible.

2.3: Not possible.

Mapping Experiment:

4.6: Emission effects disastrous.

2.3: Interferents cause problems but these are overcome by technique used.

Limb Experiment:

4.6: Atmosphere optically thick at lower altitudes of interest.

2.3: Sensitivity limits altitude but altitude range reasonable.

Spectral interferents can be overcome by the correlation interferometry technique. The chief spectral interferents in the 2.3 μm spectral region are water and methane. By using the interferogram directly, carbon monoxide can be accurately measured in the presence of atmospheric amounts of these gases which would prevent accurate measurement of CO by ordinary spectral methods. In order to accomplish the interferometric measurement it is necessary to calibrate the instrument over the entire range of density of interferents for which it will be used and to do so with variation of important atmospheric parameters over which it will be used. Thus the calibration must cover the range of methane of about 2 to 5 atmosphere cm, since this is the range that is expected to be encountered, and to cover the range of about 0.2 to 3 percipitable cm of water, since variations from dry to wet atmospheres include this range. Further, since the population of the rotational water levels are appreciably affected by temperature, variations corresponding to changes in atmospheric temperature profiles must be included in the calibration, thus necessitating calibration for conditions of a cold dry, a hot dry, a cold wet, and a hot wet atmosphere as well as conditions in between these.

The calibration determines the weighting function which multiplies the section of the interferogram in such a way as to minimize the effect of spectral interferents and maximize the effect of the gas to be measured. The choice of conditions used to determine the weighting functions is critical. The use of a wide range of conditions and interpolation between these gives much better results than use of a narrow range with extrapolation. In practice under flight conditions, it may be best to use a weighting function derived from a wide range of conditions to obtain an approximate measure of CO density and conditions and

then use a weighting function derived from a narrower range of density and conditions to obtain a more accurate CO density measurement.

The feasibility analysis thus shows the correlation interferometry technique to be capable of the measurement from a remote platform of carbon monoxide in the atmosphere over the desired range of density using the first overtone band. The measurement can be made in the mapping mode (observing sunlight reflected by the earth) and the limb mode (observing direct sunlight through the earth's limb).

Page Intentionally Left Blank

3. CORRELATION INTERFEROMETRY

3.1 Principles of Interferometry

The use of spectral techniques for the remote measurement of concentrations of trace atmospheric species is dependent on separating out the effects of the species being measured from those of all other species present in the optical path. In techniques where a part of the spectrum is measured, the separation must be obtained by spectral resolution. Thus, some separable part of the spectrum must show an appreciable effect of the species being measured and any significant effects of other species must be such that they can be eliminated. If a different technique is used effects must still be separable but the separation criteria is no longer spectral resolution but a type of resolution peculiar to that technique. Such a technique is interferometry. In this technique the separation is accomplished by a resolution of path differences, provided the data are obtained directly from the interferogram rather than from a spectrum obtained by transforming the interferogram. The instrument developed for this program is a correlation interferometer (ref. 34). The following discussion will describe the basic theory of its operation.

An interferometer is a fairly simple device (Figure 3.1). The essential elements are a beam splitter and two mirrors, plus a detector to measure the radiation output. Light from the source is incident on the beam splitter, B. At the beam splitter it is divided into two paths; one portion of the light goes to one mirror, M_1; the other portion of the light goes to the other mirror, M_2. The two portions recombine at the beam splitter and the intensity of the light once they recombine is registered by the detector, D. The intensity of the radiation received by the detector will depend on the difference between the lengths of the paths traveled by the beams in the two arms. The length of the Path F-B-M_1-B-D can be different from that of the path F-B-M_2-B-D. If the two optical paths are exactly the same, the path difference (delay*) is zero, and there is a peak in intensity. If monochromatic radiation enters the instrument, and if the path difference is increased by one-half the wavelength, the intensity reaching the detector goes down essentially to zero. Then as it increases again towards one wavelength path difference, another peak occurs. This sinusoidal oscillation about a mean level repeats at intervals of one wavelength if the light is monochromatic. The instrument actually does a Fourier transformation of the spectrum of the radiation entering. The way in which the delay is scanned, that is the way in which the path difference is changed, is in most instruments a matter of shifting one of the mirrors. One of the features of the COPE instrument is that the problem of having to scan and maintain the position of the mirror accurately is avoided by not scanning the end mirror, but, instead, scanning a plate of refractive material in one arm of the interferometer which is generally left in a fixed position. If this plate is rotated, the path length in that arm of the interferometer will vary. This will accomplish the same effect as moving one of the mirrors back and forth without the alignment problems. This is a specific advantage of the technique of this instrument.

---

*The term "delay" refers to the temporal variation of the interferometer signal. This is related to the variation of the path difference by the scan velocity.

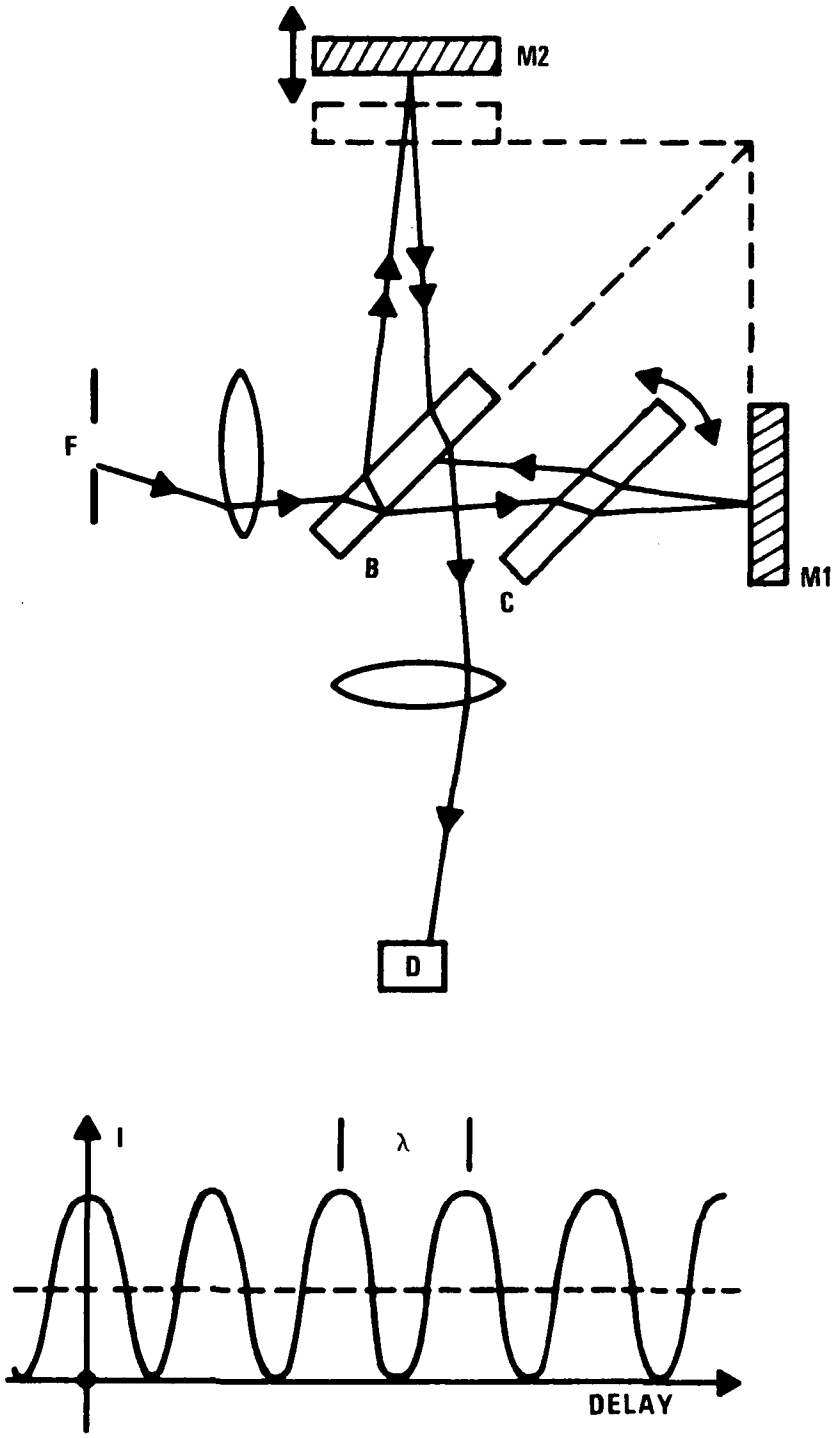

Figure 3.1 Interferometer and Interferometer Output

Other advantages, some of which are advantages of interferometry in general, include a large light throughput, multiplexing of spectral elements, a compact yet flexible instrument, and a handy output.

3.2 Relationship Between Spectra and Interferograms

In Figure 3.2 a few particular cases of the relationship between spectra and interferograms are shown. As shown on the previous figure, monochromatic spectrum produces an interferogram which is essentially a sinusoidal variation as the delay is scanned. If instead of a single monochromatic line there is a pair of monochromatic lines, then the two sinusoidals due to lines will beat together. Again a characteristic maximum is obtained at zero delay. As the oscillations beat together, they get out of phase and go through a minimum, then maximize again at a point characteristic of the line separation. If there are a number of regularly spaced lines, the beat patterns will all reinforce at zero delay again, but they very rapidly get out of step with each other and decay to very small values. Then there appears a point where they all reinforce again at a delay which is inversely proportional to the spacing between the lines. This is almost exactly the effect seen in the case of carbon monoxide as shown in Figure 3.3, which gives the actual spectrum* and interferogram. The spectrum displays fairly regularly spaced lines. There is certainly a noticeable change in the spacing from one end to the other, but it is certainly not a random spacing. As seen in the previous figure, there is reinforcement for zero delay which dies out rather rapidly, and then, at a delay which is characteristic of the spacing between the lines (about 3 cm^{-1}), the interferogram amplitude peaks up again. In general the relationship between the spectrum of the radiation and the interferogram of the radiation is given by a Fourier transformation, the cosine Fourier transformation. That is, the interferogram, apart from the constant term, is the cosine Fourier transform of the spectrum (Figure 3.4). The interferogram signal, as a function of path difference is given by:

$$I(\chi) = 2\int_0^\infty \Pi_i \ (S_i(\sigma)) \cos (2\pi\sigma\chi) \, d\sigma$$

where

σ = frequency (cm^{-1})

$S_i(\sigma)$ = spectral input at σ (ergs-cm^2-sr^{-1}-$(cm^{-1})^{-1}$-sec^{-1})

χ = path difference (cm)

Several relationships exist between the interferogram and the spectrum from which it is produced. The interferogram has a carrier frequency directly related to the mean frequency of the spectrum producing it. It will be amplitude and phase modulated, the amplitude and phase modulation being described by the band envelope shown. From an interferogram up to a given delay, the spectrum could be reconstructed with a resolution given inversely by the delay out to which the interferogram is obtained. So, from an interferogram from zero to 1 centimeter, inverse Fourier transformation reproduces a spectrum to resolu-

---

*This spectrum is that given by Plyler (ref. 17) with the mercury emission lines omitted.

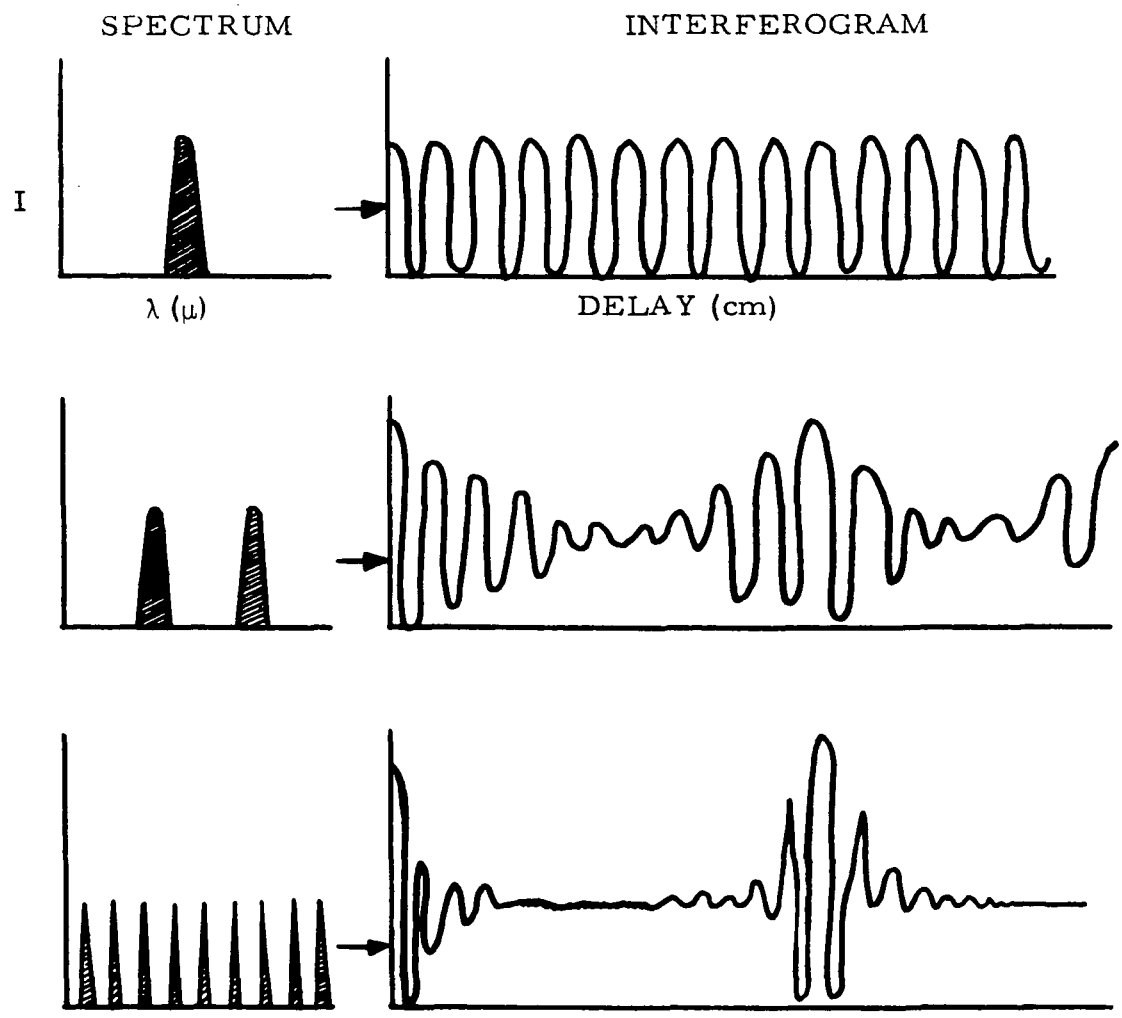

Figure 3.2 Relation of Interferogram and Spectrum

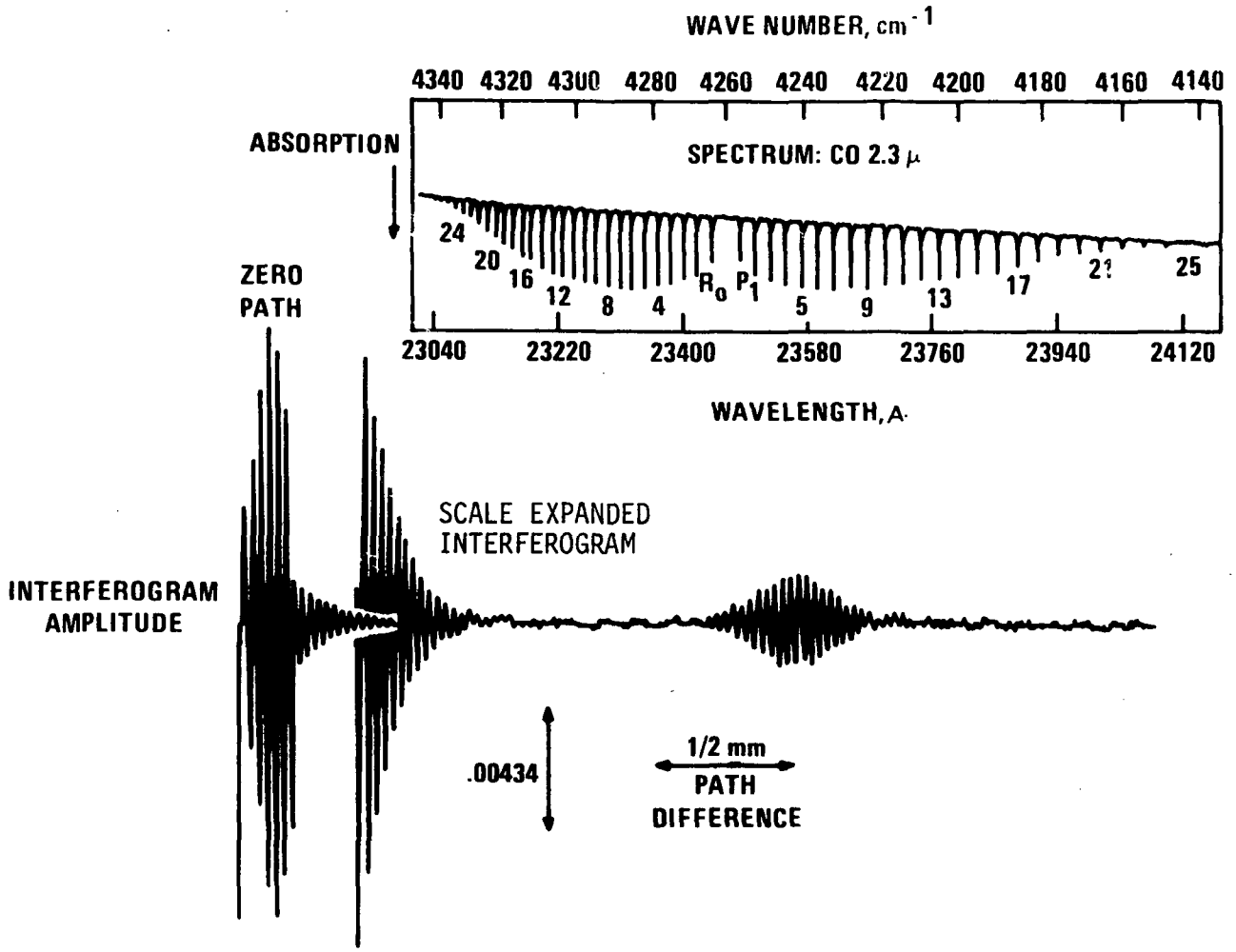

Figure 3.3 CO Spectrum and Interferogram
(of part of P branch of spectral band)

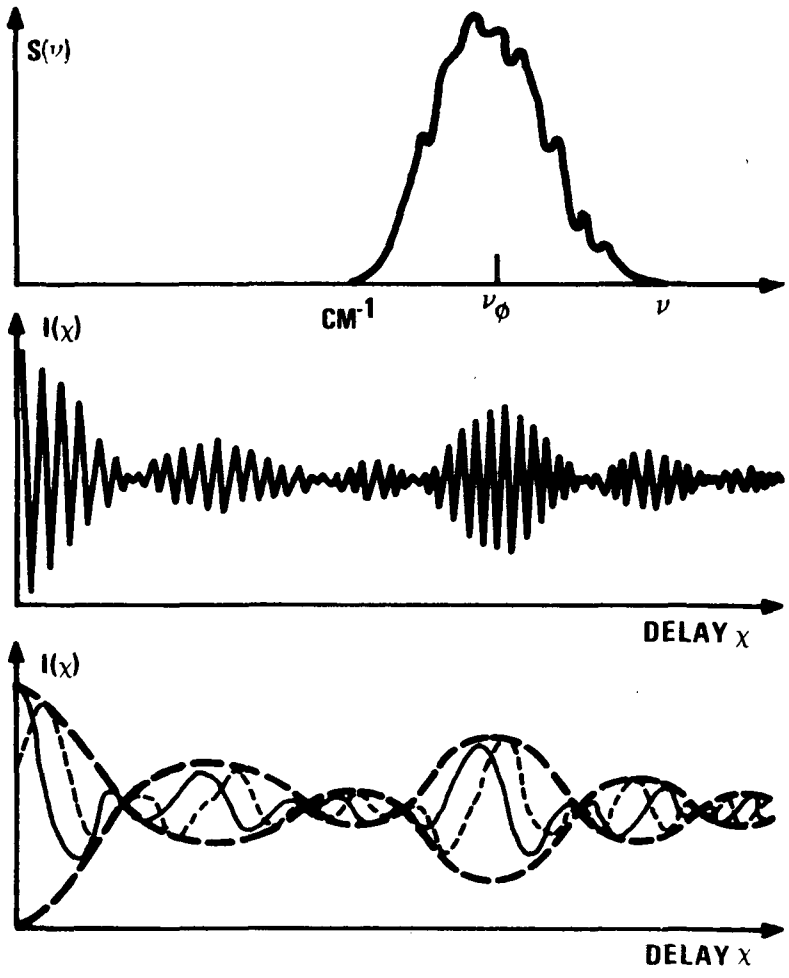

SPECTRUM
$S(\nu)$

INTERFEROGRAM

$$I(\chi) = eE\int_0^{\infty}\left[1 + \cos(\omega\chi)\right] S(\nu)d\nu$$

BEAT

$I \cdot \cos(\omega_0\chi)$ ——

$I \cdot \sin(\omega_0\chi)$ ••••

Figure 3.4 "Heterodyning" of Interferogram

tion of one wave number (cm^{-1}). Conversely, if the information characteristic of one wave number resolution is not needed, if the information need only be characterized by a 3 cm^{-1} resolution, then it is only necessary to scan the interferogram out to 1/3 cm (3 millimeters) to obtain information equivalent to a resolution of three wave numbers. It is very important to do this. Significant improvements in signal to noise ratio are obtained by limiting ourselves to scanning only the portion of the interferogram which gives the best signal to noise ratio. If essentially all the information on any given species (all the effect of that species on the interferogram) occurs over a small part of the interferogram, only that range of path difference need be scanned. The operation of the correlation interferometer involves the treatment of the interferogram data directly to obtain data on species densities rather than the use of the spectrum obtained by the Fourier transform of the interferogram. With such an operation the concept of spectral resolution loses meaning. Although the spectrum which can be obtained from an interferogram has a resolution which is the reciprocal of the path difference scanned, the ability to obtain data on one species in the presence of others by direct examination of the interferogram, is not simply dependent on the length of path-difference scan.

Probably the main objection to interferometers is that most people think in terms of using a spectrum and in order to obtain a spectrum from the interferometer, the interferogram must be transformed. This problem is avoided completely by not looking at the spectrum at all. It is not really necessary to use the spectrum. The measurement can be made quite adequately on the interferogram itself. This is a major advantage of the correlation interferometer.

Another relationship between the spectrum and the interferogram is that the spectrum of the incoming radiation can be severely band-limited by optical filters. If it is band-limited, and if an interferogram that would reproduce the spectrum only to a limited resolution is taken, then the spectrum could be characterized by a farily small number of points. On the other hand, to characterize the interferogram in this form with its very rapid oscillations (the oscillations are essentially proportional to the mean frequency and not to the width) with any degree of accuracy, a relatively large number of points, on the order of at least one per cycle of oscillation, would be needed. This would be many more points than are necessary to characterize the spectrum to a corresponding resolution. There is a lot of redundancy in the information because of the band limitation. The method used in the correlation interferometer to eliminate the redundance is simply to take the amplitude and phase modulated sinusoid and heterodyne it down with a local oscillator, where the local oscillator is the interferogram of radiation somewhere around the mean frequency of the spectrum. By heterodyning the interferogram down with a cosine or a sinusoidal variation, the interferogram is reduced to its essential variations. This is illustrated in the bottom part of Figure 3.4. All the information necessary to characterize the interferogram can be retrieved by sampling a relatively small number of points, a few points for each of the much longer cycles shown in the bottom figure. There is a slight difference whether the interferogram is beat with a sinusoid at a given wavelength or a cosine; slightly different beat-down interferograms are obtained. Actually both of them are used but, through most of the remaining discussion this fact will be ignored. In generating the local oscillator for carrying out the heterodyning, radiation which passes through the same interferometer as does the signal radiation is used. This insures that the

local oscillator always has the correct phase relationship with the signal interferogram. It also relaxes some of the accuracy needed in the knowledge of the plate drive (the scan drive). If this were not done, the scan drive would have to be known accurately to within a very small fraction of the wavelength. By having the local oscillator going through the same interferometer, this problem is alleviated.

3.3 The Measurement in the Presence of Interferents

Figure 3.5 outlines very briefly the basic principles by which the measurement on the interferogram is made. There are essentially two problems involved in a measurement of this type. We are trying to measure the CO burden on the basis of the radiation received from a satellite. The problems in making the measurement are: (1) can the measurement be made with sufficient accuracy in view of the noise limitations, and (2) can the measurement be made under conditions where the radiation received is affected not only by the gas that we are trying to measure, in this case carbon monoxide, but is also severely affected by other gases. In fact, the radiation is much more affected by such things as water vapor and methane. Ignoring for the moment this problem of the interference species, consider how a measurement would be made. Consider an interferogram due to a target signal, say CO, such as shown. There are different ways by which one could measure the CO burden which produced this signal level. One might sit at a constant delay and measure the signal level at that point. If the CO burden were doubled, the effect of CO on the intensity we would measure would be doubled (for the moment assuming variations are linear with the gas burden); the intensity would essentially be a measure of the carbon monoxide burden. If there were a constant noise level associated with the measurement of any point then the best point to make a measurement would be at the point where the signal level is maximum. If a finite range of delay were scanned, then the measurements made at all points would be combined to get some sort of average measurement of the carbon monoxide burden. In general, the optimum measurement that can be made in such circumstances is given by combining all the measurements, all the intensities of the various points, in a manner related directly to the intensity of the signal shape. That is a weighting function or correlation function is generated and this is multiplied together with the signal. The measurement made is the integral of the correlation function times the signal, the integral over the delay range which is scanned. It is integrated and the measurement obtained is directly proportional to, in this case, the carbon monoxide burden. The signal-to-noise ratio in such a measurement can be shown to be optimum when the correlation function looks exactly in shape like the target signal. That result holds when there are no interferents. Now consider another gas species which is affecting the signal received, for example, water vapor. If a point measurement of the intensity were used, the signal received would not be simply the signal due to carbon monoxide but the sum of the signals due to the carbon monoxide and to the water vapor. Even if the carbon monoxide level were to remain the same, drastically varying measurements due to variations in water vapor might be obtained so that a very poor measurement of CO would be obtained by sitting at that point. A region where a signal is unaffected by all interferents may not be available or if it is, the signal-to-noise ratio achievable at the point might not be adequate for the measurement. This problem is handled as follows. The correlation function used is not matched exactly to the

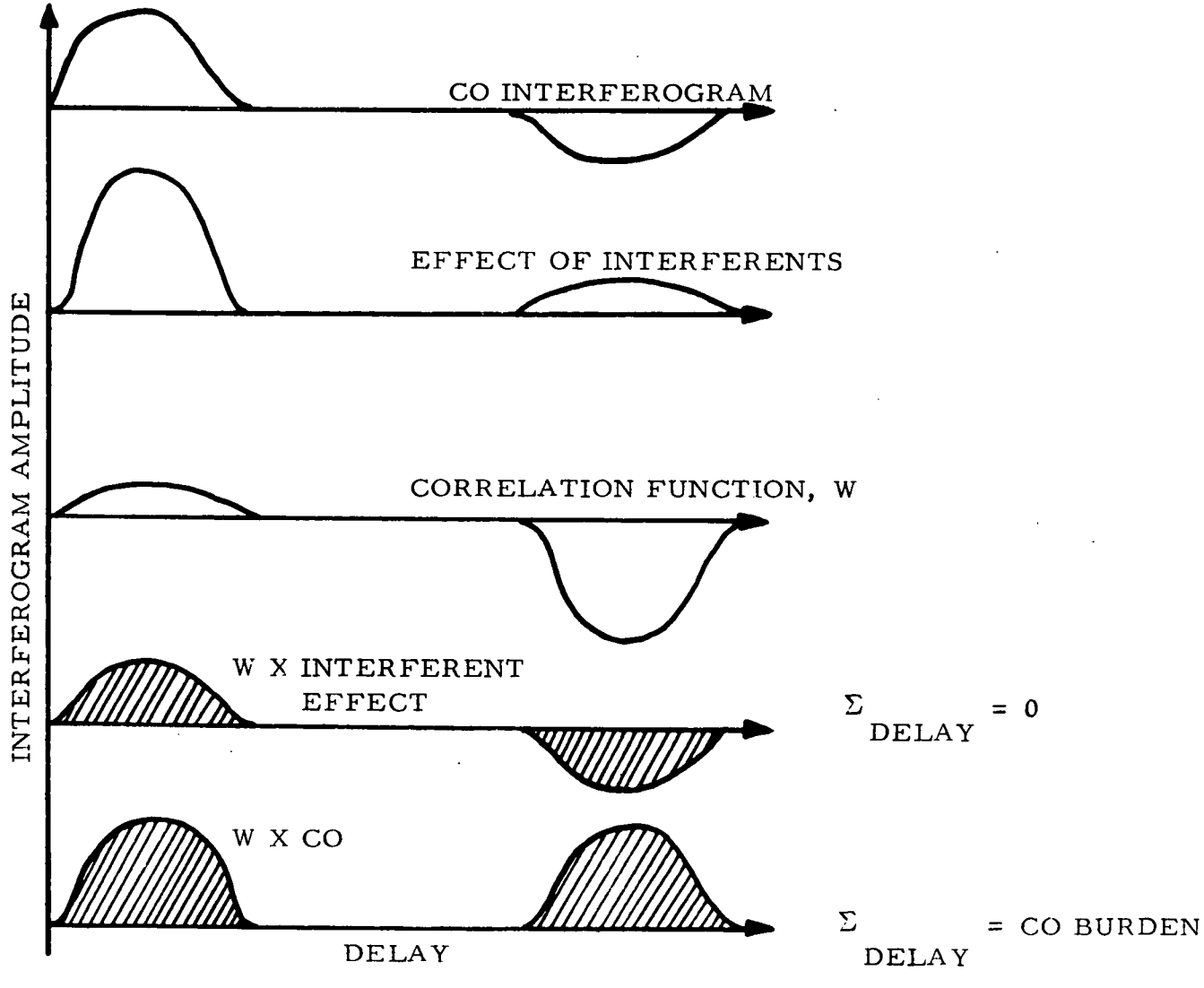

Figure 3.5 Application of Correlation Function

target gas signal shape. The correlation function (W) is adjusted so that when it is cross-correlated with the interferents and the result is integrated over the range scanned, all the positive correlation regions are balanced exactly by the negative correlation regions, so that the total area under the curve, the total result of the measurement, comes out to zero as illustrated, still maintaining the correlation function as close as possible to that constraint to the signal interferogram (target interferogram) in order to still get as large a positive correlation between the correlation function and the target gas as possible. The result of the measurement is still proportional to the carbon monoxide burden. In principle, if there are a number of interferents of this sort, rejection of these interferents can still be achieved so long as we have at least as many points to describe our correlation function as we have gases which are affecting the radiation. The measurement of the target gas can be made in real time. The first gas, in this case CO, and any other gases which significantly affect the interferogram can be measured.

In the correlation interferometer, the path difference scan is limited principally to that portion of the interferogram which is most affected by the gas whose density is being measured (excluding that portion near zero path difference). In the case of CO that portion of the interferogram obtained with path differences between 2.70 and 3.95 mm has been selected. Since the lines in the first overtone band of CO are separated by about 3 cm^{-1} on the average this shows up in that part of the interferogram centered at about 1/3 cm^{-1} = .33 cm = 3.3 mm. Thus, the CO spectrum is as shown in Figure 3.3 and the interferogram (using a spectral filter centered at 4287 cm^{-1}) is also shown in Figure 3.3. In this the major effect of the CO is seen to be in the region of 0.3 cm. Taking this portion of the interferogram between 0.27 and 0.395 cm gives essentially all of the information on CO that can be obtained from the interferogram. The determination of CO is not, however, the simple measurement of this peak in the interferogram since other gases, particularly CH_4 and H_2O also have some effect in this region. Thus, this peak is divided up into a number of sections, 32 in the case of our instrument. The effect of each gas on each of these 32 sections is determined in effect, by calibration.*

Thus, in the simplest case, a portion of the interferogram affected only by H_2O is chosen to determine the amount of H_2O** and the remainder of the interferogram is, in effect, corrected using these data and calibration information. CH_4 is dealt with similarly. Thirty-two different effects could be dealt with this way. Since in a real case portions of the interferogram affected by a single gas are not always available, the set of 32 simultaneous equations is solved to determine the amounts of individual gases causing the combined effects.

---

*Actually, the effects of specified gases, other than that being measured (such as CO), need not be specifically known by calibration. The calibration can consist of 31 different atmospheric conditions with one amount of CO and a different amount of CO with one of these conditions. The measurement of CO is then made by determining the effect on each section of the interferogram of other gases of the atmosphere as determined by a best fit of the 32 points.

**Since the H_2O spectrum and hence its interferogram is affected by temperature, two or more portions of the interferogram must be used to take this effect into account.

The output of the interferometer will be voltages, each related to the concentration (column density) of one species. The calibrations can be thought in terms of these voltages. Thus, to be able to separate out the effects of individual species it is necessary to resolve parts of the interferogram which show the effects of these species. This resolution is not attainable with the spectrum which would be produced from the interferogram obtained with this instrument. Thus, by directly using the interferogram the effects of specific species and hence its density is measurable whereas it would not be if the interferogram were converted to a spectrum and that used for the measurement. This comparatively simple measurement can be made very much faster than can a measurement of species by a high-resolution spectrometric technique, whether by a spectrometer technique or by an interferometric technique which employs the Fourier transform of a interferogram obtained over a large range of path difference.

Page Intentionally Left Blank

4. CORRELATION TREATMENT

4.1 Basic Principles

4.1.1 Instrument Output.- The interferometer receives radiation, the spectral characteristics of which are affected by a number of parameters. We wish to measure one of these parameters (CO burden), with as high accuracy as possible and as little interference as possible from variation in the other parameters. Within the instrument, optical filters limit the range of the radiation to a fairly narrow spectral region where CO absorption has the greatest relative effect on the radiation.

The correlation interferometer operates by varying the delay between the two beams of a Michelson interferometer over a defined range. As the delay is swept, a sinusoidal type signal is generated at the detector output. This signal is both amplitude and phase modulated. The band center and width are directly related to the center and width of the optical spectral filter, while the modulations are characteristic of the more detailed spectral information.

4.1.2 Preprocessing.- An important function of the interferometer electronics hardware is to reduce the high sampling rate implied by the relatively high center frequency of the interferogram signal, by synchronously detecting the signal with a reference signal, (similar to the local oscillator in a homodyne system). This reference is generated from the interferogram of radiation having stable spectral characteristics. The reference radiation passes through the same interferometer system as the signal radiation, so that to a very large extent the reference derived from its interferogram is fixed in phase relative to the interferogram of any given signal radiation, regardless of any irregularities in scan, or variations in the interferometer arm lengths.

When this synchronous detection is carried out, the result is a signal containing only the information of the sidebands of the original signal, beat down to zero frequency means. (Actually two such signals are produced, from references both in phase and in quadrature phase with the reference interferogram.) The signal's information is still band limited, by virtue of the original spectral band limitations. The signal is integrated and digitized at an interval sufficient to retrieve this information, producing a preprocessed, digitized, interferogram.

4.1.3 Final Processing.- Final processing consists of applying a linear digital filter ('weighting function' or 'weights') to the preprocessed interferogram. The filtering operation consists of taking the weights, one for each point of the interferogram, multiplying them together with the corresponding interferogram points, and summing the results. The weights are chosen, in a manner to be described below, so as to give a final result which is insensitive to variations in all parameters except the desired one. (The weights are also chosen to give a result which is optimized against a mixture of noises.) The result may be directly converted using a defined zero point and scale factor, to units of target gas burden (atm-cm, ppm-m), etc.

4.2 Determination of Weights

4.2.1 Basic Philosophy and Theory.- The determination of the weights is based on the possibility of representing any observed interferogram as a linear combination of component interferograms. The number of such component interferograms required to represent a range of actual observed interferograms to some accuracy, will depend on a number of factors depending on the range of conditions under which the interferograms are observed. The number will depend mainly on the number of parameters which vary significantly over the range of conditions, and to a lesser extent on the degree of non-linearity in the variations of the interferograms with these parameters. (Parameters will characteristically represent factors such as water vapor burden, methane burden, and temperature profile, as well as the target CO burden).

Consider then any interferogram, I, within the defined range. It may be written as a linear combination of N constituent interferograms. Using the index k to define the point on the interferogram, and j to define the particular constituent interferogram we may write

$$I(k) = \sum_{j=1}^{N} q_j \, I_j(k)$$

The q_j's are the strengths of the constituent interferograms in the particular interferogram observed. Let us assume one of these, q_{j1}, is the target gas burden.

Now the final processing consists of the application of a weighting function, H(k), to the interferogram. The resulting measurement is

$$M = \sum_k H(k) \, I(k)$$

$$= \sum_j q_j \sum_k H(k) \, I_j(k)$$

From this, it can be seen that if we can find weights H(k) that give

$$\sum_{k=1}^{Nk} H(k) \, I_j(k) = \begin{cases} 1 & j = j1 \\ \emptyset & j \neq j1 \end{cases}$$

Then the measurement will be $M = q_{j1}$, the target burden. If j varies from 1 to N, then this is a set of N equations in as many unknowns, H(k), as there are interferogram points (Nk). In order for these equations to be satisfiable, there must be at least as many interferogram points as there are constituents ($Nk \geq N$). In the case that Nk = N, there are N linear equations in N unknowns, and the solution for the H(k) is straightforward.

In the case that there are more interferogram points than there are constituent interferograms, there are many possible weighting functions which will

satisfy the N equations. It is, however, possible to choose a unique set of weights by considering the noises in making the measurement, and minimizing their effect on the measurement.

4.2.2 Noises in Measurement.- The noises operate in the following manner. The total integration time for measurement of a given point may be written D(k) (its duration, assumed unity up till now). The contribution to the final measurement for that point is actually $\Delta M(k)$.

$$\Delta M(k) = [H(k)\ D(k)]\ I(k)$$

The noise contribution for that point is significant in how it can vary this from its "correct" value. The noises may or may not decrease with integration time; that is, they may be either random or synchronous with the scan. They may or may not depend on the expected level of the interferogram itself $\langle I \rangle_k$, (an RMS value for the constituent interferogram at a given point); that is, they may be either additive or multiplicative.

A discussion of various physical origins for these noises will be presented in Section 4.2.4. However, it is sufficient at this point to be able to characterize them by four numbers, $a_1 \ldots a_4$, which represent the severities of the four possible combinations of noise type:

a_1	-	Random Additive	(RA)
a_2	-	Random Multiplicative	(RM)
a_3	-	Synchronous Addivive	(SA)
a_4	-	Synchronous Multiplicative	(SM)

The noises will combine in an RMS manner to give the mean square noise contribution $\Delta N^2(k)$ to the measurement at a particular interferogram point, and we may write

$$\Delta N^2(k) = [H(k)\ D(k)]^2 \times [(a_1 + a_2 \langle I \rangle_k^2)/D(k) + (a_3 + a_4 \langle I \rangle_k^2)]$$

$$= [H(k)\ D(k)]^2\ G(k).$$

G(k) is an effective mean square interferogram error for point k (although it may originate through error either H, D, or I).

4.2.3 Derivation of Weights.-

The total measurement is thus

$$M = \sum_k \Delta M^2(k) = \sum_k [HD]I$$

and the total squared noise is

$$N^2 = \sum_k \Delta N^2(k) = \sum_k [HD]^2\ G.$$

It is possible to choose, given the various $I_j(k)$ and the duration $D(k)$, those values for $[HD]_k$ which minimize the above noise term; subject to the constraint that $M = q_{j1}$, the target quantity, regardless of what values the other quantities may have (to the extent that the assumed linear representation is valid). The solution, derived elsewhere (ref. 35) is:

$$[HD]_k = \sum_j A^{-1}_{j,j1} \; I_j(k)/G(k),$$

where A^{-1} is the inverse of the matrix

$$A_{j,\ell} = \sum_k I_j(k) \; I_\ell(k)/G(k).$$

(Knowing $D(k)$, $H(k) = HD_k/D(k)$.)

A couple of points should be noted. First, the weights produced in this manner may be multiplied by an arbitrary scale factor, to give a new set of weights; however, the signal to noise ratio will remain unchanged. Secondly, if $G(k)$, (the squared noise at a given point) is multiplied by a scale factor; (i.e., if all noise terms a_i are increased by the same factor), then there is no change to the weights produced. In fact, $G(k)$ may be written as:

$$G(k) = \text{const} \times [1 + R \langle I \rangle^2]_k$$

where $$R = [a_2/D(k) + a_4]/[a_1/D(k) + a_3]$$

represents the relative importance of the multiplicative terms with respect to the additive terms. If we assume $D(k)$ is constant, then this one parameter will determine the weights produced; whether they optimize against multiplicative noises ($R \gg 1$), additive noises ($R \ll 1$), or some intermediate mixture. Analysis of the way R varies with the a's for reasonable values of the noises should indicate which terms will have most effect on the shape of the weights produced when varied.

Similarly, it is possible to examine the relative importance of the two multiplicative terms (in the numerator). In fact, the ratio of their contribution to the total final noise is given by $a_4 \times D/a_2$. The same is true for the two additive terms. On the other hand, to examine the total contribution of both multiplicative terms in comparison to the contribution of the additive terms, it is necessary to first calculate the weights. Once this has been done the absolute importance of the four noises may then be calculated, in the same units as those in which the target burden is measured:

$$N_1^2 = a_1 \Sigma (HD)^2/D$$
$$N_2^2 = a_2 \Sigma (HD)^2$$
$$N_3^2 = a_3 \Sigma (HD \langle I \rangle)^2/D$$
$$N_4^2 = a_4 \Sigma (HD \langle I \rangle)^2$$

4.2.4 Physical Origins for the Noise Terms.- The various noise terms may each arise due to one or more sources. Some possible sources are listed below:

RA:
- Detector noise.
- Photon noise.
- Other electrical noises.
- Digitization of integrated outputs.

RM:
- Scintillation or rapid variations in target, albedo, or illumination.
- Random errors in derivation or reference signal.
- Random variations in scan waveform.

SA:
- Presence of spectral signatures which were not represented in sample used to derive weights.
- Crosstalk from reference into signal channel.

SM:
- Inaccuracies in carrying out multiplications (truncation of weights).
- Change in scan waveform from the shape when the weights were derived.

Page Intentionally Left Blank

5. BREADBOARD MODEL CORRELATION INTERFEROMETER

Within the objective of the work on the Carbon Monoxide Pollution Experiment (COPE) program, a major goal was the development of the correlation interferometer instrument for quantitative measurement of carbon monoxide, and other trace constituents in the atmosphere. The details of the design, construction, and testing of the breadboard correlation interferometer are given in a previous report (ref. 2).

The specific objectives of this phase of the program were, by building and testing a breadboard interferometer, to establish the feasibility of the method, to gain operational experience and experimental data on the interferograms of the gases of interest and to obtain inputs for the design of an engineering model. As these objectives imply, the breadboard has provision for independently varying several of its parameters, so that the effects of these parameters could be investigated. This means that the breadboard instrument is more complex than later versions, in which these parameters will have optimum, fixed, values selected on the basis of experience with the breadboard. One such parameter was the wavelength. The breadboard was built for operation at both 2.35 μm (first overtone of CO) and at 4.6 μm (fundamental of CO). Based on the results obtained and on analytical results previously presented, the 2.35 μm band was chosen for the engineering model. The various parameters of the breadboard model are given in Table 5.1.

The laboratory tests should cover the range from 1 to something less than 0.1 atm-cm, a reasonable lower limit being 0.02 atm-cm, the limits being imposed by the mapping experiment. The ground level sinks considered cause changes of optical thickness which require that a decrease of the order of 10% be detectable. That is, the absolute limit of sensitivity should be such that a column density of 0.02 atm-cm (1/10 that of the nominal unpolluted atmosphere) is measurable.

The experiments were planned to test the ability of the breadboard model correlation interferometer to measure carbon monoxide in its optical line of sight to these levels. Since the capability of making these CO measurements with sufficient accuracy in the presence of atmospheric constituent gases which interfere spectrally with CO is the primary question to be answered, the tests set up realistic combinations of carbon monoxide and interferent gases over as wide a range as conditions as is practical.

The first series of tests were designed to verify the instrument operation in the laboratory using the General Electric multiple chamber system. In this facility the carbon monoxide and selected interferent gases can be introduced into the optical line of sight of the instrument in known quantities, and the effects of gas temperature and pressure on the measurements can be studied. The limitation of these tests is that not all of the atmospheric constituent gases can be introduced into the chambers in sufficient quantities to approximate atmospheric amounts. Water vapor is a major interferent whose effect can not be simulated in these laboratory tests. However, the laboratory tests provided a first check on the instrument operation at the minimum CO level which

TABLE 5.1 BREADBOARD SYSTEM PARAMETERS

Aperture	
Interferometer	6.6 cm diameter
Telescope	22.0 cm diameter
Field of View	
Interferometer	0.12 radian diameter
Telescope	0.034 radian diameter
Spectral Bands	4240 - 4340 cm^{-1} (2000 - 2200 cm^{-1})
Delay Scan Range	2.5 - 4.0 mm
Number of Sample Points	0 - 64
Sample Length	1 - 63 fringes
Scan Rate	1 Hz
Number of Scans Accumulated	1 - 500
Noise Equivalent Power	1.6×10^{-11} watt/$Hz^{1/2}$
Noise Equivalent CO Amount (2% Albedo, τ = 1 sec)	0.004 atm-cm
Detector 2.3 μm	LN_2 cooled PbS immersed on $SrTiO_3$
4.6 μm	LN_2 cooled InSb
Weight	
Interferometer	15 lb.
Telescope	10 lb.
Electronics	60 lb.
Power	100 watts

one wishes to detect. The laboratory tests were carried out using the 2.3 μm overtone band and using the 4.6 μm fundamental band.

The second phase of the tests was a series of outdoor measurements with the instrument looking through an actual atmospheric path at sunlight. These outdoor tests indicated the sensitivity of the correlation instrument measurement of CO over a range of atmospheric parameters which were covered in this test period. However, these tests did not permit the instrument response to be evaluated over the full range of atmospheric parameters to be encountered on a long term seasonal and latitudinal basis. The outdoor tests were carried out using the 2.3 μm overtone band.

The third phase of the tests was a series of measurements with the instrument looking through a 430-foot tunnel at NASA/LaRC. The composition of the gas in the tunnel, including an appreciable amount of water, was controlled.

The testing of the correlation interferometer showed that this technique is capable of making the desired measurements over the important range of CO in the presence of atmospheric gases.

It was found the atmospheric amounts of CO can be measured with an error of 10% or better. The instrument test confirmed the conclusion reached analytically that the use of the overtone band at 2.3 μm gives much better results than does that of the fundamental band at 4.6 μm. The range of sensitivity at 2.3 μm is much larger, the absorption being nearly linear from 0 to above 1 atm-cm and usable to at least 10 atm-cm; whereas at 4.6 μm near linearity is very limited, to a factor of about five in the range of densities of interest. The effects of gas temperatures and pressures and source temperatures are negligible using the 2.3 μm band but quite significant using the 4.6 μm band.

Carbon monoxide can be measured accurately in the presence of the major interferents for this spectral region - methane and water. The methane effect has been found to be completely separable from that of CO. These same data can be used to measure methane as well as CO with errors of less than 10% over the range of 1 to 5 atm-cm, which covers that to be expected in atmospheric measurements. The tunnel tests showed that, for water densities up to 230 atm-cm, the effect on CO accuracy is separable and minimal. The outdoor tests showed that the effect of atmospheric amounts of water can be overcome by a proper choice of correlation functions. The choice of conditions used to determine correlation functions is critical. The conditions should cover the range of variation of interferents and atmospheric parameters which affect the measurement. The use of a wide range of conditions in obtaining correlation functions and interpolation between these gives much better results than use of a narrow range with extrapolation. The outdoor tests showed that using a broad range of appropriate conditions for these functions greatly improves results.

The breadboard experimental results gave good and necessary data for obtaining design parameters for the engineering model.

Page Intentionally Left Blank

6. THE DESIGN, FABRICATION, AND GROUND-BASED TESTING OF THE ENGINEERING MODEL CORRELATION INTERFEROMETER

6.1 System Design

The design of the engineering model was based on that of the breadboard instrument, modified as indicated by the results of breadboard testing or as required by the more extended objectives of the engineering model program.

The functions to be performed by the system, subject to the constraints of aircraft and balloon operations, are as follows:

1. To collect radiation, in sufficient quantity, from a field of view appropriate to the intended flight test program.
2. To limit this radiation to the narrow spectral band where absorption by CO occurs.
3. To form the interferogram of the radiation as a function of time and convert it to a time-varying voltage for signal processing. Since the radiation is limited to an optical band of $\sigma_o \pm \Delta\sigma$ the voltage is band-limited to frequencies $S\sigma_o \pm S\Delta\sigma$ where S is rate of scanning path difference.
4. To normalize the signal amplitude in terms of the total received power in the spectral band. This is required because the observable which is related to the CO amount is the transmission of the atmosphere. This normalization should be capable of dealing with intensity changes over the entire information frequency bandwidth of the instrument (i.e., 0 to $S\Delta\sigma$).
5. To move signal frequency band (from $S\sigma_o \pm S\Delta\sigma$ to $0 \pm \Delta\sigma$) by synchronous detection and smoothing. The use of synchronous detection (or hetrodyning) gives better S/N ratio for small signals than linear or square law detection (refs. 36,37) and does not require that the signal frequency be maintained exactly at the peak of a narrow band electrical filter. Transforming to zero frequency minimizes the position accuracy required on subsequent sampling.
6. To sample the smoothed signal, at known points in the interferogram, over a range of delay centered around the CO signature. The spacing of the points to be that dictated by the bandwidth and the sampling theorem, i.e., at least one point every $1/2\ A\Delta\sigma$ units of delay.
7. To digitize the value of each sample and output this data in a form suited to telemetry and/or magnetic recording.
8. Measure and output, in suitable format, the housekeeping data required during flight testing.

The means by which these functions are implemented are shown in Figure 6.1 and described below in general terms and in detail elsewhere (ref. 3).

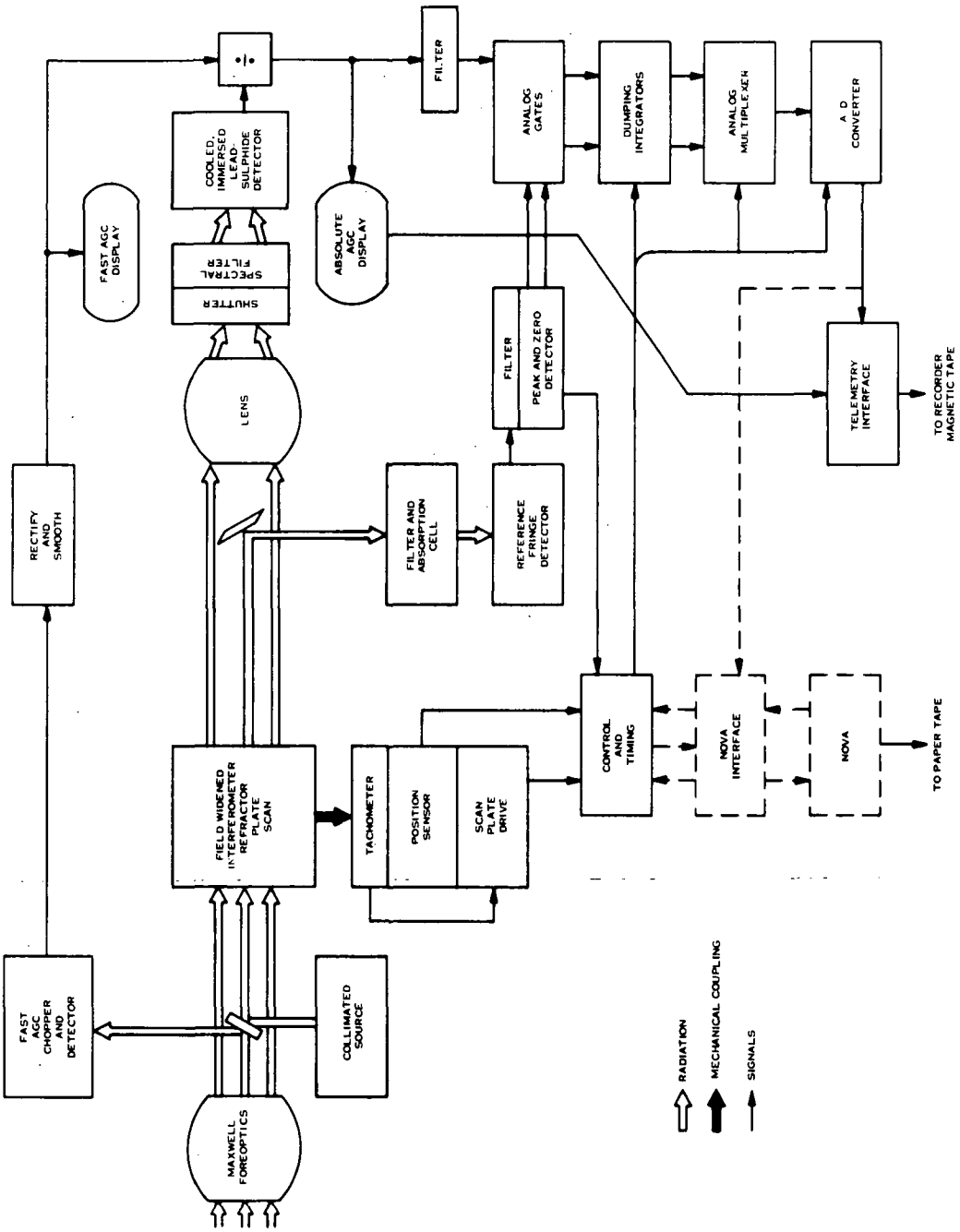

Figure 6.1 System Block Diagram

The incident radiation is collected by 4.8 inch diameter, f/4, Maxwellian fore-optics with a 7.5° field stop. The radiation then traverses the field widened, refractively scanned interferometer as a 7° beam and is then imaged onto the immersed, dry-ice-cooled, lead sulphide detector by a f/1.5 silicon lens. The spectral band is defined by a temperature controlled interference filter located at the detector housing and a rotary-solenoid-actuated shutter, directly in front of the filter, serves to interrupt the radiation, when required, for automatic gain control (AAGC).

The path difference in the interferometer is scanned by tilting the scan plate by means of a torque motor, using a drive waveform shaped so that the path difference decreases linearly over 3/4 of the scan and the plate returns rapidly to zero during the remaining 1/4. During the linear portion of the scan the main detector sees a portion of the radiation as an amplitude modulated 1 kHz sinusoid. This is the interferogram of the absorption spectrum due to the atmospheric path traversed by the radiation.

A second optical path, co-axial with the main beam, takes radiation from a quartz/iodine lamp through a collimator, a spectral filter and the interferometer, exiting, just in front of the main silicon lens, to a gas cell, a telescope and a room temperature PbS detector. The output of this detector is another 1 kHz sinusoid, the reference interferogram, whose shape is determined by the absorption in the gas cell. The reference interferogram establishes the path difference scale for the scan.

The signal from the main detector preamplifier goes to the dividend input of an analog divider, for which the divisor input is a voltage proportional to the irradiance level at the instrument. This signal, which monitors the total irradiance and its fluctuations up to 20 Hz, is generated by a bore-sighted, radiometric (fast AGC) channel, operating in the same spectral band as the interferometer.

The quotient output of the divider is then proportional to the fraction of the received radiation which is modulated by the interferometer. To maintain the proportionality constant, in spite of long-term changes in the relative responsivity of the main and FAGC channels, the radiation to the main detector is, periodically, interrupted and the amplitude of the resulting pulse is measured, at the quotient output of the divider, digitized (as the reciprocal), displayed and recorded. If the relative responsivity of the main and FAGC channels remains constant, so does the pulse, if not, the pulse amplitude is proportional to the relative responsivity and is used, during data reduction, to correct for any relative responsivity changes.

From the FAGC divider output, the main signal is filtered by 10% bandwidth filter centered at 1 kHz and then input to two synchronous rectifiers, which are just electronic switches, opened and closed by square waves derived from the peaks and zero crossings, respectively, of the reference interferogram. Two channels are used, separated by 90° in phase, because the main interferogram is, in general, out of phase with the reference interferogram.

The outputs of the synchronous rectifiers are supplied to two dumping integrators whose outputs are sampled and reset to zero at fixed increments of path

difference as determined by counting the zeros of the reference interferogram. The integrator outputs are sampled, sequentially, by a 12-bit A/D converter. The digitized values (2 per sample) are buffered and clocked out to telemetry while the next sample is being taken.

The portion of interferogram sampled is delimited by the "RUN" pulse, which goes high when the scan plate passes through a given position, as determined by a LED/photodiode sensor, and goes low after n(m + 1) - 1 zero crossings of the reference interferogram, where m is the length of a sample and n is the number of samples/scan. The integrators are allowed to run for m cycles of the reference, the remaining cycle being used to dump the accumulated charge. As a check on scan operation, the length of the run pulse is measured in terms of an internal crystal clock, displayed on the LED display and is also output.

The temperature of the main channel spectral filter and of the enclosure containing the interferometric components and the reference channel filter, are both controlled above ambient by proportional and integral controllers and thermistor sensor. Even though the path difference in the interferometer is stabilized by the use of an ultra low expansion structure and by temperature control, so that the delay is essentially controlled by the position of the scan plate, it is also advisable to have a means of monitoring the absolute delay, so as to check for any long term drifts or displacements due to mechanical shock. The number of reference interferogram peaks occurring between the mechanically generated start of scan pulse and a pulse denoting the position of a local maximum in the reference interferogram is counted and displayed.

For test and checkout purposes, the system can be interfaced with a Nova mini-computer, so that the resulting system very closely resembles the breadboard model of the correlation interferometer.

As well as storing and accumulating the sample values, the Nova can be used to control the engineering model system, as was done in the breadboard instrument. The control program is conversational, via a teletype, and permits the operator to set the number of samples/scan and the number of scans to be co-added and to have the accumulated sample values either printed out and/or punched on paper tape or to have them multiplied by any one of a set of 8 stored correlation functions and output the sum of the resulting products. The stored correlation functions are input, as required, from paper tape and there is also the facility to re-enter a previous set of sample values from tape and treat it with correlation functions. All operator input points in the program are trapped to prevent accidental overwriting of stored program or data and the A/D converter data is trapped for overflow.

Comparing the engineering model with the breadboard model of the correlation interferometer, the major changes in functional blocks are the addition of control, telemetry and "housekeeping" blocks to replace the Nova mini-computer, the provision of "fast" AGC, the substitution of unit-magnification Maxwellian fore-optics for the Newtonian telescope used in the breadboard and the separation of the main and reference channels so that they no longer share a single field stop and spectral filter.

6.2 System Parameters

The data and operating experience gained during the construction and testing of the breadboard model correlation interferometer (ref. 2) showed that, while there were several areas in which the design could be improved, the major radiometric and interferometric parameters were well chosen. Accordingly, these parameters (etendue, detector NEP, operating wavelength and scan range) were carried over to the engineering model design. The external field of view was changed from 2 x 2° to 7 x 7° (equal to the internal field of view of the interferometer) to give a ground resolution element compatible with the V/h characteristics of the intended flight vehicles. This change in field permitted a reduction in instrument size by the elimination of the fore-optics telescope used with the breadboard.

The Engineering Model Correlation Interferometer is shown in Figure 6.2. The light-colored object in the left center is the frame made of ultra-low-expansion material. The gray object seen through the frame opening is the oscillating compensating plate. The two fixed mirrors are shown on the extreme left and in the center. The detector is on the upper right.

The major system parameters for the engineering model are listed in Table 6.1. The bulk of the changes from the breadboard design occurred at the subsystem level.

6.3 Engineering Model Correlation Interferometer Testing

In order to properly evaluate the performance of the engineering model correlation interferometer a series of tests of the instrument was carried out. These consisted of tests in the laboratory, outdoors at Valley Forge, Pa. and Hampton, Va., on board a Falcon Fan-Jet and on board a Jet Ranger Helicopter. The flight tests are described in sections 7 and 8 of this report.

6.3.1 Multiple Chamber Test Facility.- The multiple chamber test facility was designed to permit known amounts of test gas to be introduced into the optical path of the instrument between the source and the fore-optics. Since it was necessary for the complete 7° field of view of the instrument to be filled by an extended area source of nearly uniform radiance, the cells were constructed with an inside diameter of 30.5 cm (12.0 in.). This permitted cells with a total length of 150 cm (59.05 in,) to be connected together, and still allowed the conical field of view of the instrument to clear the inside surfaces of the cells and view the source. The details of the test facility are shown in Figures 6.3 and 6.4.

Each of the three cells which comprise the multiple chamber system is equipped with a vacuum gauge which is used for testing for leaks and for determining when the cell is sufficiently evacuated to be filled with test gas. The cells can be isolated from a common manifold which is used for evacuating the cells and for filling them with the proper gas mixture. The pressure of the gas in the pumping mainfold, and hence the pressure in the individual cells with the appropriate valves opened, is determined by means of a mercury manometer.

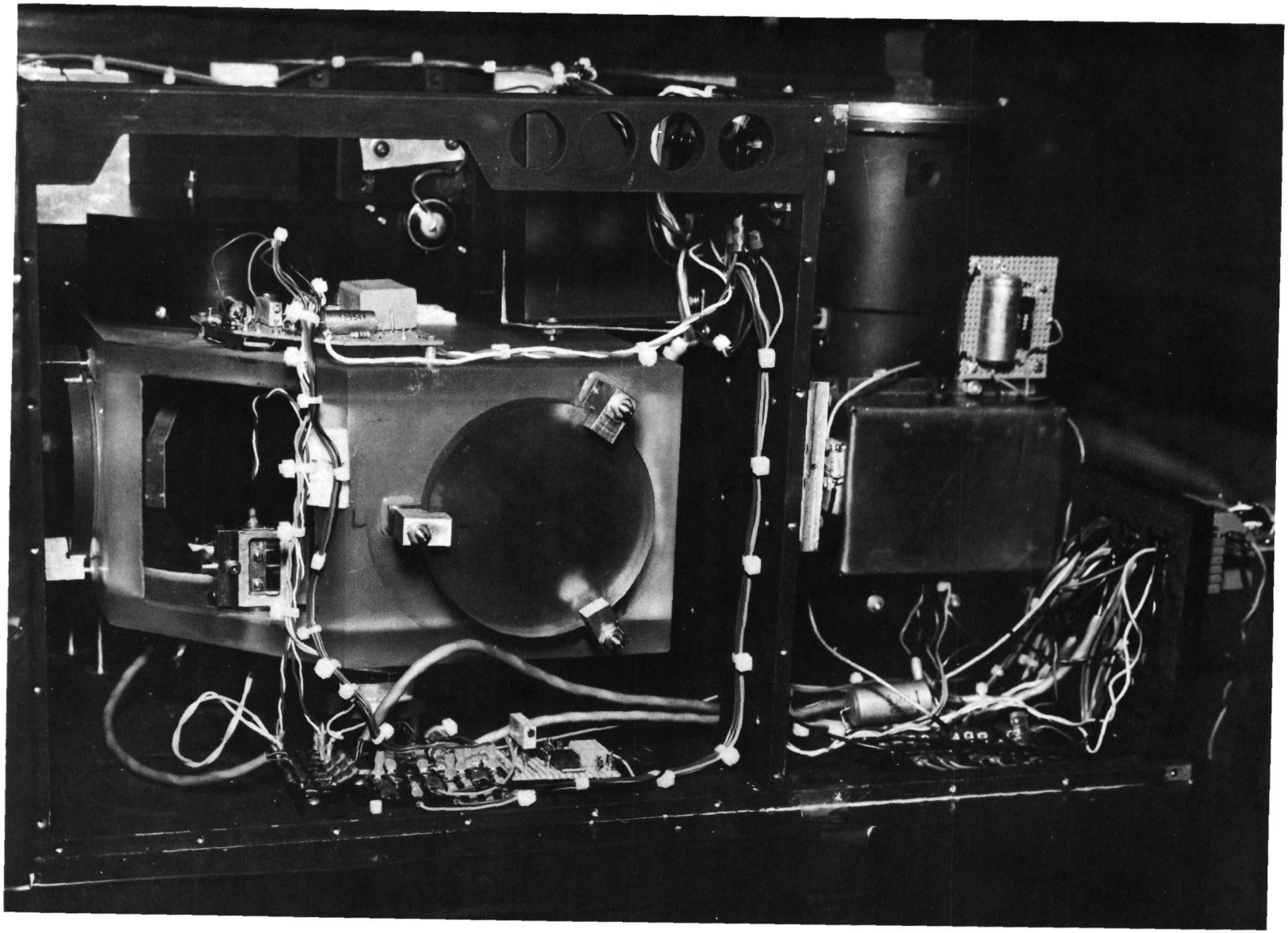

Figure 6.2 Engineering Model Correlation Interferometer Sensor

TABLE 6.1 ENGINEERING MODEL SYSTEM PARAMETERS

Aperture	
Interferometer	6.6 cm diameter
Field of View	
Interferometer	0.12 radian diameter
Spectral Band	4260 - 4400 cm^{-1}
Delay Scan Range	2.5 - 3.9 mm
Number of Sample Points	0 - 64
Sample Length	1 - 63 fringes
Scan Rate	1 Hz
Noise Equivalent Power	1.6 x 10^{-11} watts/$Hz^{1/2}$
Noise Equivalent CO Amount (2% Albedo, τ = 1 sec.)	0.004 atm-cm
Detector	Cooled (195 °K) PbS Immersed on $SrTiO_3$
Weight	
Interferometer	55 lb.
Electronics	41 lb.
Power	168 watts at 24 volts

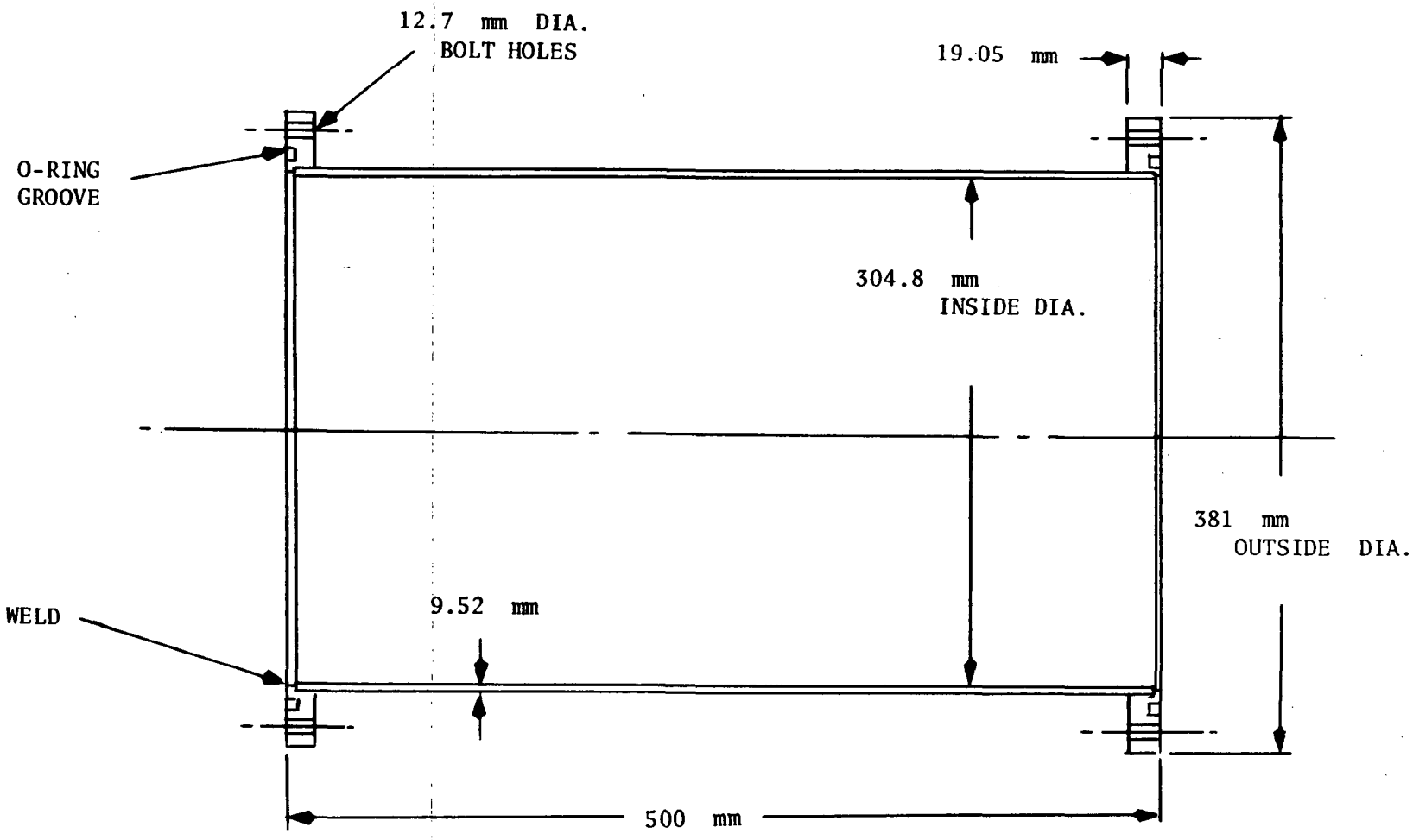

Figure 6.3 Test Cell

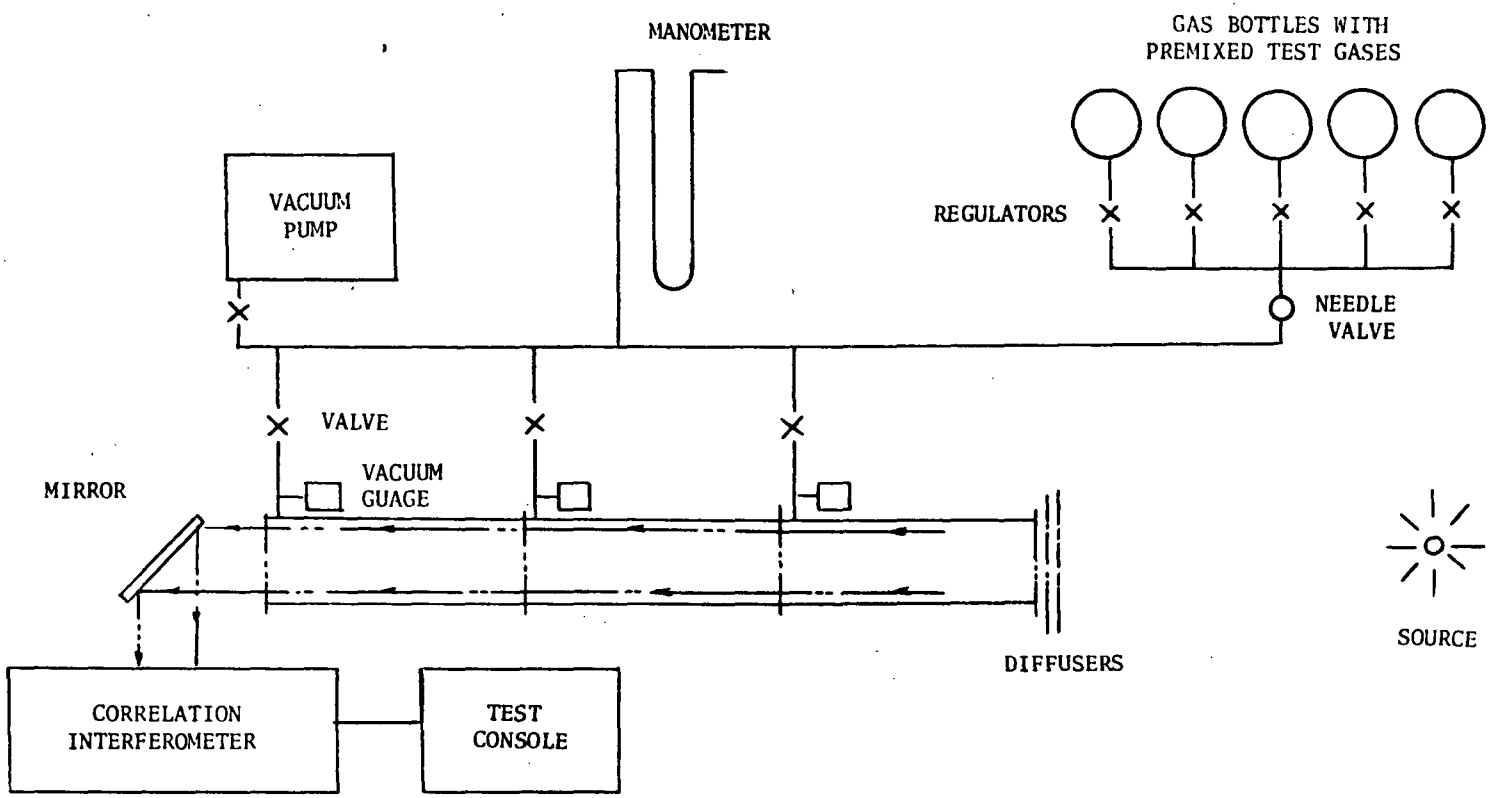

Figure 6.4 Multiple Test Facility

The individual cells are constructed from aluminum pipe with an inside diameter of 30.5 cm (12.0 in.). Aluminum flanges are welded to each end of the pipe to make each cell a self-contained unit which can be used individually or bolted together with other cells to form a longer optical path. The windows, which are 2.54 cm (1.0 in.) thick polished pyrex plate glass, are clamped between the cells and sealed with O-rings to provide a leak-free system. Each cell forms a unit with an optical path length of 50 cm (19.68 in.).

A tungsten halogen lamp provides the infrared energy source for the tests. The lamp illuminates a set of three sheets of pyrex plate glass with a rough ground surface. These scatter and diffuse the energy to provide a uniform diffuse source for the interferometer to look at. A variable voltage transformer is used to control the lamp power and hence the light output. For outdoor testing the sun's rays are directed parallel to the axis of the cell system onto the diffuser plates by means of plane or concave mirrors.

The cells, the source, the pumping manifold, and the correlation interferometer were all mounted on a laboratory table provided with wheels. This makes the complete system mobile and quite easily moved outdoors for tests.

6.3.2 Laboratory Tests of the Correlation Interferometer.- The laboratory tests of the instrument were designed to determine the sensitivity of the correlation interferometer to carbon monoxide in the presence of interferents when the measurement light levels were equivalent to an earth albedo of 30 to 40%. The laboratory tests of the breadboard (ref. 2) demonstrated the ability of the interferometer to make the type of carbon monoxide measurements required. The lead sulphide detector initially installed in the engineering model correlation interferometer is the same detector which had been used in the breadboard instrument. It became necessary to use the same detector when the detector manufacturer was unable to supply a new detector with higher sensitivity in time for the instrument tests.

All of the interferent gases cannot be introduced into the test cells in the quantities present in the atmosphere. Water, which is a significant interferent at 2.35 μm cannot be introduced in significant quantities in the 150 cm (59.05 in.) cell length available. However, the effects of methane and carbon monoxide can be studied with realistic atmospheric amounts. A study of the correlation interferometer response to combinations of these two gases is sufficient to determine its operating parameters.

The gases used for these tests were various premixed gases (30% methane in nitrogen, 5.21% methane in nitrogen, 2.1% carbon monoxide in nitrogen, 1% carbon monoxide in nitrogen, and 0.1% carbon monoxide in nitrogen) together with pure nitrogen for use in diluting the available mixtures when necessary. The optical thickness of gas desired is introduced into the system by (1) evacuating the system, (2) filling one or more cells with the required mixture, (3) re-evacuating the remaining system, and (4) repeating the procedure until all needed cells are filled.

The nominal background amounts of carbon monoxide and methane in a double vertical path through the atmosphere are given as:

1. 0.18 atm-cm of carbon monoxide (corresponding to a constant mixing ratio of carbon monoxide of 0.1 ppm)

2. 2.80 atm-cm of methane (corresponding to a constant mixing ratio of methane of 1.6 ppm)

These gas quantities have been computed from atmospheric concentration models for carbon monoxide and methane which have been discussed previously (ref. 5).

The laboratory tests were conducted with a small matrix of methane and carbon monoxide conditions. The methane consisted of 3 amounts from 1.75 to 3.50 atm-cm and the carbon monoxide consisted of up to 5 amounts ranging from 0 to 1.0 atm-cm. The test matrix with a range of carbon monoxide and methane mixtures is necessary to permit computation of a correlation function applicable over the range of test gases selected. The basic procedure in generating a set of data to be used in determining a suitable correlation function for the methane and carbon monoxide mixture, is the following:

1. A test condition is set up in the gas cells which corresponds to a nominal background amount of the gases used. In this case 2.6 atm-cm of methane and 0.2 atm-cm of carbon monoxide was used since this corresponded to approximately the amount of gas in a vertical atmospheric column for a double pass through the atmosphere.

2. A series of interferogram scans is then obtained and coadded at some predetermined sampling interval. In this case interferograms each consisting of 31 sampling points equally spaced over the selected path difference interval were collected. A minicomputer data handling system collects and formats the data, and outputs a punched paper tape record.

3. The nominal amount of carbon monoxide in the cell is then increased by a predetermined amount, known as the target amount, which was 0.30 atm-cm for the purposes of the tests. The interferogram for this methane and carbon monoxide condition is then sampled as above.

4. This is repeated for a series of test conditions in which the carbon monoxide is maintained at 0.2 atm-cm and the methane is varied. For these experiments the three methane amounts varied from 1.75 to 3.5 atm-cm.

The measurements were run twice to provide duplicate measurements to be used as test cases. In addition, some other combinations of methane and carbon monoxide were run as test cases.

The data is all recorded on punched paper tape and then is input through the GE time-share computer system for storage on disc. Using these stored in-

terferograms, various correlation functions can be computed and applied to interferograms of test cases to obtain a measure of the carbon monoxide in the path.

The procedure for computing the correlation functions is described in Section 4.2. The application of the correlation function to a measured interferogram to yield a corresponding value of CO or CH_4 is as follows:

1. The interferogram consists of a set of 31 in-phase points, [I(k)], and 31 quad-phase points, [Q(k)], due to the synchronous detection process.

2. The correlation function similarly has values H[I(k)] and H[Q(k)] corresponding to each of the interferogram points.

3. The measured value of CO, for example, is given by the expression

$$q(CO) = \sum_{k=1}^{31} \left\{ H[I(k)]I(k) + H[Q(k)]Q(k) \right\} \times \frac{N_c}{N_m} \times \left\{ q(CO)_{target} - q(CO)_{nominal} \right\} + q(CO)_{nominal}$$

where:

$q(CO)$	is the measured value of CO
$q(CO)_{target}$	is the value of CO in the interferogram used as a target increment in the correlation function matrix
$q(CO)_{nominal}$	is the value of CO in the interferogram used as a background amount in the correlation matrix.
N_c	is the number of scans co-added to form the matrix of correlation interferograms
N_m	is the number of scans co-added in the interferogram to be measured.

In a similar manner it is possible to set up a matrix of test cases to measure methane (or other gases) and compute a correlation function.

Following the September 1973 flights in Ottawa, Canada, the interferometer was found to have had a mechanical displacement in the torque motor which drives the oscillating refractor plate. This was corrected and some modifications were also made in the detector pre-amplifier circuit and in the temperature control circuits which stabilize the interferometer temperatures. When these modifications were completed the new lead sulphide detectors were available and one of

these was installed before further laboratory testing was initiated. The new detectors (designated #001 and #992) were found to have a nitrogen hold time of about 6 hours at room temperature, and when installed in the interferometer the hold time with dry ice and methanol was better than 12 hours. Methanol or acetone was used in the detector in place of the glycol when it was found that the glycol became quite viscous at dry ice temperatures raising the possibility that the detector temperature might not be constant.

With the new detector installed, matrices of test cases were run to again verify instrumental noise and offsets from sources other than detector noise. The new detector and its spare were replaced and interchanged to determine the magnitude of inaccuracies which might result if replacement of a detector became necessary. In addition, a series of measurements was conducted with the incident light level chopped at frequencies between 5 and 60 Hz to attempt to simulate the effects of varying ground albedo on the measurements. These data are given later in the section describing the results of laboratory tests.

6.3.3 Outdoor Correlation Interferometer Tests.- After the operation of the engineering model correlation interferometer had been verified in the laboratory, it was taken outdoors to make measurements using radiation which has traversed a real atmospheric path. The outdoor tests were designed to demonstrate the ability of the instrument in making measurements of carbon monoxide and methane in the presence of large amounts of water vapor, which is an interferent at 2.35 μm.

The primary purpose of the outdoor tests was to obtain a set of interferograms from the correlation interferometer covering a wide range of atmospheric conditions. Some of these interferograms were then used to generate correlation functions which were optimized for detecting carbon monoxide and methane against their background atmospheric interferent gases over the range of test conditions for which the data were generated.

The multiple chamber system used during the laboratory tests was taken outdoors for use in adding increments of known amounts of carbon monoxide and methane to the optical path which included a single atmospheric path. For these tests the light source is the sun itself. A 35.6 cm (14.0 in.) square mirror was used to direct the sunlight into the cells approximately parallel to the axis of the cells and the instrument. The sunlight was diffused at the entrance window of the cells by directing the sunlight onto a ground pyrex diffuser plate which covered the entire cell aperture. A total of three diffuser plates was employed to attenuate the sunlight at the interferometer to a value which corresponds to that seen by the instrument looking at a sunlit body with an albedo in the range of 30 to 40%.

A number of outdoor measurements were made with the apparatus shown in Figure 6.5 using sunlight in the vicinity of the General Electric Valley Forge Space Center. The solar evaluation angles during the test were such that the atmospheric air mass covered varied by a factor of about 3, with a corresponding variation in the range of carbon monoxide and interferent gases.

The test procedure was as follows:

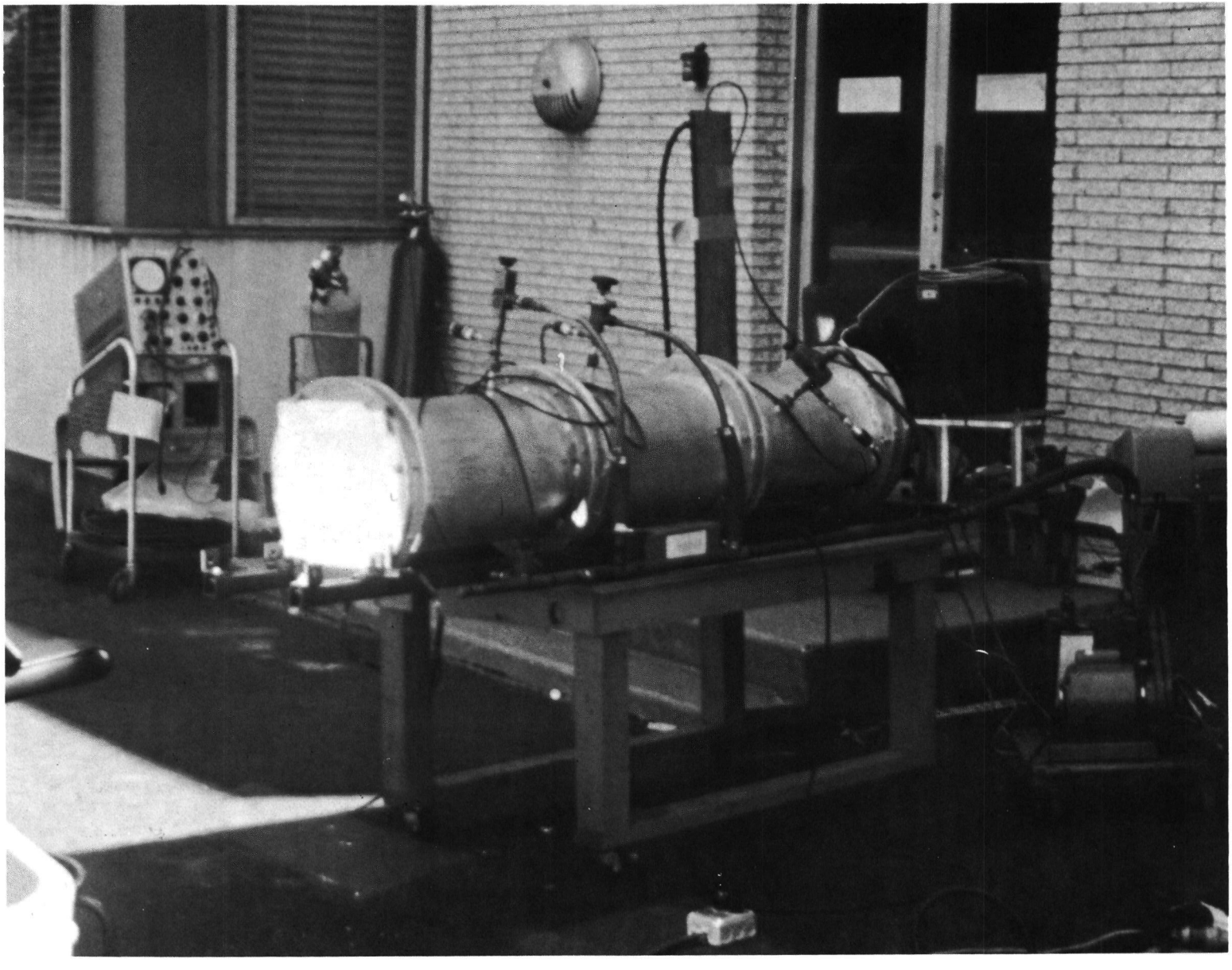

Figure 6.5 Outdoor Experimental Setup

1. An inteferogram was obtained with the cells evacuated and only the background atmospheric amounts of carbon monoxide and interferents in the optical path.

2. The carbon monoxide in the path was then successfully incremented by 0.5, 1.0, and 1.5 atm-cm by introducing the bottled carbon monoxide mixture into the cells, and the corresponding interferograms obtained.

3. The carbon monoxide was pumped out of the cells and the methane was then incremented by 1.5, 3.0, or 4.5 atm-cm and the interferograms obtained.

4. Other combinations of carbon monoxide and methane increments were also run, and interferograms for the atmospheric background amounts of gas were also obtained at regular intervals.

The purpose of collecting a large number of interferograms during the course of a day was to obtain a matrix of test cases which covered the range of carbon monoxide, methane, and water anticipated during flight testing of the instrument. The outdoor tests provided a set of measurements which was used in computing correlation functions for carbon monoxide and methane, which were then applied to the outdoor data (not used in generating the correlation functions) as a test of the instrument's measurement capabilities.

6.3.4 Corroborative Measurements.- At the same time that outdoor measurements were being made with the correlation interferometer, auxiliary solar spectral absorption measurements were being made in order to define the atmospheric amounts of carbon monoxide and methane at the time of the measurements. This measurements program was carried out by NASA Langley Research Center personnel operating from their instrumented van located at Valley Forge, Pa. The instrumentation within the van consisted primarily of a Fourier transform spectrometer with a maximum spectral resolution of 0.1 cm^{-1}. A sun tracker mounted on the roof of the van permitted the sun's rays to be continuously directed into the spectrometer to obtain atmospheric absorption spectra. The solar absorption spectrum covered the carbon monoxide fundamental band at 4.6 μm and the tail of the methane band in the region of 3.7 μm. These spectra were obtained at a resolution of 0.25 cm^{-1} using a liquid nitrogen cooled HgCdTe detector. Although the interferometer spectrometer has a maximum resolution of 0.1 cm^{-1}, the spectra were obtained at a resolution of 0.25 cm^{-1} in order to provide spectra with acceptable signal to noise in a reasonable measurement time. Since the sun tracker did not provide perfect tracking it was necessary to compromise on the spectral resolution. The measurement time for the 0.25 cm^{-1} spectra was up to 2 minutes. This resolution was found to be acceptable for the purpose of determining the atmospheric levels of carbon monoxide and methane. The atmospheric spectra were obtained at periodic intervals during the day while the measurements with the correlation interferometer were being made.

In order to relate the spectra with specific amounts of carbon monoxide and methane, calibration absorption spectra of known amounts of carbon monoxide and methane in a cell were obtained. These were used to generate calibration

curves of line absorption vs gas amount for the carbon monoxide and methane lines which were least overlapped by water vapor lines in the atmospheric spectra. These calibrations were then used to determine the amounts of carbon monoxide and methane in the atmospheric absorption spectra taken during the time that atmospheric measurements were being made with the correlation interferometer.

Following the Canadian flights in April 1974, the correlation interferometer was taken to NASA Langley Research Center for calibration and determination of weighting functions to be applied to the flight data. The calibration was carried out using the multiple chamber test facility in a manner similar to that described in Section 6.3.3. The instrumented NASA van was also employed at this time to provide the spectral data needed to determine the CO and CH_4 in the atmospheric path at the same time that the calibration measurements were being made with the correlation interferometer

6.4 Engineering Model Test Results

6.4.1 Laboratory Tests.- The laboratory tests conducted with the engineering model were mainly designed to determine the instrumental measurement noise and stability. Since the lead sulphide detector used in the instrument during these initial tests was that from the breadboard interferometer, the noise and sensitivity characteristics were not as good as calculated, based on the specifications of the detectors on order.

The laboratory data in Table 6.2 were computed from the test matrix with a nominal carbon monoxide value of 0.197 atm-cm and a target carbon monoxide value of 0.55 atm-cm. In these tests, conducted in May 1973, the nominal case was chosen to have carbon monoxide and methane values close to their expected values during outdoor measurements. The target case then increments only the carbon monoxide by a pre-selected amount. In this way the instrument response to a known amount of carbon monoxide was determined. In this case the test data were computed on the basis of 128 co-added scans. Table 6.3 indicates that the measurement accuracy is generally much better than 10%. Extrapolation of the carbon monoxide values to 1.00 atm-cm yields a lower measured value of the carbon monoxide by 5% or less. However, the breadboard tests indicated that the carbon monoxide absorption is becoming non-linear for these larger amounts of carbon monoxide and hence the lower measured value of carbon monoxide is expected. Extrapolation of the carbon monoxide to low or zero values results in a slight offset to the data which amounts to about -0.021 atm-cm. The rms measurement noise is of the order of 0.005 to 0.008 atm-cm.

Table 6.3 shows the same data matrix computed on the basis of 8 co-added scans. This data shows the same trends as the data discussed in Table 6.2 except that the measurement noise level appears to be higher in general. The rms measurement noise is 0.015 atm-cm of carbon monoxide.

In March and April of 1974 a series of laboratory tests of the interferometer were conducted with the new lead sulphide detectors installed in the instrument. A matrix of test cases similar to those obtained for the breadboard detector gave the data in Tables 6.4 and 6.5. Figure 6.6 is a plot of the 31

TABLE 6.2 LABORATORY CARBON MONOXIDE MEASUREMENTS
MAY 1973

NOMINAL CO = 0.197 atm-cm
TARGET CO = 0.500 atm-cm
NOMINAL CH_4 = 2.60 atm-cm
OTHER CH_4 = 1.75, 3.50 atm-cm
MEASUREMENT TIME = 128 Scans
BREADBOARD DETECTOR (193 K)

CH_4 atm-cm	CO atm-cm	MEASURED CO atm-cm	ACCURACY %
1.75	.197	.211	7.1
1.75	.197	.211	7.1
2.60	0	- .030	---
2.60	0	- .010	---
2.60	0	- .025	---
2.60	.025	.005	- 80.0
2.60	.025	- .006	124.0
2.60	.025	- .005	120.0
2.60	.197	.178	- 9.6
2.60	.197	.186	- 5.6
2.60	.500	.491	- 1.8
2.60	.500	.493	- 1.4
2.60	1.000	.950	- 5.0
2.60	1.000	.959	- 4.1
2.60	1.000	.971	- 2.9
3.50	.197	.192	- 2.5
3.50	.197	.209	6.1

TABLE 6.3 LABORATORY CARBON MONOXIDE MEASUREMENTS
MAY 1973

NOMINAL CO = 0.197 atm-cm
TARGET CO = 0.500 atm-cm
NOMINAL CH_4 = 2.60 atm-cm
OTHER CH_4 = 1.75, 3.50 atm-cm
MEASUREMENT TIME = 128 Scans
BREADBOARD DETECTOR (193 K)

CH_4 atm-cm	CO atm-cm	MEASURED CO atm-cm	ACCURACY %
1.75	.197	.209	6.1
1.75	.197	.196	- 0.5
1.75	.197	.211	7.1
2.60	0	- .042	---
2.60	0	- .006	---
2.60	0	- .021	---
2.60	.025	.027	8.0
2.60	.025	- .015	160.0
2.60	.025	.008	- 68.0
2.60	.197	.168	- 14.7
2.60	.197	.192	- 2.5
2.60	.197	.211	7.1
2.60	.500	.553	10.6
2.60	.500	.490	- 2.0
2.60	.500	.494	- 1.2
2.60	1.000	.915	- 8.5
2.60	1.000	.974	- 2.6
3.50	.197	.185	- 6.1
3.50	.197	.158	- 19.8
3.50	.197	.193	- 2.0

TABLE 6.4 LABORATORY CARBON MONOXIDE MEASUREMENTS
APRIL 1974

NOMINAL CO = 0.208 atm-cm
TARGET CO = 0.525 atm-cm
NUMBER OF SCANS = 128

NOMINAL CH_4 = 2.60 atm-cm
OTHER CH_4 = 1.74, 3.48 atm-cm
DETECTOR #002 (193 K)

ACTUAL CH atm-cm	ACTUAL CO atm-cm	MEASURED CO atm-cm	ACCURACY ACCURACY %
1.74	0.208	.214	2.9
1.74	0.208	.214	2.9
2.60	0	.031	---
2.60	0	.019	---
2.60	0	.028	---
2.60	0.208	.209	0.4
2.60	0.208	.208	0.0
2.60	0.525	.480	- 8.6
2.60	0.525	.473	- 9.9
3.48	0.208	.185	-11.1
3.48	0.208	.164	-21.2

TABLE 6.5 LABORATORY CARBON MONOXIDE MEASUREMENTS
APRIL 1974

NOMINAL CO = 0.208 atm-cm
TARGET CO = 0.525 atm-cm
NUMBER OF SCANS = 8

NOMINAL CH_4 = 2.60 atm-cm
OTHER CH_4 = 1.74, 3.48 atm-cm
DETECTOR #002 (193 K)

ACTUAL CH atm-cm	ACTUAL CO atm-cm	MEASURED CO atm-cm	ACCURACY %
1.74	0.208	.242	16.4
1.74	0.208	.219	5.3
1.74	0.208	.234	12.5
2.60	0	.015	---
2.60	0	.019	---
2.60	0.208	.206	- 1.0
2.60	0.208	.193	- 7.2
2.60	0.208	.178	-14.4
2.60	0.525	.438	-16.6
2.60	0.525	.480	- 8.6
2.60	0.525	.468	-10.9
3.48	0.208	.181	-13.0
3.48	0.208	.170	-18.3
3.48	0.208	.182	-12.5

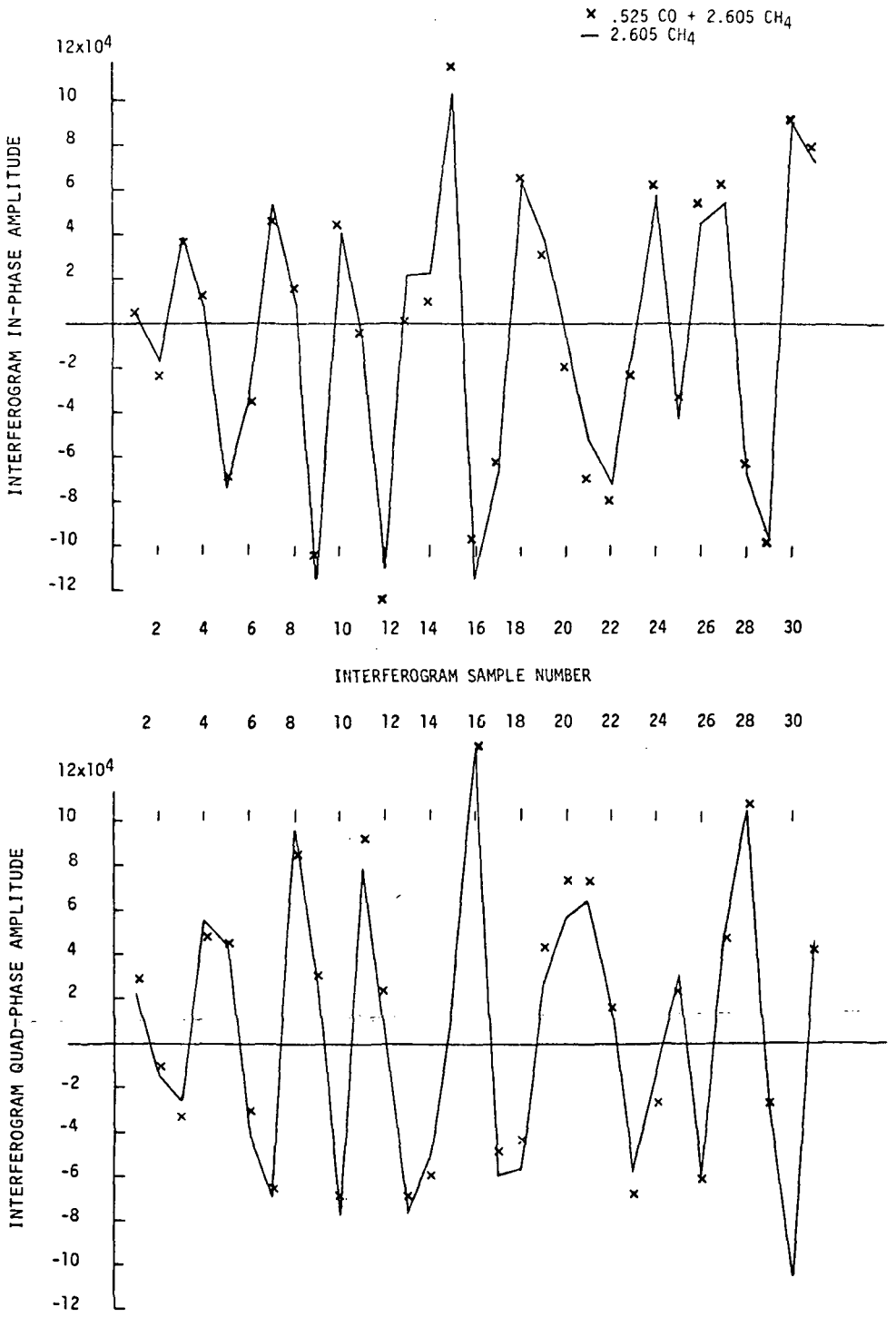

Figure 6.6 Interferogram In- and Quad-Phase Sample Values for 128 Co-added Scans for Laboratory Measurements

interferogram sample points for the in-phase and quad-phase components of the interferogram co-added for 128 scans for two gas conditions in the cells. This actually represents 112 data scans due to the operation of the AAGC shutter. The interferogram output consists of 31 separate values for each phase. In Figure 6.6 these points are connected to show the general shape of the interferogram. However the values between the 31 sample points do not represent interferogram values for a different sampling condition. The continuous interferogram curve shown would change for each sampling condition chosen. This is also true for the other interferograms plotted in Figure 6.8 and Figure 6.10. One case had 2.605 atm-cm of CH_4 and the other case had the same amount of CH_4 with an added increment of 0.525 atm-cm of CO. The second case is designated by x's in Figure 6.6 and indicates the change in the interferogram due to CO. Table 6.6 indicates the weighting function values derived from the data matrix shown in Table 6.7 The weighting function consists of one value for each of the interferogram sample points.

6.4.1.1 Effect of removing or changing detectors: In the testing of the interferometer it was important to determine the effect on the measurement of removing a detector and then re-installing it again, or of replacing one detector with another if one of them should fail. That is, determine if a calibration were performed with a particular detector, would the measurements with the other detector, or the re-installed detector be acceptable. The measurement sequence followed was:

1. To obtain a matrix of measurements with detector #002.
2. Remove the detector and replace it with detector #001.
3. Obtain another measurement matrix.
4. Remove the detector and replace it with detector #002 again.
5. Obtain the same measurement matrix again.
6. Generate a set of weights based on the last test matrix and apply them to the other measurements.

These data are tabulated in Tables 6.4, 6.8, and 6.9.

Comparing the measurements obtained when the detectors are changed it is evident that no significant changes have occurred in the measurement interferograms. The measurement accuracies are generally better than 10%. The few cases which are more than 10% do not indicate a failure of the weights to apply but rather an infrequent transient noise in the system which causes a greater than normal error in the measurement. In Table 6.9 the zero carbon monoxide measurements show an offset of 0.050 atm-cm in the measured carbon monoxide value. However, the measurement of zero carbon monoxide in Table 6.4 (i.e., the matrix used in generating the weights) shows an offset of 0.026 atm-cm. Thus the real difference in the two sets of measurements is only 0.024 atm-cm of carbon monoxide. In actual measurements a correction could be found and applied.

TABLE 6.6 WEIGHTING FUNCTIONS APPLIED TO LABORATORY, OUTDOOR AND FLIGHT DATA

CO LAB WEIGHT		CO LaRC/LAB WEIGHT		CH_4 LaRC WEIGHT	
IN-PHASE	Q-PHASE	IN-PHASE	Q-PHASE	IN-PHASE	Q-PHASE
0	0	0	0	0	0
-2165	-13	-2423	5046	-963	3103
1447	-5013	-3357	808	-1353	1402
2643	-1708	263	-2797	-3981	2667
6034	1905	7172	-3169	-3368	-3360
998	7554	-3118	7618	3290	-4383
-7792	3059	-10438	1436	3475	-165
5756	-9043	4038	-8492	-2617	5495
10589	-6428	4938	-2436	-2210	548
7659	4528	1395	3866	882	-2750
-2975	13121	-3807	3549	3722	1643
-7627	8580	-4692	3303	-8067	8794
-11382	6634	-7506	7780	-2338	-4170
-4515	-5240	-6128	-8631	-3811	3307
6032	-7914	9589	-7476	735	-2367
7895	1203	11056	-1294	-2050	2362
7006	4862	5262	7026	864	237
61	10301	-970	7264	-2480	6821
-4634	11529	-8191	10228	-8923	4832
-9129	8134	-12446	11504	-4557	-3308
-14185	5133	-13089	2978	1594	-4736
-9889	-5624	-5367	-5119	3099	-1960
-4613	-6557	-260	-6594	638	0
789	-9319	4442	-10431	1041	1422
9605	-6995	4721	-1067	-5283	2221
7186	-1327	-1023	494	2804	-7160
3604	-9	842	-6295	6864	-1164
604	-417	9633	183	210	6098
4043	-2618	-4186	7823	-7198	5277
159	3084	6102	-11294	0	-1475
-398	835	6011	-2681	-1296	2481

N.B. The weighting functions are derived from interferograms with 112 scans of actual data. The values should be reduced by a factor of 2×10^9 when applied to interferograms.

TABLE 6.7 INTERFEROGRAMS EMPLOYED IN THE COMPUTATION OF WEIGHTING FUNCTIONS

	CO LAB WEIGHT		CO LaRC/LAB WEIGHT		CH_4 LaRC WEIGHT	
	CO atm-cm	CH_4 atm-cm	CO atm-cm	CH_4 atm-cm	CO atm-cm	CH_4 atm-cm
NOMINAL	.208	2.60	.154	1.78	.115	1.44
TARGET	.525	2.60	.487	1.69	.135	2.38
OTHER	.208	1.74	.115	1.44	.422	1.46
	.208	3.48	.120	1.55	.198	2.48
			.124	3.50		
			.128	2.93		
			.135	2.38		
			.141	1.83		
			.208	2.60		
			.208	3.48		

TABLE 6.8 LABORATORY CARBON MONOXIDE MEASUREMENTS MARCH 1974

NOMINAL CO = 0.207 atm-cm
TARGET CO = 0.525 atm-cm
NUMBER OF SCANS = 128

NOMINAL CH_4 = 2.60 atm-cm
OTHER CH_4 = 1.74, 3.48 atm-cm
DETECTOR #001 (193 K)

ACTUAL CH_4 atm-cm	ACTUAL CO atm-cm	MEASURED CO atm-cm	ACCURACY %
1.74	0.207	0.206	- 0.5
1.74	0.207	0.205	- 1.0
1.74	0.207	0.209	- 1.0
2.60	0	- .011	---
2.60	0	- .010	---
2.60	0	- .011	---
2.60	0.207	0.185	-10.6
2.60	0.207	0.184	-11.1
2.60	0.207	0.178	-14.0
2.60	0.525	0.478	- 9.0
2.60	0.525	0.510	- 2.9
2.60	0.525	0.527	0.4
3.48	0.207	0.165	-20.3
3.48	0.207	0.202	- 2.4
3.48	0.207	0.191	- 7.7

6.4.1.2 Effects of incident light modulation: When the interferometer is mounted in a flight vehicle looking down at the earth, the energy incident on the instrument will vary depending on the type of terrain being covered. The fast automatic gain control system (FAGC) is intended to compensate for light intensity changes which occur with frequency components up to 20 Hz.

A set of tests were performed to exercise the instrument FAGC system over a range of signal frequencies and amplitude modulations which might be expected in flight. These tests were carried out using the multiple chamber test facility with the light source modulated by a variable speed chopper. Figure 6.7 illustrates the source modification made to vary the light intensity. The lamp in front of the chopper was adjusted to provide a mean light level for the measurements. Another lamp behind the chopper illuminated a diffuser which provided a light source which could be chopped at a predetermined frequency. The amplitude of the chopped light was controlled by varying the voltage to the lamp. A gas test condition amounting to 0.208 atm-cm of carbon monoxide and 2.60 atm-cm of methane was set up in the cells and the lamps were adjusted to give a mean light ground albedo of about 30%. The light level as indicated by the FAGC panel display was 8.10. A set of measurements of the carbon monoxide in the cells was made by co-adding 8 scans of data. The rms measurement noise level with this unchopped light condition was .0179 atm-cm of carbon monoxide. The chopped light amplitude was then adjusted to give an FAGC reading of 8.13 ± 1.13 or a light variation of about 14%. Sets of 8 scan measurements were then made as the chopper frequency was varied from 5, 10, 15, 20, 30, 40, and 60 Hz. The amplitude of the chopped light was then changed to a FAGC value of 8.0 ± 2.0 or a light variation of ± 25% and the measurements repeated. The rms noise levels of these measurements were computed and are tabulated in Table 6.10.

The FAGC system design was intended to compensate for light level changes as fast as 20 Hz. However it is seen that the higher frequencies did not cause significantly higher measurement noise. The amplitude of the light variation appears to have a greater effect on the measurement noise than does the frequency of the light variation. Thus in flying over non-uniform terrain with greatly differing values of albedo one might expect the measurements to show more scatter.

6.4.1.3 Variation of measurement noise with indicent light: Most of the measurements were performed at a FAGC value of about 8 which corresponds to a ground albedo of about 30%. Since the FAGC value during flights had been observed at times to fall below this value, it was of interest to determine the measurement noise associated with lower FAGC values. The incident light was adjusted to give values of 2.4 and 4.06 and a set of 8 scan carbon monoxide measurements with o.208 atm-cm of carbon monoxide and 2.60 atm-cm of methane in the cells was made for each of the light levels. The rms noise levels at the lower light levels were as follows:

FAGC	RMS NOISE (atm-cm)
8.0	.018
4.0	.059
2.4	.065

TABLE 6.9 LABORATORY CARBON MONOXIDE MEASUREMENTS
MARCH 1974

NOMINAL CO = 0.207 atm-cm
TARGET CO = 0.525 atm-cm
NUMBER OF SCANS = 128

NOMINAL CH_4 = 2.60 atm-cm
OTHER CH_4 = 1.74, 3.48 atm-cm
DETECTOR #002 (193 K)

ACTUAL CH atm-cm	ACTUAL CO atm-cm	MEASURED CO atm-cm	ACCURACY %
1.74	0.207	.220	6.3
1.74	0.207	.212	2.4
1.74	0.207	.197	- 4.8
2.60	0	.058	---
2.60	0	.058	---
2.60	0	.062	---
2.60	0.207	.224	8.2
2.60	0.207	.218	5.3
2.60	0.207	.218	5.3
2.60	0.525	.460	-12.3
2.60	0.525	.468	-10.9
2.60	0.525	.458	-12.8
3.48	0.207	.208	0.5
3.48	0.207	.190	- 8.2
3.48	0.207	.206	- 0.5

TABLE 6.10 RMS NOISE LEVELS IN CARBON MONOXIDE MEASUREMENTS WITH THE INPUT LIGHT CHOPPED (8 SCANS)

FREQUENCY (Hz)	RMS NOISE (atm-cm) FAGC = 8.13 ± 1.13	FAGC = 8.0 ± 2
0	.0179	.0179
5	.0282	.0456
10	.0314	.0491
15	.0109	.0352
20	.0260	.0184
30	.0322	.0410
40	.0140	.0228
60	.0342	.0130

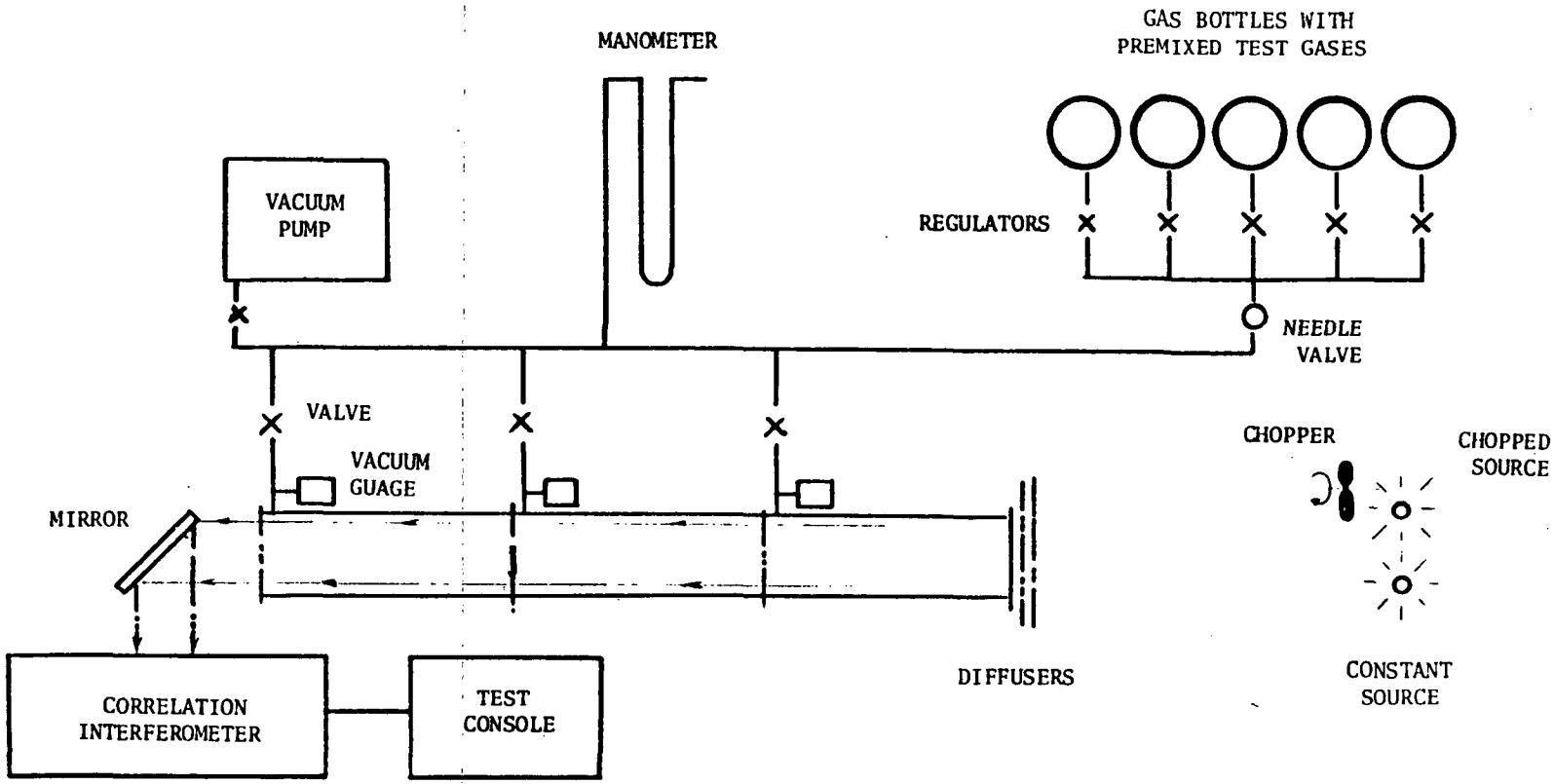

Figure 6.7 Multiple Test Facility with Chopped Source

The noise values do not scale linearly with the light level, but since the computed noise values have a tendency to show some scatter even for similar sets of data, the data do show a general inverse scaling with light level.

6.4.2 Outdoor Tests.- Following the flight tests of the correlation interferometer in May 1973, the instrument was returned to the General Electric Valley Forge Space Center for a series of outdoor measurements which were then used for a determination of correlation functions for carbon monoxide and methane. On June 14th and 15th approximately 60 interferograms were obtained for various combinations of carbon monoxide and methane in the cells as the atmosperic background amounts of carbon monoxide, methane, and water varied during the course of the measurements.

The procedure used for processing the outdoor calibration data was the following:

> The solar absorption spectra were examined and the carbon monoxide lines in the 4.6 μm region, which were found to be the least overlapped with water and nitrous oxide lines, were located. The absorption for the individual lines was measured and compared with the measured carbon monoxide calibration using known carbon monoxide in a gas cell. This provided a carbon monoxide measurement for each of the seven carbon monoxide lines used. An average carbon monoxide level was then determined and a standard deviation computed. The primary carbon monoxide calibration was performed with the gas at 760 torr. Since the real atmosphere contains carbon monoxide at total pressures ranging from 760 torr to very low pressure, and the line absorption for amounts in the range from 0.1 to 0.2 atm-cm are quite strong, it was believed that some correction to the data might be necessary (ref. 7). As a first order correction, carbon monoxide calibrations were obtained for 0.2 atm-cm of carbon monoxide at 760 and 380 torr, and the ratio of the line absorptions calculated. From this data the computed atmospheric values of carbon monoxide were increased by a factor of 1.12. A more accurate correction was not considered justified since the scatter in the spectral data were much greater. The atmospheric carbon monoxide in the path was then plotted as a function of time during the day and a smooth curve drawn through the data points. This permitted interpolation between the data points to obtain carbon monoxide in the atmosphere at times when measurements were made with the correlation interferometer. Table 6.11 shows the background carbon monoxide as a function of time on June 14-15, 1973.
>
> The solar spectral data were treated in a similar manner to extract information regarding the methane in the atmospheric path. The methane spectrum in the vicinity of 3.7 μm was examined for this purpose. Table 6.11 also shows the background methane as a function of time on June 14-15, 1973.
>
> These spectral data were then added to any carbon monoxide or methand increment which may have been in the gas cells at the time that the interferograms were being collected with the correlation interferometer. The interferometer along with carbon monoxide and methane amounts in the

path were input to the computer system for computation of correlation functions for carbon monoxide and methane. It should be noted that not more than 10 test cases were used in computing the correlation function which means that there were approximately 50 interferograms available to use as tests of the applicability of the correlation function.

The computed methane in the path (using the correlation function which appeared to be the best over the complete range of test data) is tabulated in Table 6.12. The corresponding carbon monoxide data (for atmospheric measurements within the range of applicability of the best carbon monoxide correlation functions) are tabulated in Table 6.13. In each case the errors in the spectral measurements of the background gas are shown. If the errors involved in determining the amount of gas in the path spectrally are taken into account, the correlation interferometer measurements of carbon monoxide and methane agree quite well with the known amounts.

Following the April 1974 flights a series of outdoor measurements were made at Hampton, Virginia for calibration purposes. From the matrix of test conditions in the multiple chamber cells, interferograms were obtained from which weighting functions were derived for application to the flight data recorded on the Falcon and helicopter flights. Figure 6.8 illustrates the interferograms collected during the outdoor calibration. One interferogram is for the amount of CO and CH_4 in the atmospheric path with no gas in the cells, i.e., 0.154 atm-cm CO + 1.78 atm-cm CH_4. The second interferogram includes the addition of 0.333 atm-cm of CO for a total amount of 0.487 atm-cm CO + 1.69 atm-cm CH_4.

Table 6.6 indicates a weighting function for CO (CO LaRC/LAB) derived from a combination of the outdoor calibration interferograms and some laboratory interferograms which do not have any effect from water vapor (Table 6.7). Table 6.6 also lists a methane weight (CH_4 LaRC) derived from the Langley calibration interferograms.

A series of flight measurements were made at NASA Langley Research Center with the correlation interferometer mounted on a Bell Jet Ranger 206 helicopter (Figure 6.9). These flights are described in Section 8.

The interferograms collected during the Falcon and helicopter flights have the same general shape as those collected during the outdoor calibration tests. Figure 6.10 is an interferogram measured during the Churchill flights described in Section 7.

TABLE 6.11 CARBON MONOXIDE AND METHANE MEASUREMENTS
USING THE IF-6 INTERFEROMETER
VALLEY FORGE, PA. JUNE 14-15, 1973

DATE	LOCAL TIME	CO (atm-cm)	CH_4 (atm-cm)	
6/14/73*	1100	.090 ± .016	1.03 ± .16	*Strong winds.
	1255	.088 ± .020	1.11 ± .19	
	1445	.107 ± .023	1.16 ± .19	
	1555	.119 ± .033	1.11 ± .23	
	1632	.167 ± .044	1.28 ± .23	
6/15/73	0909	.165 ± .044	1.68 ± .18	

TABLE 6.12 CORROBORATIVE MEASUREMENT OF METHANE
SOLAR LOOKING EXPERIMENT
VALLEY FORGE, PA. JUNE 14-15, 1973

BACKGROUND + CELL INCREMENT atm-cm	CORRELATION INTERFEROMETER atm-cm
1.02 ± .16	0.93
	1.02
	1.03
	1.07
	1.11
1.09 ± .18	0.87
	0.91
1.34 ± .23	1.22
1.40 ± .23	1.25
1.68 ± .18	1.38
	1.46
	1.54
	1.68
2.08 ± .20	2.08
2.55 ± .20	2.45
	2.46
	2.55
3.07 ± .18	2.90
3.31 ± .20	2.82
3.80 ± .20	3.90
4.03 ± .20	4.09
	4.22
4.50 ± .22	4.25
5.27 ± .23	5.24
6.73 ± .23	6.70

TABLE 6.13 CORROBORATIVE MEASUREMENT OF CARBON MONOXIDE
SOLAR LOOKING EXPERIMENT
VALLEY FORGE, PA. JUNE 14-15, 1973

BACKGROUND + CELL INCREMENT atm-cm	CORRELATION INTERFEROMETER atm-cm
.082 ± .020	.082
	.108
.084 ± .020	.084
.085 ± .020	.049
	.085
.088 ± .020	.076
.095 ± .020	.124
	.144
.100 ± .023	.063
	.100
.122 ± .033	.112
.124 ± .033	.156
.155 ± .040	.167
.202 ± .045	.260
.220 ± .045	.265
.267 ± .045	.235
	.250
.583 ± .020	.552
.584 ± .020	.591
.593 ± .020	.558
	.616
.605 ± .023	.620
.630 ± .035	.680
.667 ± .044	.658
	.681
.682 ± .045	.657
1.08 ± .016	.991
1.09 ± .016	1.06
	1.06
1.58 ± .020	1.56
	1.57
	1.57

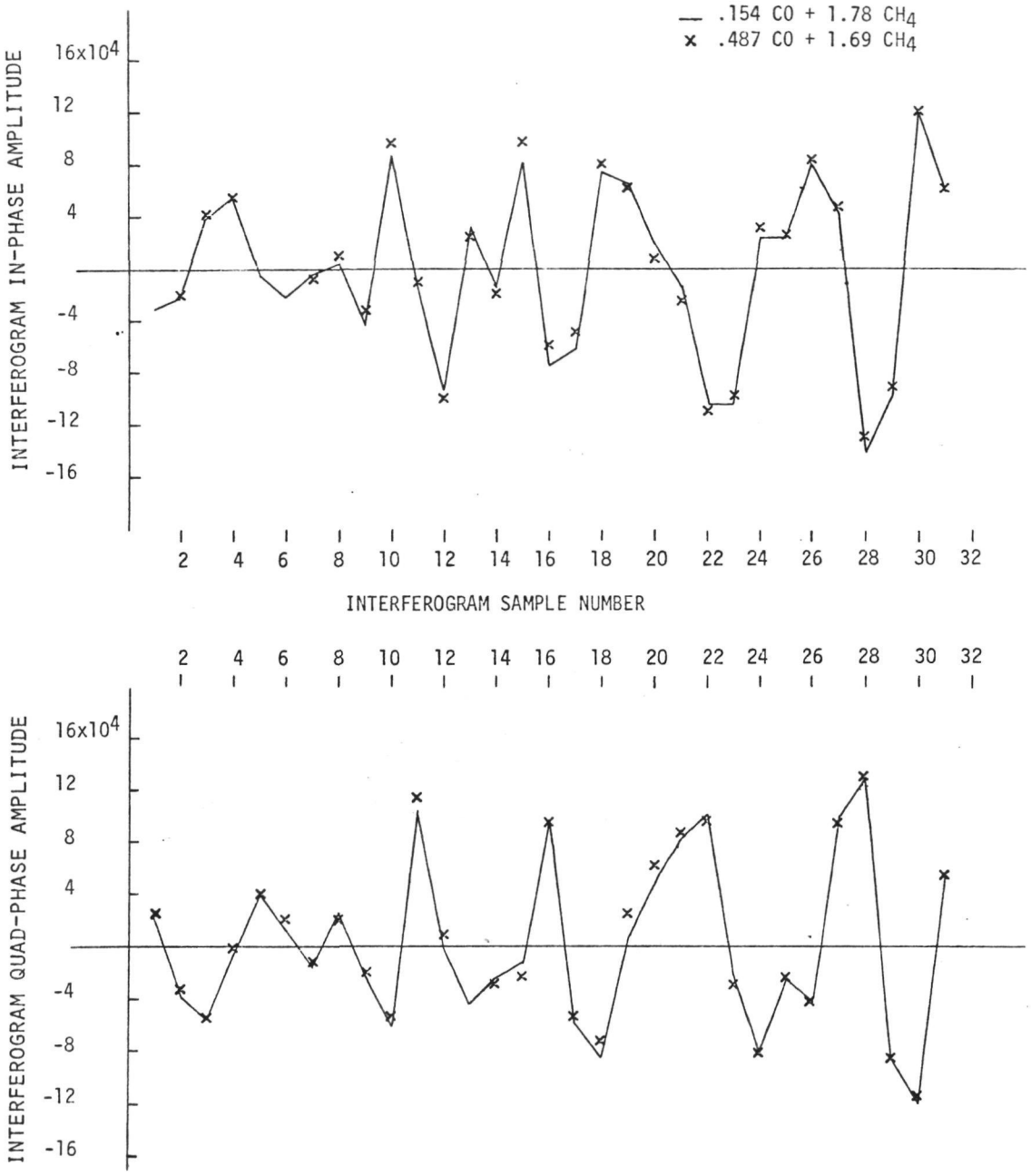

Figure 6.8 Interferogram for In- and Quad-Phase Sample Values for 128 Co-added Scans for Outdoor Measurements at NASA Langley

Figure 6.9 The Helicopter Platform Over the NASA Van

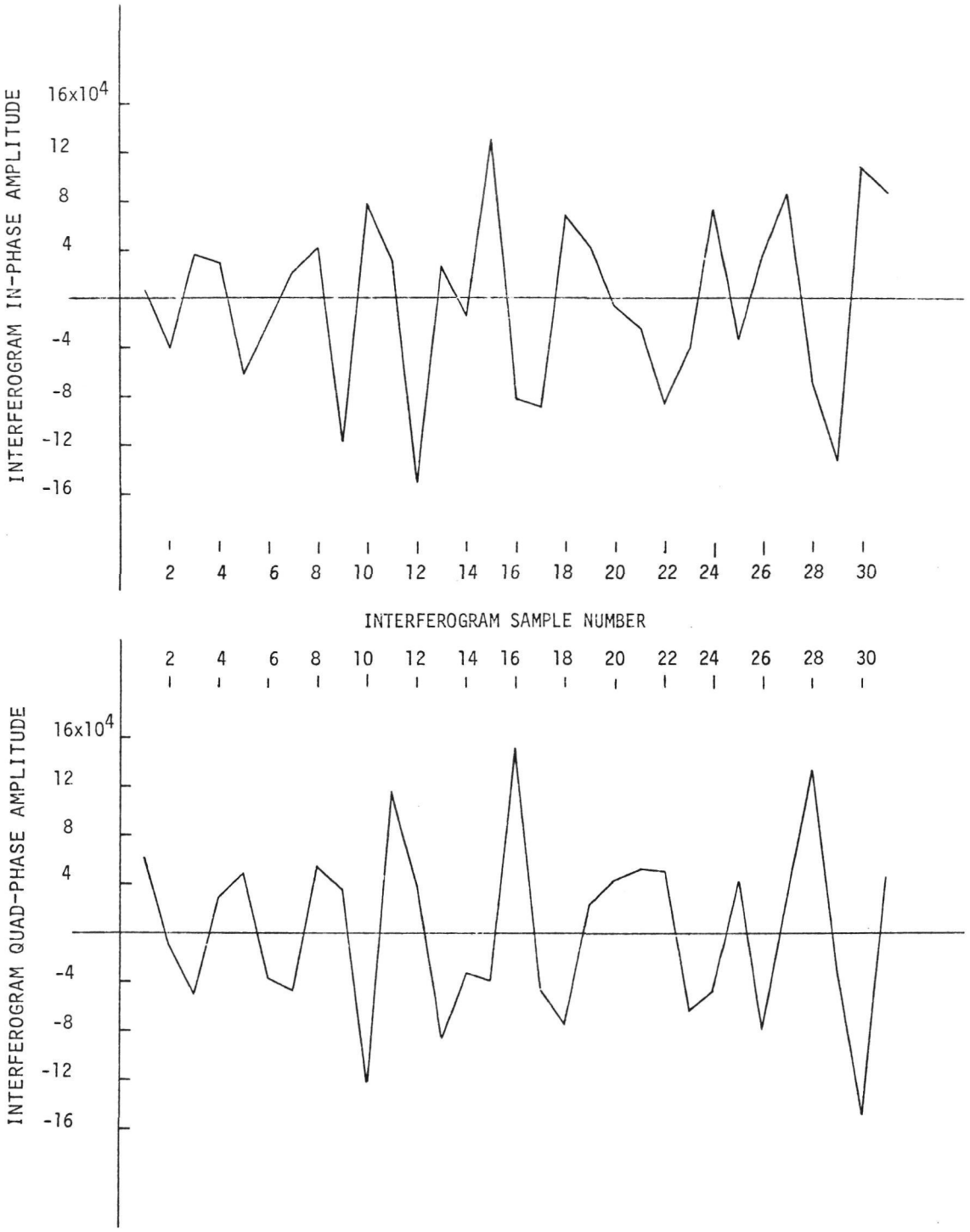

Figure 6.10 Interferogram In- and Quad-Phase Sample Values for 128 Co-added Scans for the Flights Over Churchill, Canada

Page Intentionally Left Blank

7. ENGINEERING MODEL AIRCRAFT FLIGHT TESTS

7.1 Platform and Interface

The Engineering Model Correlation Interferometer was mounted on board a Falcon Fan-Jet Aircraft. This aircraft was owned and operated by the Airborne Sensing Unit of the Canada Centre for Remote Sensing. It was equipped with two windows in the floor which permitted downward viewing. The interferometer was mounted over the more forward of these windows which was in line with the door of the aircraft. The Falcon is shown in Figure 7.1. The red box in the open doorway is the sensor. A mounting plate was made to fit into mounting positions above the window. Four shock mounts (Barry Controls Model 2K2-BA-25) were placed on the plate. The sensor is shown in position in Figure 7.2. The window can be seen below the instrument. The interferometer was mounted on a second plate which was mounted on shock mounts. Over the aft window was positioned a Panasonic TV camera which looked directly down with a 75° field of view. The 7° field of view of the interferometer was always within that of the TV camera. The TV camera output was recorded on tape which also contained a voice track on which could be put orally any comments and information desired during the flight.

The output of the interferometer was, in general, recorded by a Mincom 14-channel magnetic tape recorder. The following information was recorded:

Interferogram data
2 timing pulses
Interferometer scan time
Fast AGC
Ratio of main channel to FAGC
Time from time code generator
Reference interferogram

The electronics for the interferometer were installed in standard 19" racks which were built into the aircraft. These electronics comprised 3-units -- the power supply, the processor, and the NOVA interface. The NOVA 1200 mini-computer and the teletype units were mounted in the aircraft to permit an occasional on-the-spot determination of the approximate amount of CO burden and a check by use of the standard cell.

A Systron-Donner Corporation time-code generator of IRIG-B format was also mounted on board in such a way that the time -- using a pre-set reference time -- was input onto the data tape and visually displayed. The visually displayed time could then be orally put onto the video tape. For the helicopter flights, to be covered later, a NASA, 36-bit, 100 pulse per second, 1000 cycle carrier, time-code generator was used.

7.2 Data Processing

Processing of the data from the FM recorder tapes recorded during the flights is a two step procedure. The first step is to play the recorded analog

Figure 7.1 Falcon Fan Jet Aircraft with Correlation Interferometer

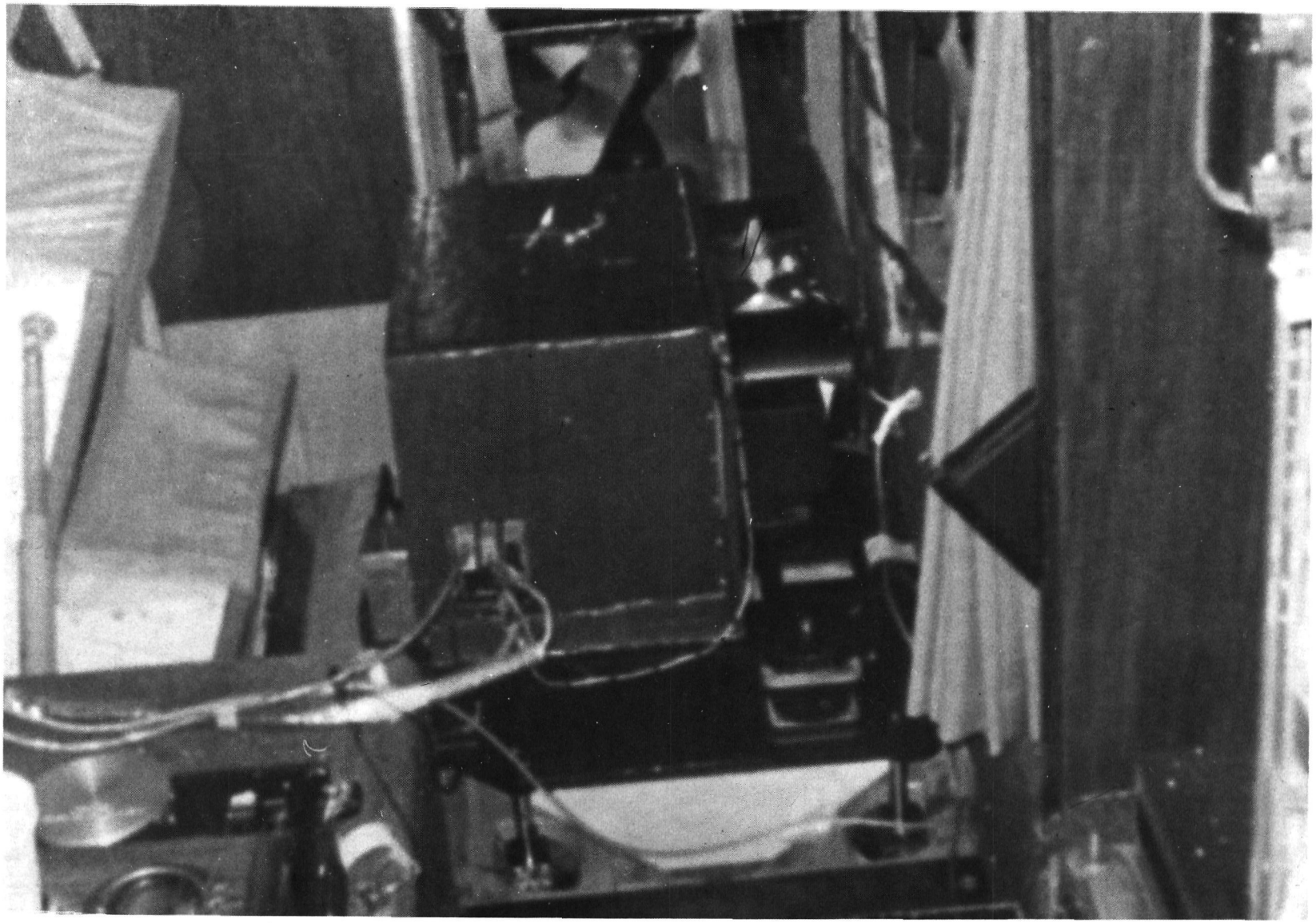

Figure 7.2 Correlation Interferometer Installed Above Falcon Window

tapes into a computer through an interface unit to produce another data tape which contains the interferogram points and timing data in binary format. This binary tape is then available for further processing of the interferogram on another computer.

The four analog data tracks used in the processing are: 1) the digitized interferogram samples in NRZ serial form, and also a single 16-bit word indicating the duration of scan or absolute AGC value which is output during the scan plate flyback; 2) a clock track which provides the timing pulses to tell the computer when to sample the interferogram data track, the clock track provides 24 sampling pulses for each of the 31 interferogram sample points; 3) a clock track which provides the timing pulses to tell the computer when to sample the duration of scan or absolute AGC data, this clock track provides 16 sampling pulses for the single data word; 4) a time code track which provides absolute timing information to permit the interferogram data to be related to positional information as provided by the TV camera system, the time code is NASA 36-bit with a 100 pps code on a 1000 cps carrier.

The interferogram data track and the two clock tracks are played into the computer through an interface which combines the two clock tracks and adds a sync word for each frame of data. The computer then checks for a sync word within each frame and counts the clock pulses to ensure that the correct number of data bits are generated within the duration of a single frame of data. This error check eliminates almost all questionable data which may be generated by noise pulses on the clock track.

The time code track is played into a reader which is also interfaced with the computer. This adds the time of the data frame in binary form as part of the data record for a single scan of the interferometer.

The digital tape which is thus obtained can then be processed further on an SDS-930 computer. The data tape is first unpacked to yield another binary tape which formats the interferogram data into the in-phase and quad-phase components, similar to the format output by the NOVA when used with the instrument, and separates out the time, duration of scan information and absolute AGC data. This tape can now be processed to output interferogram values on a single scan basis or after co-adding any specified number of scans. In addition, correlation functions can be generated on the GE 605 time share computer system using previously input calibration interferograms obtained with the NOVA computer on paper tape. The correlation functions can then be applied by the SDS-930 to the recorded interferogram either on a single scan basis or after co-adding any number of scans to yield a measurement of CO or CH as a function of time.

7.3 Canada Flights - May 1973

In May 1973, two flights were made on board the Falcon Fan-Jet aircraft. These were undertaken mainly to test the operation of the correlation interferometer under flight conditions. It was felt that it would also be helpful to determine the response of the instrument over various surfaces with different albedos. The routes for these two flights are shown in Figure 7.3. Both flights generally followed the Ottawa River (with data recording being begun

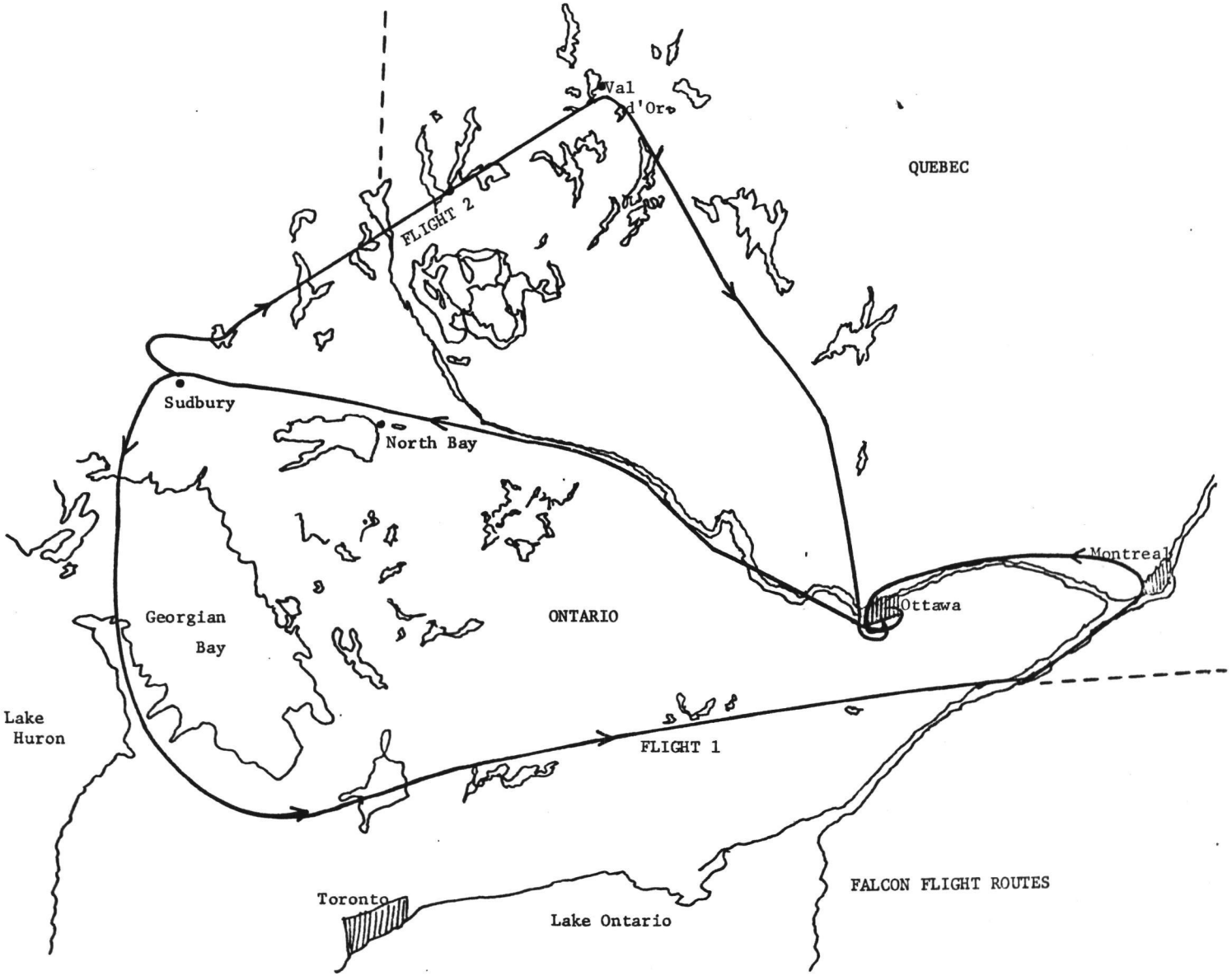

Figure 7.3 Routes of Canada Flights - May 1973

around Petawawa) and then going over the North Bay and Sudbury areas. Flight one then went south over Georgian Bay; Owen Sound, Ontario; Perth, Ontario and Cornwall, Ontario, to the Montreal area, then back to the Ottawa area; over the city of Ottawa, and finally over the area east of Ottawa. Flight two turned northeast from Sudbury to Val d'Or, Quebec and back to Ottawa. During flight two there was extensive cloud cover and the data were much less useful than in flight one. In flight one, the video tape was improperly recorded so that the location could only be approximated by use of time and flight speed information together with a rough plot of the flight path.

The useful data were those obtained by use of the NOVA and teletype. Table 7.1 gives the column density measurements of CO and CH_4 along with the approximate locations where these data were obtained. Each of these measurements (described briefly by Goldstein, ref. 38) were averaged over about two minutes. The actual measurements are of the total column densities, expressed in atmosphere-centimeters; the quantities noted as ppm are obtained by assuming a constant mixing ratio throughout the column, undoubtedly a poor assumption, but suitable to give a rough idea of the lower atmosphere concentrations. The first measurements, particularly over the Petawawa area, were over a cloud covered region. The measurements noted as Georgian Bay were over the water of that bay and provided very little signal and hence the measurements are not meaningful. The areas around Cornwall, Montreal, and, to some extent, Ottawa, are industrial areas. The high burdens of CO reflect that condition. The Ottawa area measurements were made over areas south and west of the city, quite removed from the city. The measurements near Alfred show a high level of CO which may or may not be true. For these measurements there were no other measurements with which these could be compared. Therefore, the accuracy of the measurements cannot be determined.

From these measurements it was concluded that on the first airborne tests of the correlation interferometer the instrument operated properly. The measurements, both of CO and CH_4 were reasonable and showed logical variations with the environment.

7.4 Test Flights - September 1973

In September 1973 a second series of flights were undertaken in order to further test the operation of the correlation interferometer under aircraft flight conditions with a variety of atmospheric and surface conditions. The scan time of the oscillating plate of the correlation interferometer changed both during the flights and the times of calibration. Thus, none of the calibrations could be used nor could any calibration suitable for the treatment of the flight data be obtained. In addition to the major cause of error and noise, the varying scan velocity, electronic cross-talk developed contributing further to the noise. Although both of these problems were subsequently detected and corrected, the flight data could not be said to be meaningful.

7.5 Canada Flights - April 1974

A third series of flights were made in April 1974 aboard the Falcon. This series consisted of three flights. The first was made in the Churchill, Manitoba area; the second was made in southern Ontario countryside; the third was made over Toronto.

7.5.1 Churchill Area Flight.- The flight in the Churchill area was made for the purpose of obtaining data over a large area having a uniform surface, thus providing a test for the repeatability of the instrument operation. Although the flight originated in Winnipeg, Manitoba, the instrument was not put into operation until shortly before reaching the actual area selected for the repetitive measurements because, due to the very low temperatures above the window and, hence, around the instrument, the scan time was significantly lower than normal operating values. Even during about the first third of the first pass this condition prevailed. Three passes were made over the same area, as shown in Figure 7.4. This area was almost completely covered with fresh snow which could be distinguished from older (presumably recrystallized) snow by its much greater reflectivity (of the order of 10% and 25%, respectively). The terrain in this area was essentially free of any vegetation. Most of the rivers and creeks were still frozen and snow-covered, although the ice in the center of some of the larger rivers had started to break up, giving the only variation in albedo. However, such covered only a small part of the field of view which, for the altitude of 31,000 feet, was about 3700 feet, and thus the variation was not significant. In comparing the data all of the straight portions of the three passes was used except for the first one-third of pass one. That was eliminated because of the still increasing scan time and because this was over a slightly different area, some of which had significant vegetation.

The weighting functions used in obtaining the CO and CH_4 burdens from the interferograms were ones obtained from the use of laboratory data only. These had essentially no water in the path. For the cold atmosphere of the Churchill region this was thought to be most suitable. For all subsequent measurements discussed in this report, the weighting functions employed several points of calibration data obtained at NASA Langley in May 1974, and several points obtained in the laboratory. It is believed that these spanned the burdens of water and other gases encountered in the measurments.

The results of these measurements is shown in Table 7.2. These are presented as single-scan data, and as data averaged over a number of scans -- 2, 8, 16, and 32. The average absolute deviation from the average is given in each case. For CO this is 44% for 1 scan, 31% for 2 scans, 18% for 8 scans, 12% for 16 scans and 10% for 32 scans. For CH_4 the average deviation is 10% for 1 scan and 2% for 32 scans. The single-scan data for both CO and CH_4 for the three passes of the Churchill flights are given in Appendix I as an example of data of this type.

The values of the total burdens (in atm-cm) of CO and CH_4 was converted to values of concentration (in ppm) by assuming a constant mixing ratio thoughout the atmosphere and by taking into account the total amount of gas in the path, here equivalent to 2.1 vertical columns of atmospheric gas. This is a reasonable assumption in this remote area although the mixing ratio is likely to de-

TABLE 7.1 FLIGHT MEASUREMENTS OF CO AND CH_4 OVER CANADA, MAY 24, 1973

	CO		CH_4		
	atm-cm	ppm	atm-cm	ppm	
Petawawa	.074		1.50	0.84	80% cloud cover*
North Bay	.176		1.45		40% cloud cover*
Sudbury	.216	.141	1.43	0.84	10% cloud cover*
Georgian Bay	.091	.060	1.09	0.71	Over water
Owen Sound	.275	.180	1.63	1.07	
Perth	.148	.094	1.62	1.03	
Cornwall	.486	.307	2.53	1.59	
Montreal Area	.479	.296	2.08	1.28	Some water
Ottawa Area	.149	.104	1.38	0.96	Descending
Ottawa	.389	.288	1.72	1.27	
Alfred	.431	.315	1.63	1.19	Bog

*Clouds at 8000 ft.

TABLE 7.2 MEASUREMENTS IN THE CHURCHILL AREA

	CO atm-cm	CH_4 atm-cm
32 SCANS		
Pass 1	.278 ± .048	3.71 ± 0.08
Pass 2	.275 ± .011	3.74 ± 0.03
Pass 3	.267 ± .022	3.74 ± 0.06
16 SCANS		
Pass 1	.279 ± .053	
Pass 2	.275 ± .011	
Pass 3	.267 ± .032	
8 SCANS		
Pass 1	.279 ± .060	
Pass 2	.271 ± .035	
Pass 3	.267 ± .049	
2 SCANS		
Pass 1	.278 ± .096	
Pass 2	.271 ± .077	
Pass 3	.267 ± .082	
1 SCAN		
Pass 1	.278 ± .135	3.71 ± 0.33
Pass 2	.271 ± .103	3.74 ± 0.41
Pass 3	.267 ± .125	3.74 ± 0.32

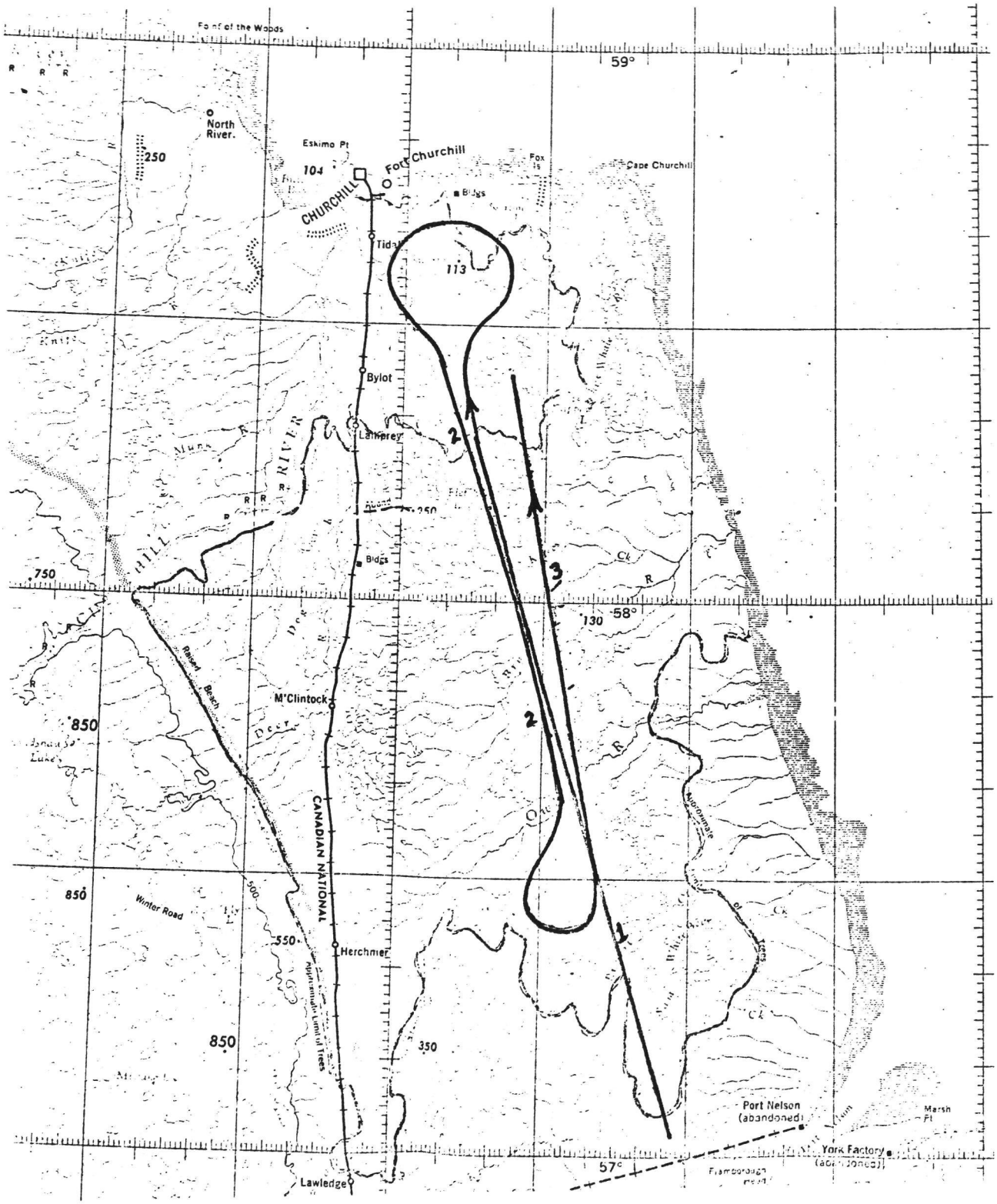

Figure 7.4 Churchill Area Flight Paths

crease in the stratosphere. Thus the concentrations in the stratosphere should possibly be slightly lower than given by a constant mixing ratio. The values obtained with this assumption are compared with other measurements made in the Arctic in Table 7.3. The measurements of Wilkness (ref. 39) were made in the Arctic Ocean area at approximately latitude 70 - 80 °N, and those of Seiler (ref. 40) were made in the polar area. Thus these were at higher latitudes than were those of this work (57°40' - 58°25' N). It can be seen that the agreement for both CO and CH_4 is good. The Churchill measurements show that the correlation interferometer gives consistent values of the gas burden.

7.5.2 Southern Ontario Flights.- The flights in the Southern Ontario area were made for the purpose of determining the effect of rapidly varying surface characteristics on the measurements. In this area the surface cover does vary rapidly with various types of vegetation, fields plowed in various ways, roads, rivers and creeks, etc. It was planned to traverse the same path several times each with a different value of V/H (speed ÷ altitude in sec^{-1}) by changing the values of one or both of these parameters. The actual six passes are shown on the map in Figure 7.5. The paths are actually different because of the difficulty in exactly repeating a path in a high-speed aircraft and because of a request by air-traffic control, after the first three passes, to change the area. The changes did not change the surface characteristics appreciably.

For each of the six passes a region which was judged to encompass the most rapidly varying surface characteristics was chosen for comparision. In Table 7.4 these data for each of the six passes are given in terms of the average of single scan data and the average absolute deviation therefrom. The values of V/H for each pass is given. It is seen that the average absolute deviation does not increase with V/H even though the values of V/H encountered were more than twice as high as the maximum value designed for (.05 sec^{-1}). It is concluded that the instrument can make consistent measurements over rapidly varying terrain with values of V/H in excess of 0.1 sec^{-1}.

7.5.3 Toronto Flights.- The flights over Toronto were made at the request of and in conjunction with the Ontario Ministry of the Environment. Nine passes were made in various regions over the city and its environs. These are shown in Figure 7.6. The first pass and part of several others were made over the waters in Lake Ontario and a very low signal was obtained. The results are presented as 32-scan averages in the map in Figure 7.6. It can be seen that the higher values were found in the downtown region and along the heavily traveled freeways, the Queen Elizabeth Way (along the South shore) and Rt. 401 (along the north side of the most populous area). The area to the north shows lower values as do, to a lesser extent, the area along the pass which more or less followed the Don River Valley.

Point samples were obtained by the Ontario Ministry of the Environment who provided the data listed in Table 7.5.

TABLE 7.3 ARCTIC MEASUREMENTS (ppm)

	CO	CH_4
THIS WORK*	0.14	1.89
WILKNESS		
TROPOSPHERE		
WINTER	0.22	1.62
SUMMER	0.09	1.38
STRATOSPHERE	0.12	1.59
SEILER		
STRATOSPHERE	0.11	

*Based on constant mixing ratio througout the atmosphere. Winter conditions prevailed at time of these measurements.

TABLE 7.4 SOUTHERN ONTARIO FLIGHT DATA

PASS	CO (atm-cm)	V/H (sec^{-1})
1	.248 ± .079	.014
2	.270 ± .111	.045
3	.261 ± .106	.029
4	.277 ± .103	.044
5	.237 ± .076	.059
6	.232 ± .106	.121

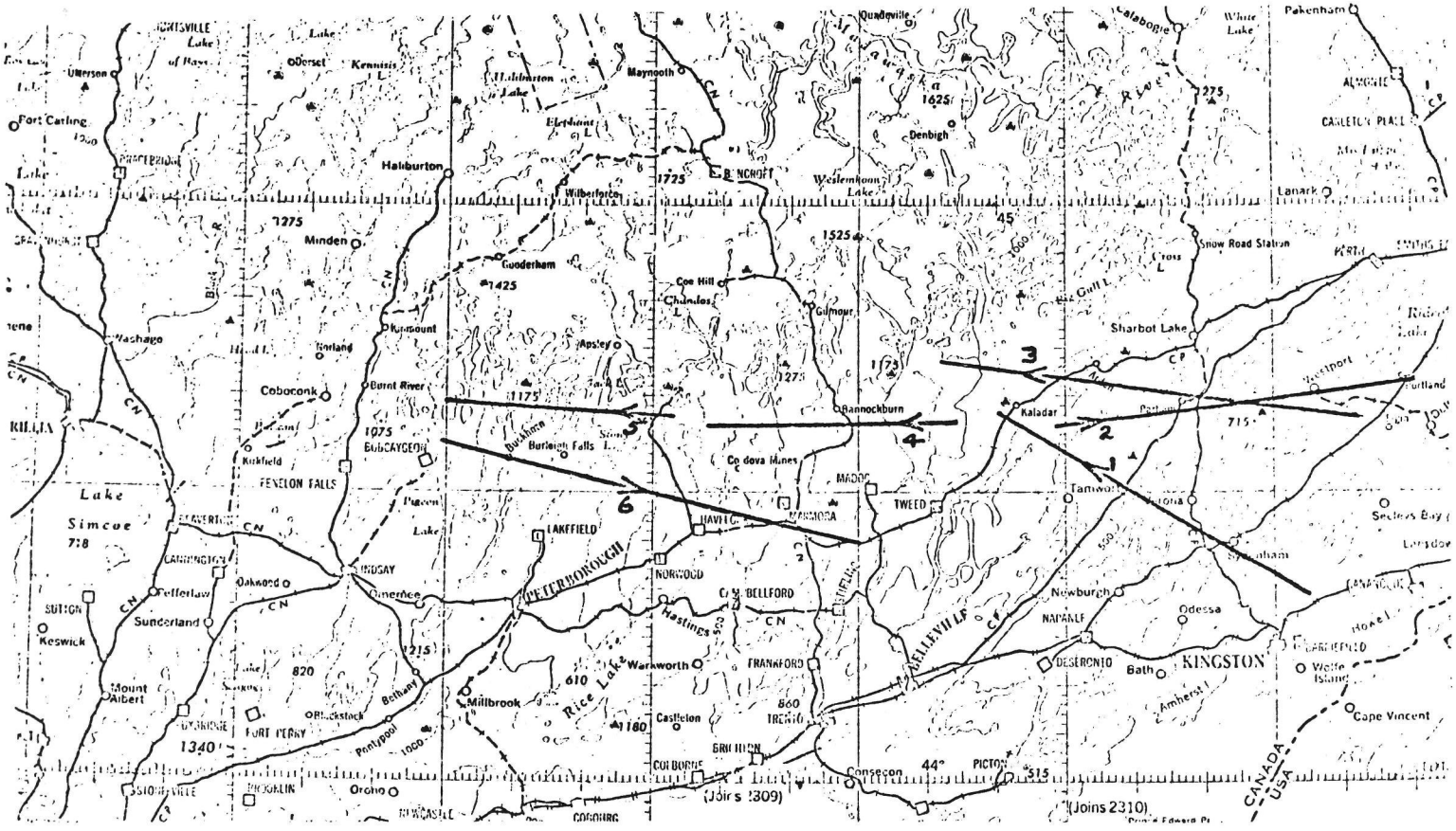

Figure 7.5 Flights In Southern Ontario

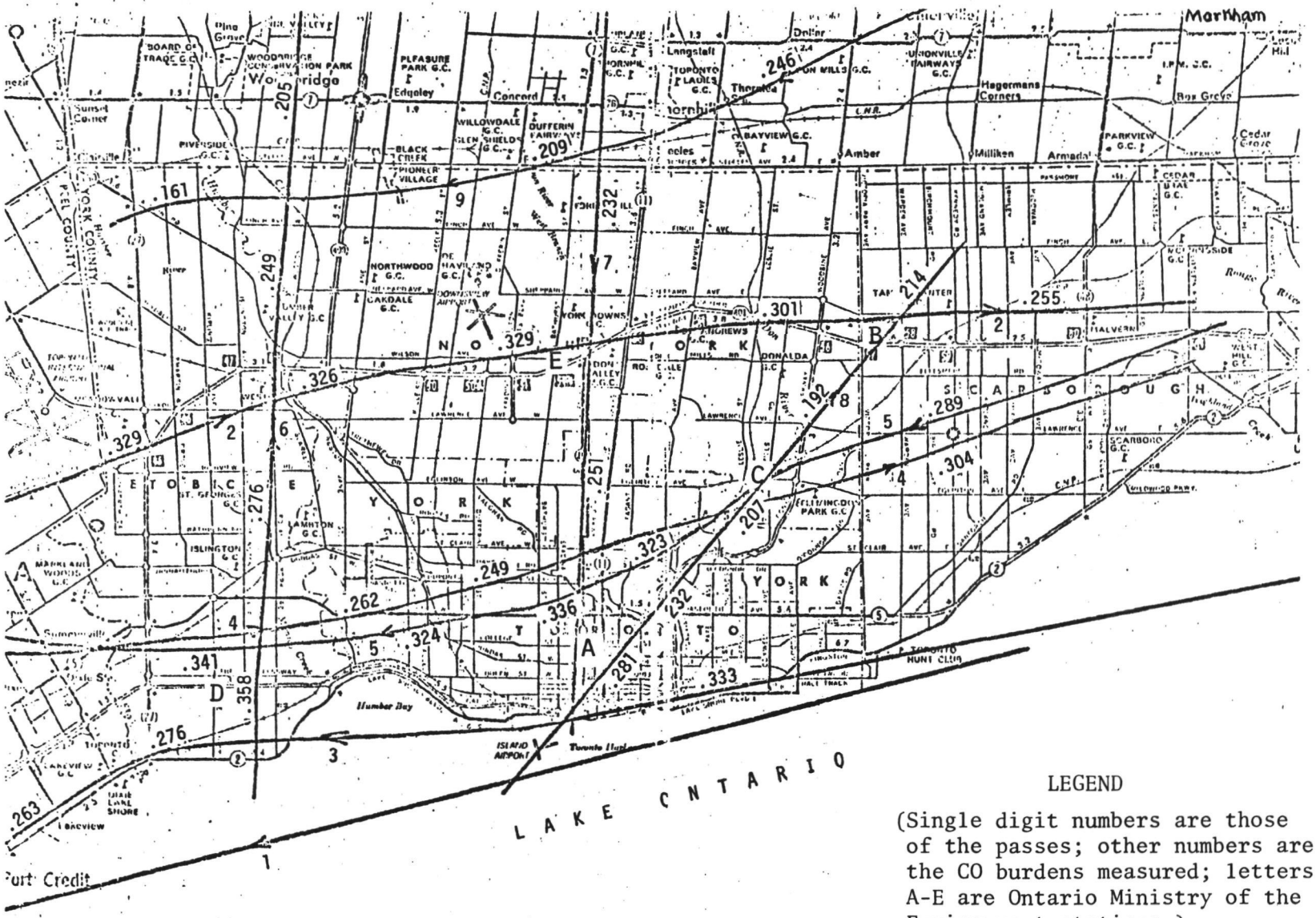

LEGEND

(Single digit numbers are those of the passes; other numbers are the CO burdens measured; letters A-E are Ontario Ministry of the Environment stations.)

Figure 7.6 Toronto Flight Paths and Data

TABLE 7.5 ONTARIO MINISTRY OF THE ENVIRONMENT CO (ppm) DATA

Station	1100	1200	1300
A	2	2	1
B	3	3	3
C	1	2	1
D			2
E	1	2	2

These results show variations which follow the same trends as do the remote data. Of course, these data are coarse and no direct comparison can be made between column density measurements and ground samples. It is planned by the Ontario Ministry of the Environment to make computer runs using a dispersion model to calculate what values each of these two types of measurements should give and thus how they compare with each other and with the models. At present it can merely be said that the results over polluted areas are reasonable.

8. ENGINEERING MODEL HELICOPTER FLIGHT TESTS

8.1 Platform and Interface

As a further test of the Engineering Model Correlation Interferometer, the instrument was mounted on board a Bell Jet Ranger 206 Helicopter owned and operated by Keystone Helicopter, Inc. of West Chester, Pa. This aircraft is shown in Figure 8.1. Keystone provided a downward-looking port in the helicopter for these tests. A pyrex window was installed in this port for the CO and CH_4 measurements in the 2.3 μm region. A mounting on which the interferometer shock mounts were placed was designed and fabricated and the instrument was installed thereon in a position over the rear left seat and the floor in front of it. A Sangamo Model 3568 14-channel tape recorder was used for this work and mounted on the same frame as the shock-mounted interferometer. The sensor and the recorder are shown mounted on the helicopter in Figure 8.2. The electronics, Figure 8.3, including a time-code generator, were placed in the luggage compartment. The time-code generator and a clock on the dashboard of the helicopter were set so that the readings were coordinated. A Sony Model AVC 3400 video tape recorder was placed in the nose of the helicopter with a downward-looking 68° field of view which included the 7° field of view of the instrument. This recorder also had a voice channel using a built-in microphone so that the operator in the left-front seat could put times, locations, speeds, altitudes, and other comments on the tape. With the microphone located several feet from the operator much of the helicopter noise was picked up. Thus, on the recorded tapes, the voice was somewhat difficult to pick up but was, in general, satisfactory.

8.2 Pennsylvania Flights

Two short flights were made over a suburban area about thirty miles west of Philadelphia in order to test the operation of the correlation interferometer using the helicopter as a platform. The paths for these flights are shown in Figure 8.4. The measurements obtained are given in Table 8.1. It can be seen that these data, which are averages and average absolute deviation of single scan measurements, show precisions about the same as that of the data obtained on the jet aircraft -- of the order of 40%. The one exception to this is the value obtained at a high value of V/H (about 1 sec^{-1}) and is presumed to be due to the magnitude of V/H which is more than twenty times the V/H for which the instrument was designed.

8.3 NASA Langley Area Flights

A series of flights was made in the vicinity of NASA Langley with the objective of obtaining correlation interferometer measurements to compare with other measurements obtained with ground-based instrumentation to provide both comparative and calibration data. These flights were also desired in order to further test the operation of the instrument on the helicopter, to test the repeatability of the instrument response and to test the response and operation over various terrains including areas of high and low reflectivity.

Figure 8.1 Bell Jet Ranger 206 Helicopter

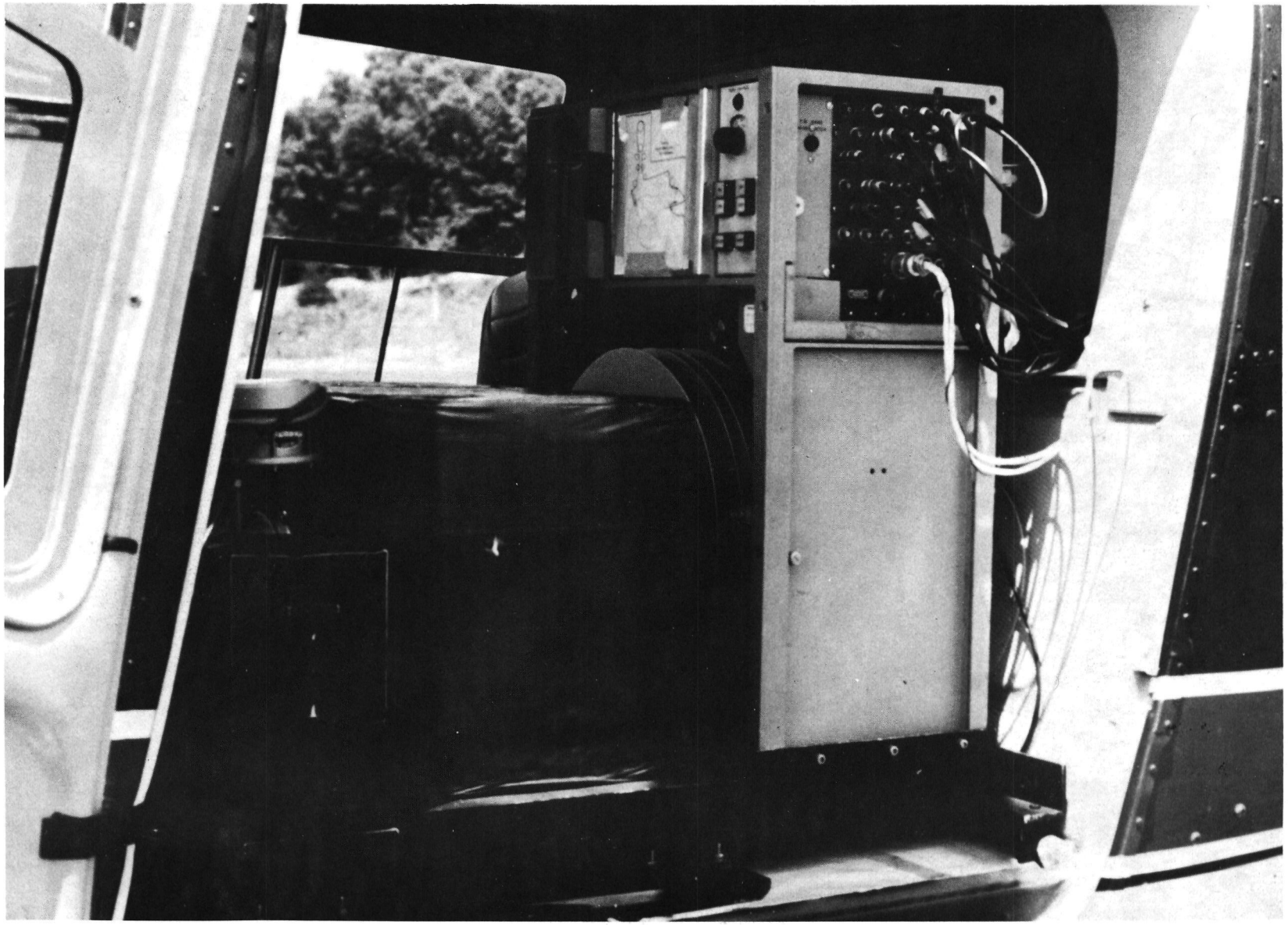

Figure 8.2 Correlation Interferometer and Recorder Installed in the Helicopter

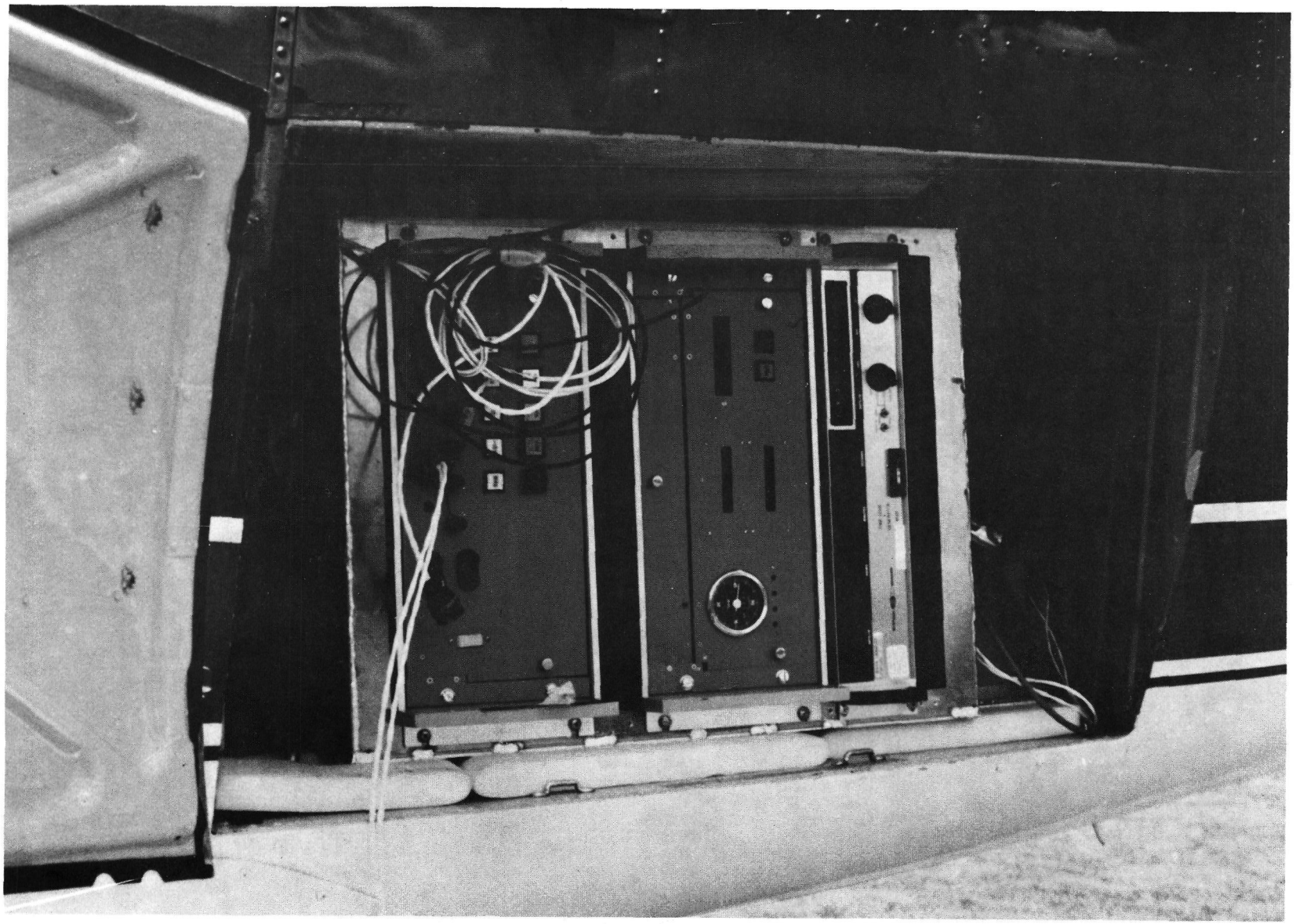

Figure 8.3 Electronics Installed in Helicopter Baggage Compartment

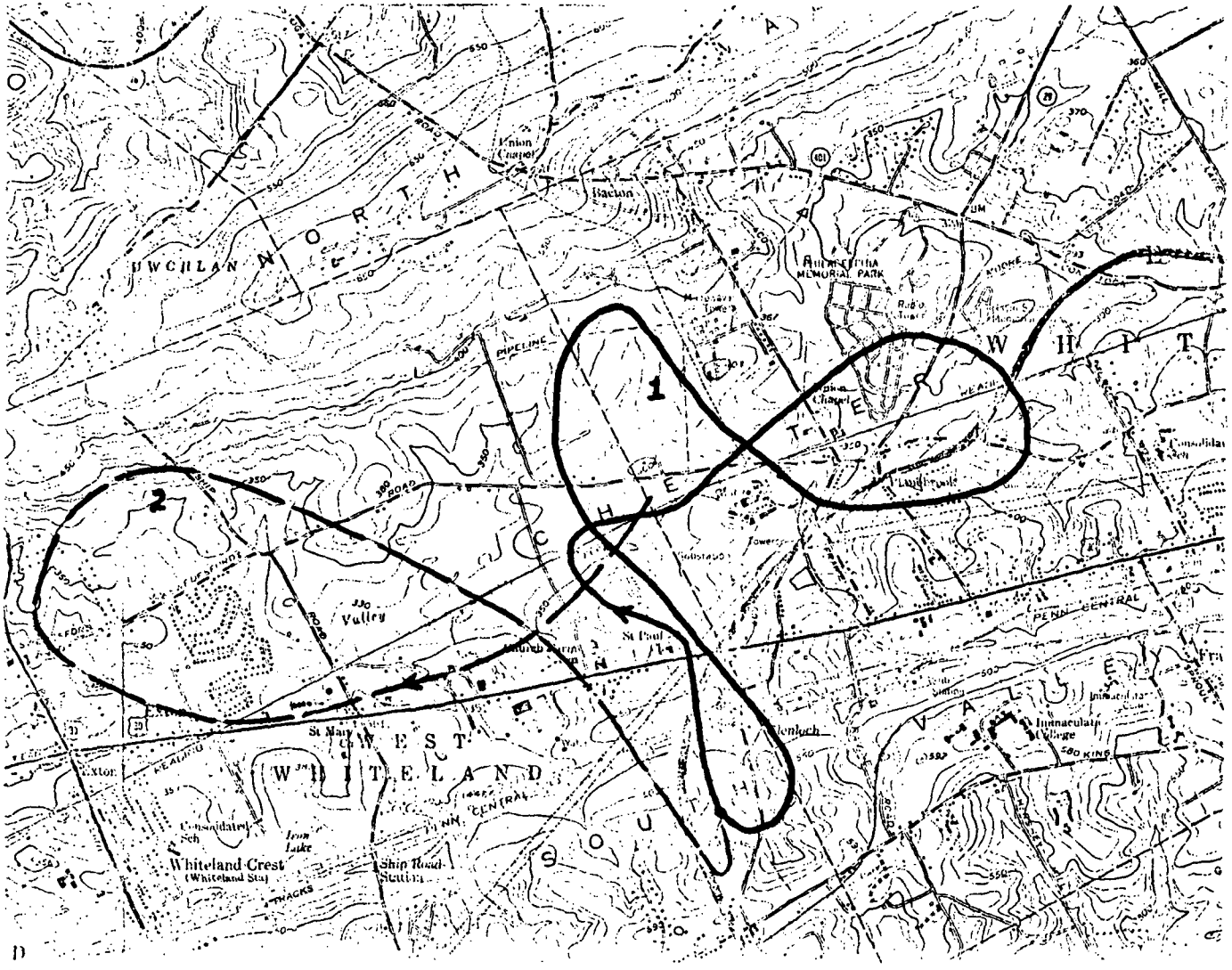

Figure 8.4 Helicopter Flight Paths - June 1974

TABLE 8.1 HELICOPTER MEASUREMENTS IN PA.

CO (atm-cm)	CH_4 (atm-cm)	
.240 ± .084	1.82 ± .22	
.208 ± .088	1.86 ± .21	
.233 ± .071	1.32 ± .29	
.228 ± .086	1.45 ± .33	
.229 ± .067	1.43 ± .28	
.226 ± .096	1.17 ± .38	
.242 ± .193	1.51 ± .69	V/H $\approx$ 1

Ground-based column density measurements were obtained with NASA's Idealab IF-6 interferometer of 0.1 cm^{-1} resolution operated by P. J. LeBel. Many passes were made over the van containing that instrument and a chromatograph with which ground-level concentrations were obtained. The IF-6 interferometer integrated signals over a period of about two minutes, and transformed the interferograms into spectra, and obtained the CO and CH_4 burdens therefrom. For each of the many passes of the helicopter over the van, Table 8.2 gives data averaged over a uniform area, shown in Figure 8.5, east and west of the van, which, in general, consisted of 10 to 19 scans except for pass number 18 which was obtained by hovering for 210 scans, and the data obtained by the instrumentation in the NASA van. The GE and NASA data are also shown graphically -- the CO for June 8 and 9 in Figures 8.6 and 8.7, respectively, and the methane for June 8 and 9 in Figures 8.8 and 8.9, respectively. The agreement is, in general, quite good -- with the error limits which are of the order of 20% for each instrument. The altitude of the helicopter was only a few hundred feet above the ground so that this part of the radiation path added very little to the total burden as compared with the interferometer looking up from the ground.

The scatter in the correlation interferometer measurements was found to be about the same as those obtained when measurements were made using the Falcon Jet as the platform. Measurements made during the six-minute period of hovering (Figures 8.10 and 8.11) show no increase in the CO or the CH_4 burden indicating no effect of the exhaust. The helicopter thus appears to be a suitable as well as convenient and useful platform.

Further measurements were made during this series of flights. However, difficulties arose in the form of frequent dropout of interferogram data and culminating finally in the finding of a broken wire. Hence data obtained after the first appearance of this trouble were not deemed usable. The broken wire was more likely due to rough ground transportation rather than the comparatively smooth flights. The only problem which may have been introduced by roughness in

TABLE 8.2 DATA FROM PASSES OVER VAN AT NASA LANGLEY

DATE	GE RUN NO.	NASA RUN NO.	TIME HR:MIN:SEC	GE CO	NASA CO	GE CH_4	NASA CH_4
6/18/74		1	9:25		.17		1.97
		2	10:00		.15		1.72
		3	11:00		.105		1.36
		4	12:50		.09		.90
	1		14:03:57	.24		.86	
	2		14:06:30	.17		1.01	
	3		14:09:41	.15		.84	
	4		14:11:50	.13		.86	
	5		14:15:23	.15		.82	
	6		14:18:01	.13		1.09	
	7		14:21:46	.13		1.05	
	8		14:27:32	.13		.96	
	9		14:46:52	.19		1.05	
	10		14:50:40	.15		1.20	
	11		14:53:45	.17		.93	
	12		14:56:51	.10		.87	
	13		14:59:31	.20		.99	
	14		15:02:49	.18		1.05	
	15		15:05:10	.22		1.34	
	16		15:07:35	.14		1.02	
	17		15:15:33	.14		1.33	
		6	15:30		.11		1.55
		7	16:00		.12		1.67
		8	16:15		.13		1.82
		9	16:30		.15		1.95
	18		16:31:30	.14		.88	
	19		16:36:36	.20		.56	
	20		16:40:12	.14		.76	
		10	16:45		.17		2.03
		11	16:49		.18		2.22
6/19/74		1	9:10		.19		2.13
		2	9:55		.15		1.73
		3	10:20		.14		1.62
		4	10:35		.14		1.42
		5	10:45		.14		1.46
	21		10:50:20	.16		1.08	
	22		10:52:13	.15		.88	
	23		10:59:40	.14		.90	
		6	11:00		.13		1.34
	24		11:01:40	.11		.85	
	25		11:05:10	.10		.72	
	26		11:07:03	.13		.95	
		7	11:33		.16		1.30
		8	13:00		.12		1.18
		9	13:25		.12		1.19
		10	15:00		.13		1.36
		11	15:30		.16		1.50
		12	15:40		.16		1.64

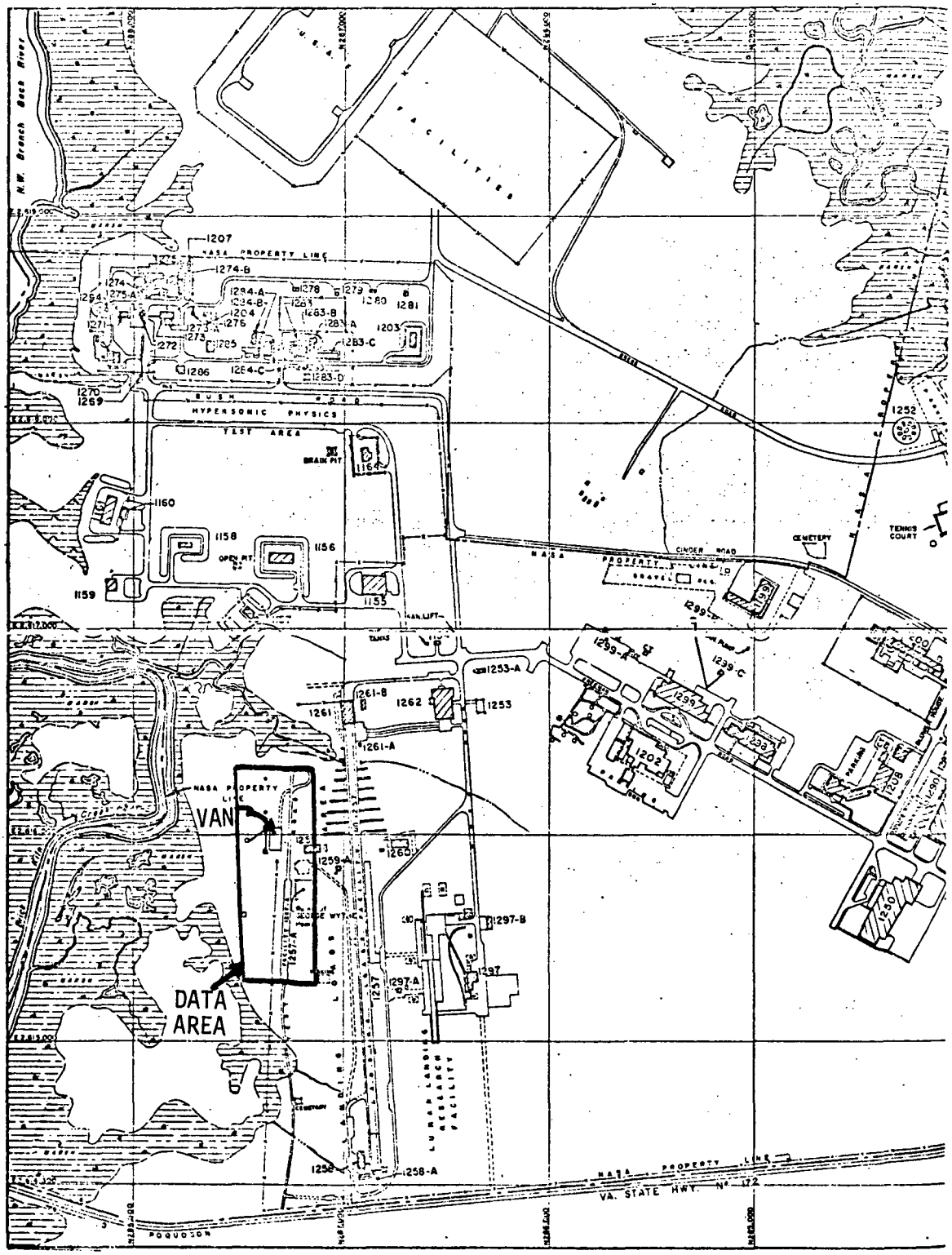

Figure 8.5 Area of Flights at NASA Langley

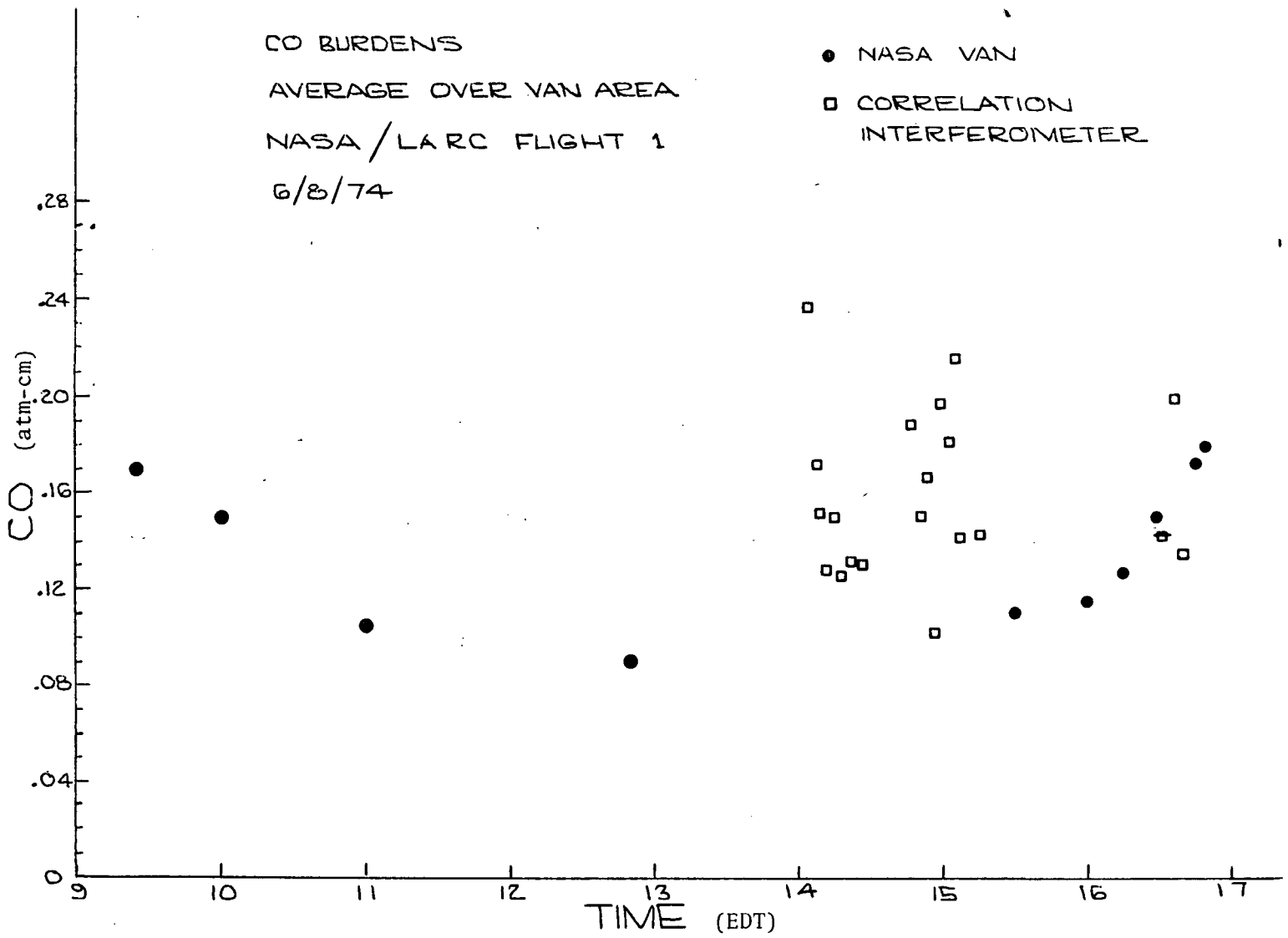

Figure 8.6 CO Burdens - Flight 1 - 8 June 1974
(Average Over Van Area - NASA LaRC)

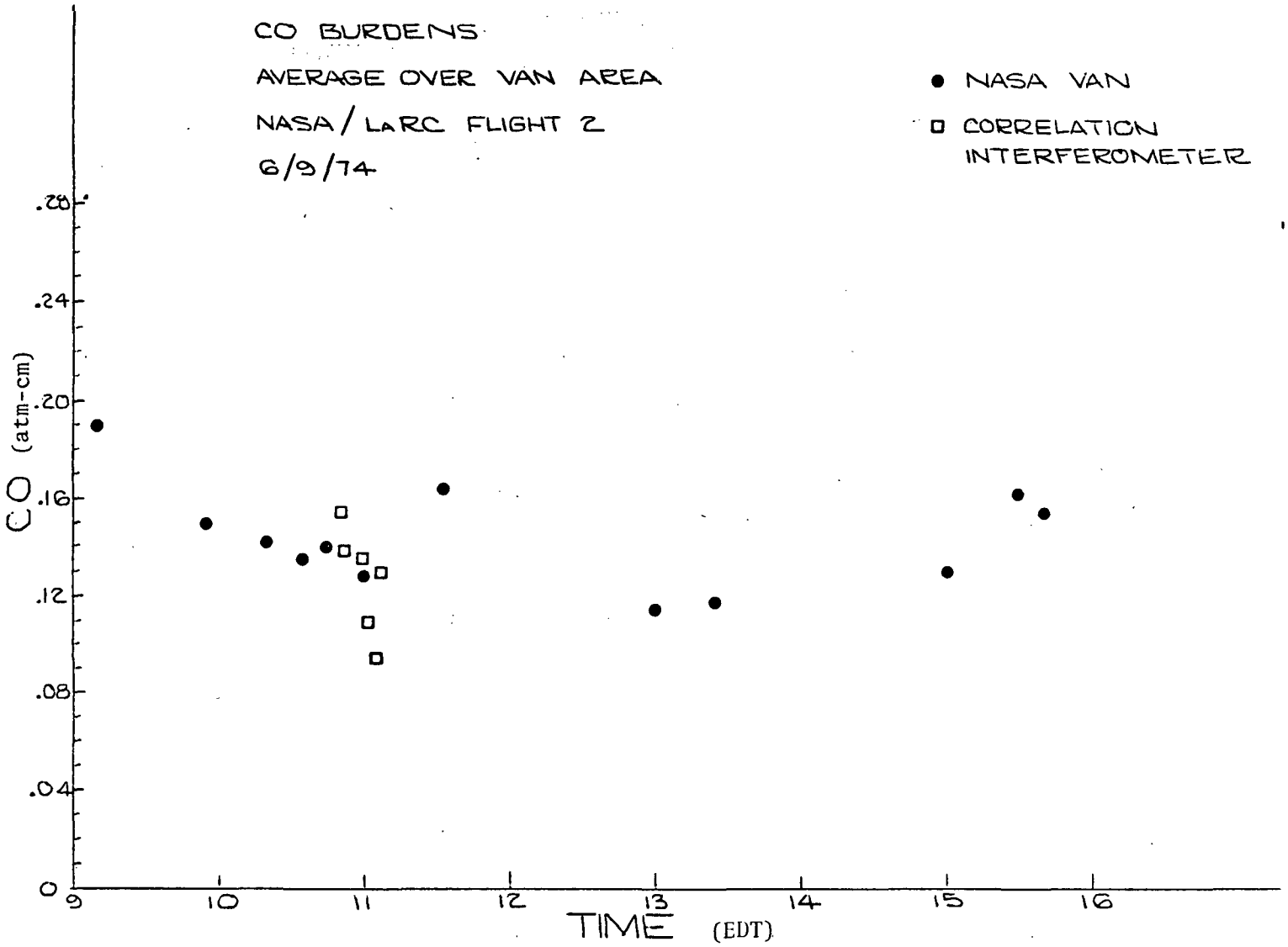

Figure 8.7 CO Burdens - Flight 2 - 9 June 1974
(Average Over Van Area - NASA LaRC)

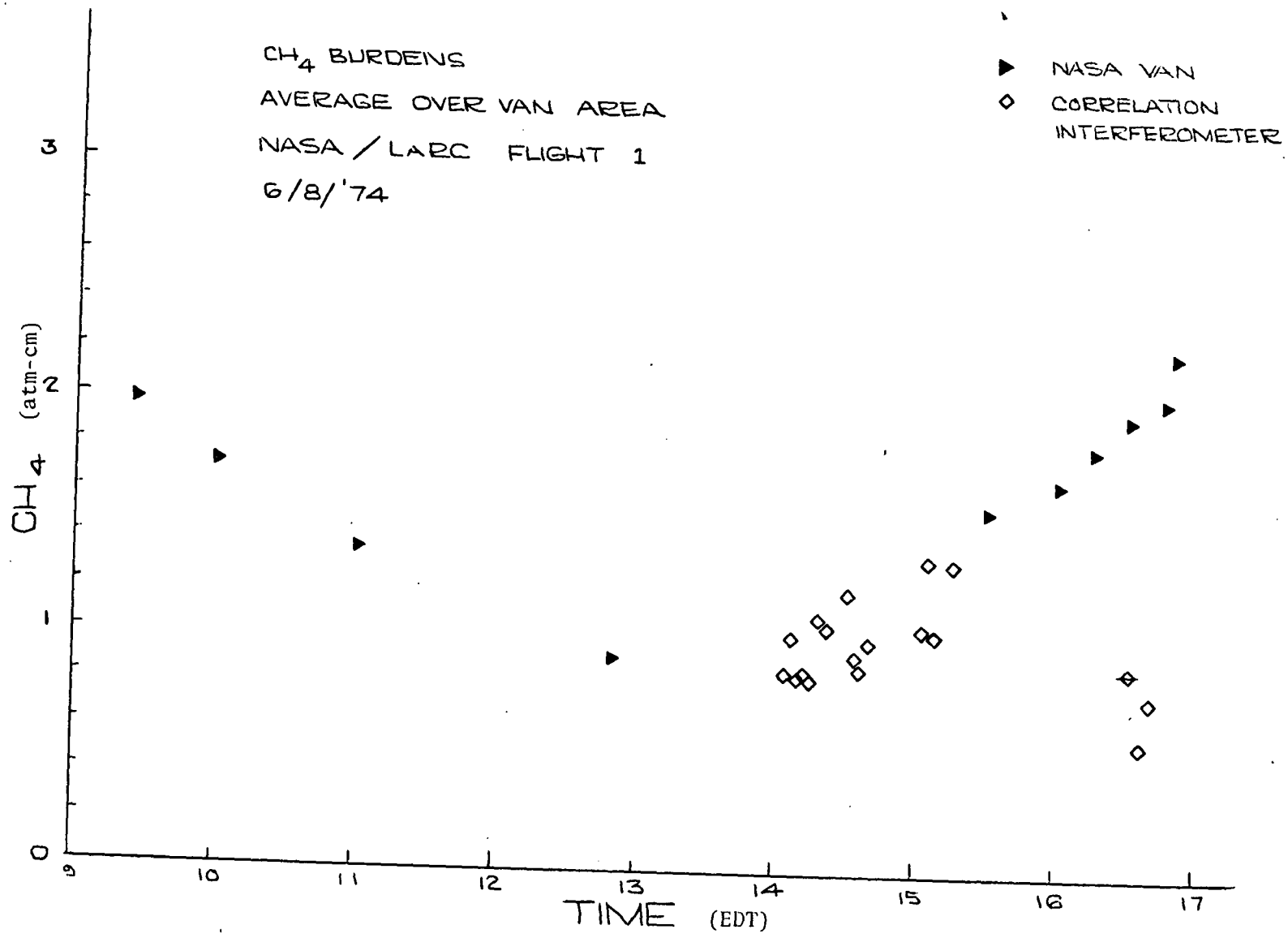

Figure 8.8 CH_4 Burdens - Flight 1 - 8 June 1974
(Average Over Van Area - NASA LaRC)

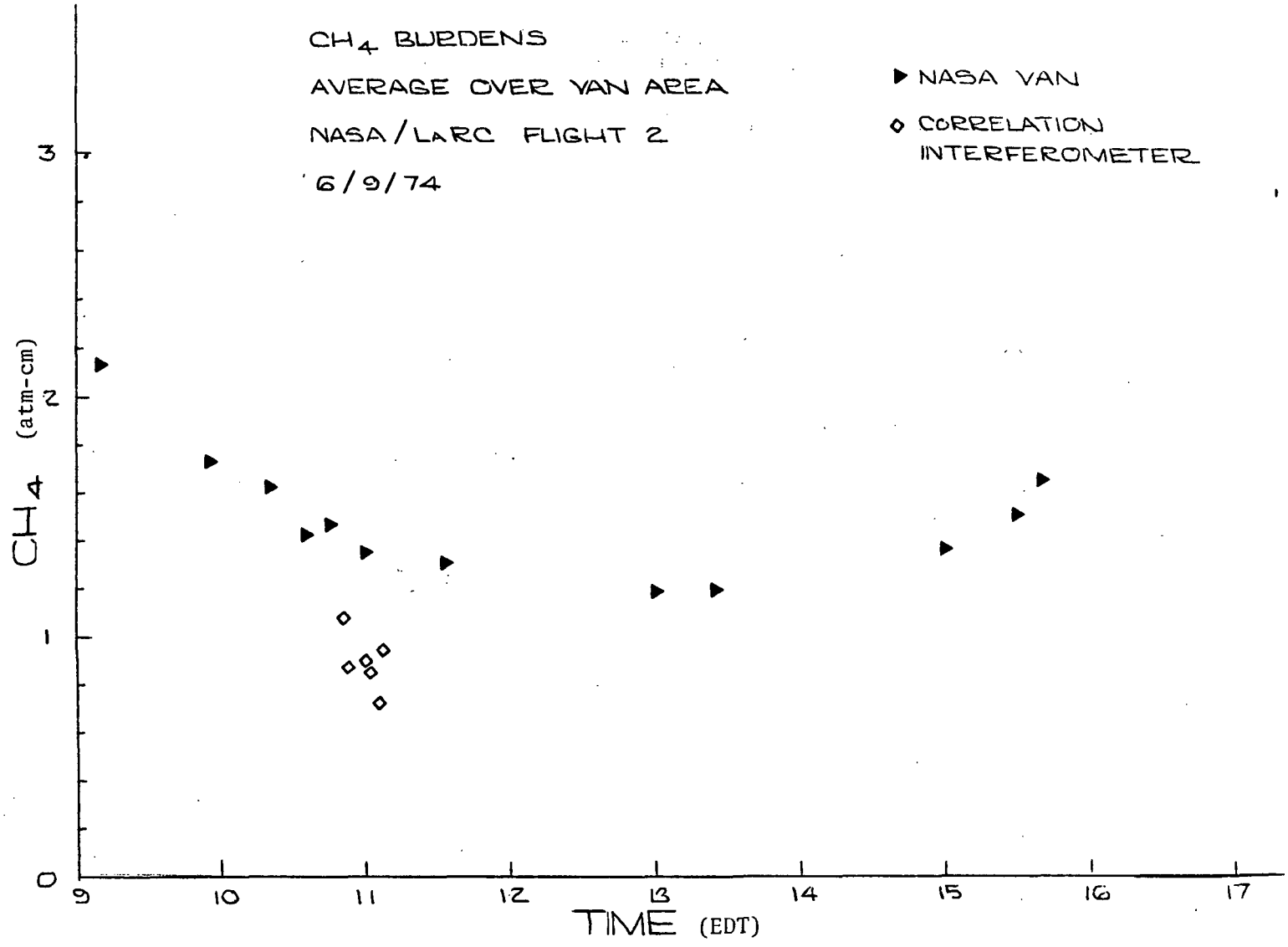

Figure 8.9 CH_4 Burdens - Flight 2 - 9 June 1974
(Average Over Van Area - NASA LaRC)

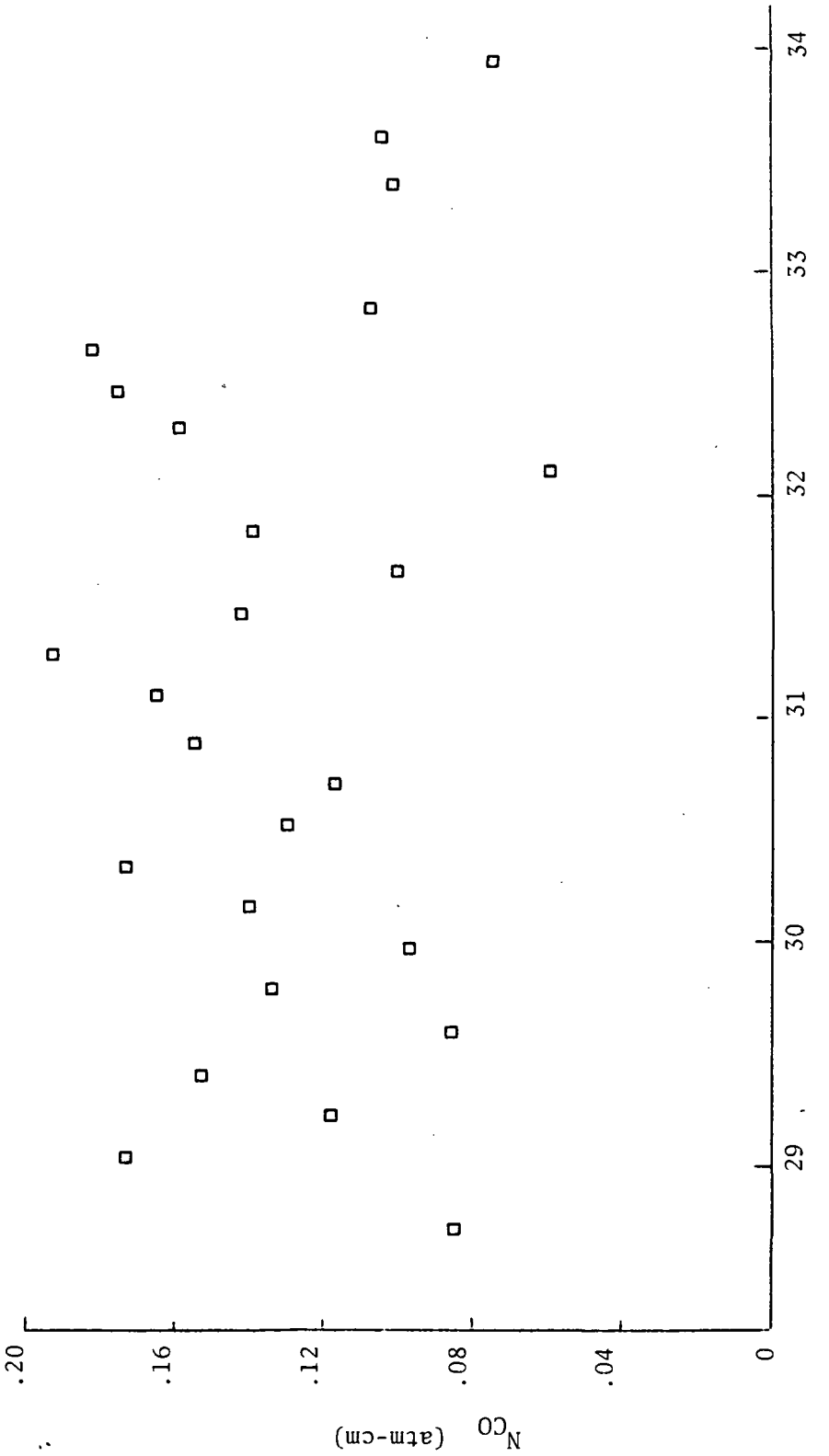

Figure 8.10 CO Burdens Measured During Hovering Period

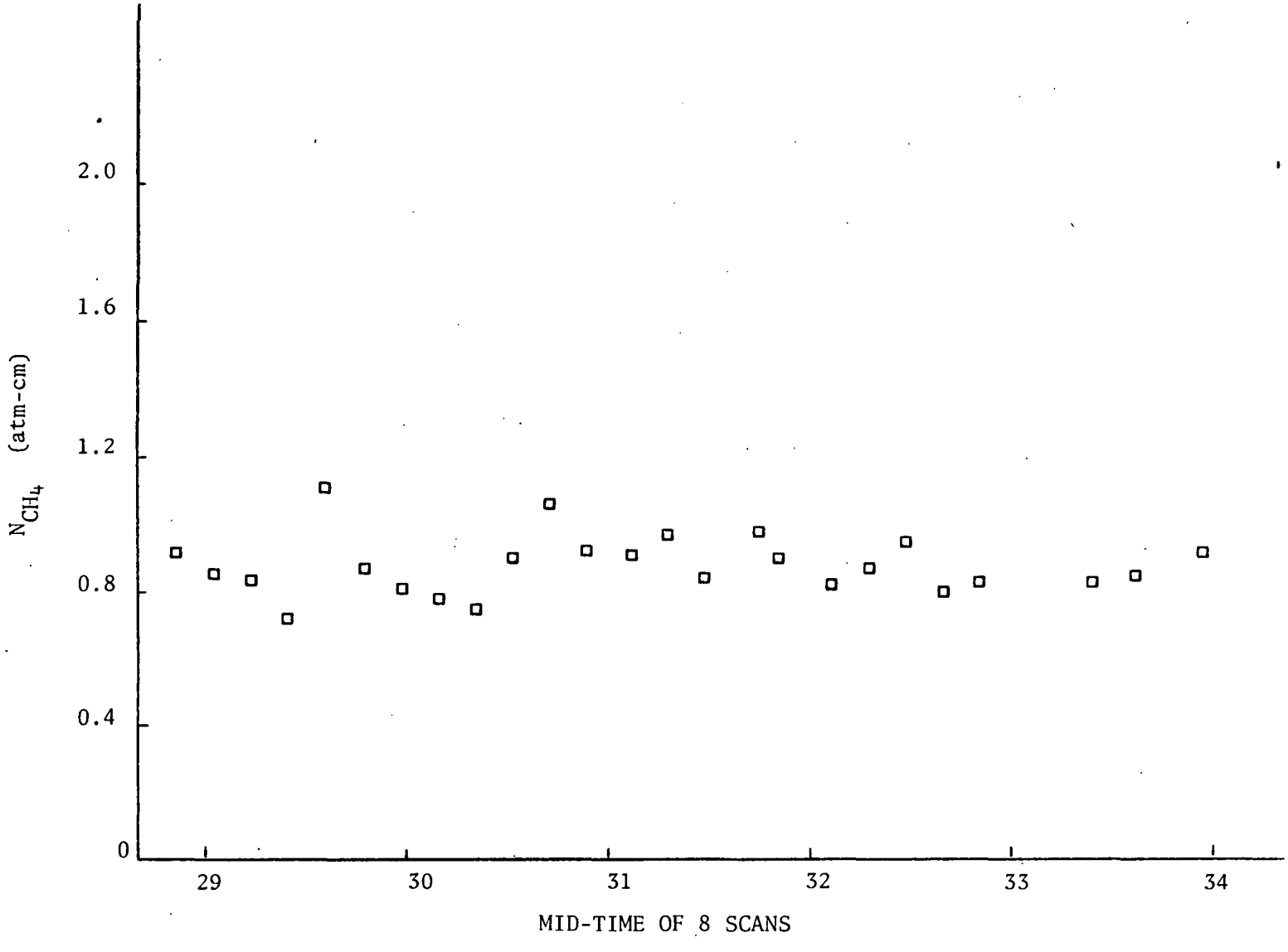

Figure 8.11 CH_4 Burdens Measured During Hovering Period

flight is thought to be a possible problem with the recorder at the higher speeds used in flights away from Langley since the tape recorder was not shock-mounted at that time. All the data on the later flights were suspect. These flights included ones over Hampton, Newport News, the Hog Island area, the Dismal Swamp, and the beach area south of Virginia Beach. The data for these were therefore not used.

The main objective of these flights was met. Data were obtained from the helicopter platform. These data were comparable with those data obtained from the ground by the IF-6 interferometer. These data gave acceptable comparison.

8.4 Washington Area Flights

A series of flights were made in the Washington, D.C. area in order to test the ability of the correlation interferometer on board a helicopter to make meaningful measurements in the urban areas and in doing so to compare such measurements with those made by various other instruments in the same area at about the same time. In addition to the correlation interferometer, column density data were also obtained with the NASA interferometer and sample data were obtained with the NASA chromatograph at ground level, the NRL chromatograph at ground levels and at various altitudes including above the mixing layer, and the State of Maryland infrared gas analyzer which obtained ground-level measurements.

A direct comparison of the correlation interferometer data with that from the IF-6 can be made. The part of the path of the radiation between the ground and the platform adds only a few percent as compared to the path between the sun and the ground. The comparative data are shown in Table 8.3 and in Figures 8.12, 8.13, 8.14 and 8.15. The GE data are averages for periods of 15 seconds over a region extending from the van in a direction away from an adjacent highway. The NASA data were integrated over periods of one to two minutes. The agreement is again seen to be quite good. The NRL data shown are total burdens calculated for a vertical column using the NRL sample data (taken over a period of about an hour) and a logical extrapolation into the stratosphere.

8.5 Other Flights

These flights have shown that the helicopter is a very suitable platform for tests of and measurements by the correlation interferometer just as is the Jet aircraft. A series of flights was made in September, 1974 for Columbia Gas Systems to test the ability of the correlation interferometer to detect natural gas leaks by measurement of ethane, methane, and the ratio of these two gases. For this work the instrument was converted to operate in the 3.3 μm range. The flights took place in rural areas of Kentucky, Tennessee, Virginia, and West Virginia. The results will be reported elsewhere at a later date.

TABLE 8.3 COMPARISON OF HELICOPTER DATA WITH GROUND-TRUTH MEASUREMENTS

DATE	GE RUN NO.	NASA RUN NO.	START TIME HR:MIN:SEC	STOP TIME HR:MIN:SEC	GE CO	NASA CO	GE CH_4	NASA CH_4
7/11/74		1	15:10:00	15:11:16		.10		1.43
	6-1		15:31:02	15:31:15	.17		1.05	
		2	15:34:00	15:36:32		.12		1.57
		3	16:05:00	16:07:32		.14		1.78
	6-2		16:06:33	16:06:52	.21		0.95	
		4	16:45:00	16:46:16		.16		2.48
7/12/74		1	09:23:00	09:24:16		.13		2.31
		2	10:03:50	10:05:06		.14		1.84
		3	10:17:35	10:18:51		.16		1.80
		5	10:49:00	10:50:16		.15		1.61
	7-11		11:01:15	11:01:31	.20		1.08	
	7-12		11:03:05	11:03:17	.17		1.10	
	7-13		11:06:06	11:06:22	.21		1.11	
	7-15		11:10:02	11:10:14	.20		1.18	
		6	11:10:50	11:12:06		.11		1.52
	7-16		11:11:41	11:11:53	.14		1.05	
	7-17		11:14-23	11:14:38	.18		1.25	
	7-19		11:17:19	11:17:35	.21		0.97	
	7-20		11:19:08	11:19:18	.16		1.26	
	8-1		11:32:30	11:32:37	.19		1.22	
		7	11:44:50	11:46:06		.14		1.43
		8	12:27:20	12:28:36		.13		1.43
		9	13:51:05	13:52:21		.14		1.50
	9-1		14:19:57	14:20:12	.26		1.31	
		10	14:20:45	14:22:01		.17		1.67

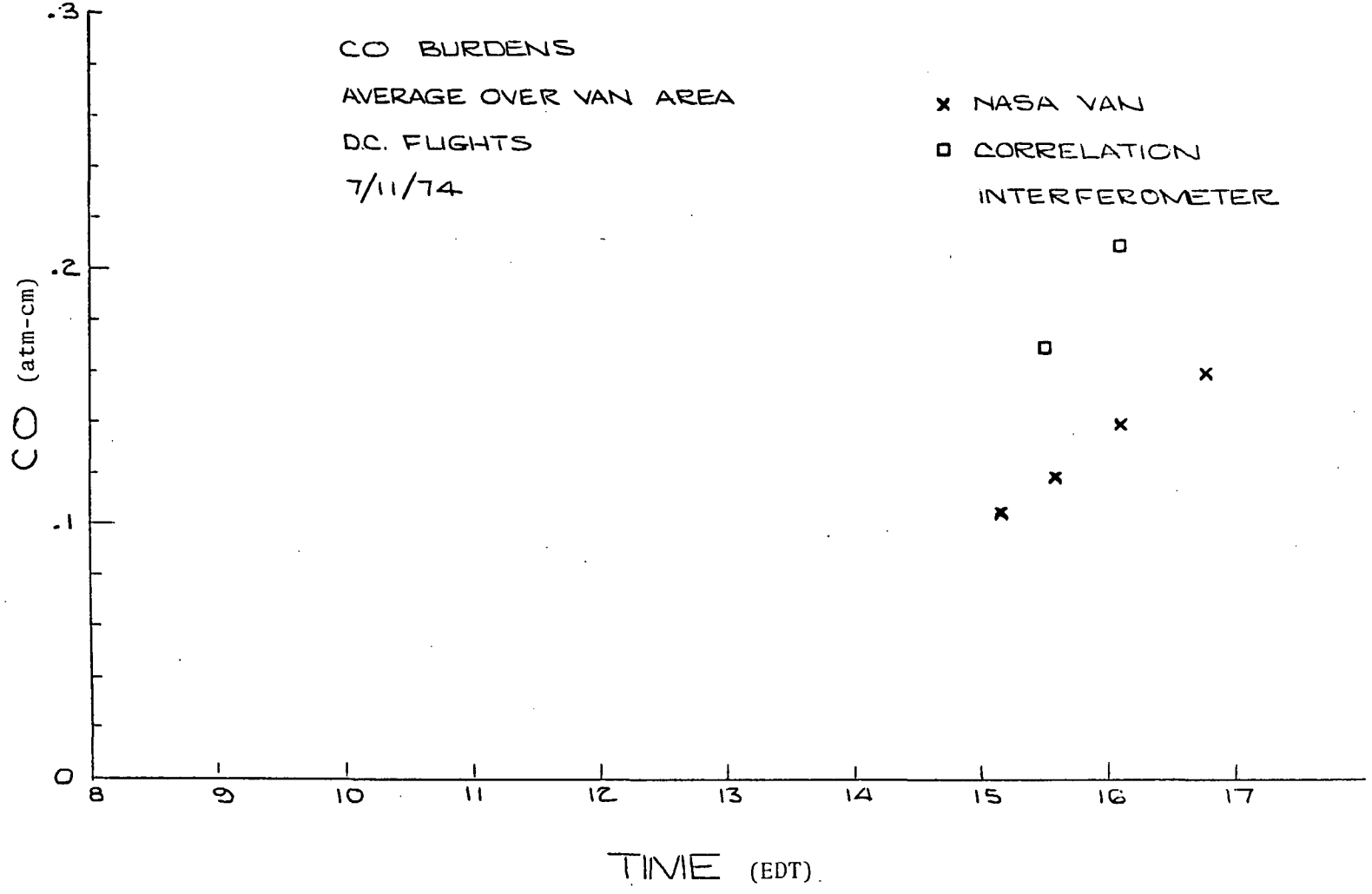

Figure 8.12 CO Burdens - D. C. Flights - 11 July 1974
(Average Over Van Area)

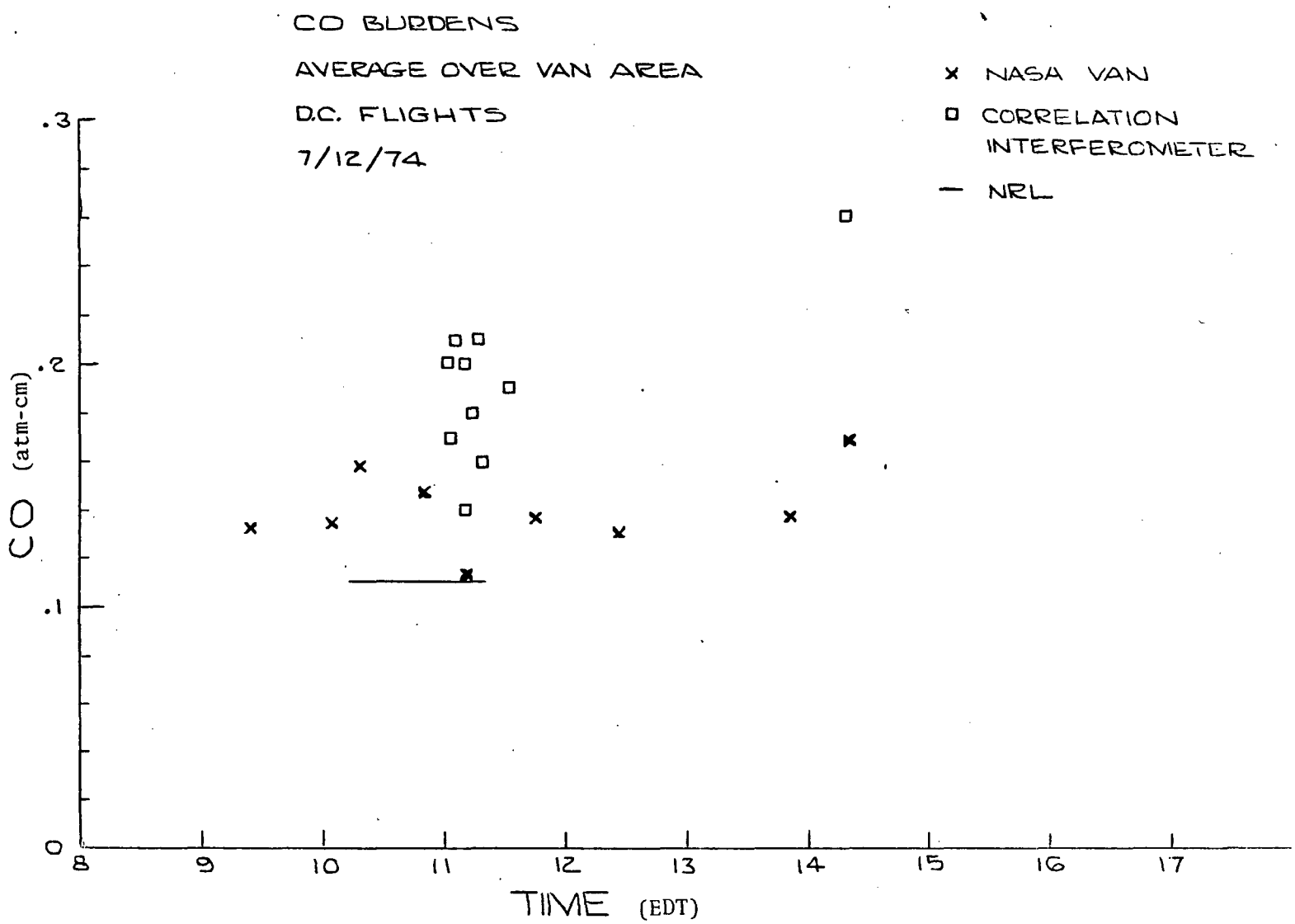

Figure 8.13 CO Burdens - D. C. Flights - 12 July 1974
(Average Over Van Area)

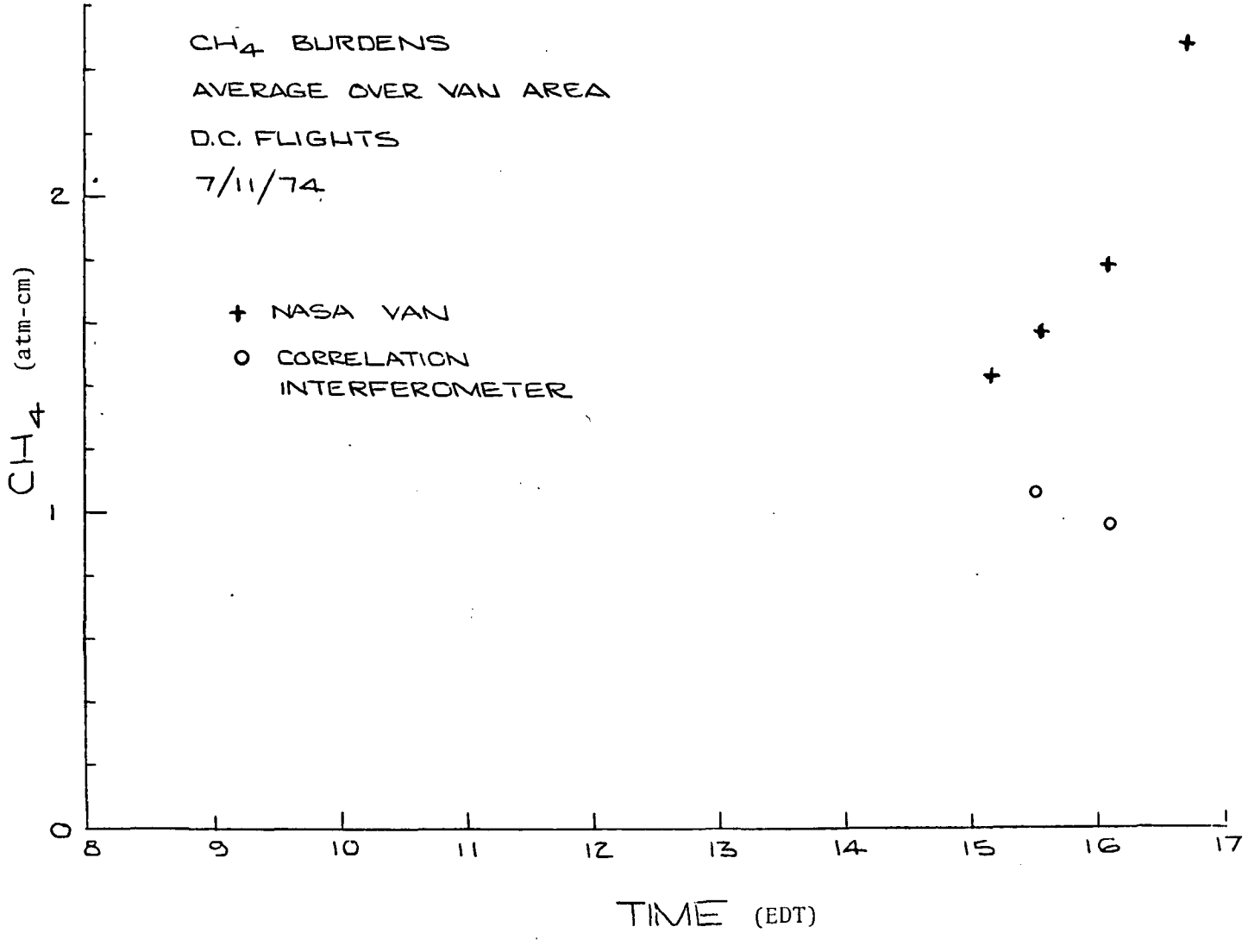

Figure 8.14 CH_4 Burdens - D. C. Flights - 11 July 1974
(Average Over Van Area)

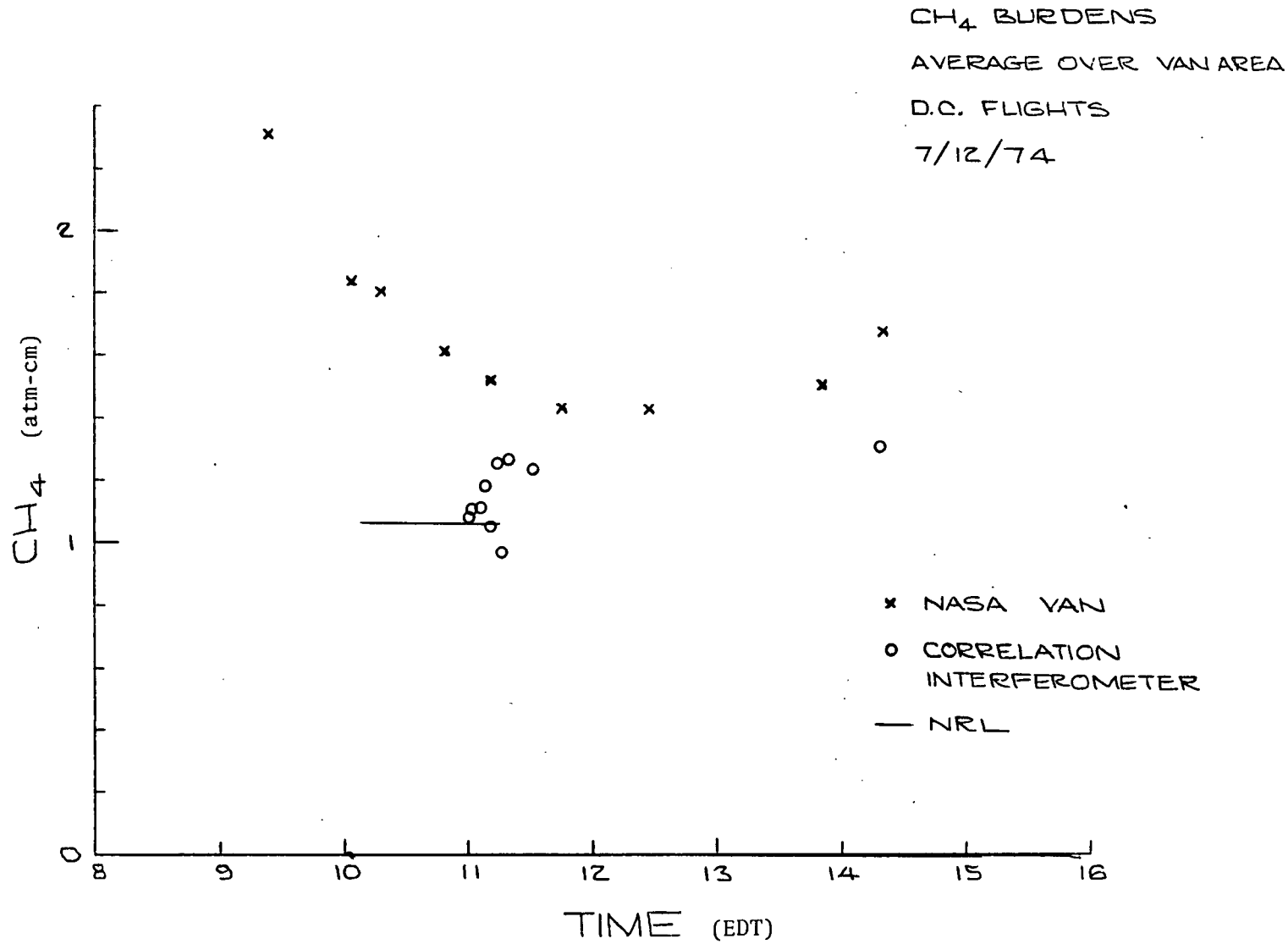

Figure 8.15 CH_4 Burdens - D. C. Flights - 12 July 1974
(Average Over Van Area)

9. A STUDY OF THE FEASIBILITY OF THE REMOTE MEASUREMENT OF TRACE ATMOSPHERIC SPECIES BY CORRELATION INTERFEROMETRY

A correlation interferometer was developed for the measurement of carbon monoxide and methane in the troposphere and in the stratosphere using absorption in the 2.35 μm region. Based on positive results obtained with this instrument, a study was undertaken to determine the feasibility of using this instrument for a large variety of atmospheric trace gases. This study will be discussed in detail after a brief discussion of the instrumental technique.

The 2.35 μm band of carbon monoxide was chosen since in this region, the non-thermal infrared, the main contribution to the observed radiation is that of the light reflected from the earth's surface. This makes the contribution of an absorbing molecule essentially independent of its altitude and the interpretation of the data is simpler than in the thermal infrared. For solar-looking measurements this consideration is negligible. It is not always possible to find suitable absorption bands in the non-thermal infrared and thermal infrared bands must be used. This is the case for three of the gases examined in the multi-gas analysis given below.

The basic interferometer is shown schematically in Figure 3.1. It is to be noted that the two mirrors are fixed in the instrument and the variation in path length difference is attained by the oscillation of the compensating plate. For the results given below, a thirteen degree oscillation was used giving a path length difference from 2.7 to 3.95 μm.

Figure 3.3 shows the spectrum of carbon monoxide in the 2.35 μm region and the corresponding interferogram. Since the spectral lines have a separation of the order of 3 cm^{-1}, the interferogram has a peak at 1/3 cm^{-1} or about 3 mm. The correlation interferometer uses only this part of the interferogram since most of the information on CO is contained therein (2.7 to 3.95 mm). The instrument operates directly on this interferogram section and does not transform it into a spectrum. Indeed, a spectrum obtained from the transformation of a portion of an interferogram would have little meaning. 32-scan measurements in the laboratory and outdoors show accuracies with approximately 10% error for CO and 2% error for CH_4.

For the measurement of a specific gas the optimum wavelength range and delay range must be known. The wavelength range determines the needed spectral filter, detectors and optics. The optimum wavelength range is determined by the absorption spectra of the gas and of other (interferent) gases of the atmosphere, by the identity and strength of the light source, by detector sensitivity, and to a slight extent, by the availability of optical materials. The breadboard and engineering models of the correlation interferometer have employed optical filters with a full width, at half maximum transmittance, of the order of 45 cm^{-1}, centered at about 4280 cm^{-1} (2.34 μm). Only the radiation transmitted by this filter affects the interferogram. Each gas has a specific spectral range which is best to use, although these may be very nearly the same for some gases with the effects still being separable by the correlation interferometer technique, since the interferogram on which the direct measurements are made is determined by line spacing which may vary significantly while still

being in the same wavelength range. This is the case with methane and carbon monoxide.

The other major parameter to be set is the delay range. The line spacings of the absorption spectra for each species is somewhat different. For measurement it is very convenient if these are such that the interferometric effects are nearly but not exactly the same, as with CH_4 and CO, as mentioned above. It is also quite convenient if the interferometric effects are nearly the same -- that is, occur over the same delay range -- but the spectral effects are found in a somewhat different spectral range, This occurs when the rotational energy level differences of two gases are nearly equal but the vibrational level differences are not nearly equal. It is not entirely fortuitous that this is often the case for similar molecules. Thus examination of spectra and interferograms for ammonia, NH_3, and nitric oxide, NO, as well as methane and carbon monoxide, each show major effects on the interferogram in the 2.7 to 4.0 mm range for spectral absorptions which are in different wavelength ranges. Thus these four gases could be measured using the same delay range, i.e., the same difference in the path lengths of the two arms of the interferometer, just by the use of different optical spectral filters.

For some other gases, optimum results would be obtained using a different delay range. However, it can be expected that any other delay range can be used for more than one other gas, again just by the use of appropriate spectral filters. Later the optimum wavelength ranges and path differences (delay ranges) are determined for several gases. However, it will also be seen that there is a single delay range which is suitable for at least most of the gases of interest.

In the first study the following steps comprised each calculation:

1. Spectra with 0.5 cm^{-1} resolution were obtained for individual gases at specific optical thicknesses using the Digilab FTS-14 interferometer-sepctrometer and ratioing to the background spectrum.
2. By use of computer techniques, spectra of various combinations of gases were obtained with appropriate optical filters.
3. From each spectrum, an interferogram was generated.
4. For each gas of interest an interferogram for the combination of the interferent gases and that gas was compared with an interferogram for the combination of the interferent gases without the gas of interest. The difference is the effect of the gas of interest in the presence of interferents.

The gases studied were:

CH_4	-	Methane
CO	-	Carbon Monoxide
CO_2	-	Carbon Dioxide
H_2O	-	Water

NH_3	-	Ammonia
NO	-	Nitric Oxide
NO_2	-	Nitrogen Dioxide
N_2O	-	Nitrous Oxide
SO_2	-	Sulfur Dioxide
C_2H_6	-	Ethane
C_2H_4	-	Ethylene

Table 9.1 lists the spectra which were obtained, arranged in order of increasing wavelength.

In addition to the spectra of these gases, spectra of water are needed. Since it has not been practical, in the laboratory, to obtain spectra for atmospheric amounts of water (for which a path-length of several kilometers is needed) these were obtained by use of a computer. All spectral regions where water is a significant interferent in the spectra given above were covered. The amount of water used was 2150 atm-cm, as given by Gutnick (ref. 9)(1962). Multiples of this from 0.1 to 10 were used.

Various combination spectra were generated, from which the corresponding interferograms were obtained. For these calculations a Lorentzian filter was assumed and filter width was taken of the order of 1/2 to 1% of its center frequency.

The interferograms with and without the gases of interest (the gases to be measured) are shown in Figures 9.1 through 9.11 for atmospheric burdens of CH_4, CO, CO_2, H_2O, NH_3, NO, NO_2, N_2O, SO_2, C_2H_6, and C_2H_4, respectively. The effect of the gas of interest is shown by the difference in the two interferograms plotted for that gas. Quantitative estimates of the sensitivities and accuracies for the gases are obtained by comparing the interferogram showing the CO effect (Figure 9.4) and the experimental accuracies of CO measurements from studies such as those mentioned above. Table 9.2 gives the estimated sensitivities relative to CO. Thus, correlation interferometry can be a very useful technique for the stratospheric and tropospheric measurement of these important trace atmospheric species.

To further study the feasibility of the measurement of several of the atmospheric trace gases listed above, in situations simulating their optical thicknesses in the atmosphere, a second systematic study has been carried out to simulate the performance of the correlation interferometer in the qualitative measurement of these gases. Because of the extensive computer calculations required, the complete study was not carried out for all of the gases.

Each calculation consisted of the first three steps of the calculation described above and the following three steps:

4. Various combinations of these interferograms were used to obtain weighting functions.
5. Using one or more appropriate weighting function(s), each interferogram was tested to determine the optical thickness the correlation interferometer technique would indicate.

TABLE 9.1 SPECTRA USED FOR INTERFEROGRAMS

$\nu(cm^{-1})$	Gas	Optical Thickness (atm-cm)
5156 - 4900	CO_2	250
	NH_3	0.036, 0.36
5048 - 4792	CO_2	250
	NH_3	0.0036[x]
4538 - 4282	CH_4	5.4
	CO	0.36
	NH_3	0.0036[x], 0.036, 0.36
	NO_2	0.014[x]
	N_2O	0.9
4358 - 4102	CH_4	5.4
	CO	0.36
	NO_2	0.014[x]
3778 - 3522	CO	0.36
	CO_2	250
	NH_3	0.0036[x]
	NO	0.016[x]
	N_2O	0.9
3578 - 3322	CO_2	250
	NH_3	0.0036[x]
	NO_2	1.08[x]
	N_2O	0.9
3416 - 3160	NH_3	0.036
	N_2O	0.9
3116 - 2860	CH_4	5.4
	NO_2	0.014, 0.14
	N_2O	0.9
	C_2H_6	0.00162, 0.00288, 0.00405, 0.0120, 0.0205, 0.102, 0.507
	C_2H_4	0.0206, 0.0615, 0.1850
3038 - 2782	CH_4	5.4
3800 - 2700	C_2H_6	0.013, 1.3, 13, 99
	C_2H_4	99.8
3600 - 2700	C_2H_4	0.013, 1.3
	C_2H_4O	0.026, 0.13, 45.4
	$C_2H_6O_2$	0.013, 0.59
	α - $C_{10}H_{16}$	0.012, 0.5
	β - $C_{10}H_{16}$	0.012, 0.36
2668 - 2412	CH_4	5.4
	N_2O	0.9
	SO_2	0.072
2598 - 2342	SO_2	0.072
2286 - 2030	CO	0.36
	CO_2	250
	N_2O	0.9
2018 - 1762	CO_2	250
	NH_3	0.0036[x], 0.036
	NO	0.004, 0.016
1810 - 1554	NH_3	0.0036
	NO_2	0.014
1506 - 1250	CH_4	5.4
	NO_2	0.014[x]
	N_2O	0.9
	SO_2	0.0036

x - No significant absorption.

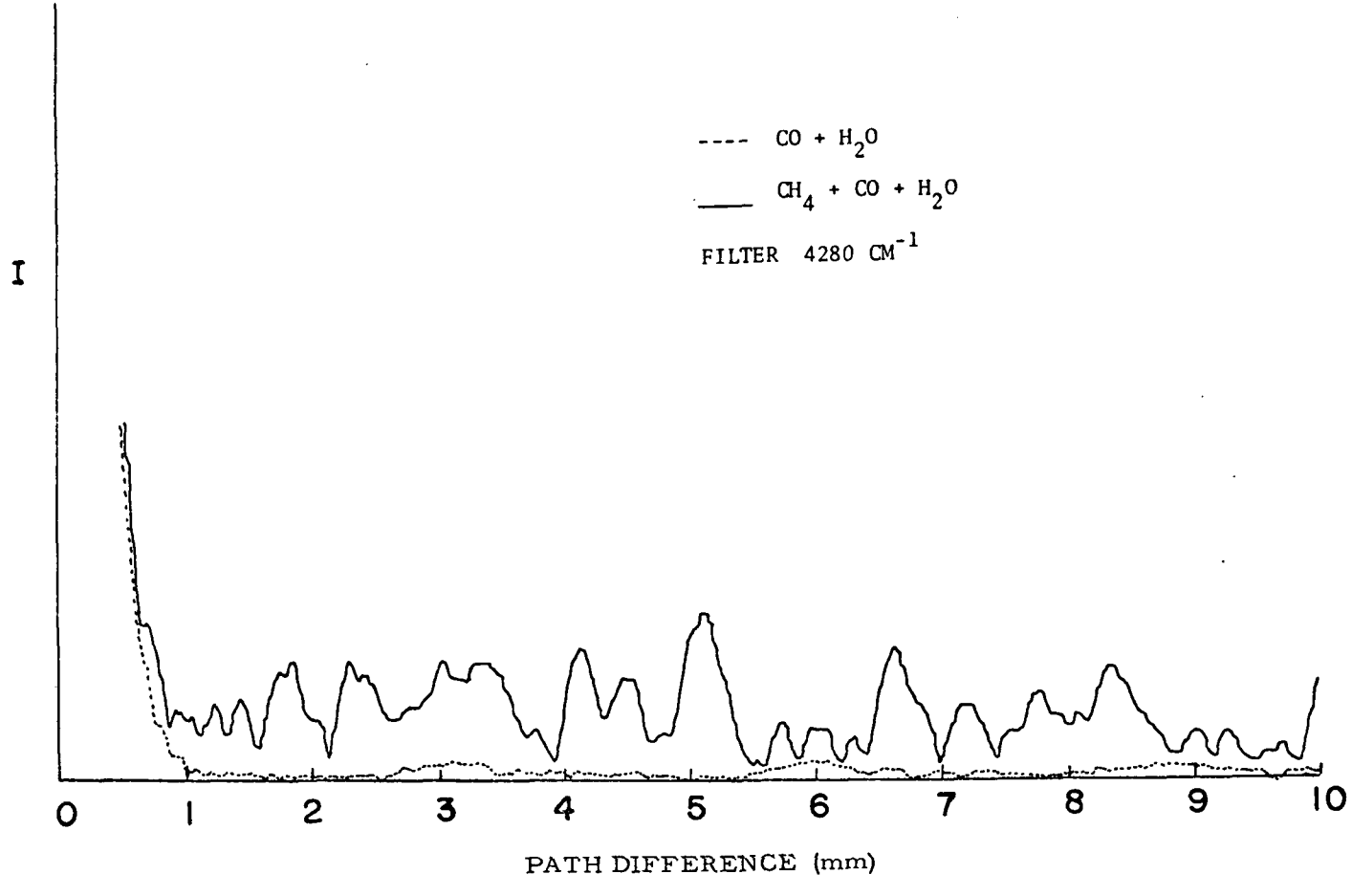

Figure 9.1 The Effect of CH_4 on the Interferogram Signal (Arbitrary Units) as a Function of Path Difference

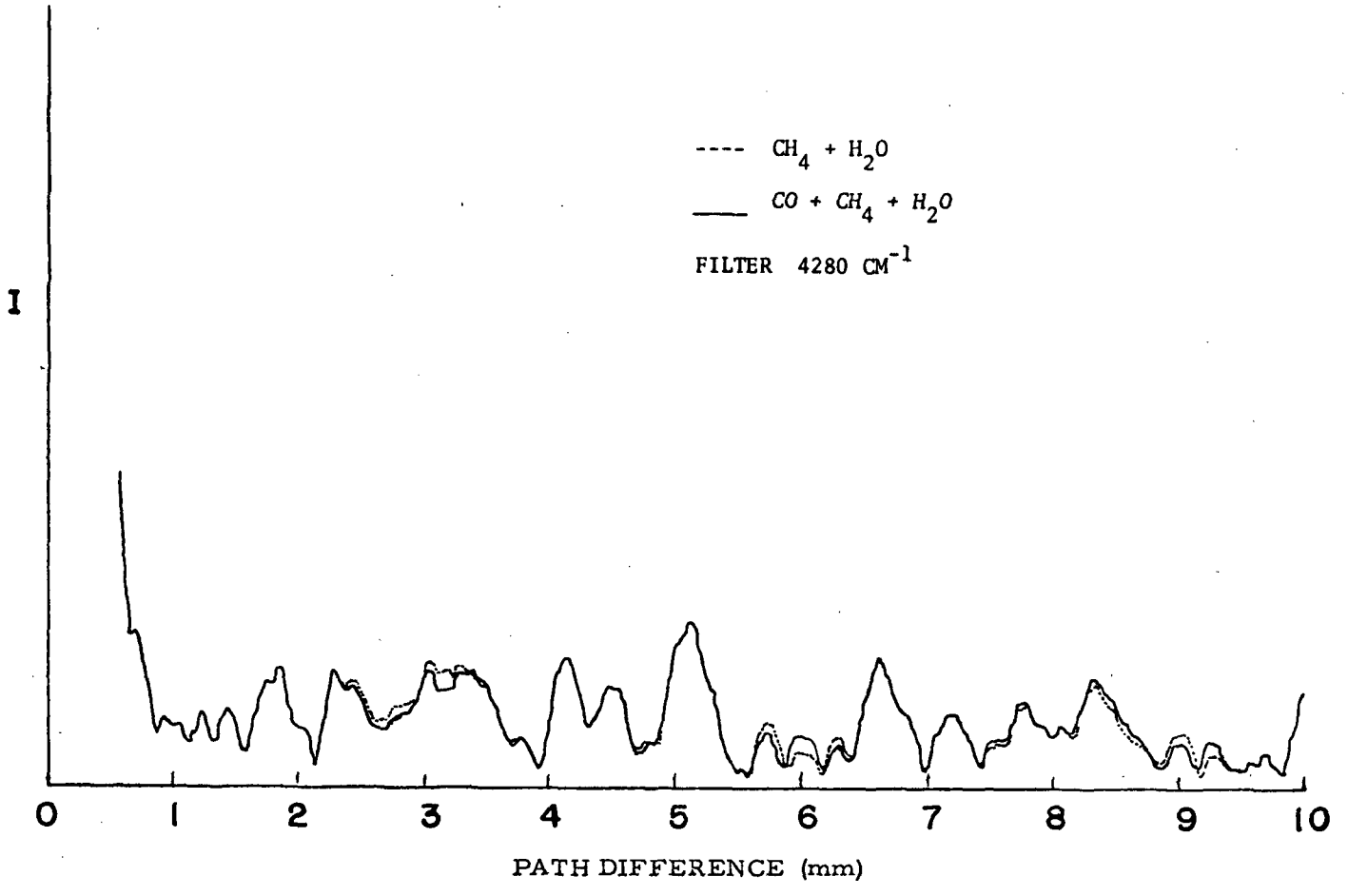

Figure 9.2 The Effect of CO on the Interferogram Signal (Arbitrary Units) as a Function of Path Difference

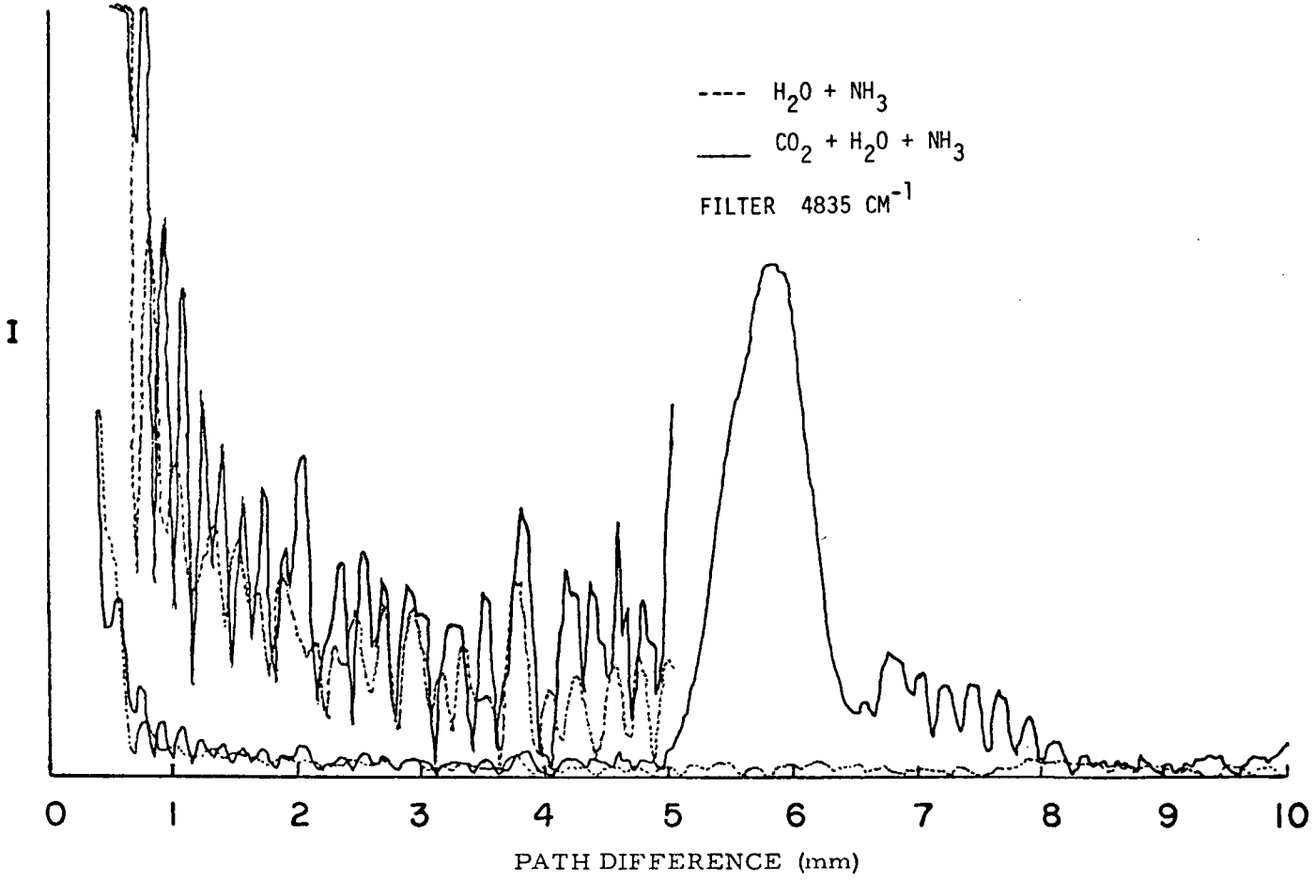

Figure 9.3 The Effect of CO_2 on the Interferogram Signal (Arbitrary Units) as a Function of Path Difference

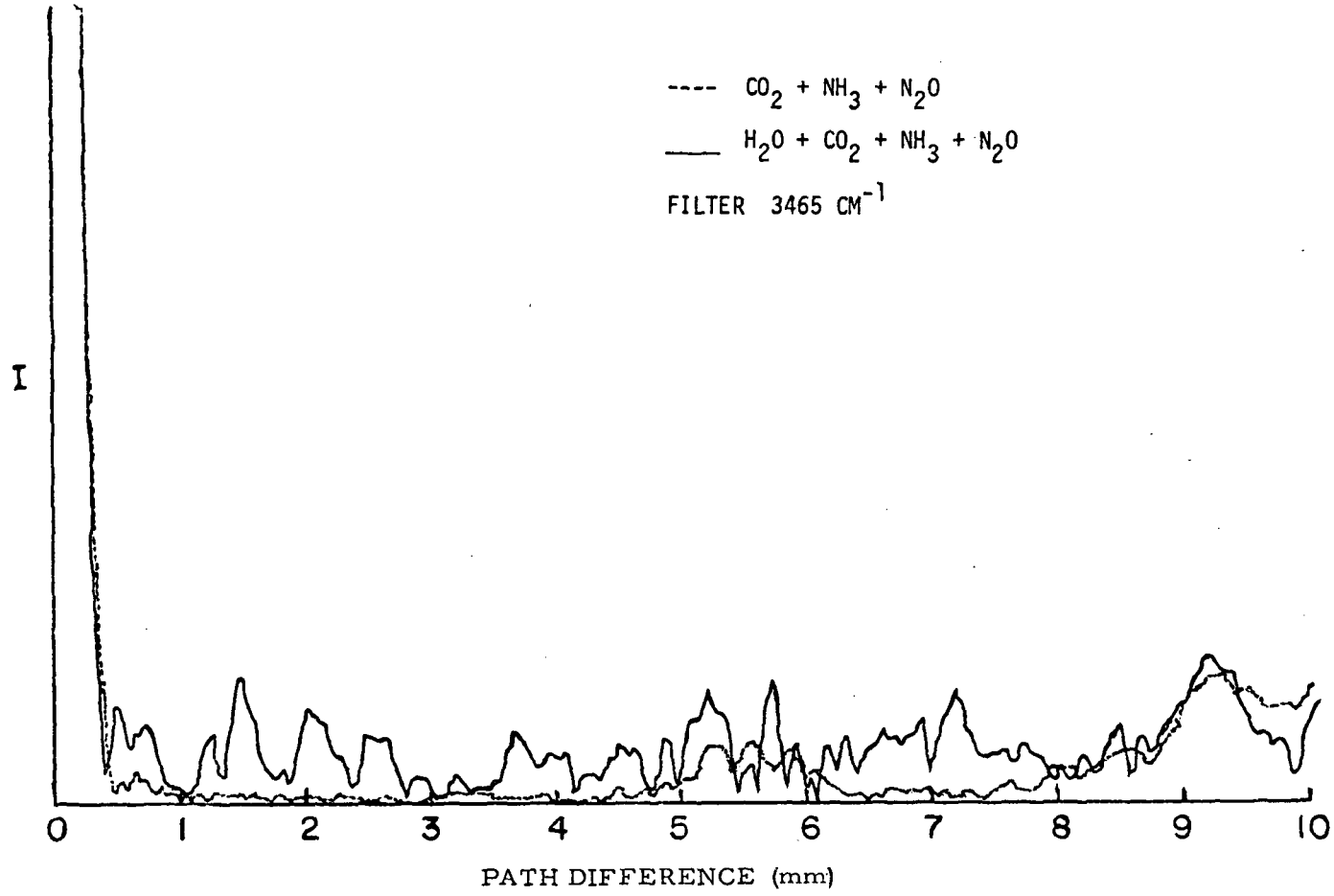

Figure 9.4 The Effect of H_2O on the Interferogram Signal (Arbitrary Units) as a Function of Path Difference

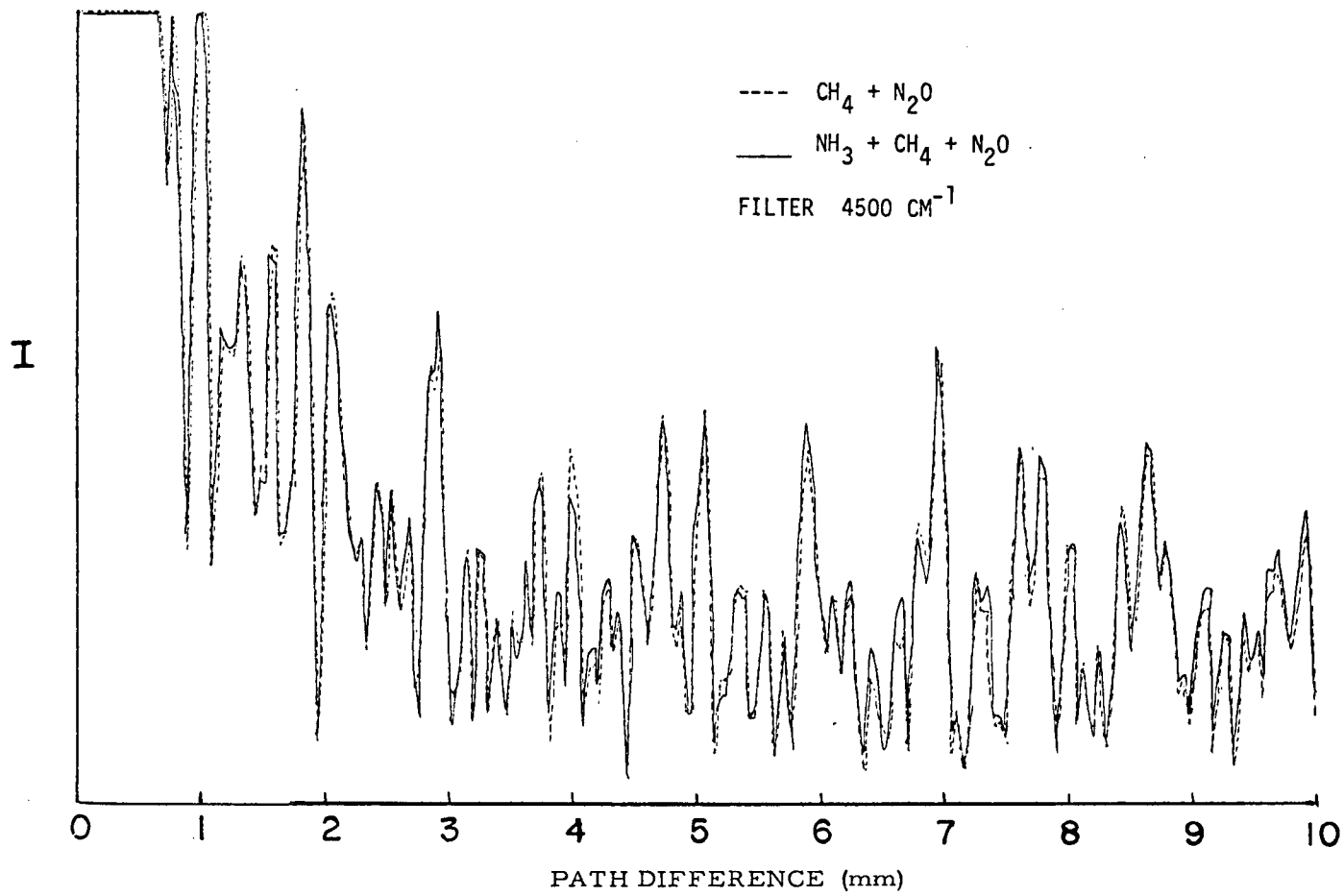

Figure 9.5 The Effect of NH_3 on the Interferogram Signal (Arbitrary Units) as a Function of Path Difference

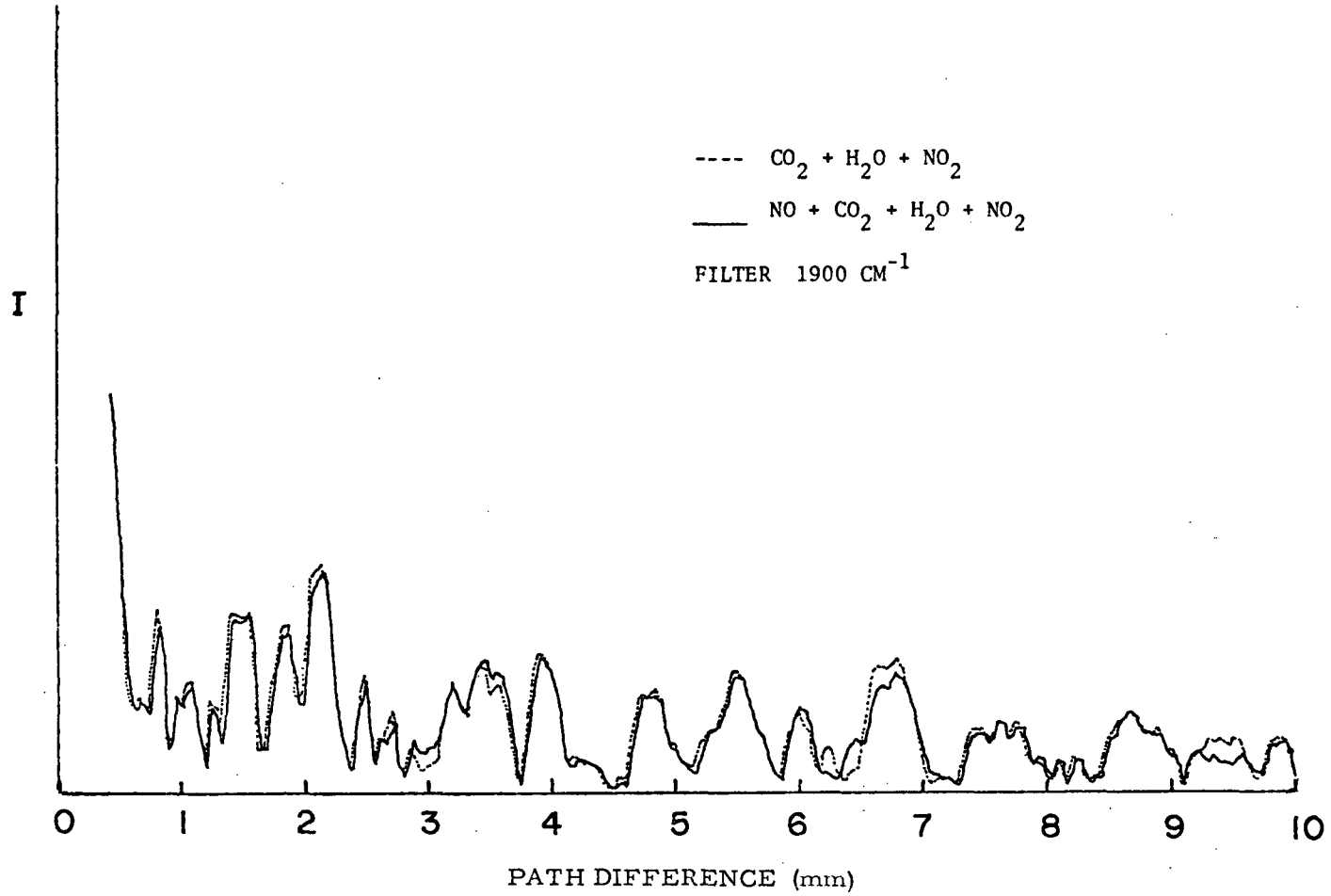

Figure 9.6 The Effect of NO on the Interferogram Signal (Arbitrary Units) as a Function of Path Difference

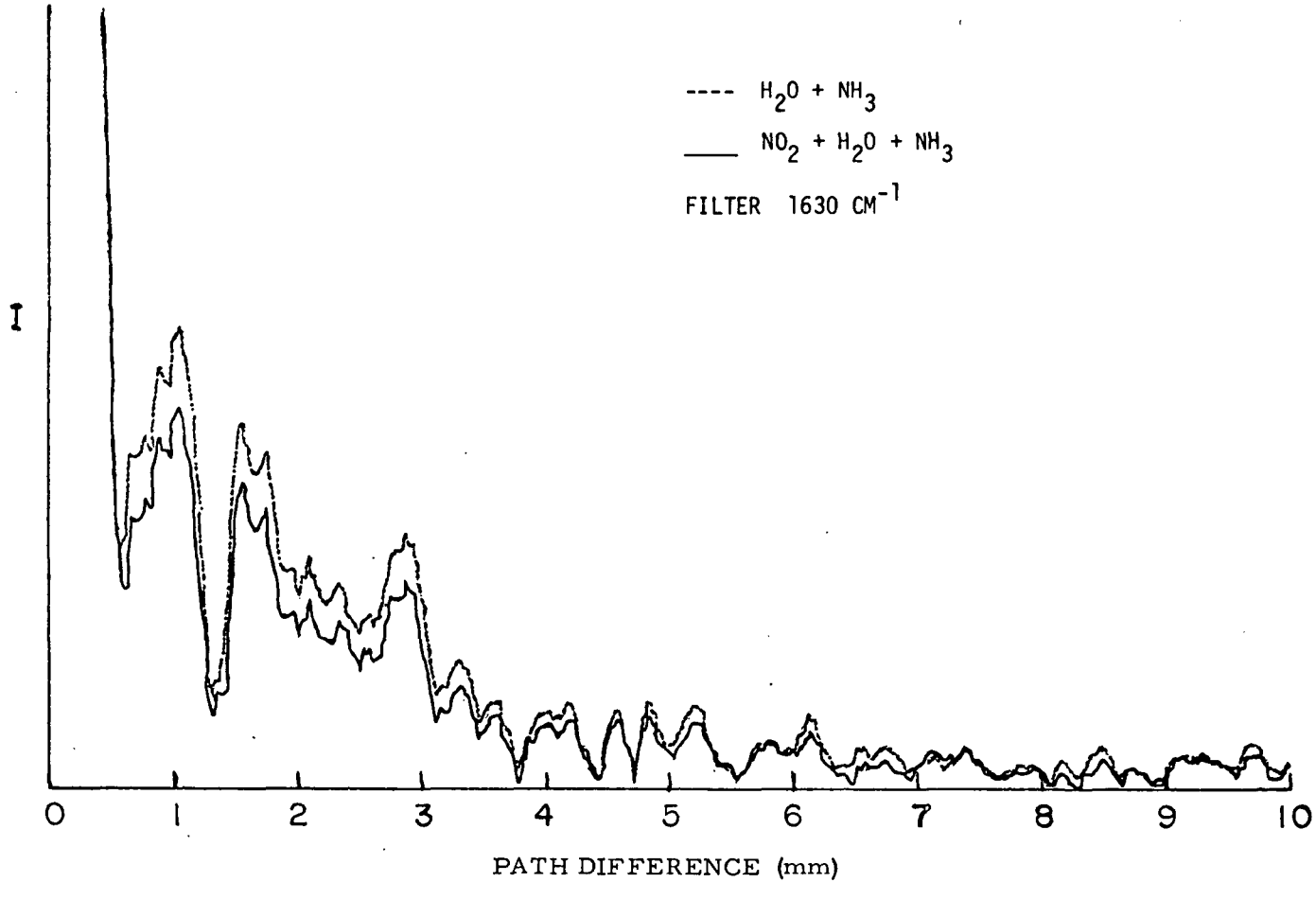

Figure 9.7 The Effect of NO_2 on the Interferogram Signal (Arbitrary Units) as a Function of Path Difference

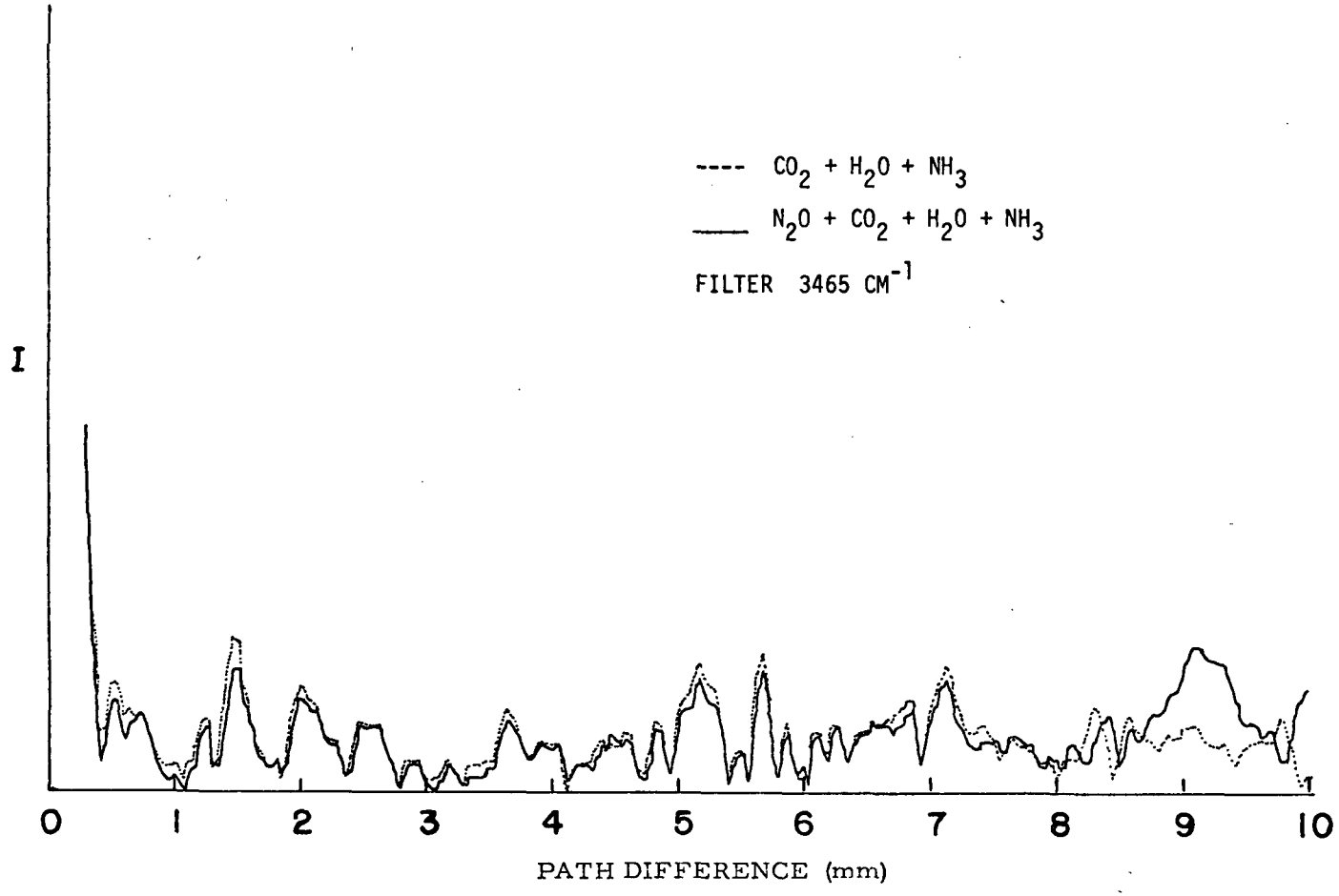

Figure 9.8 The Effect of N_2O on the Interferogram Signal (Arbitrary Units) as a Function of Path Difference

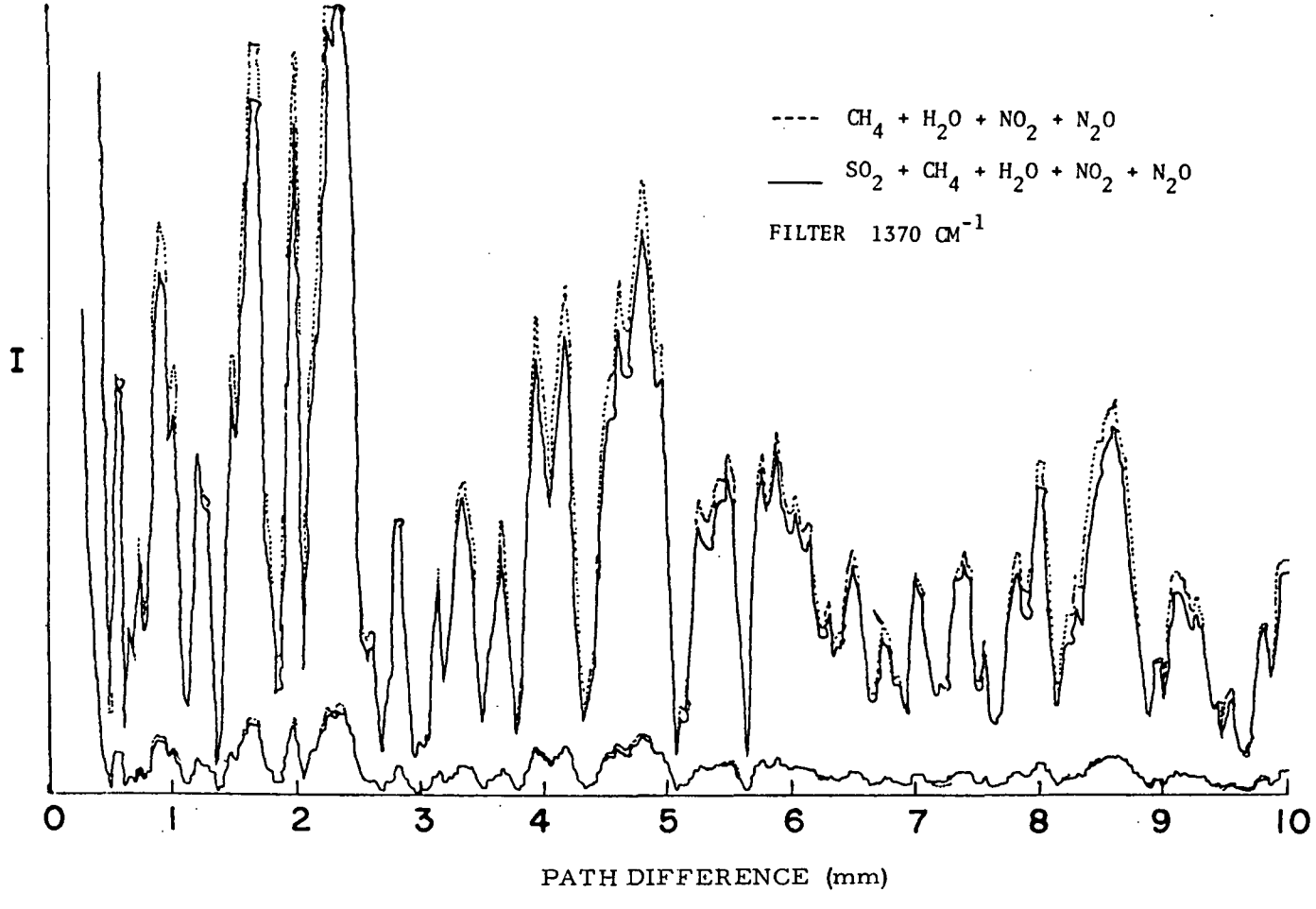

Figure 9.9 The Effect of SO_2 on the Interferogram Signal (Arbitrary Units) as a Function of Path Difference

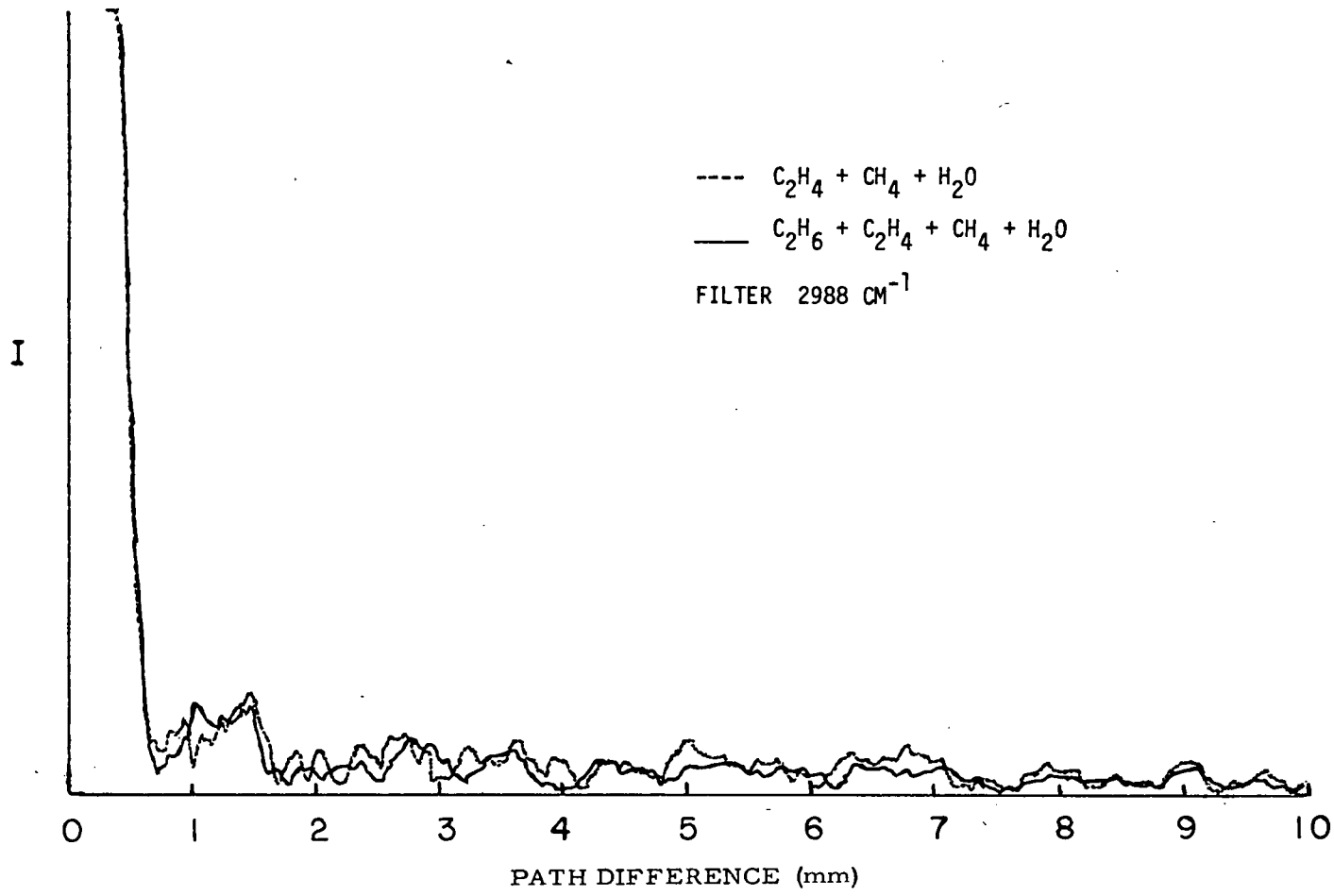

Figure 9.10 The Effect of C_2H_6 on the Interferogram Signal (Arbitrary Units) as a Function of Path Difference

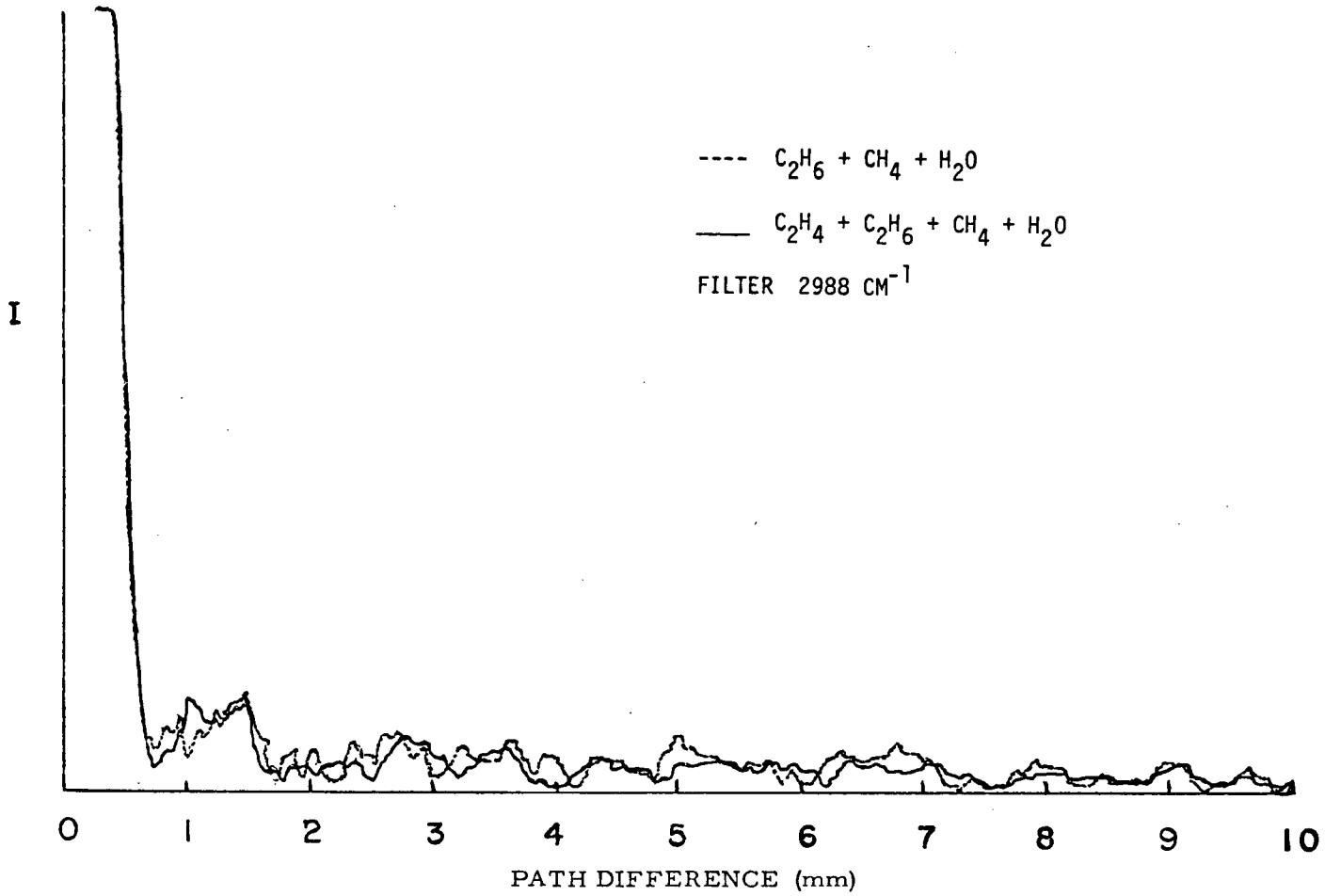

Figure 9.11 The Effect of C_2H_4 on the Interferogram Signal (Arbitrary Units) as a Function of Path Difference

TABLE 9.2 ESTIMATED SENSITIVITIES - SOLAR LOOKING - RELATIVE TO CO (CO = 0.04 atm-cm)

SPECIE	FILTER CENTER FREQUENCY cm^{-1}	(μm)	DELAY RANGE mm	RELATIVE BURDEN
CH_4	4280	(2.34)	5.5 - 6.4	5
			All Other	2
CO	4280	(2.34)	2.3 - 3.5	
			5.6 - 6.3	1
			7.4 - 9.4	
CO_2	4835	(2.07)	5.0 - 6.0	2
			6.0 - 8.0	125
			All Other	1250
H_2O	3465	(2.89)	All	1250
NH_3	4500	(2.22)	2.6 - 4.0	5
			6.3 - 7.5	10
N_2O	3465	(2.89)	3.0 - 3.6	5
			8.5 - 9.7	.5
NO†	1900	(5.26)	2.8 - 3.7	.2
			5.8 - 7.0	.08
			9.0 - 9.5	.08
NO_2†	1630	(6.13)	0.5 - 4.0	.06
			All Other	
SO_2†	1370	(7.30)	∿ 2.0	.03
			2.5 - 4.0	.2
			4.5 - 5.7	.2
			8.0 - 9.5	.3
C_2H_4†	2988	(3.35)	1.0 - 4.0	.5
			4.5 - 5.5	.2
			6.0 - 8.5	.5
C_2H_6†	2988	(3.35)	1.0 - 4.0	.02
			5.0 - 7.5	.008
			7.5 - 9.2	.02

†Detector with a $D^* \simeq 3 \times 10^{10}$ cm $Hz^{1/2}$ w^{-1}; all other species assume detector with a $D^* \simeq 10^{11}$ cm $Hz^{1/2}$ w^{-1}.

6. The indicated optical thicknesses were compared with the actual optical thicknesses to assess the accuracy of the technique and its sensitivity.

From this study conclusions can be drawn concerning the best delay range, and best spectral range, and the expected accuracy and sensitivity for the measurement of each of the gases. These conclusions are shown in Table 9.3.

A critical examination of the results of these two types of calculations, as given in Tables 9.2 and 9.3, shows the correlation interferometer to have the needed sensitivity and accuracy to measure atmospheric amounts of most of the atmospheric trace species.

TABLE 9.3 CALCULATED ACCURACIES AND SENSITIVITIES FOR MEASUREMENT OF ATMOSPHERIC TRACE GASES AS DETERMINED BY APPLICATION OF CORRELATION INTERFEROMETER ALGORITHM

GAS	SPECTRAL REGION (cm^{-1})	DELAY RANGE (mm)	ACCURACY FOR ATMOSPHERIC BURDEN (%)	SENSITIVITY (atm-cm)
CH_4	4280	2.58 - 3.83	10	
CO	4280	2.58 - 3.83	10	.01
H_2O	4865	2.58 - 3.83	25	
NO	1900	5.78 - 7.19	10	.001
		2.58 - 3.83	20	.002
N_2O	3465	2.58 - 3.83	10	.1
SO_2	1370	8.28 - 9.69	15	.002
		2.58 - 3.83	25	.005

Page Intentionally Left Blank

10. REFERENCES

1. Bortner, M. H.; Kummler, R. H.; and Jaffe, L. S.: "A Review of Carbon Monoxide Sources, Sinks, and Concentrations in the Earth's Atmosphere," NASA CR-2081, June 1972; and Water, Air, and Soil Pollution 3, 17 (1974).

2. Bortner, M. H.; Dick, R.; Goldstein, H. W.; Grenda, R. N.; and Levy, G. M.: "Development of a Breadboard Model Correlation Interferometer for the Carbon Monoxide Pollution Experiment," NASA CR-112212, Mar. 1973.

3. Dick, R.; Grenda, R. N.; Goldstein, H. W.; and Bortner, M. H.: "Design, Fabrication, and Testing of an Engineering Model Correlation Interferometer for the Carbon Monoxide Pollution Experiment," GE Rpt. (NASA Contract NAS1-10139), Nov. 1974.

4. Kummler, R. H.; Grenda, R. N.; Baurer, T.; Bortner, M. H.; Davies, J. H.; and MacDowell, J.: Satellite Solution of the Carbon Monoxide Sink Anomaly, Paper presented at 50th Annual Meeting, Am. Geophys. Union (Washington, D.C.), Apr. 1969.

5. Bortner, M. H.; Alyea, F. N.; Grenda, R. N.; Liebling, G. R.; and Levy, G. M.: "Analysis of the Feasibility of an Experiment to Measure Carbon Monoxide in the Atmosphere," NASA CR-2302, Oct. 1973.

6. Bortner, M. H.; and Kummler, R. H.: "The Chemical Kinetics and the Composition of the Earth's Atmosphere," General Electric Co. Rpt., GE-9500-ESC-SR-1, July 1968.

7. CIRA: COSPAR International Reference Atmosphere 1965. North Holland Publishing Co., Amsterdam, 1965.

8. Cadle, R.; and Powers, J.: Tellus 18, 176 (1966).

9. Gutnick, M.: "Mean Moisture Profiles to 31 m for Middle Latitudes," Interim Notes on Atmospheric Properties No. 22, Geophysical Research Directorate, AFCRL, 1962.

10. Oppel, G. E.: and Pearson, F. A.: "Infrared Model Atmospheres," Lockheed Missile & Space Co., 1963.

11. Lindquist, G.: "A Water Vapor Profile from the CARDE Solar Spectra," (U), in Semiannual Report of the Ballistic Missile Radiation Analysis Center (U) (1 July through 31 December 1964), Volume I: General Review, Report No. 4613-33-P(1), Inst. of Sci. & Tech., Univ. of Mich., pp. 23-47. Mar. 1965 (SECRET).

12. Anding, D.: "Band Model Methods for Computing Atmospheric Slant-Path Molecular Absorption," Univ. of Mich., Infrared & Optical Sensor Lab., NAVSO, P-24499-1, Feb. 1967.

13. AFCRL: U. S. Standard Atmosphere, 1966 Supplement, ARCRL (1966).

14. Keneshea, T. J., Zimmerman, S. P., and George, J. D.: The Latitudinal Variation of Major and Minor Neutral Species in the Upper Atmosphere, 14th COSPAR Meeting (Seattle), 1971.

15. Valley, S. L., ed.: Handbook of Geophysics and Space Environments, Chapters 10 and 16, AFCRL, McGraw Hill, 1965.

16. Burch, D. E.; and Williams, D.: Appl. Optics 1, 587 (1962).

17. Pyler, E. K., Benedict, W. S., and Silverman, S.: J. Chem. Phys. 20, 175 (1952).

18. Penner, S. S.; and Weber, D.: J. Chem. Phys. 19, 807 (1951).

19. Benedict, W. S.; Herman, R., Moore, G. E.; and Silverman, S.: Ap. J. 135, 277 (1962).

20. Bowen, T. R.: Blackbody Radiation Tables, U.S. Army Missile Command Rpt. TN-AMSMI-RNR-1-63, May 1963.

21. Thekaekara, M. P.: Solar Electromagnetic Radiation, NASA SP-8805, Rev. 1971.

22. Kostkowski, H. J.; and Bass, A. M.: J. Quant. Spect. & Rad. Transfer 1, 177 (1961).

23. Chandrasekhar, S.: Radiative Transfer, Dover Publ., N.Y., 1960.

24. Kulander, J. L.: "Non-Equilibrium Radiation," General Electric Co. Rpt. GE 71SDR64SD41, June 1964.

25. Armstrong, B. H.: J. Quant. Spect. & Rad. Transfer 7, 61 (1967).

26. Penner, S. S.: Quantitative Molecular Spectroscopy and Gas Emissivities, p. 20, Addision-Wesley, Reading, Mass., 1959.

27. Houghton, J. T.; and Smith, S. D.: Proc. Roy. Soc., London, A320, 23 (1970).

28. Abel, P. G.; Ellis, P. J.; Houghton, J. T.; Peckham, G.; Rogers, C. D.; Smith, S. D.; and Williamson, E. J.: Proc. Roy. Soc., London, A320, 35 (1970).

29. Abel, P. G.; Houghton, J. T.; Matley, J. B.; and Williamson, E. J.: Proc. Roy. Soc., London, A320, 57 (1970).

30. Ludwig, C. B.: Private Communication, 1970.

31. Cooley, J. W.; and Turkey, J. W.: Math. of Computation 19, 297 (1965).

32. Gentlemen, W. M.; and Sande, G.: Fast Fourier Transforms for Fun and Profit," Proc. Fall Joint Computer Conf., pp. 563-578 (1966).

33. Tuller, S. E.: Monthly Weather Rev. 96, 785 (1968).

34. Dick, R.; and Levy, G.: Correlation Interferometry, Proceedings Aspen International Conference on Fourier Spectroscopy, AFCRL-71-0019, 1971.

35. Grenda, R. N.; Bortner, M. H. ; LeBel, P. J.; Davies, J. H.; and Dick, R.: Carbon Monoxide Pollution Experiment (I). A Solution to the Carbon Monoxide Sink Anomoly. Paper presented at the Joint Conference on Sensing of Environmental Pollutants (Palo Alto), AIAA Paper #71-1120 (Nov. 1971).

36. Rice, S. O.: Bell Sys. Tech. J. 23, 282 (1944).

37. Rice, S. O.: Bell Sys. Tech. J. 24, 46 (1945).

38. Goldstein, H. W.; Bortner, M. H.; Grenda, R. N.; Karger, A. M.; Dick, R.; David, F.; and LeBel, P. J.: Proc. Second Joint Conf. on Sensing of Environmental Pollutants, pp. 17-20 (1973).

39. Wilkness, P. E.; Swinnerton, J. W.; Bressan, D. J.; Lamontagne, R. A.; and Larson, R. E.: J. Atmos. Sci. 32, 158 (1975).

40. Seiler, W.; and Junge, C.: Tellus 21, 447 (1969).

Page Intentionally Left Blank

APPENDIX I.

CHURCHILL AREA SINGLE SCAN DATA

Page Intentionally Left Blank

CHURCHILL AREA SINGLE SCAN DATA
PASS 1

SCAN NO.	CO (atm-cm)	CH_4 (atm-cm)	SCAN NO.	CO (atm-cm)	CH_4 (atm-cm)
494	.4414	3.7672	544	.3136	3.9275
495	.4986	4.4806	545	.4003	3.9303
496	.5834	2.6820	546	.5506	3.2858
497	.5461	3.5357	548	.3609	3.5575
498	.1959	4.0735	549	.3490	3.7733
500	.2991	3.5077	551	.3918	2.9152
501	.2508	3.4481	552	.2251	3.6841
502	.5335	3.5612	553	.3788	3.1893
503	.0699	4.0531	554	.3182	3.7687
504	.3953	3.3726	556	.3594	4.2140
505	.5877	3.7486	557	.3791	3.3390
506	.1340	3.7339	558	.3199	3.3341
508	.4385	3.8813	559	.5116	3.8152
509	.5378	3.7410	560	.4895	3.3166
511	.1575	3.3294	561	.4313	3.3375
512	.2267	3.4253	562	.4729	3.9021
513	.4746	3.1921	564	.4199	4.3725
514	.5798	3.7908	565	.2257	3.8922
516	.3726	3.6776	566	.3114	3.8468
517	.4056	3.6653	567	.1593	3.6139
518	.3220	3.6270	568	.3274	3.8792
519	.4874	3.1220	569	.3465	3.9123
520	.4473	3.2826	570	.2569	3.9997
521	.4193	3.7929	572	.4523	3.5903
522	.3614	3.4855	573	.3978	3.4034
524	.2707	3.4323	574	.4786	3.5605
525	.4848	3.7762	575	.3902	3.6289
526	.5151	3.1855	576	.2325	3.0639
527	.3613	3.7536	577	.3253	3.4836
528	.1847	3.6481	578	.2243	3.9457
529	.2983	3.7990	580	.4323	3.5026
530	.5388	2.7415	581	.3865	3.6278
532	.0715	3.7033	583	.3436	3.6203
533	.1201	3.1972	584	.3223	3.4526
534	.2481	3.1434	585	.1240	3.8160
535	.5632	3.6784	586	.3688	3.6374
536	.5896	3.5374	588	.2345	3.9257
537	.2399	3.7466	589	.2110	3.6411
538	.3963	3.8850	590	.3756	3.2890
540	.3539	4.1497	591	.3687	3.3935
541	.2059	4.0138	592	.2288	4.2965
542	.3146	3.4315	593	.3858	3.5786
543	.2150	3.1389	594	.2403	3.3953

CHURCHILL AREA SINGLE SCAN DATA
PASS 1 - Continued

SCAN NO.	CO (atm-cm)	CH_4 (atm-cm)	SCAN NO.	CO (atm-cm)	CH_4 (atm-cm)
596	.3420	3.6490	645	.1698	3.4495
597	.4998	4.0172	646	.2159	3.9573
598	.1575	3.5603	647	.2975	3.9574
599	.4247	3.6813	648	.3897	4.1862
600	.1871	4.0481	649	.3530	3.7326
601	.4109	2.8514	650	.2701	3.4851
602	.0738	3.7007	652	.4806	4.3353
604	.2770	4.3084	653	.2577	3.9929
605	.1902	3.3382	654	.3638	3.3630
606	.3259	3.8206	655	.1426	3.6467
607	.6268	3.4115	656	.1945	3.0471
608	.2454	3.9162	657	.1821	4.4800
609	.6068	3.6687	658	.0765	3.9314
610	.2014	3.4794	660	.0952	3.4958
612	.0636	3.9554	661	.2014	3.1061
613	.1637	3.5953	662	.1318	4.0710
614	.1598	3.3301	663	.1806	3.4139
615	.4952	2.8475	664	-.0237	4.0238
616	.2567	3.1798	665	.3453	4.1098
617	.1964	4.0099	666	.3767	3.7916
618	.2597	3.3153	668	.1223	4.1844
620	.3280	4.0318	669	.3660	3.5951
621	.1745	3.6790	670	.3890	3.7040
622	.2370	3.0848	671	.4051	3.6560
623	.2564	3.6807	672	.3410	3.2676
624	.4429	3.2533	673	.2633	3.3534
625	.2260	3.4534	674	.2179	4.1237
626	.5785	3.5117	676	.2404	3.6888
628	.0345	4.1203	677	.1029	3.0505
629	.0911	4.2961	678	.3956	3.6307
630	.3291	3.8378	679	.3354	4.6841
631	.5265	3.7049	680	.2938	3.1424
632	.2200	3.6815	681	.1257	3.3827
633	.3670	4.3242	682	.1061	3.7920
634	.3427	3.3690	684	.2738	3.7112
636	.0978	3.7733	685	.2990	3.6155
637	.4875	3.2260	686	.1042	4.3178
638	.3020	3.5784	687	.4345	3.0503
639	.3368	4.1089	688	.5124	3.6762
640	.5475	4.0242	689	.0850	4.1894
641	.1255	3.7961	690	.3401	2.9083
642	.4205	3.5003	692	.2436	3.8055
644	.2406	3.7924	693	.3398	3.3031

CHURCHILL AREA SINGLE SCAN DATA
PASS 1 - Continued

SCAN NO.	CO (atm-cm)	CH_4 (atm-cm)	SCAN NO.	CO (atm-cm)	CH_4 (atm-cm)
694	.3076	4.3462	744	.4508	3.7579
695	.3713	3.2095	745	.1594	3.9547
696	.4556	4.0562	746	-.1225	3.4149
697	.2858	3.8356	748	.0680	3.9513
698	.1800	3.2073	749	.4829	3.9301
700	.3621	4.0038	750	.1912	4.1199
701	.2143	4.0279	751	.3706	3.5468
702	.2713	4.0246	752	.4301	4.0245
703	.1784	4.4967	753	.4228	3.7420
704	.3720	3.6151	754	.2892	3.2673
705	.1834	3.6815	756	.2149	4.3044
706	-.0569	4.1049	757	.0567	4.5085
708	.6185	3.8038	758	.0615	3.3264
709	.1904	4.3701	759	.2124	3.2652
710	.1444	3.9782	760	.0273	3.5825
711	.3881	3.3063	761	-.1602	2.7442
712	.3480	4.0239	762	.4504	2.6617
713	.0640	3.3514	764	.2331	3.6278
714	.3616	3.4833	765	.3066	3.6287
716	.0595	4.2171	766	.2902	3.9451
717	.1483	3.4260	767	-.1197	3.5703
718	.2130	3.4244	768	-.0771	3.9907
719	.2451	3.9875	769	.1431	3.5658
720	.5476	3.7732	770	.2710	3.0198
721	.1647	3.9809	772	.7107	3.5736
722	.2888	4.3687	773	.0825	3.7305
724	.3865	3.8327	774	.1034	4.6591
725	.3539	4.1933	775	.3308	3.4203
726	.0724	4.7648	776	.3864	3.7169
727	.1117	3.6538	777	.0950	4.3656
728	.3261	3.2113	778	.2872	4.1862
729	.3331	3.7831	780	.1945	3.7804
730	.2872	3.8079	781	.0562	3.5782
732	.1860	4.1111	782	.1747	3.1294
733	.2303	4.3677	783	.1416	4.3846
734	.2011	3.5780	784	-.0149	4.2199
735	.7204	3.3603	785	.2157	3.6093
736	.0884	3.2708	786	.0437	3.9714
738	.2493	4.4892	788	.1421	3.7192
740	.0621	3.6423	789	.1959	3.6568
741	.3798	3.8247	790	.3478	3.9927
742	.0702	3.7184	791	.1979	3.9617
743	.3426	3.1718	792	.3212	3.9463

CHURCHILL AREA SINGLE SCAN DATA
PASS 1 - Concluded

SCAN NO.	CO (atm-cm)	CH_4 (atm-cm)	SCAN NO.	CO (atm-cm)	CH_4 (atm-cm)
793	-.1623	3.8937	842	.3565	3.0860
794	.4649	3.4827	844	.2006	3.8706
796	.1711	4.1553	845	.1495	4.4679
797	.5779	3.4853	846	.5773	2.9689
798	.2556	4.7868	847	.1363	3.0891
799	.1145	3.4708	848	.6451	2.9528
800	.2770	3.9799	849	.1011	3.0967
801	-.1993	4.1181	850	.2870	4.6828
802	.0291	3.8873	852	.1108	2.9207
804	.1867	3.9052	853	.4763	4.6941
805	-.2203	3.8315	854	.3277	3.5806
806	.2408	3.8482	855	.3452	3.7967
807	.2968	3.2358	856	.3588	2.8560
808	.1217	4.3579	857	.1715	4.7654
809	.2357	4.6650	858	.3163	3.6580
810	.2469	3.7579	860	.1646	3.6162
812	.4798	4.1364	861	.3266	3.3507
813	.3800	2.8540	862	.0192	4.2168
814	.1409	3.8365	863	.3085	3.7707
815	-.0038	4.5899	864	-.0857	4.3306
816	.0569	4.1330	865	.6671	3.7557
817	.1821	3.7697	866	.3210	3.6373
818	.1022	3.5541	868	.0924	3.5251
820	.4318	3.9949	869	.1156	4.4565
821	.5142	3.6458	870	.0735	4.0488
822	.2843	4.4395	871	.1572	3.9825
823	.2944	3.7261	872	.4748	3.2381
824	.3971	3.6872	873	.2498	3.4621
825	.0944	4.2770	874	.1974	4.2047
826	.6754	3.0305	876	.4012	3.7691
828	.4526	3.9432	878	.3086	2.6420
829	.0879	4.2668	879	.3653	3.1910
830	.0456	3.9784	880	.4595	4.1029
831	.4843	3.9239	882	.5578	4.6950
832	.0996	3.4931	883	.3745	3.6817
833	.3206	3.0610	884	.2809	3.1809
834	.2953	3.7912	885	.1022	4.0699
836	.0359	3.8679	886	.1786	3.7063
837	-.0350	3.3926	887	.3628	3.4542
838	.2541	3.7200	888	.2206	3.8038
839	.3229	2.4168			
840	.2155	3.7555			
841	.0374	3.4919			

CHURCHILL AREA SINGLE SCAN DATA
PASS 2

SCAN NO.	CO (atm-cm)	CH_4 (atm-cm)	SCAN NO.	CO (atm-cm)	CH_4 (atm-cm)
1005	.2868	4.1674	1054	.2282	4.4830
1006	.4163	3.0810	1056	.1722	3.2463
1008	.2698	3.5252	1057	.0227	3.7654
1009	.4106	4.0497	1058	.4300	3.6119
1010	.4125	3.2554	1059	.3394	3.5375
1011	.2376	2.8463	1060	.1983	4.9188
1012	.1571	3.6803	1061	.3380	4.2097
1013	.3713	3.8110	1062	.4366	4.1020
1014	.4311	4.0535	1064	.1444	4.2077
1016	.1959	3.7383	1065	.2345	3.2104
1017	.3348	3.1565	1066	.4154	3.4784
1018	.2712	3.1903	1067	-.0278	3.5251
1019	.3131	3.4222	1068	.2004	4.0226
1020	.5567	4.2075	1069	.2713	3.4799
1021	.2495	3.5897	1070	.4688	2.7993
1022	.1119	4.0217	1072	.2308	3.5638
1024	.3633	3.8737	1073	.2481	3.2826
1025	.5056	4.0399	1074	.3383	3.6115
1026	.2043	3.7509	1075	.3795	3.6156
1027	.0512	4.2556	1076	.0610	5.0027
1028	.2602	3.8406	1077	.2162	4.3663
1029	.1773	4.3095	1078	.6051	3.8921
1030	.4623	3.0569	1080	.4799	2.9864
1032	.0762	3.9604	1081	.2043	3.4243
1033	.3713	3.5240	1082	.2707	3.4847
1034	.4023	3.6930	1083	.2524	3.7960
1035	.2207	3.1706	1084	.3950	3.2422
1036	.3655	3.8404	1085	.2688	3.6131
1037	.2895	4.2679	1086	.2864	3.7740
1038	.0719	3.3185	1088	.3211	4.3087
1040	.1879	3.7050	1089	.1156	3.8293
1041	.4165	3.9070	1090	.0618	3.5096
1042	.3008	3.4111	1091	.0952	3.4909
1043	.3597	3.8848	1092	.1608	4.3698
1044	.2708	4.0655	1093	.2489	3.9753
1045	-.0734	3.6664	1094	.3202	3.4073
1046	.1542	3.4808	1096	.2521	3.6283
1048	.6799	3.0064	1097	.2940	3.7519
1049	.3843	3.6562	1098	.0685	3.1820
1050	.2082	4.4672	1099	.4139	3.7106
1051	.5057	3.7472	1100	.2434	3.6845
1052	.2054	3.4425	1101	-.0613	3.4410
1053	.4103	3.7695	1102	.3622	3.9003

CHURCHILL AREA SINGLE SCAN DATA
PASS 2 - Concluded

SCAN NO.	CO (atm-cm)	CH_4 (atm-cm)
1104	.0384	4.3229
1105	.2016	3.7565
1106	.2451	4.0009
1107	.3988	3.3109
1108	.3941	4.6328
1109	.1494	4.0542
1110	.1759	3.9237
1112	.2208	4.2733
1113	.1911	2.9248
1114	.5337	3.1117
1115	.0853	3.7637
1116	.2206	4.1741
1117	.2121	3.5599
1118	.3904	3.9989
1120	.0752	3.4651
1121	.2110	3.0374
1122	.3609	3.7407
1123	.5880	3.7233
1124	.2753	3.0305
1125	.0788	2.9862
1126	.6016	3.8256
1128	.4166	3.7921
1129	.1936	3.8989
1130	.1040	3.7903
1131	.1879	3.8463
1132	.0515	4.0103
1133	.5241	3.5129
1134	.2733	3.6744
1136	.3361	3.8689
1137	.2747	3.4437
1138	.2213	3.2364
1139	.0939	3.3710
1140	.3368	3.3618
1141	.4734	4.1248
1142	.4334	4.6006
1144	.1556	4.0145
1145	.2519	4.0727
1146	.2339	3.4130
1147	.2511	3.7755
1148	.3221	3.5119
1149	.1358	3.3880
1150	.1780	3.4276
1152	.2006	3.9702

CHURCHILL AREA SINGLE SCAN DATA
PASS 3

SCAN NO.	CO (atm-cm)	CH_4 (atm-cm)	SCAN NO.	CO (atm-cm)	CH_4 (atm-cm)
1477	.4768	3.3745	1522	.0873	3.4279
1478	.2175	3.9028	1523	.3473	3.3312
1479	.5268	3.8084	1525	.1845	4.2121
1480	.0510	3.5577	1526	.2708	3.5464
1481	.3010	4.4073	1527	.1676	4.4597
1482	.3408	4.0858	1528	.0015	3.5720
1483	.1356	4.3624	1529	.4998	3.8104
1485	.1366	3.9919	1530	.3240	3.4525
1486	.0420	3.9280	1531	.1640	3.5448
1487	.4430	3.1901	1533	.2804	4.6137
1488	.3065	3.5991	1534	.2389	3.9817
1489	.5330	4.1067	1535	-.0078	3.5343
1490	.1082	4.3858	1536	.1355	4.1415
1491	.3474	3.9523	1537	.1432	3.5880
1493	.1574	3.6289	1538	.3692	4.0141
1494	.1642	3.6896	1539	.2251	3.6787
1495	.4520	3.7801	1541	.2245	3.1454
1496	.4135	3.7834	1542	.1874	3.8629
1497	.0583	3.7813	1543	.0626	4.4396
1498	.1686	3.8327	1544	.2862	4.1641
1499	.1752	3.6347	1545	.2066	3.6483
1501	.2093	3.1881	1546	.2179	3.6191
1502	.3324	3.8098	1547	.1164	3.3416
1503	.2178	3.5156	1549	.1625	3.6864
1504	.2450	4.0570	1550	.1110	4.2651
1505	.0790	3.1762	1551	.4476	4.1902
1506	.2745	4.7297	1552	.5530	3.5514
1507	.6113	4.0112	1553	.1712	3.5763
1509	.4603	3.5867	1554	.3242	3.7022
1510	.5168	3.6849	1555	.2087	3.5765
1511	.2081	3.5694	1557	.2237	3.6872
1512	.2314	3.5827	1558	.4336	3.8788
1513	.2073	3.9886	1559	.3563	4.2715
1514	.0252	3.9828	1560	.4939	3.4884
1515	.2130	3.9023	1561	.4564	3.6975
1517	.3302	2.7942	1562	.3355	3.8744
1518	.2266	3.6323	1563	.1661	4.0055
1519	.3755	3.7126	1565	.3041	3.3584
1520	.0644	4.4009	1567	.1825	3.8688
1521	.4109	3.8127	1568	.2839	4.1946

CHURCHILL AREA SINGLE SCAN DATA
PASS 3 - Continued

SCAN NO.	CO (atm-cm)	CH_4 (atm-cm)	SCAN NO.	CO (atm-cm)	CH_4 (atm-cm)
1569	.4193	3.2297	1616	.3507	3.9522
1570	.4676	4.0736	1617	.2929	3.3857
1571	.5647	3.3441	1618	.3855	3.9930
1573	.4292	3.8105	1619	.1323	3.9168
1574	.3105	4.1281	1621	.3549	3.5629
1575	.2955	3.8639	1622	.3696	3.3663
1576	-.1501	4.0385	1623	.2620	3.7535
1577	.1515	4.0345	1624	.2991	3.6925
1578	.2033	3.5296	1625	.4078	4.0020
1579	.2469	3.6731	1626	.2930	4.0952
1581	.3189	3.5239	1627	.4781	3.4514
1582	.3703	3.1980	1629	.2214	3.8439
1583	.1622	3.8813	1630	.3075	3.6544
1584	.2139	4.5345	1631	.4059	3.9219
1585	.1871	4.6585	1632	.3370	3.5830
1586	.3040	3.4062	1633	.3876	3.5376
1587	.2533	4.4232	1634	.2906	4.4530
1589	.2944	3.5255	1635	.3088	4.0479
1590	.2776	3.4718	1637	.1345	3.7847
1592	.2295	3.5109	1638	.3436	3.2425
1593	.3023	3.5502	1639	.2335	3.6080
1594	.2582	3.8130	1640	.3038	3.5825
1595	.1553	4.2368	1641	.2734	4.2928
1597	.2526	3.5529	1642	.1000	3.3930
1598	.2053	3.8751	1643	.2067	4.1527
1599	.2513	3.5342	1645	.3409	3.5819
1600	.0728	3.5339	1646	.1387	4.0837
1601	.4043	3.8289	1647	.4962	4.0801
1602	.4416	3.5767	1648	.4216	3.7687
1603	.3673	3.3965	1649	.1031	3.0630
1605	.1656	3.3766	1650	.5030	4.0007
1606	.3975	3.2749	1651	.4021	4.1301
1607	.1302	3.2493	1653	.1253	3.6392
1608	.2440	3.9672	1654	.5550	3.9279
1609	.3484	3.4985	1655	.3558	4.3770
1610	.1883	4.3553	1656	.1539	3.5717
1611	.2395	3.8755	1657	.3974	3.1919
1613	.5238	3.6800	1658	.2791	3.5581
1614	.2722	4.2438	1659	.3003	3.2392
1615	.2565	3.5113	1661	.3284	3.9508

CHURCHILL AREA SINGLE SCAN DATA
PASS 3 - Continued

SCAN NO.	CO (atm-cm)	CH_4 (atm-cm)	SCAN NO.	CO (atm-cm)	CH_4 (atm-cm)
1662	.2057	3.2993	1707	.2418	3.9159
1663	.4011	4.4723	1709	.0265	4.0695
1664	.2549	3.9832	1710	.1649	3.8324
1665	.3413	3.8486	1711	.6964	4.1459
1666	.2601	3.8580	1712	.1956	3.6005
1667	.2563	4.0266	1713	.1561	3.3155
1669	.3478	3.1449	1714	.2875	4.2316
1670	.1428	3.5879	1715	.3306	4.0059
1671	.4092	3.8860	1717	.3304	3.8309
1672	.2615	4.3452	1718	.2696	3.4067
1673	.0493	3.8809	1719	.2311	3.5805
1674	.1587	3.6117	1720	.1524	4.1449
1675	.1909	3.1674	1721	.1479	3.7665
1677	.2223	3.6277	1722	.2902	3.2383
1678	.3434	3.6318	1723	.3526	4.3002
1679	.1242	4.1511	1725	.1315	3.6202
1680	.4242	4.1712	1726	.4002	3.3151
1681	.1966	4.0987	1727	.0820	3.6546
1682	.2446	4.0355	1728	.3533	3.4064
1683	.3025	3.9236	1729	.5358	3.7462
1685	.3292	3.5373	1730	.3063	3.3754
1686	.2191	4.1675	1731	.1196	4.1177
1687	.3927	3.8789	1733	.4239	3.3292
1688	.2069	3.2807	1734	.0977	3.8958
1689	.1119	3.4802	1735	.3787	3.9266
1690	.3089	3.9911	1736	.5194	4.1238
1691	.2975	3.2313	1737	.0385	3.8903
1693	.0465	3.2169	1738	.2405	3.8801
1694	.1650	4.1514	1739	.0694	3.9135
1695	.3675	3.5476	1741	.1990	3.2134
1696	.1479	3.7486	1742	.3508	3.9128
1697	.3809	4.1470	1743	.0186	3.8950
1698	.2397	3.6515	1744	.3966	3.5590
1699	.1737	3.9723	1745	.0070	4.6462
1701	.2938	3.8524	1746	.1026	3.6716
1702	.2279	3.8987	1747	.3544	3.7890
1703	.2377	3.5570	1749	.3167	3.7640
1704	.5202	3.3562	1750	.1184	3.5218
1705	-.0024	4.2962	1751	.2873	3.9571
1706	.0543	3.8803	1752	.1813	4.1515

CHURCHILL AREA SINGLE SCAN DATA
PASS 3 - Concluded

SCAN NO.	CO (atm-cm)	CH_4 (atm-cm)
1753	.5271	3.6298
1754	.2216	3.7671
1755	.1377	3.3227
1757	.0433	3.2476
1758	.1901	3.8724
1759	.2451	3.8785
1760	.4655	2.9977
1761	.2384	3.1290
1762	.0368	3.9787
1763	-.0076	3.7299
1765	.2749	3.8975
1766	.4816	4.0721
1767	.2008	3.6595
1768	.1766	3.0828
1769	.2061	4.1099
1770	.3258	4.3265
1771	.4176	3.7880
1773	.4276	4.0791
1774	.4462	3.7716
1775	.1772	3.5431
1776	.0023	3.9505
1777	.3958	4.3587
1778	.3135	3.7452
1779	.5307	3.5998
1781	.4194	3.6877
1782	.3288	3.6862
1783	.3251	4.0213
1784	.5216	3.7277
1785	.1629	3.2293
1786	.1498	3.4528
1787	.4086	3.4054
1789	.1951	4.1959
1790	.5041	3.3472
1791	.3898	3.4420
1792	.4213	3.9977
1793	.2694	4.3403
1794	.3919	3.6098
1795	.4340	3.8411
1797	.1741	3.3817
1798	.3412	3.1748
1799	.0135	3.9825
1800	.7353	3.9083